University of Alberta

Development and application of a capillary electrophoresis immunoassay for DNA lesions induced by ultraviolet light

by

Alevtina Goulko

A thesis submitted to the Faculty of Graduate Studies and Research
in partial fulfillment of the requirements for the degree of
Doctor of Philosophy

Department of Chemistry

Edmonton, Alberta
Spring 2011

Abstract

Ultraviolet (UV) light is one of the most abundant DNA damaging agents. The major DNA lesions, such as cyclobutane pyrimidine dimers (CPDs) and (6-4) pyrimidine pyrimidone (64PPs) photoproducts, are carcinogenic and mutagenic. Studies of the formation, repair and mutagenicity of these DNA lesions induced by environmentally relevant doses of UV irradiation require sensitive and specific techniques for their detection.

This thesis focuses on the development and application of an immunoassay combining capillary electrophoresis (CE) separation with laser induced fluorescence (LIF) detection. Primary monoclonal antibodies binding to either CPDs or 64PPs were used as the affinity recognition probes. A fluorescently labeled secondary antibody fragment (F_{ab}) was used to bind to the primary antibody. The immunocomplexes of the DNA lesions with the antibodies were separated from the excess amounts of antibodies by using CE. The fluorescent intensities of the immunocomplexes containing the DNA lesions were measured for quantitative determination of CPDs and 64PPs. Synthetic standard oligonucleotides (16 bases in length) containing a single CPD or 64PP were used for quantitative calibration. Successful determination of CPDs in UV-irradiated 80-nucleotide (nt) DNA library, calf thymus DNA, human placenta DNA and human fibroblast cells demonstrated the applicability of this CE-LIF immunoassay. Irradiation of the random

oligonucleotide sequences, naked DNA and cells with varying doses of UVB and/or UVC provided useful information on the relative yield of the formation of the UV-induced DNA lesions. The yield of CPD formation in the cellular DNA of CRL-2522 fibroblasts (3.6 ± 0.8 lesions per 10^3 nt per J/cm^2) following irradiation with low doses of UVB (< 0.3 J/cm^2) was approximately 7 times lower than that in the naked calf thymus DNA (26.8 ± 1.4 lesions per 10^3 nt per J/cm^2).

A fluorescently labeled oligonucleotide (90nt in length) containing a single CPD was designed, synthesized and partially characterized. It could potentially be used as a probe to study interactions between CPD-containing DNA and nucleotide excision repair proteins, or as a probe to screen for binding proteins or antibodies. The CE-LIF immunoassay takes advantage of antibody affinity, CE separation and highly sensitive LIF detection. Further potential applications include studies of DNA repair, monitoring of DNA damage and environmental biomarker development.

<u>Acknowledgements</u>

I would like to express my gratitude to everybody who helped, inspired and guided me throughout my doctoral program.

I owe my deepest and sincerest gratitude to my supervisor, Dr. X. Chris Le, whose mentorship and scholarship have impressed me deeply and benefited me in my life. I cannot thank him enough for his understanding, patience, kindness and guidance during my journey. His expertise, valuable conversations, stimulating suggestions and challenging tasks helped me a great deal during the ups and downs of research and throughout the completion of this thesis.

I wish to express my sincere thanks to Dr. Michael Weinfeld, my co-supervisor, for his full support, guidance and encouragement. I also want to thank him for allowing me to work in his lab and for his motivating energy and enthusiasm.

My thanks and appreciation also go to my thesis supervisory committee, Dr. Charles Lucy and Dr. Robert Campbell for their constructive comments, wise advice, kind encouragement and support.

In addition I would like to thank Dr. Glen Loppnow for letting me use his laboratory and for providing very useful comments during the candidacy exam and every time we had a conversation.

Table of Contents

List of Tables

List of Figures

List of Abbreviations

#64PP(s)	Number of 6-4 photoproduct lesions
#CPD(s)	Number of cyclobutane pyrimidine dimer lesions
16nt or 16mer	Single-stranded oligonucleotide of 16 bases long
26mer	Single-stranded oligonucleotide of 26 bases long
Ab*	A monoclonal antibody fluorescently labeled with secondary antibody
Ab*-DNA	A complex formed by DNA with UV lesions and a fluorescently labeled monoclonal antibody
*Fab	Fluorescently labeled F_{ab} fragment (secondary antibody)
64PP-16mer	Single-stranded 16 base long oligonucleotide with a single 64PP lesion
64PP(s)	6-4 pyrimidine pyrimidone dimer or (6-4) photoproduct(s)
80nt	Single stranded oligonucleotide of 80 bases long
90mer	Single stranded 90 bases long oligonucleotide or double-stranded oligonucleotide containing 90 base pairs
A	Adenosine
Ab	Monoclonal antibody
Ab*	Monoclonal antibody fluorescently labeled by secondary antibody
Ab*-Ag	Complex formed by an antigen and fluorescently labeled antibody
Ab*-DNA	Complex formed by DNA and Ab*
Ab-UV-Std*	Complex formed by fluorescently labeled oligonucleotide with single UV lesions (UV-Std*) and a monoclonal antibody (Ab)
ACN	Acetonitrile
AFM	Atomic force microscopy
AP	Apurinic apyrimidinic

ATP	Adenosine-5'-trophosphate
B[a]P	Benzo[a]pyrene
BCC	Basal cell carcinoma
bp	Base pair
BPDE	Benzo[a]pyrene diol epoxide
C	Cytosine
CE	Capillary electrophoresis
CHO cells	Chinese hamster ovary cells
CIE	Commission Internationale de l'Éclairage
CPD(s)	Cyclobutane pyrimidine dimer(s)
CPD*-16mer	Fluorescently labeled single stranded 16 bases long oligonucleotide with a single CPD lesion
CPD-16mer	Single-stranded 16 bases long oligonucleotide with a single CPD lesion
CPD-26mer	Single stranded 26bases long oligonucleotide with a single CPD lesion
CPD*-90mer	Fluorescently labeled 90-nt ling oligonucleotide with a single CPD lesion
CRL-2522	Normal human fibroblasts from fore skin
CRL-DNA	DNA extracted from CRL-2522 cells
CT	Calf thymus
CZE	Capillary zone electrophoresis
DDW	Distilled deionized water
DewPP	Dewar isomer of (6-4) photoproduct
DMA$^{(III)}$	Dimethylarsinous acid
DMA$^{(IV)}$	Dimethylarsinic acid
DNA	Deoxyribonucleic acid
DPC(s)	DNA-protein cross-link(s)
dR	Deoxyribose
DSB	Double strand breaks

E.coli	*Escherichia coli*
EDTA	Ethylenediamine tetraacetic acid
ELISA	Enzyme-linked immunosorbent assay
EOF	Electroosmotic flow
ESI	Electrospray ionization
F_{ab}-Ab	Conjugate of monoclonal antibody (Ab) and fluorescently labeled secondary antibody (F_{ab})
F_{ab}-KTM-50	KTM-50 antibody fluorescently labeled with F_{ab}
F_{ab}-KTM-53	KTM-53 antibody fluorescently labeled with F_{ab}
G	Guanine
GS	Gas chromatography
HAc	Acetic acid
hIgG	Human immunoglobulin type G
HP	Human placenta
HPLC	High performance liquid chromatography
iAs$^{(III)}$	Inorganic arsenic (III)
iAs$^{(IV)}$	Inorganic arsenic (IV)
kDa	Kilo Dalton
KTM-50	A monoclonal antibody against 64PP
KTM-53	A monoclonal antibody against CPDs
LIF	Laser induced fluorescence
LMPCR	Ligation-mediated polymerase chain reaction
MEM	Minimum essential medium
MMA$^{(III)}$	Monomethylarsinous acid
MMA$^{(IV)}$	Monomethylarsinic acid
MS	Mass spectroscopy
NER	Nucleotide excision repair
NIR	Near infrared region of the light

nt	Nucleotide
oligo	Oligonucleotide
P	Phosphate
PA	Peak area
PAtotal	Peak area for an antibody signal
PA_{cmplx}	Peak area for a complex signal
PAGE	Polyacrylamide gel electrophoresis
PAH	Polycyclic aromatic hydrocarbons
PCI	Peripheral component interconnect
PCR	Polymerase chain reaction
PBS	Phosphate buffered saline
PMT	Photomultiplier tube
PNK	Polynucleotide kinase
PR	Photoreactivation
R_s	Resolution
RIA	Radioimmunoassay
RP-HPLC	Reversed-phase high performance liquid chromatography
SCC	Squamous cell carcinoma
SM-16mer	Single stranded 16 base long oligonucleotide with no UV-induced lesions (starting material)
ss	Single strand
SSB	Single strand breaks
T	Thymine
TDM-2	A monoclonal antibody against CPD lesions
TEAA	Tetraethylammonium acetate
TG	Tris-Glycine
THF	Tetrohydrofuran
THP1 cells	Human acute monocytic leukemia cell line

TLC	Thin layer liquid chromatography
UV	Ultraviolet light
UVX	Ultraviolet light of either A, B, or C region
UVA	Ultraviolet light, A region (315 – 400 nm)
UVB	Ultraviolet light, region B (280 – 315 nm)
UVC	Ultraviolet light, regon C (100 – 280 nm)
UV-CRL-DNA	DNA extracted from CRL-2522 cells exposed to UV light
UV-DNA	UV-irradiated DNA or DNA with UV-induced lesions
UvrABC	Type of exonuclease
Vis	Visible region of the light
WHO	World Health Organization

Chapter One

General Introduction

1.1. Damaging effect of UV light on DNA

Everyone is exposed to ultraviolet (UV) radiation from the sun and/or other sources used in industry, commerce and recreation. UV radiation is divided into three regions: UVA (315 – 400 nm), UVB (280 – 315 nm) and UVC (100 – 280 nm). As sunlight passes through the atmosphere virtually all UVC radiation and approximately 90% of UVB radiation are absorbed by the ozone layer. Therefore, the UV radiation reaching the Earth is largely composed of UVA radiation and a small amount of UVB radiation. Figure 1.1 shows how we may be exposed to UV light.

Small amounts of UV radiation are beneficial to humans and essential in the production of vitamin D. UV radiation is also known to treat several diseases, including rickets, psoriasis and eczema [1]. However extended exposure to solar UV radiation may result in acute and chronic health effects on the skin, eyes and immune system. Sunburn and tanning are the best known acute effects of excessive UV radiation. Chronic effects include skin aging and cancer. Two major public health problems related to chronic exposure to excessive UV include skin cancers and cataracts [1, 2]. Skin cancer is the most common human cancer. The two main common types of non-melanoma skin cancer are basal cell carcinoma (BCC) and squamous cell

carcinoma (SCC). BCC accounts for about 80% of all non-melanoma skin cancer. Epidemiological studies have shown that people who work outdoors are more likely to develop skin cancer than indoor workers. Malignant melanoma is a tumor derived from the pigment cells (melanocytes) of the skin. Unlike non-melanoma, which can be treated surgically, melanomas have marked tendency to metastasize [2]. Between two and three million non-melanoma skin cancers and approximately 130,000 melanoma skin cancers occur globally each year [1]. Another major health problem that might be related to chronic effect of UV exposure is cataracts. Twelve to fifteen million people are blind from cataracts. According to the World Health Organization (WHO) estimates, up to 20% of these cases of blindness may be caused or enhanced by sun exposure, especially in India, Pakistan and other countries close to the equator [1]. All of these health effects are closely related to the intensity and duration of UV exposure.

The UV Index for a typical summer midday in Edmonton, Alberta, Canada, is 7, which is considered high [3]. This value can be converted into a daily DNA damage UV dose of ~0.2 J/cm^2 and erythemal daily UV dose of ~0.4 J/m^2 respectively [4]. The conversion of UV index into the daily DNA damage UV dose is derived from an action spectrum, which describes the effect of UV radiation on DNA in human skin, proposed by Setlow [5]. The conversion of UV index into the erythemal daily UV dose is derived from the action spectrum for the susceptibility of the Caucasian skin to sunburn (erythemal) by UV radiation, adopted as a standard by the International

Commission on Illumination, CIE (Commission Internationale de l'Éclairage). Conversion of UV index provided us with the environmentally relevant UV exposure.

Questions concerning the primary processes taking place in human skin exposed to sunlight can be answered by studying human cells in culture. UV exposure of cells and tissues results in the formation of a number of different photoproducts in DNA.

Even though virtually no UVC reaches the earth, most of the experiments on the effect of UV radiation on cells are performed using UVC because of its efficiency in producing damage to cells, especially to their DNA since DNA highly absorbs at 260 nm. UV radiation produces many types of photochemical alterations in DNA, RNA and proteins, as well as to structures such as membranes. DNA, however, is the major target for the deleterious effects of UV radiation because it is the largest molecule in the cell, it is present in the fewest copies, it carries the genetic information for a cell and it absorbs UV radiation very efficiently [7, 8].

A large number of differing types of damage are produced in DNA by UV irradiation. These include the modification of individual purine and pyrimidine bases (e.g. deamination), the production of pyrimidine dimers (covalent linkage of adjacent pyrimidines in DNA), the addition of other molecules to the purines and pyrimidines (e.g., water (photohydrate), DNA-protein cross-links) and single- and double-strand breaks in DNA [9-11].

Pyrimidine dimers account for the majority of UV-induced lesions in DNA. The pyrimidines are ten times more sensitive than purines and thus are primary sites of damage. UV radiation acts on DNA mainly through a direct excitation process of the nucleobases and further reactions proceed in an oxygen-independent manner. This leads mainly to the cyclobutane pyrimidine dimers (CPDs). The second most common DNA photoproduct is 6-4 pyrimidine pyrimidone, also called (6-4) photoproduct (64PP). 64PP has an absorption maximum at ~320 nm. At high doses of 313 nm light 64PP formed between two thymines undergo an efficient photoconversion into its Dewar isomer [12, 13]. Figure 1.2 shows structures of the main UV-photolesions.

UVB radiation is highly mutagenic [14] and it mostly induces mutations at bipyrimidine sites in cellular DNA [15]. A similar mutation spectrum was also observed in the *p*53 gene of the cells from skin tumors [16, 17]. However, cells of many species have a defensive mechanism against UV-induced photolesions. For example, photoreactivation (PR) is the recovery from biological damage caused by UVC or UVB radiation by simultaneous or subsequent treatment with light of longer wavelength [18]. Photoreactivation was heavily studied using *Escherichia coli* as well as other types of organisms (i.e., viruses, yeast, nonplacental mammals) [19]. Unfortunately, photoreactivaiton is not present in placental mammals, including humans [20]. In humans CPDs, 64PPs and Dewar isomers are

repaired via nucleotide excision repair (NER). This repair mechanism is designed to cleave and repair bulky DNA adducts [18, 21].
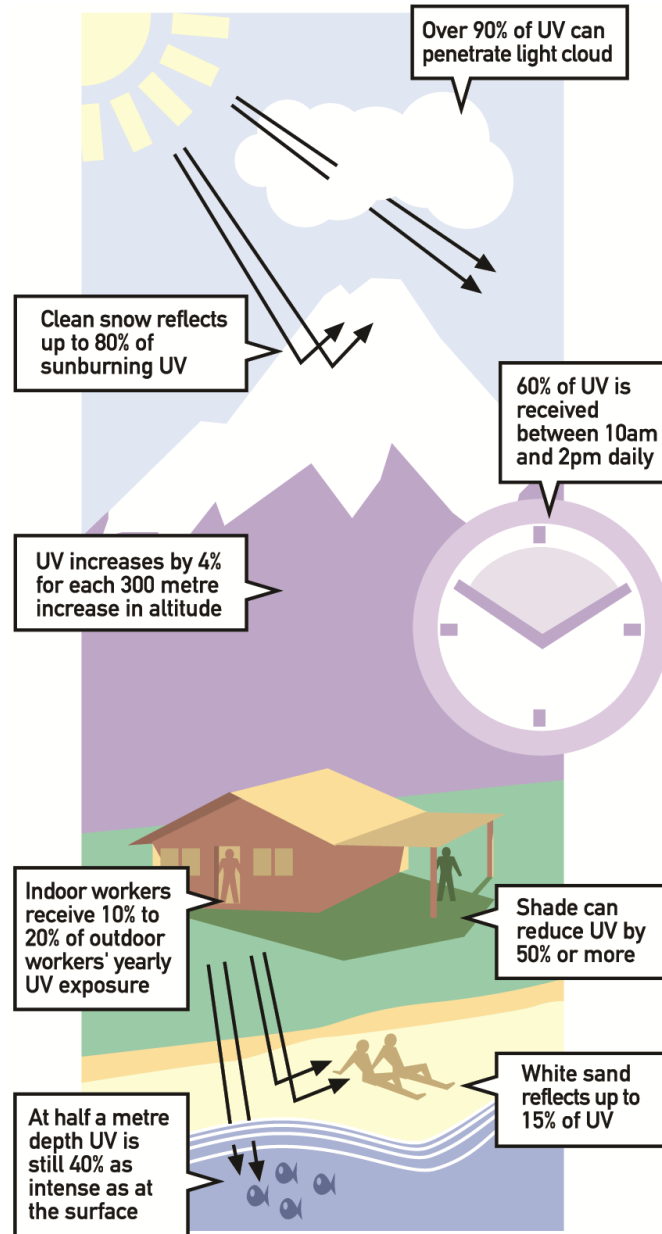
Figure 1.1. Distribution of UV radiation and possible exposure by humans on Earth [1]

Reprinted with permission from the World Health Organization.
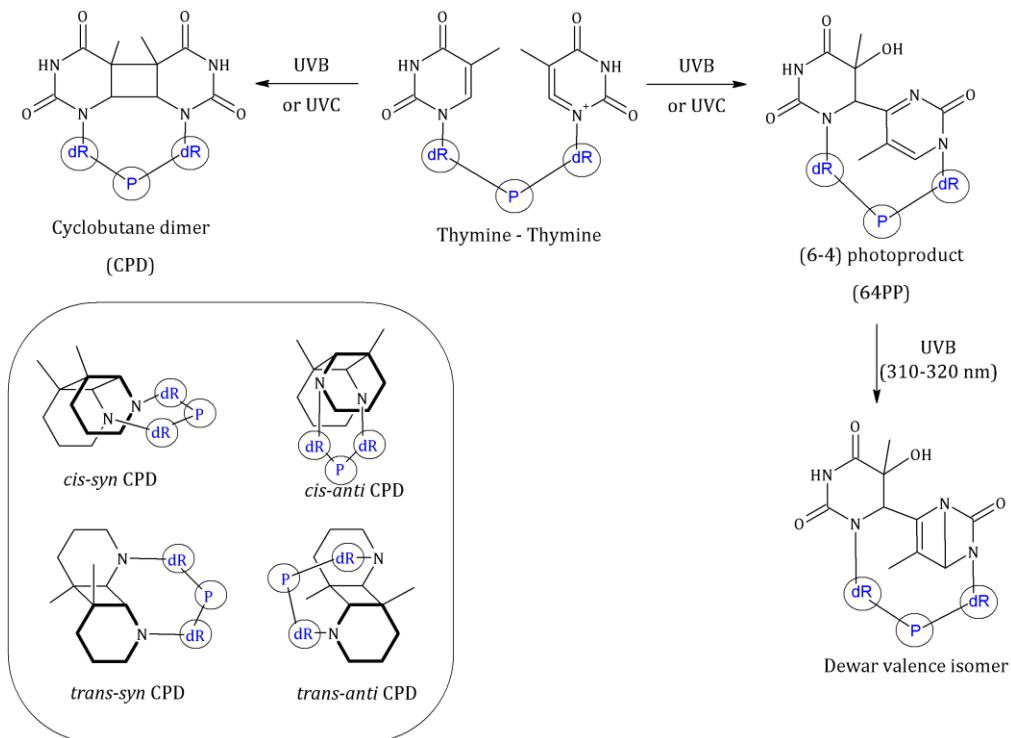
Figure 1.2. Structures of the main UV-induced photoproducts

The insert shows four possible structural isomers of CPD lesions.

dR: 2-deoxyribose; P: phosphate

1.2. Assays for photodamage in DNA

Because UV-induced photolesions are mutagenic and carcinogenic there have been numerous reports on the development of methods to monitor the formation and repair of these lesions in the last four to five decades. Methods used to study the formation of UV damage in DNA can be divided into two major subcategories: methods that measure individual UV-induced lesions in bases and methods that measure UV-induced lesions in general. Both approaches are in use to address different scientific questions.

1.2.1. Assays based on chromatography

Initially, paper chromatography was used to study 64PP in DNA at fairly low UVC doses (up to 0.05 J/cm^2) [22]. This method involved chromatographic analysis of radioactive-labeled DNA. Then in the mid-1980s HPLC provided higher resolution to separate UV-induced lesions in DNA [23-26]. At that time only radioactive measurements were sensitive enough, which required pre-labeling of samples with [^{3}H]-thymidine. Also these methods require a complete hydrolysis of DNA to individual nucleosides, which was time consuming and may require a large amount of sample. Later a non-radioactive HPLC method was suggested for monitoring the formation of 64PP [27]. In this method HF-pyridine was used to stabilize the unstable 64PP derivatives, which preserved the integrity of 64PP for quantitative measurement. 64PP derivatives exhibited fluorescence around 380 nm and

thus could be detected using a fluorescence detector. Unfortunately this method had a relatively low sensitivity of the steady-state fluorescence detector, which was not applicable for monitoring the formation of 64PP in cellular DNA extracted from UVB- or UVC-irradiated cells. It also could not be applied toward measuring CPD since these photoproducts do not fluoresce [27, 28].

TLC and HPLC combined with ^{32}P-postlabeling assay were also used to measure the formation and repair of CPD and 64PP in cellular DNA. These methods involve the initial digestion with DNAse I and then venom phosphodiesterase digestion releases the targeted lesions. This is followed by phosphorylation in the presence of ^{32}P-ATP and then HPLC separation of the radiolabeled lesions [29-31]. ^{32}P-postlabeling allows detection of both CPD and 64PP at low doses. Advantages of ^{32}P-postlabeling are not only high sensitivity and requirement of low amount of DNA, but also the possibility to study different types of UV-induced lesions (CPD, 64PP, Dewar isomers) in one sample. The major advantages of [^{32}P]-HPLC over [^{32}P]-TLC are higher resolution and reproducibility, however [^{32}P]-HPLC has lower absolute (mass) sensitivity than [^{32}P]-TLC. The disadvantage of chromatography-based assays is that some UV-induced lesions can co-migrate, thus resulting in the poor selectivity among the UV lesions.

Recently, an HPLC Electrospray (ESI) MS/MS was used to measure dimeric pyrimidine photoproducts [32-36]. Isolated or cellular DNA

extracted from UV-irradiated cells was eznymatically digested by a mixture of several enzymes [29]. For better separation of pyrimidine dimers formed beween thymines and cytosines, cytosine-containing UV-lesions were quantitatively converted into their corresponding uracil derivatives through deamination. The derivatives were then analyzed by HPLC-MS/MS. This method measures all possible bi-pyrimidine adducts in both UV-irradiated isolated and cellular DNA [32-36]. Using the same hydrolysis procedure the formation of CPD lesions in isolated DNA has been monitored using capillary GC-MS. This method involved chemical digestion of DNA followed by trimethylsilylation as well as the use of internal standards labeled with stable isotopes [37].

1.2.2. Assays based on the specific DNA cleavage

Cleavage of DNA at CPD and/or 64PP lesions with dimer-specific UV endonuclease followed by alkaline agarose gel electrophoresis has also been used to study the formation of UV-induced lesions in DNA [38-40]. Under mild conditions of alkaline hydrolysis the 64PP were converted to alkali-labile sites that appear as single-strand breaks (SSB) [38]. T4 endonuclease V was used to cleave DNA specifically at the CPD sites and then formation of the breaks was quantified by electrophoretic techniques [21, 39, 40]. A slot blot method was also used to detect CPD and 64PP simultaneously using T4 DNA polymerase-associated (3'→5') exonuclease digestion, which is blocked

by both CPD and 64PP lesions and thus can be used to detect both lesions [39, 41].

1.2.3. PCR-based assay

Ligation-mediated polymerase chain reaction (LMPCR) has been applied to monitor the formation of photoproducts in cellular DNA [42-44]. This method is important because it allows one to sequence the position of CPD and 64PP in DNA by mapping the lesions using alkaline cleavage and then amplifying the product. The mapping is done at nucleotide resolution of dimeric photoproducts. The LMPCR takes advantages of the PCR amplification to achieve high sensitivity [45, 46]. Measurements of CPDs in DNA of the basal layer of engineered human skin [47] using this technique led to the conclusion that the upper layer of the epidermis is protected against the genotoxic effects of UVC but not against the UVB radiation. By using LMPCR it was also shown that CPDs in DNA generate the vast majority of UVB-induced mutations in mammalian cells [48].

1.2.4. Immunoassays

Chromatography based assays such as GC-MS, ^{32}P-postlabeling and HPLC-MS/MS, require digestion of the DNA prior to analysis, which has the potential for artifactual formation of DNA damage. Immunochemical techniques avoid excessive digestion of DNA. For over 20 years immunological approaches have been used to measure the dimeric

photoproducts in DNA from cultured cells and tissues as well as their excision repair kinetics [49, 50]. Numerous monoclonal and polyclonal antibodies were raised against CPDs, 64PPs and even Dewar isomers. These antibodies have been used for ELISA, radioimmunoassay (RIA) and immuno-dot-blot assay of lesions in nuclear DNA, together with immunostaining of photoproducts in tissues [51-55].

There are many studies on the measurements of CPDs and 64PPs in isolated DNA, cellular DNA and tissues using various immunoassays for various purposes. For instance, RIA with polyclonal antibodies against both CPDs and 64PPs has been used for DNA repair studies in UVB-irradiated mouse skin [56]. RIA also was used to identify that TiO_2 containing sunscreen partially prevents the formation of CPDs and 64PPs in engineered human skin after exposure to solar simulated light [57]. RIA is widely used to study repair kinetics of CPDs and 64PPs in a wide range of UV-irradiated samples, such as healthy human skin [58], skin from xeroderma pigmentosum patients [59, 60] and many others [56, 61-63]. However, RIA has two limitations: (i) as a competitive binding assay it measures relative rather than absolute numbers of lesions in DNA; and (ii) photolesions may structurally modify the binding sites in DNA thus making it unrecognizable by antibodies, resulting in inaccurate measurement of photolesions. Monoclonal antibodies were also used to detect sequence specific damage after DNA digestion with restriction enzymes [62, 64].

Other immunoassays used to study photolesions in different samples are immunofluorescence microscopy [65, 66], chemiluminescence-based Western blot assay [67] and application of ^{125}I-radiolabeled secondary antibodies to indirectly measure the CPDs in whole prokaryotic cells [66].

1.2.5. Comet assays

The comet assay or single-cell gel electrophoresis is a well established and highly sensitive method for detecting strand breaks in DNA of single cells. A modified comet assay also allows the immunofluorescent detection of CPD and 64PP in the cellular DNA by introducing a lesion-specific endonuclease [68, 69]. However, quantitation and calibration of this method is a downside. In the comet assay DNA is visualized by fluorescence microscopy and then the use of available software with image analysis or visual scoring provides information on the degree of breakage in DNA. These results are then calibrated using the standard method, which involves irradiation of sample cells with γ- or X-rays to induce a known number of SSB in DNA [70]. Then the number of SSB can be related to the number of UV-lesions in DNA. An issue of using the comet assay for CPD and 64PP detection is the background of the SSB and DSB that are also produced by UV light [69, 70, 72].

1.2.6. Assays based on the recognition of DNA adducts by repair proteins

DNA repair proteins are known for their recognition of bulky DNA-adducts. For instance Uvr ABC complex is known to recognize DNA-adducts produced by UV-light, BPDE, etc. [21]. Uvr ABC, or *E. coli* ABC excision nuclease, was used as a probe to assay for DNA-damages [73]. Uvr ABC was also used in combination with another *E. coli* DNA repair enzyme, DNA photolyase, to measure CPDs and 64PPs [74]. Uvr ABC detects both photolesions. Photolyase combined with light treatment can repair only CPDs but not 64PPs [75, 76], thus allowing measurement of only 64PP after this treatment [74].

Application of assays that involve repair protein recognition of the DNA-adducts is very useful for understanding how the repair proteins work and recognize damage [77]. However, two points should be kept in mind when using the repair proteins systems for detection of photolesions: firstly, repair proteins are not not lesion-specific and incisions by an excinuclease are dependent on the extent of base modification at any site [74]; secondly, an excinuclease does not cleave 100% of the adducts under in vitro conditions [73]. Thus the amount of photolesions cannot be determined accurately.

1.3. Capillary electrophoresis – laser induced fluorescence assays

This thesis research makes use of capillary electrophoresis (CE) coupled with laser-induced fluorescence (LIF) in combination with immuno-recognition of UV-damage by monoclonal antibodies. The objective is to develop a sensitive and fast assay to detect CPD and 64PP in cellular DNA exposed to UVB at environmentally relevant doses. Immunoassays were introduced earlier. Thus CE-LIF is briefly introduced here.

Capillary electrophoresis is a technique that employs narrow-bore capillaries to perform high-efficiency electrophoretic separations of both large and small molecules. There are different modes of capillary electrophoresis. Capillary zone electrophoresis is the mode used in this research.

1.3.1 Capillary zone electrophoresis

Capillary zone electrophoresis (CZE), also known as free solution CE, is the simplest, most commonly used form of CE. The separation is based on differences in the migration time of solutes (based on charge-to-mass ratio) in an electric field. Very high electrical fields (100 – 500 V/cm or higher) can be applied to the capillary. Due to large surface-to-volume ratio Joule heating generated from the large electrical field efficiently dissipates. The use of the high electrical fields results in short analysis times, high resolution and high efficiency [78-80].

14

One of the best features of CZE is the simplicity of the instrumentation. A schematic diagram of a generic CE system is shown in Figure 1.3.
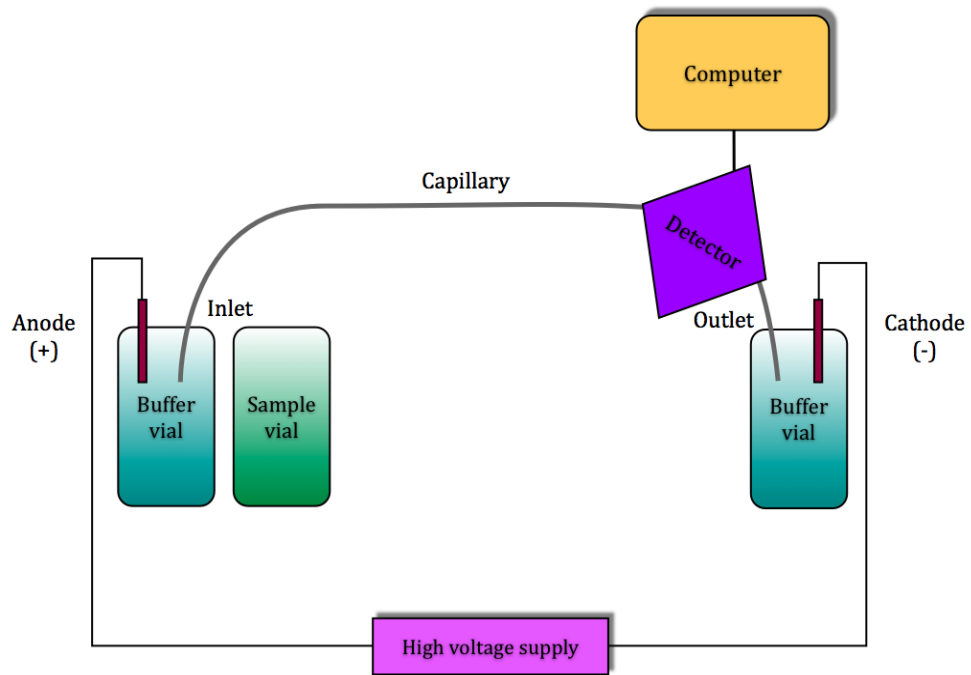
Figure 1.3. Schematic representation of a generic capillary electrophoresis system

Briefly, the ends of fused silica capillary are placed in buffer reservoirs whose content is identical to that inside the capillary. The sample is then loaded into the capillary by replacing the reservoir at the anode end with a sample reservoir. An electrical field is applied (electrokinetic injection) or the level of the sample reservoir is raised (hydrostatic injection) for a short period (typically a few seconds). After the sample is injected, the buffer reservoir is replaced and the electric field is applied for the separation. A detector is placed at or near the cathode end of the capillary. The signal from the detector is then sent to a data-handling device such as a computer. The final result is displayed as electropherograms, which represents the detector response versus the time that voltage has been applied.

One of the advantages of CZE is that charged (positive or negative) and neutral species can all be detected at the cathode end of the capillary. This is possible due to the phenomenon called electroosmotic flow (EOF) that drives all solute molecules toward the cathode end. EOF is caused by the charges on the walls of the capillary. Fused silica capillary, which is typically used in CZE, has ionizable silanol groups. These groups are in constant contact with a buffer and their degree of ionization can be controlled by the buffer pH. Therefore, negatively charged walls of the capillary are in constant contact with cations present in the buffer. This results in the formation of a double-layer and the creation of a potential difference known as zeta potential. When voltage is applied, the cations forming the double-layer are drawn towards the cathode. Since cations are solvated they drag the bulk of

the solution toward the cathode. Given that EOF is greater than the mobility of all species and the net mobility is in the direction of EOF, cations, anions and neutral molecules can be detected at the same end. Cations will migrate faster than EOF; neutral molecules will migrate at the velocity of EOF; and anions will migrate slower than EOF since they are attracted to the anode but still carried by the EOF.

Another advantage of CZE is the ability to control separation of species by changing the EOF [82-85]. There are different parameters that can change EOF. The most common parameter is the pH of the separation buffer because it changes the degree of ionization of the silanol groups. Other parameters that also alter the EOF are ionic strength of the buffer, temperature [81, 86-90], covalent coating of the capillary inner wall [91-93] and the use of surfactants for dynamic coating [94-96].

1.3.2. CE coupled with laser induced fluorescence

CE has been coupled with a wide variety of detectors: ultraviolet absorbance; mass spectrometry; conductivity; fluorescence; etc. The advantages of fluorescence detection are low detection limits and versatility. Detection limits of around $10^{-20} - 10^{-21}$ mole have been reported [97, 98]. A variety of different lasers can be used in LIF detection: helium-neon, helium-cadmium, argon and diode lasers. Unfortunately the amount of background signal is relatively high for the on-column detection, due to scattering at the capillary walls. To decrease the background signal, Dovichi's group

introduced post-column detection based on the sheath flow cuvette [99-101]. In sheath flow the background scattering is greatly minimized and the analyte molecules are hydrodynamically focused to match the size of the incident laser beam. Thus detection limits are lowered to hundreds of molecules [102, 103].

Applications of CE-LIF were demonstrated in a wide range of applications: DNA sequencing; studies of antibody-antigen interactions; and determination of a variety of macromolecules and drugs among others [104-109].

1.4. Rationale and Scope of the Thesis

The brief reviews in the previous section illustrate that many methods have been developed for detection of UV-induced DNA damage: immuno-dot-blot assays [48, 110], radioactive labeling followed by gel electrophoresis on sequencing gels [111] combined with enzymatic reactions, immunocyto- and immunohistochemistry [51, 112, 113], high performance liquid chromatography coupled with mass spectrometry (HPLC-MS) [32, 34, 114], electrospray/tandem mass spectrometry (ES/MS) [35] and comet assays [68, 115, 116]. Because of the important roles of DNA damage in many biological processes, there has been continued interest in developing new assays for trace levels of DNA damage. Recent examples also include molecular beacons and smart probes [117-119], atomic force microscopy (AFM) [71, 72] and

Raman spectroscopy [120, 121].

The objective of this thesis is to develop a capillary electrophoresis - laser induced fluorescence (CE-LIF) immunoassay that will complement and improve on current assays. This method requires minimum DNA treatment and has the advantages of specific immunorecognition, fast CE separation and highly sensitive LIF detection. The target is the UV-induced lesions because they are difficult to measure at trace levels.

This thesis consists of six chapters and an appendix.

Chapter 1 introduces general background on DNA damage and reviews the methods that are in use to measure UV-induced damage. Advantages and some limitations of these methods are also discussed.

Chapter 2 describes the development of a CE-LIF immunoassay method for detection of CPD and 64PP in an 80-nt DNA library and isolated human placenta DNA (HP-DNA) and calf-thymus DNA (CT-DNA).

Chapter 3 shows quantitation of UV-induced lesions by developing a calibration using synthetic standards. This calibration was applied to quantification of UV lesions in the 80-nt DNA library, HP-DNA and CT-DNA samples. The quantitative measures provide information on the yield of the formation of DNA lesions

Chapter 4 applies the developed CE-LIF immunoassay to the determination of CPD photoproducts in DNA extracted from the CRL-2522

cells radiated with UVB light at different doses. Experimental results are compared to those using the standard ^{32}P-postlabeling method. An application of the CE-LIF immunoassay to study co-mutagenesis of UV light and exposure to BPDE is also briefly demonstrated.

Chapter 5 describes the synthesis and partial characterization of a longer fluorescently labeled CPD-standard (90nt). This fluorescently labeled oligonucleotide containing a single lesion could be used in future studies of interactions between nucleotide excision repair proteins and DNA with CPD lesions.

Chapter 6 summarizes the conclusions from the research, discusses implications and suggests future directions for research.

Appendix A summarizes the optimization of experimental conditions used to develop the CE-LIF immunoassay. These results complement those shown in Chapters 2 and 3.

Appendix B lists data of HPLC separation, purification and MS characterization of the custom synthesized 16 nucleotide long standards with either CPD or 64PP lesion.

Appendix C shows the integration methods used in analyses of data obtained form CE-LIF immunoassay experiments.

Appendix D briefly outlines a proposed future project.

1.5. References

1. World Health Organization (2002), Global Solar UV Index: A practical guide.

2. B.L. Diffey, (1991), Solar ultraviolet radiation effects on biological systems, Phys. Med. Biol., *36*, 299-328.

3. Environment Canada. Weather and Meteorology (last access was on February 1, 2011):
    http://www.ec.gc.ca/uv/default.asp?lang=En&n=C74058DD-1

4. Tropospheric Emission Monitoring Internet Service (TEMIS), last access was on February 17, 2011:
    http://www.temis.nl/uvradiation/

5. R.B. Setlow (1974), The wavelength in sunlight effective in producing skin cancer: a theoretical analysis, Proc. Natl. Acad. Sci. U.S.A., *71*, 3363-3366.

6. J. Van Geffen, R. van der A, M. van Weele, M. Allaart and H. Eskes (2004), Surface UV radiation monitoring based on GOME and SCIAMACHY, article is available via web link at http://www.temis.nl/uvradiation/UVindex.html (last access was on February 1, 2011).

7. J. Moan, M.J. Peak (1989), Effects of UV radiation on cells, J. Photochem. Photobiol. B: Biol., *4*, 21-34.

8. K.C. Smith (2009) Basic ultraviolet radiation photobiology, at www.photobiology.info/UVphotobiology.html (last access was on December 12, 2010).

9. J.-S. Taylor (1994), Unraveling the molecular pathway from sunlight to skin cancer, Acc. Chem. Res., *27*, 76-82.

10. J. Cadet, M. Berger, T. Douki, B. Morin, S. Raoul, J.-L. Ravanat and S. Spinelli (1997), Effects of UV and visible radiations on DNA – final base damage, J. Biol. Chem., *378*, 1275-1286.

11. J.-L. Ravanat, T. Douki and J. Cadet (2001), Direct and indirect effects of UV radiation on DNA and its components, J. Photochem. Pbotobiol. B: Biol., *63*, 88-102.

12. J.-S. Taylor and M.P. Cohrs (1987), DNA, light and Dewar pyrimidones: The structure and biological significance to TpT_3, J. Am. Chem. Soc. *109*, 2834-2835.

13. J.-S. Taylor, D.S. Garrett and M.P. Cohrs (1988), Solution-state structure of the Dewar photoproduct of thymidylyl-$(3'\rightarrow5')$-thymidine, Biochemistry *27*, 7206-7215.

14. T.P. Coohill, M.J. Peak and J.G. Peak (1987), The effects of the ultraviolet wavelengths of radiation present in sunlight on human cells *in vitro*, Photochem. Photobiol., *46*, 1043-1050.

15. J.H. Miller (1985), Mutagenic specificity of ultraviolet light, J. Mol. Biol., *182*, 45-65.

16. N. Dumaz, C. Drougard, A. Sarasin and L. Daya-Grosjean (1993), Specific UV-induced mutation spectrum in the p53 gene of skin tumors from DNA-repair-deficient xeroderma pigmentosum patients, Proc. Natl. Acad. Sci., *90*, 10529-10533.

17. H. Nakazawa, D. English, P.L. Randell, K. Nakazawa, N. Martel, B.K. Armstrong and H. Yamasaki (1994), UV and skin cancer: specific p53 gene mutation in normal skin as a biologically relevant exposure measurement, Proc. Natl. Acad. Sci. U.S.A., *91*, 360-364.

18. J. Jagger, (2008) Photoreactivation, at www.photobiology.info/Jagger.html#TOP (last access was on December 12, 2010).

19. G.B. Sancar (2000), Eznymatic photoreactivation: 50 years and counting, Mutat. Res., *451*, 25-37.

20. A. Sancar (2008), Structure and function of photolyase and in vivo enzymology: 50th anniversary, J. Biol. Chem., *283*, 32153-32157.

21. E.C. Freidberg, G.C. Walker and W. Siede (1995), DNA repair and mutagenesis, ASM Press, Washington, D.C.

22. A.J. Varghese and R.S. Day, III (1970), Excision of cytosine-thymine adduct from the DNA of ultraviolet-irradiated *Micrococcus Radiodurans*, Photochem. Photobiol., *11*, 511-517.

23. J. Cadet, N.E. Gentner, B. Rozga and M.C. Paterson (1983), Rapid quantitation of ultraviolet-induced thymine-containing dimers in human cell DNA by reverse-phase high performance liquid chromatography, J. Chromatogr., *280*, 99-108.

24. H.J. Niggli and P.A. Cerutti (1983), Cyclobutane-type pyrimidine formation and excision in human skin fibroblasts after irradiation with 313 nm ultraviolet light, Biochemistry, *22*, 1390-1395.

25. W.A. Franclin and W.A. Haseltime (1984), Removal of UV light-induced pyrimidine-pyrimidon (4-6) products from *Escherichia coli* DNA requires the *uvrA, uvrB* and *uvrC* gene products, Proc. Natl. Acad. Sci. USA, *81*, 3821-3824.

26. D.E. Brash, W.A. Franklin, G.B. Sancar, A. Sancar and W.A. Haseltine (1985), *Eschericia coli* photolyase reverses cyclobutane pyrimidine dimers but not pyrimidine-pyrimidone (64) photoproducts, J. Biol. Chem., *260*, 11438-11441.

27. T. Douki, L. Voituriez and J. Cadet (1995), Measurement of pyrimidine (6-4) pyrimidine photoproducts in DNA by a mild acidic hydrolysis-HPLC fluorescence assay, Chem. Res. Toxicol., *8*, 244-253.

28. J. Cadet, E. Sage and T. Douki (2005), Ultraviolet radiation-mediated damage to cellular DNA, Mutat. Res., *571*, 3-17.

29. M. Liuzzi, M. Weinfeld and M.C. Paterson (1989), Enzymatic analysis of isomeric trithymidylates containing ultraviolet light-induced cyclobutane pyrimidine dimers. I. Nuclease P1-mediated hydrolysis of the intradimer phosphodiester linkage, J. Biol. Chem, *264*, 6355-6363.

30. M. Weinfeld, M. Liuzzi and M.C. Paterson (1989), Enzymatic analysis of isomeric trithymidylates containing ultraviolet light-induced cyclobutane pyrimidine dimers. II. Phosphorylation by phage T4 polynucleotide kinase, J. Biol. Chem, *264*, 6364-6370.

31. V.J. Bykov and K. Hemminki (1995), UV-induced photoproducts in human skin explants analyzed by TLC and HPLC-radioactivity detection, Carcinogenesis, *16*, 3015-3019.

32. T. Douki, M. Court, S. Sauvaigo, F. Odin and J. Cadet (2000), Formation of the main UV-induced thymine dimeric lesions within isolated and cellular DNA as measured by high performance liquid chromatography-tandem mass spectrometry, J. Biol. Chem., *275*, 11678-11685.

33. T. Douki and J. Cadet (2001), Individual determination of the yield of the main UV-induced dimeric pyrimidine photoproducts in DNA suggests a high mutagenicity of CC photolesions, Biochemistry, *40*, 2495-2501.

34. S. Frelon, T. Douki, J.-L. Ravanat, J.-P. Pouget, C. Tornabene and J. Cadet (2000), High performance liquid chromatography-tandem mass spectrometry measurement of radiation-induced base damage to isolated and cellular DNA, Chem. Res. Toxicol., *13,* 1002-1010.

35. T. Douki, M. Court and J. Cadet (2000), Electrospray – mass spectrometry characterization and measurement of far-UV-induced thymine photoproducts, J. Photochem. Photobiol. B: Biol. *54*, 145-154.

36. T. Douki and J. Cadet (2003), Formation of the spore photoproduct and other dimeric lesions between adjacent pyrimidines in UVC-irradiated dry DNA, Photochem. Photobiol. Sci., *2*, 433-436.

37. I.D. Podmore, M.S. Cooke, K.E. Herbert and J. Lunec (1996), Quantitative determination of cyclobutane thymine dimers in DNA by stable isotope-dilution mass spectrometry, Photochem. Photobiol., *64*, 310-315.

38. Mitchel D.L., Brash D.E. and Nairn R.S. (1990), Rapid repair kinetics of pyrimidine (6-4) pyrimidine photoproducts in human cells are due to excisions rather than conformational change, Nucleic Acids Res., *18*, 963-971.

39. X. Liu and M.J.Smerdon (1995), A slot blot method for detection of ultraviolet photoproducts in DNA, Anal. Biochem., *229*, 323-328.

40. S.E. Freeman, A.D. Blackett, D.C. Monteleone, R.B. Setlow, B.M. Sutherland and J.C. Sutherland (1986), Quantitation of radiation-, chemical-, or enzyme-induced single strand breaks in nonradioactive DNA by alkaline gel electrophoresis: Application to pyrimidine dimers, Anal. Biochem., *158*, 119-129.

41. P.W. Doetsch, G.L. Chan and W.A. Haseltine (1985), T4 DNA polymerase (3'-5') exonuclease, an enzyme for the detection and quantitation of stable DNA lesions: the ultraviolet light example, Nucleic Acids Res., *13*, 3285-3304.

42. G.P. Pfeifer, R. Drouin, A.D. Riggs and G.P. Holmquist, (1991), In vivo mapping of a DNA adduct at nucleotide resolution: detection of pyrimidine (6-4) pyrimidone photoproducts by ligation-mediated

polymerase chain reaction, Proc. Natl. Acad. Sci. U.S.A., *88*, 1374-1378.

43. G.P. Pfeifer, R. Drouin and G.P. Holmquist (1993), Detection of DNA adducts at the DNA sequence level by ligation-mediated PCR, Mutat. Res., *288*, 39-46.

44. R. Drouin and J.P. Therrien (1997), UV-induced cyclobutane pyrimidine dimer frequency correlates with skin cancer mutation hotspots in *p53*, Photochem. Photobiol., *66*, 719-726.

45. S. Tornaletti, D. Rozek and G.P. Pfeifer (1993), The distribution of UV photoproducts along the human *p53* gene in relation to mutations and skin cancer, Oncogene, *8*, 2051-2057.

46. S. Tommasi, M.F. Denissenko and G.P. Pfeifer (1997), Sunlight induces pyrimidine dimers preferentially at 5'-methylcytosine bases, Cancer Res., *57*, 4727-4730.

47. J.-P. Therrien, M. Rouabhia, E.A. Drobetsly and R. Drouin (1999), The multilayered organization of engineered human skin does not influence the formation of sunlight-induced cyclobutane pyrimidine dimers in cellular DNA, Cancer Res., *59*, 285-289.

48. Y.-H. You, D.-H. Lee, J.-H. Yoon, S. Nakajima, A. Yasui and G.P. Pfeifer (2001), Cyclobutane pyrimidine dimers are responsible for the vast majority of mutations induced by UVB irradiation in mammalian cells, J. Biol. Chem., *276*, 44688-44694.

49. D.L. Mitchell and J.M. Clarkson (1981), The development of a radiommunoassay for the detection of photoproducts in mammalian cell DNA, Biochim. Biophys. Acta, *655*, 54-60.

50. D.B. Yarosh, S. Boumakis, S. Brown, M.T. Canning, J.W. Galvin, D.M. Both, E. Kraus, A. O'Connor and D.A. Brown (2002), Measurement

of UVB-induced DNA damage and its consequences in models of immunosuppression, Methods, *28*, 55-62.

51. M.S. Cooke, I.D. Podmore, N. Mistry, M.D. Evans, K.E. Herbert, H.R. Griffiths and J. Lunec (2003), Immunochemical detection of UV-induced DNA damage and repair, J. Immunol. Methods, *280*, 125-133.

52. L. Roza, K.J.M. Van der Wulp, S.J. MacFarlane, P.H.M. Lohman and R.A. Baan (1988), Detection of cyclobutane thymine dimers in DNA of human cells with monoclonal antibodies raised against a thymine-dimer containing tetranucleotide, Photochem. Photobiol., *48*, 627-634.

53. T. Mori, M. Nakane, T. Hattori, T. Matsunaga, M. Ihara and O. Nikaido (1991), Simultaneous establishment of monoclonal antibodies specific for either dimer or (6-4) photoproduct form the same mouse immunized with ultraviolet-irradiated DNA, Photochem. Photobiol., *54*, 225-232.

54. T. Mizuno, T. Matsunaga, M. Ihara and O. Nikaido (1991), Establishment of a monoclonal antibody recognizing cyclobutane-thymine dimer in DNA: a comparative study with 64M1 antibody specific for 6-4 photoproducts, Mutat. Res., *254*, 175-184.

55. T. Matsunaga, Y. Hatakeyama, M. Ohta, T. Mori and O. Nikaido (1993), Establishment and characterization of a monoclonal antibody recognizing the Dewar isomers of (6-4) photoproducts, Photochem. Photobiol., *57*, 934-940.

56. D.L. Mitchell, R. Greinert, F.R. de Gruijl, K.L.H. Guikers, E.W. Breitbart, M. Byrom, M.M. Gallmeier, M.G. Lowery and B. Volkmer (1999), Effect of chronic low-dose ultraviolet B radiation on DNA damage and repair in mouse skin, Cancer Res., *59*, 2875-2884.

57. M. Rouabhia, D.L. Mitchell, M. Rhainds, J. Claveau and R. Drouin (2002), A physical sunscreen protects engineered human skin against artificial solar ultraviolet radiation-induced tissue and DNA damage, Photochem. Photobiol. Sci., *1*, 471-477.

58. H. Stege, L. Roza, A.A. Vink, M. Grewe, T. Ruzicka, S. Grether-Beck and J. Krutmann (2000), Enzyme plus light therapy to repair DNA damage in ultraviolet-B-irradiated human skin, Proc. Natl, Acad. Sci. U.S.A., *97*, 1790-1795.

59. F. Bernerd, D. Ausselineau, C. Vioux, O. Chevallier-Lagente, B. Bouadjar, A. Sarasin and T. Magnaldo (2001), Clues to epidermal cancer proneness revealed by reconstruction of DNA repair-deficient xeroderma pigmentosum skin in vitro, Proc. Natl. Acad. Sci. U.S.A., *98*, 7817-7822.

60. E. Otoshi, T. Yagi, T.Mori, T. Matsunaga, O. Nikaido, S.-T. Kim, K. Hitomi, M. Ikenaga and T. Todo (2000), Respective roles of cyclobutane dimers, (6-4) photoproducts and minor photoproducts in ultraviolet mutagenesis of repair-deficient xeroderma pigmentosum A cells, Cancer. Res., *60*, 1729-1735.

61. D. Perdiz, P. Grof, M. Mezzina, O. Nikaido, E. Moustacchi and E. Sage (2000), Distribution and repair of bipyrimidine photoproducts in solar UV-irradiated mammalian cells, J. Biol. Chem., *275*, 26732-26742.

62. G. Spivak, Y. Itoh, T. Matsunaga, O. Nikaido, P. Hanawalt and M. Yamaizumi (2002), Ultraviolet-sensitive syndrome cells are defective in transcription-coupled repair of cyclobutane pyrimidine dimers, DNA Repair, *1*, 629-643.

63. Y. Nishiwaki, N. Kobayashi, K. Imoto, T.-A. Iwamoto, A. Yamamoto, S. Katsumi, T. Shirai, S. Sugiura, Y. Nakamura, A. Sarasin, S. Miyagawa and T. Mori (2004), Trichothiodystrophy fibroblasts are

deficient in the repair of ultraviolet-induced cyclobutane pyrimidine dimers and (6-4) photoproducts, J. Invest. Dermatol., *122*, 526-532.

64. L. Riou, E. Eveno, A. van Hoffen, A.A. van Zeeland, A. Sarasin and L.H.F. Mullenders (2004), Differential repair of the two major UV-induced photolesions in Trichothiodystrophy fibroblasts, Cancer Res., *64*, 889-894.

65. B.H. Al-Adhami, R.A.B. Nichols, J.R. Kusel, J.O'Grady and H.V. Smith (2007), Detection of UV-induced thymine dimers in individual *Cryptosporidium parvum* and *Cryptosporidium hominis* oocysts by immunofluorescence microscopy, Appl. Environ. Microbiol., *73*, 947-955.

66. J. Peccia and M. Hernandez (2002), Rapid Immunoassay for detection of UV-induced cyclobutane pyrimidine dimers in whole bacterial cells, Appl. Environ. Microbiol., *68*, 2542-2549.

67. P.A. Rochelle, S.J. Upton, B.A. Montelon and K. Woods (2005), The response of Cryptosporidium to UV light, Trends Parasitol., *21*, 81-87.

68. S. Sauvaigo, C. Serres, N. Signotini, N. Emmonet, M.-J. Richard and J. Cadet (1998), Use of the single cell gel electrophoresis assay for the immunofluorescent detection of a specific DNA damage, Anal. Biochem., *259*, 1-7.

69. M. Duşinská and A. Collins (1996), Detection of oxidized purines and UV-induced photoproducts in DNA of single cells by inclusion of lesions-specific enzymes in the comet assay, Alter. Lab. Anim., *24,* 405-411.

70. A. Collins (2004), The comet assay for DNA damage and repair, Mol. Biotechnology, *26*, 249-261.

71. M. Lysetska, A. Knoll, D. Boehringer, T. Hey, G. Krauss and G. Krausch (2002), UV-light-damaged DNA and its interaction with human replication protein A: an atomic force microscopy study, Nucleic Acid Res., *30*, 2686-2691.

72. Y. Jiang, C. Ke, P.A. Mieczkowski and P.E. Marszalek (2007), Detecting ultraviolet damage in single DNA molecules by atomic force microscopy, Biophysical Journal, *93*, 1758-1767.

73. D.C. Thomas, A.G. Morton, V.A. Bohr and A. Sancar (1988), General method for quantifying base adducts in specific mammalian genes, Proc. Natl. Acad. Sci. U.S.A., *85*, 3723-3727.

74. D.C. Thomas, D.S. Okumoto, A. Sancar and V.A. Bohr (1989), Preferential DNA repair of (6-4) photoproducts in the dihydrofolate reductase gene of Chinese hamster ovary cells, J. Biol. Chem., *264*, 18005-18010.

75. D.E. Brash, W.A. Franklin, G.B. Sancar, A. Sancar and W.A. Haseltine (1985), *Escherichia coli* DNA photolyase reverses cyclobutane pyrimidine dimenrs but nor pyrimidine-pyrimidone (6-4) photoproducts, J. Biol. Chem., *260*, 11438-11441.

76. G.M. Myles, B. van Houten and A. Sancar (1987), Utilization of DNA photolyase, pyrimidine dimer endonucleases and alkali hydrolysis in the analysis of aberrant ABC excinuclease incisions adjacent to UV-induced DNA photoproducts, Nucleic Acids Res., *15*, 1227-1243.

77. H. Wang, M. Lu, M.-S- Tang, B. van Houten, J.B.A. Ross, M. Weinfeld and X.C. Le (2009), DNA wrapping is required for DNA damage recognition in the Escherichia coli DNA nucleotide excision repair pathway, Proc. Natl. Acad. Sci.U.S.A., *106*, 12849-12854.

78. D.R. Baker, Capillary electrophoresis, John-Wiley & Sons, New York, NY, 1995.

79. D. Heiger, High performance capillary electrophoresis, Agilent Technologies, 2000.

80. J.P. Lander, Handbook of capillary electrophoresis (2nd ed), CRC Press, Boca Raton, FL, 1996.

81. K.D. Bartle and P. Myers (2001), Theory of capillary chromatography, J. Chromatogr. A, *916*, 3-23.

82. K. K.-C. Yeung and C. A. Lucy (1997), Suppression of electroosmotic flow and prevention of wall adsorption in capillary zone electrophoresis using zwitterionic surfactants, Anal. Chem., *69,* 3435-3441.

83. K. K.-C. Yeung and C. A. Lucy (1998), Improved resolution of inorganic anions in capillary electrophoresis by modification of the reversed electroosmotic flow and the anion mobility using mixed surfactants, J. Chromatogr. A, *804*, 319-325.

84. A. G. Diress and C. A. Lucy (2004), Electroosmotic flow reversal for determination of inorganic anions by capillary electrophoresis with methanol-water buffers, J. Chromatogr. A, *1027*, 185-191.

85. A. M. MacDonald, M.A. Sheppard and C. A. Lucy (2005), Enhancement of electroosmotic flow using zwitterionic additives", Electrophoresis, *26*, 4221-4228.

86. K.D. Bartle, R.A. Carney, A. Cavazza, M.G. Cikalo, P. Myers, M.M. Robson, S.C.P. Roulin and K. Sealey (2000), Capillary electrochromatography on silica columns: factors influencing perfomance, J. Chromatogr. A, *892*, 279-290.

87. P. Schmitt-Kopplin and A. Feketa (2008), The CE way of thinking: "all is relative!", Methods in Mol. Biol., *384 (Capillary Electrophoresis)*, 611-629.

88. H. Ahmadzadeh, M. Prescott, N. Muster and A. Stoyanov (2008), Revising electroosmotic flow: an important parameter affecting separation in capillary and microchip electrophoresis, Chem. Eng. Comm., *195*, 129-146.

89. W. Thormann, J. Caslavska and R.A. Mosher (2007), Modeling of electroosmotic and electrophoretic mobilization in capillary and microchip isoelectric focusing, J. Chromatogr. A, *1155*, 154-163.

90. G.L. Erny and A. Cifuentes (2006), Field amplified separation in capillary electrophoresis: A capillary electrophoresis mode, Anal. Chem., *78*, 7557-7562.

91. B.R. Reschke, J. Schiffbauer, B.F. Edwards and A.T. Aaron (2010), Simultaneous separation and detection of cations and anions in microfluidic device with suppressed electroosmotic flow and a single injection port, Analyst, *135*, 1351-1359.

92. R. Knob, S. Gerstmann, R. Cabala and H. Frank (2009), Polypyrrole-coated and polysulfate-modified CE capillaries, Chromatographia, *69*, 1431-1435.

93. M. Spanila, J. Pazourek and J. Havel (2006), Electroosmotic changes due to interactions of background electrolyte counter-ions with polyethyleneimine coating in capillary zone electrophoresis of proteins, J. Sep. Sci., *29*, 2234-2240.

94. J.E. Melanson, N.E. Baryla and C. A. Lucy (2001), Dynamic capillary coatings for electroosmotic flow control in capillary electrophoresis, TrAC, *20*, 365-374.

95. C.A. Lucy, A. M. MacDonald and M.D. Gulcev (2008), Non-covalent capillary coatings for protein separations in capillary electrophoresis, J. Chromatogr. A, *1184*, 81-105.

96. M.D. Gulcev, T.M. McGinitie, M.F. Bahnasy and C.A. Lucy (2010), Surfactant bilayer coatings in narrow-bore capillaries in capillary electrophoresis, Analyst, *135*, 2688-2693.

97. L. Tao and R.T. Kennedy (1996), On-line competitive immunoassay for insulin base on capillary electrophoresis with laser induced fluorescence. Anal. Chem., *68*, 3899-3907.

98. X.C. Le, J.Z. Xing, J. Lee, S.A. Leadon and M. Weinfeld (1998), Inducible repair of thymine glycol detected by an ultrasensitive assay for DNA damage, Science, *280*, 1066-1069.

99. Y.F. Cheng and N.J. Dovichi (1988), Subattomole amino acid analysis by capillary zone electrophoresis and laser-induced fluorescence, Science, *242*, 562-564.

100. S. Wu and N.J. Dovichi (1989), High-sensitivity fluorescence detector for fluorescein isothiocyanate derivatives of amino acids separated by capillary zone electrophoresis, J. Chromatogr., *480*, 141-151.

101. S. Wu and N.J. Dovichi (1992), Capillary zone electrophoresis separation and laser-induced fluorescence detection of zemtomole quantities of fluorescein thiohydantoin derivatives of amino acids, Talanta, *39*, 173-178.

102. H. Swerdlow, J.Z. Zhang, D.Y. Chen, H.R. Harke, R. Grey, S.L. Wu, N.J. Dovichi and C. Fuller (1991), Three DNA sequencing methods using capillary gel electrophoresis and laser-induced fluorescence, Anal. Chem., 63, 2835-2841.

103. D.Y. Chen and N.J. Dovichi (1994), Yoctomole detection limit by laser-induced fluorescence in capillary electrophoresis, J. Chromatogr. B, *657*, 265-269.

104. Q.H. Wan and X.C. Le (1999), Capillary electrophoresis coupled with laser-induced fluorescence polarization as a hybrid approach to ultrasensitive immunoassays, J. Chromatogr. A., *853*, 555-562.

105. Q.H. Wan and X.C. Le (1999), Capillary electrophoretic immunoassay for digoxin and gentamicin with laser-induced fluorescence polarization detection, J. Chromatogr. B, *734*, 31-38.

106. Q.H. Wan and X.C. Le (1999), Fluorescence polarization studies of affinity interactions in capillary electrophoresis, Anal. Chem., *71*, 4183-4189.

107. Q.H. Wan and X.C. Le (2000), Studies of protein-DNA interactions by capillary electrophoresis/laser induced fluorescence polarization, Anal. Chem., *72*, 5583-5589.

108. M.T. Lam and X.C. Le (2002), Competitive immunoassay for vancomycin using capillary electrophoresis with laser-induced fluorescence detection, Analyst, *127*, 1633-1637.

109. H. Fu, J.W. Guthrie and X.C. Le (2006), Study of binding stoichiometries of the human immunodificiency virus type 1 reverse transcriptase by capillary electrophoresis and laser-induced fluorescence polarizaton using aptamers as probes, Electrophoresis, *27*, 433-441.

110. D. Perdiz, P. Grof, M. Mezzina, O. Nikaido, E. Moustacchi and E. Sage (2000), Distribution and repair of bypyrimidine photoproducts in solar UV-irradiated mammalian cells, J. Biol. Chem., *275*, 26732-26742.

111. D.L. Mitchell, J. Jen and J.E. Cleaver (1991), Relative induction of cyclobutane pyrimidine dimers and cytosine photohydrates in DNA irradiated in vitro and in vivo with ultraviolet-C and ultraviolet-B light, Photochem. Photobiol., *54*, 741-746.

112. M. Yamada, M.U. Udono, M. Hori, R. Hirose, S. Sato, T. Mori and O. Nikaido (2006), Aged human skin removes UVB-induced pyrimidine dimers from the epidermis more slowly than younger adult skin in vivo, Arch. Dermatol. Res., *297*, 294-302.

113. H. Backvall, C. Wassberg, B. Berne and F. Ponten (2002), Similar UV responses are seen in a skin organ culture as in human skin in vivo, Experimental Dermatology, *11*, 349-356.

114. S. Courdavault, C. Baudouin, M. Charveron, B. Canguilhem, A. Favier, J. Cadet and T. Douki (2005), Repair of the three main types of bipyrimidine DNA photoproducts in human keratinocytes exposed to UVB and UVA radiations, DNA Repair, *4*, 836-844.

115. M.P. Sastre, M. Vernet and S. Steinert (2001), Single-cell gel/comet assay applied to the analysis of UV readiation-induced DNA damage in *Rhodomonas sp.* (*Cryptophyta*), Photochem. Photobiol., *74*, 55-60.

116. J.P. Pouget, T. Douki, M.J. Richard and J. Cadet (2000), DNA damage induced in cells by γ and UVA radiation as measured by HPLC/GC-MS and HPLC-EC and comet assay, Chem. Res. Toxicol., *13*, 541-549.

117. S. Yarasi, C. McConachie and G.R. Loppnow (2005), Molecular beacon probes of photodamage in thymine and uracil oligonucleotides, Photochem. Photobiol., *81*, 467-473.

118. S.A. Oladepo and G.R. Loppnow (2010), The effect of tryptophan on UV-induced DNA photodamage, Photochem. Photobiol., *86*, 844-851.

119. S.A. Oladepo and G.R. Loppnow (2010), Self-quenching smart probes as a Platform for the détection of sequence-specific UV-induced DNA photodamage, Anal. Bioanal. Chem., *397*, 2949-2957.

120. Y.-L. Tang and Z.-Y. Guo (2005), Raman spectroscopic analysis of the effect of ultraviolet radiation on calf thymus DNA, Acta Biochim. Biophys. Sin., *37*, 39-46.

121. W. Ke, D. Zhou and J. Wu (2005), Effects of UV irradiation on calf thymus DNA in aqueous solution. A Raman spectroscopic study, J. Raman Spectrosc., *36,* 39-44.

Chapter Two

Development of a non-competitive CE-LIF immunoassay
for detection of UV-lesions

2.1. Introduction

The fast and efficient separation by capillary electrophoresis (CE) and small sample volume requirement make CE a powerful technique for biochemical and clinical analysis [1-6]. Laser induced fluorescence (LIF) offers extremely sensitive detection for CE [7-11], leading to a detection limit of a single molecule [9-11]. However, fluorescent labeling of trace levels of analyte in the presence of a sample matrix can be problematic because of non-quantitative derivatization and matrix interference on the labeling reaction.

By developing innovative combinations of affinity recognition with CE/LIF, these problems could be circumvented. Several research groups, including those of Arriaga [12], Bowser [13, 14], Britz-McKibbin [15, 16], Chen [17, 18], Harrison [19, 20], Heegaard [21-23], Karger [24, 25], Kennedy [26-29], Krull [30, 31], Krylov [32, 33], Le [34-38], McGown [39, 40], Novotny [41], Pawliszyn [42, 43], Regnier [44, 45] and Whitesides [46, 47], to name a few, have demonstrated the potential of affinity recognition with CE for a variety of biological and environmental applications. The primary objective

of this chapter is to develop a sensitive assay for UV-induced DNA lesions by building on the advantages of the affinity recognition, CE separation and LIF detection.

My primary research focuses on detecting trace amounts of DNA damage caused by environmentally relevant doses of UV exposure. A major analytical challenge in quantifying a few lesions in a DNA molecule of several million to a billion base pairs is the need for high selectivity and sensitivity. Our approach uses a monoclonal antibody to recognize the specific DNA lesion, which can provide selectivity. We use LIF detection to achieve the required detection limit. To make the DNA damage detectable with high sensitivity LIF, we use a fluorescently labeled antibody fragment to provide an affinity probe.

Briefly, a mouse monoclonal primary antibody (Ab), raised against a specific DNA damage, recognizes and binds to the DNA at its damaged site. A fluorescently labeled secondary anti-mouse antibody fragment ($^*F_{ab}$) recognizes and binds to the F_c region of the primary antibody (Ab*), thereby providing the capability for LIF.

To achieve complete formation of the fluorescent complex so that the DNA lesions can be quantified, we use excess amounts of the $^*F_{ab}$ to saturate the Ab and excess Ab to saturate the DNA damage. The final mixture is separated using capillary electrophoresis (CE) and the fluorescent species are detected using laser-induced fluorescence (LIF). The overall process is

schematically shown in Figure 2.1.

The assay can also be represented as the following equation:

$$nDNA + mAb + z*F_{ab} \rightarrow (Ab*)_x\text{-}(DNA)_n + (m\text{-}x)Ab*_{(excess)} + (z\text{-}x)*F_{ab(excess)}$$

<div align="right">(eq. 2-1)</div>
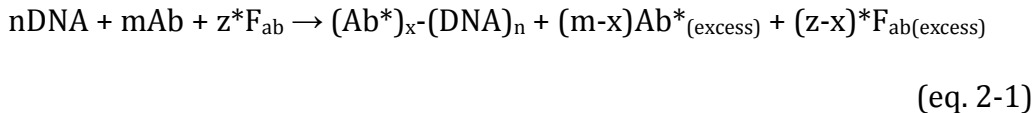
Where Ab*-DNA denotes the ternary complex ($*F_{ab}$-Ab-DNA) of DNA lesion with the primary antibody that in turn binds to the fluorescent secondary antibody fragments; $Ab*_{(excess)}$ represents the complex ($*F_{ab}$-Ab) between the primary antibody and the fluorescent secondary antibody fragment. (n, m, z, x represent the stoichiometry of species.)

The concept of the CE-LIF immunoassay has been demonstrated from the detection of DNA adducts of benzo[a]pyrene in DNA (BPDE; generated by a typical chemical carcinogen) and thymine glycol (Tg; typical oxidative DNA damage induced by ionizing radiation) [51]. The present research extends the development of ultrasensitive assays to cyclobutane pyrimidine dimers (CPDs) and 6-4 photoproducts (64PPs) generated by UV radiation. These lesions are difficult to detect and there has been no CE-LIF method for their detection.

To verify that CE-LIF immunoassay is applicable for the detection of UV-induced lesions in DNA a series of experiments were carried out, which included detection of CPDs and 64PPs in a single stranded 80-nucleotide long DNA library, isolated single stranded calf thymus DNA (CT-DNA) and human

placenta DNA (HP-DNA) after being exposed to either UVB or UVC light at different doses. Also different commercially available primary antibodies were compared in this non-competitive assay. Choice of experimental conditions for CE-LIF is described in Appendix A.
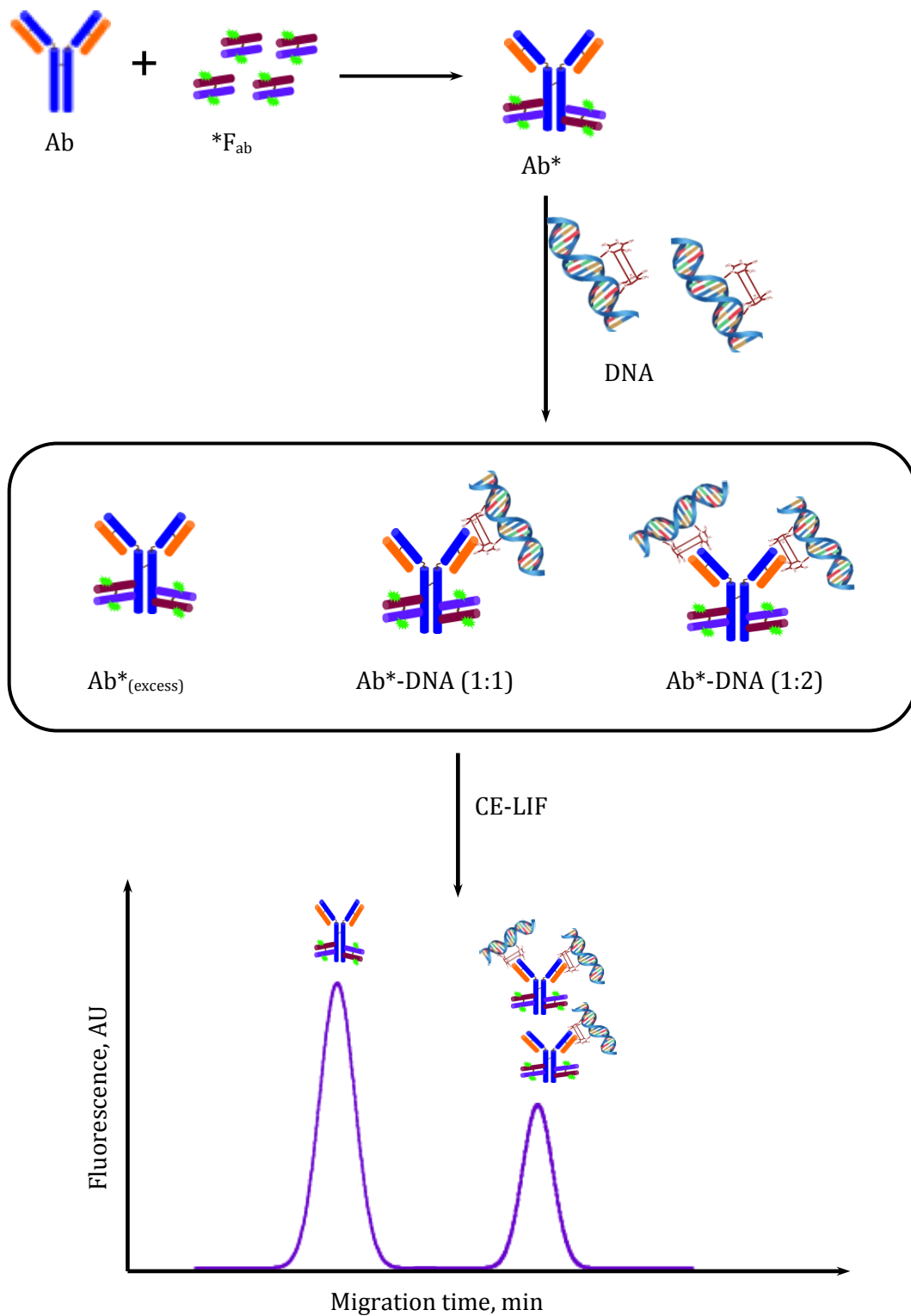
Figure 2.1. Schematic representation of CE-LIF immunoassay for detection of UV-lesions

2.2. Experimental

2.2.1. Reagents

Tris-glycine buffer solutions (TG, 25 mM Tris and 192 mM Glycine) were prepared from 10x TG buffer (Bio-Rad Laboratories, Hercules, CA, USA) by diluting with 18.2 MΩ distilled deionized water (DDW) from a Milli-Q Gradient Water System (Millipore, Nepean, ON, Canada). The pH of TG buffer for incubation was adjusted to 7.5 and the pH of the TG buffer for CE separation was 8.3. The single-stranded 80 nucleotide random DNA library (80nt DNA) used in this study was synthesized by IDT (Integrated DNA Technologies, Inc., Caralville, IA, USA). The DNA library had the following sequence: 5'-AGC AGC ACA GAG GTC AGA TG (N)$_{40}$ CCT ATG CGT GCT ACC GTG AA-3', where N is any of the four bases. Single-stranded human placental DNA (HP-DNA) was obtained from Fluka BioChemika (Buchs, Switzerland). Single-stranded calf-thymus DNA (CT-DNA) was obtained from Sigma-Aldrich (St. Louis, MO, USA). Monoclonal mouse anti-thymine dimer antibody (clone KTM-53, IgG$_1$ isotype) and monoclonal mouse anti-(6-4) photoproduct antibody (clone KTM-50, IgG$_1$ isotype) were purchased from Kamiya Biomedical Company (Seattle, WA, USA). Goat anti-mouse F$_{ab}$ fragment (*F$_{ab}$), supplied in a Zenon® Alexa Flour® 546 (λ_{ex} = 556 nm, λ_{em} = 573 nm) mouse IgG$_1$-labeling kit (Molecular Probes, Eugene, OR, USA), was used as a secondary antibody to fluorescently label KTM-53 and KTM-50.

2.2.2. UVB and UVC irradiation

The 80nt DNA, HP-DNA and CT-DNA were irradiated in a UV chamber with overhead UVB or UVC lamps (Luzchem Research Ltd., Ottawa, ON, Canada) located at approximately 12.5 cm from the target. These UVB and UVC lamps have a spectral range of 235 - 850 nm. The emission spectrum of the UVB lamps has the following characteristics: 32% UVA (315-400 nm), 54% UVB (281-315 nm), 3% UVC (235-280 nm), 10% visible (401-700 nm) and less than 1% NIR (701-850 nm) regions. The emission spectrum of the UVC lamps has the following characteristics: 1.67% UVA (315-400 nm), 1.98% UVB (281-315 nm), 88.59% UVC (235-280 nm), 7.21% visible (401-700 nm) and less than 1% NIR (701-850 nm) regions.

UV doses were measured using a UVX digital radiometer with a UVB sensor (UVX-31, 310 nm, UVP Inc., Upland, CA, USA) and a UVC sensor (UVX-25, 254 nm, UVP Inc., Upland, CA, USA) in mW/cm^2 and later converted to J/cm^2 based on different irradiation times. The 80nt DNA, HP-DNA and CT-DNA solutions were put into 60-mm Petri dishes and placed into the UV chamber for either UVB or UVC irradiation.

2.2.3. Instrumentation

The laboratory-built capillary electrophoresis laser induced fluorescence (CE-LIF) system (Figure 2.2) used for these studies was described previously [35, 51-55]. Briefly, uncoated fused silica capillaries (20

μm i.d., 150 μm o.d., Polymicro Technologies, Phoenix, AZ, USA) were used for separation. Electrophoresis was powered by a high-voltage power supply (CZE1000R, Spellman, Plainview, NY, USA). Injection and separation conditions (times and voltages) were controlled by LabView software program (National Instruments, Austin, TX, USA) run on a Macintosh computer. The injection end of the capillary and the electrode connected to the power supply (positive polarity) were placed into the sample vial or into the vial with the running buffer. The other end of the capillary and the other electrode were placed into the waste vial. The polyimide coating-free area of the capillary for the on-column detection was fixed in the grounded holder. The laser was a 1.0 mW green helium-neon laser (Melles Griot, Irvine, CA, USA) with an excitation wavelength of 543.5 nm. The laser beam was focused onto the capillary through a microscope objective (6.3x) and the fluorescence signal was collected with a 60x microscope objective lens (0.7 NA, Universe Kogaku, Oyster Bay, NY, USA) at 90° from the direction of the laser beam. The focused light was then filtered using a 580 nm band-pass filter; the signal was detected by photo-multiplier tube (Hamamatsu Photonics, Japan) and recorded by a Macintosh computer equipped with a PCI data acquisition board and running LabView software. An auxiliary microscope (10×, 0.25 NA) was used to align the laser beam with the capillary, focusing optics and PMT.

He-Ne laser 543.5 nm

PMT

Filter 580 nm

Instrument control and data processor

Pinhole

Capillary

Electrode

Microscope 60× objective

Cuvette

Mirror

Focusing 6.3× objective

Samples

High voltage power supply

Waste

Laser beam

to PMT

capillary

sample injection
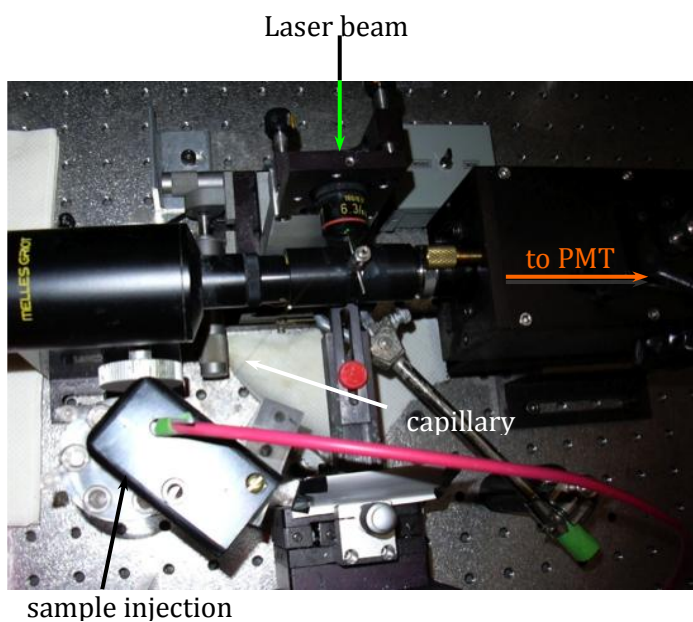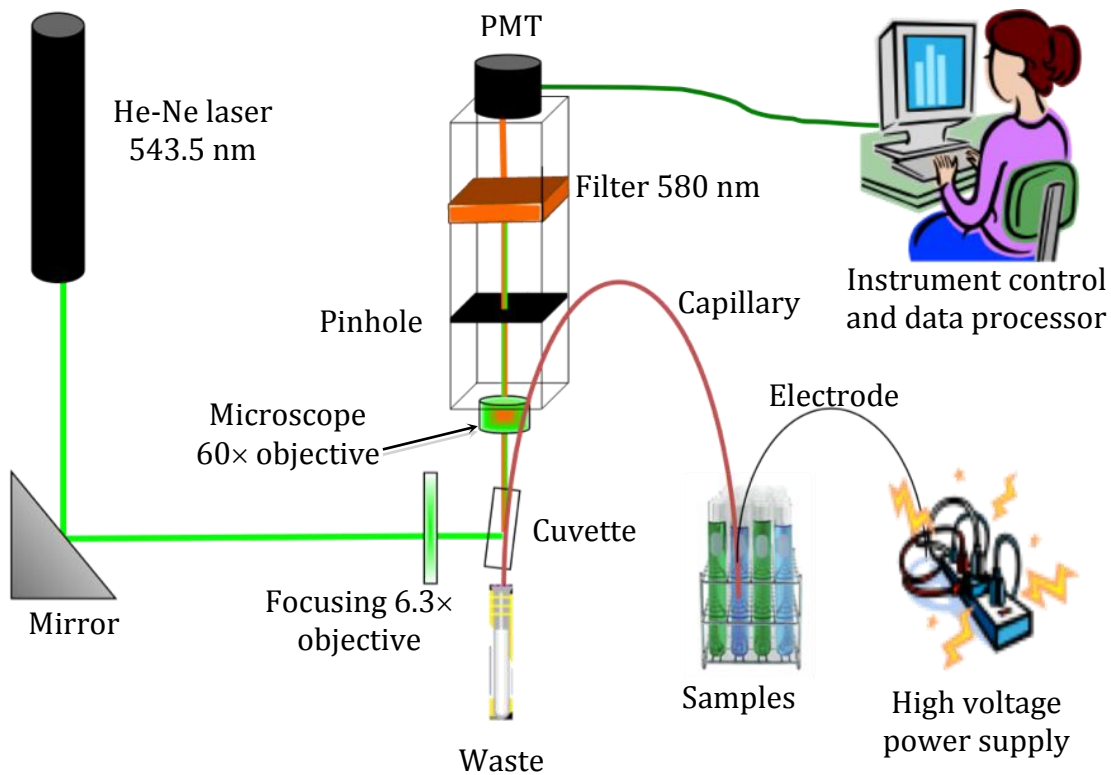
Figure 2.2. Diagram and photographs of the laboratory-built capillary electrophoresis laser-induced fluorescence (CE-LIF) instrument used in this research

2.2.4. Detection of CPDs and 64PPs in DNA samples

The primary anti-CPD (KTM-53) and anti-64PP (KTM-50) antibodies were mouse IgG_1 type antibodies. The primary antibodies were labeled using the Zenon® mouse IgG labeling kit (Molecular Probes). The kit included Zenon® mouse IgG labeling reagent, which is the fluorescently labeled goat F_{ab} fragment selective for the F_c portion of the mouse IgG_1 type. F_{ab} fragment is conjugated to an Alexa Fluor® 546 dye ($*F_{ab}$). It was the only type of the fluorophore available in the Zenon® labeling kit. Based on the Table 2.1, [56-58] Alexa Fluor® 546 was chosen due to its higher quantum yield at 543 nm.

Table 2.1. Spectroscopic properties of fluorescent dyes*

Fluorophore	λ_{ex} (nm)	λ_{em} (nm)	Extinction coefficient ($M^{-1} \cdot cm^{-1}$)	Quantum yield
TMR	555	580	103,000	0.20
Cy3	550	570	150,000	0.15
Alexa Fluor® 546	554	575	104,000	0.79
Alexa Fluor® 555	555	565	150,000	0.10

(*) Data provided for free dyes only.

Fluorescent labeling of the antibody using the Zenon® labeling kit is simple and quick [59]. Three to four fold molar excess of fluorescently labeled goat F_{ab} fragment was added to the solution with the primary antibody; 100 μg/ml of nonspecific *h*IgG was also added to prevent non-specific binding of DNA to the primary antibody as well as to bind excess F_{ab} fragments. Previous work showed that the F_{ab}-antibody complex was formed in less than 5 minutes [59]. To ensure the complete reaction, we let the solutions incubate at room temperature for 15 minutes. After formation of F_{ab}-Ab conjugates, the "master mix" was added to single stranded DNA samples and solutions were incubated for 20 minutes at room temperature prior to the CE-LIF analysis. Solutions were incubated in 1×TG buffer (25 mM Tris and 192 mM Glycine) at pH 7.5. An aliquot of the prepared solution was electrokinetically injected into the capillary by applying an injection electric field of 500 V/cm for 5 sec. Separation was carried out at room temperature with 1×TG running buffer, pH 8.3, at an applied electric field of 500 V/cm. The capillary was washed after every injection with 20 mM NaOH, distilled deionized water and 1×TG, pH 8.3, for a period of at least 3 minutes for each wash step.

To minimize variations and potential errors due to possible changes in fluorescent intensity signal from the fluorophore, adsorption of label and protein complexes on the capillary wall, variations in electroosmotic flow (EOF) and possible signal drift due to possible movement of the capillary, we used the relative peak areas to measure the level of UV lesions in DNA.

Relative peak area ($PA_{relative}$) was defined as the ratio of peak area for the complex (PA_{cmplx}) over the total peak area of all fluorescent species (PA_{total}). The relative PA values enabled reproducible results for experiments even when absolute fluorescence intensities vried due to new alignment of the instrument or the change of new capillaries.

2.3 Results and discussion

To develop a CE-LIF immunoassay that could be useful for a range of potential applications, we chose three types of DNA samples representing different sizes: 80nt DNA library, single-stranded calf-thymus DNA (CT-DNA) and single-stranded human placenta DNA (HP-DNA). The HP-DNA is 530 – 830 bases long and the CT-DNA is approximately 50,000 bases long. The 80nt DNA library contains random sequences of oligonucleotides. The library is the same as that used in the experiments for the selection of DNA aptamers [75]. In the present research, these different DNA samples were irradiated with varying doses of UVB and UVC light to produce DNA photolesions, including CPDs and 64PPs. A CE-LIF immunoassay was then developed and applied to the detection of DNA photolesions in the irradiated DNA samples. The following sub-sections describe the detection of CPD and 64PP lesions in the three types of DNA samples. Further details on the optimization of experimental conditions are shown in Appendix A.

We detected both photoproducts in all DNA samples after irradiation with either UVB or UVC light. It has been previously reported that irradiation to UVB and UVC light results mainly in CPD photoproducts and much less in 64PP lesions [60-64]. Results of our experiments supported the previous findings, which also help validate the application of the CE-LIF immunoassay.

2.3.1. Detection of the CPD and 64PP lesions in UVB irradiated 80nt DNA library

Figure 2.3 shows example electropherograms obtained from CE-LIF analyses of solutions containing the fluorescent secondary antibody fragment F_{ab} (*F_{ab}), the primary antibody (Ab*) to either CPD or 64PP and the DNA samples. The DNA sample was an 80nt DNA library containing approximately 10^{13} sequences. This DNA library was irradiated with UVB (0.0 – 5.4 J/cm^2) prior to the CE-LIF immunoassay.

The main peaks in Figure 2.3 are due to the LIF detection of fluorescent species, including the excess *F_{ab}, the complex of the *F_{ab} with Ab (Ab*) that recognizes CPD or 64PP and the ternary complex of the DNA lesions with the primary antibody (Ab*-DNA) (Figure 2.1). Under free zone CE conditions used here, the *F_{ab} and Ab* are not resolved and migrate as a single peak (Ab* in Figure 2.3). Upon binding to DNA, the introduction of multiple negative charges by the DNA to the ternary complex results in a substantial mobility shift from the antibody alone. With the increase in (negative) charge-to-mass ratio, the Ab*-DNA complex migrates slower to

the cathode where the LIF detector is located (Figure 2.2). The resolution (R_s) between the Ab* and the Ab*-DNA peaks is approximately 0.99 ± 0.08.

The relative intensity of the Ab*-DNA peak is used to measure the amount of the CPD or 64PP lesions in the DNA sample. Figure 2.3 shows an increase in the Ab*-DNA peak intensity with the increase of UVB dose.

Figure 2.4 shows the dose response for a wider range of UVB doses. The relative peak area of the Ab*-DNA complex ($PA_{relative}$) is proportional to the amount of UV damage present in DNA. Thus the higher the value of $PA_{relative}$ the more UV damage is present in the DNA sample. Figure 2.4 also shows that the $PA_{relative}$ is much lower for the 64PPs compared to CPDs in the irradiated 80nt DNA library. Thus lower amounts of 64PPs compared to CPD lesions have been formed in DNA. These results agree with the findings that UVB light produces more CPD photoproducts than 64PP [65]. The relative frequency of production of the different products depends on the spectrum of the UV source, the types of cells or tissue used and the exposure conditions. Previous reports [66-69] concluded that the most frequent lesions in DNA were CPDs when the UV irradiation wavelength was below 365 nm. Only in certain specific DNA sequences did the yield of 64PP approach that of CPDs [66].
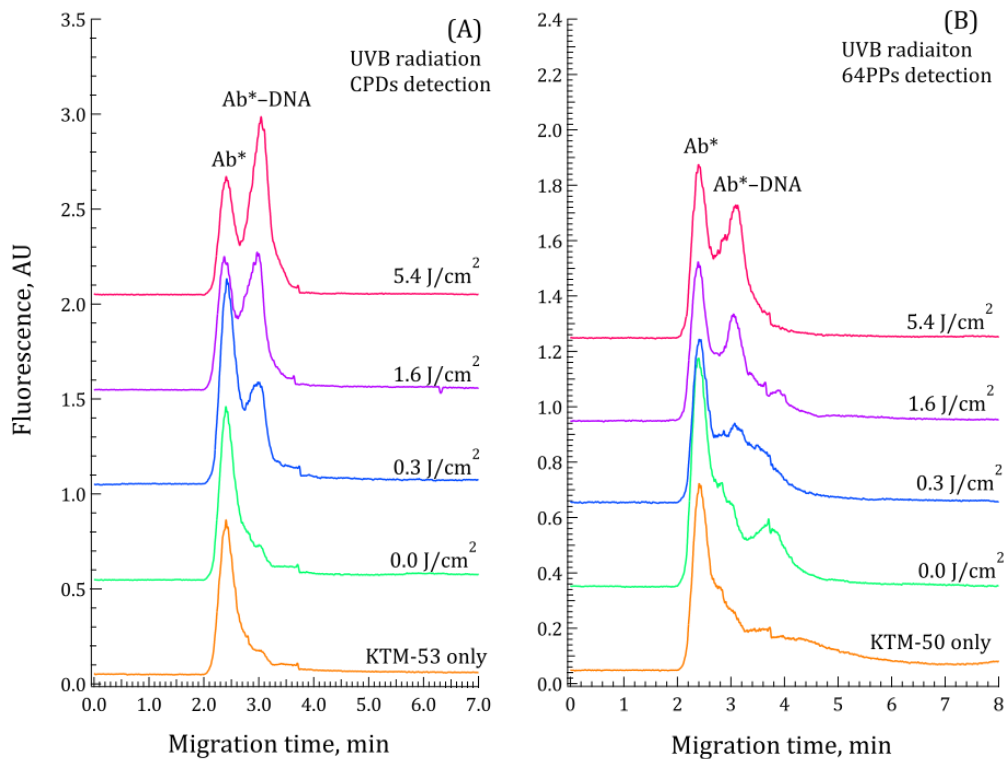
Figure 2.3. Electropherograms from CE-LIF immunoassay of CPD (A) and 64PP (B) in UVB-irradiated 80-nt DNA library

The peak labeled Ab*-DNA represents the ternary complex between the DNA lesions (CPD or 64PP) and the antibody recognizing the specific lesion.

The peak denoted with Ab* represents the excess fluorescent secondary antibody fragment F_{ab} (*F_{ab}) and its complex (*F_{ab}-Ab) with the primary antibody.

Figure 2.4A illustrates the dose response for CPD photoproducts. At UVB doses <5 J/cm^2 there is a noticeable linear increase in signal with the increase of UVB dose. However, at UVB doses >5 J/cm^2 the signal reaches a plateau. The plateau may be the result of either saturation of the antibody by CPD lesions (not enough Ab to detect all CPD damage) or DNA strands saturated by the CPD lesions (no more sites available to produce CPD damage). Environmentally relevant UVB doses are below 3.0 J/cm^2, therefore the working range for detection of CPD lesions in DNA samples was at the UVB doses under 3.0 J/cm^2.

Figure 2.4B shows an increase in the formation of 64PPs up to the UVB dose of ~2 J/cm^2 and then at the higher doses a decrease in the formation of 64PPs. References [70-72] reported that the higher doses of UV light at 300 – 350 nm result in photochemical conversion of 64PP into its Dewar isomer. The anti-64PP antibody used in the present work (KTM-50 clone) does not bind to 64PP Dewar isomers. Therefore, at UVB doses higher than 2 J/cm^2, if 64PPs were photochemically converted into Dewar isomers, the latter would not be detected by the CE-LIF immunoassay. This would be consistent with the observed decrease in the signal response at the UVB doses higher than 2 J/cm^2. The observed plateau for 64PP at UVB doses greater than 3 J/cm^2 may also suggest that the system reached steady-state meaning that no more 64PP are produced or photochemically converted.
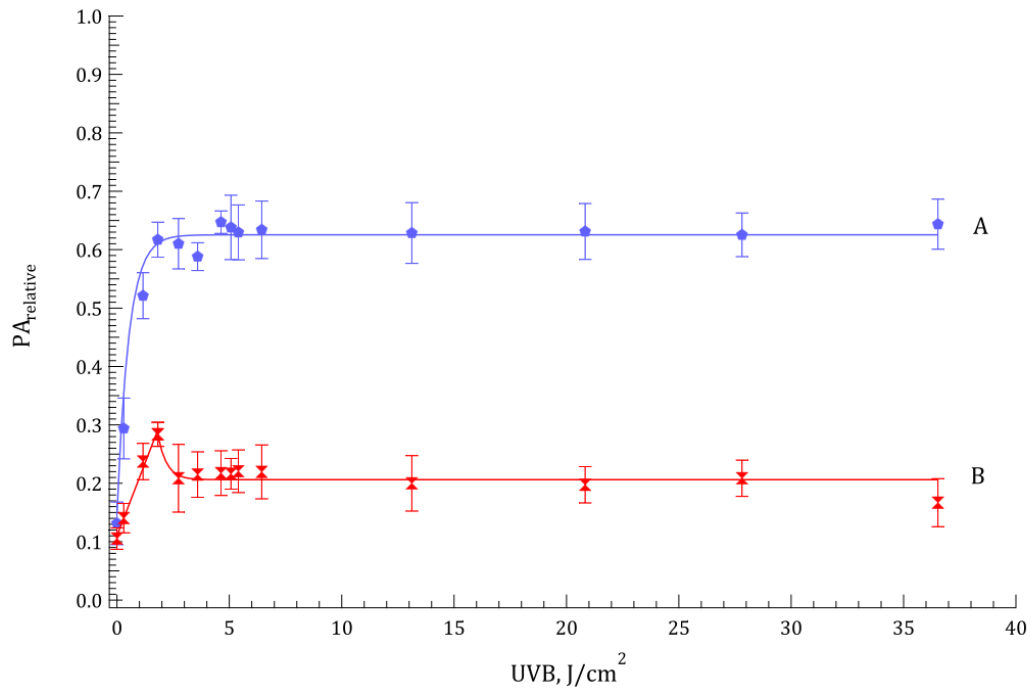
Figure 2.4. Dose response for CPD (A) and 64PP (B) lesions formed in 80nt DNA library irradiated with a wide range of UVB doses

Each data point represents the mean value and the error bars represent ± standard deviation from a minimum of three independent experiments.

Note: the lines connecting data points serve to show trends. The lines were not generated from any data-fitting program.

Since this research focuses on the detection of the UV lesions in DNA exposed to environmentally relative doses of UV light (UV doses < 3.0 J/cm^2), our interest was on UVB doses below 2.0 J/cm^2. Therefore the issue of the photochemical conversion of 64PPs at higher UVB doses was not explored further.

Figure 2.5 shows the linear range of the dose response *vs.* UVB dose for both CPD and 64PP lesions in the 80nt DNA library. Within this low range (up to 2.0 J/cm^2), the amounts of CPD and 64PP increase with increasing doses of UVB radiation.
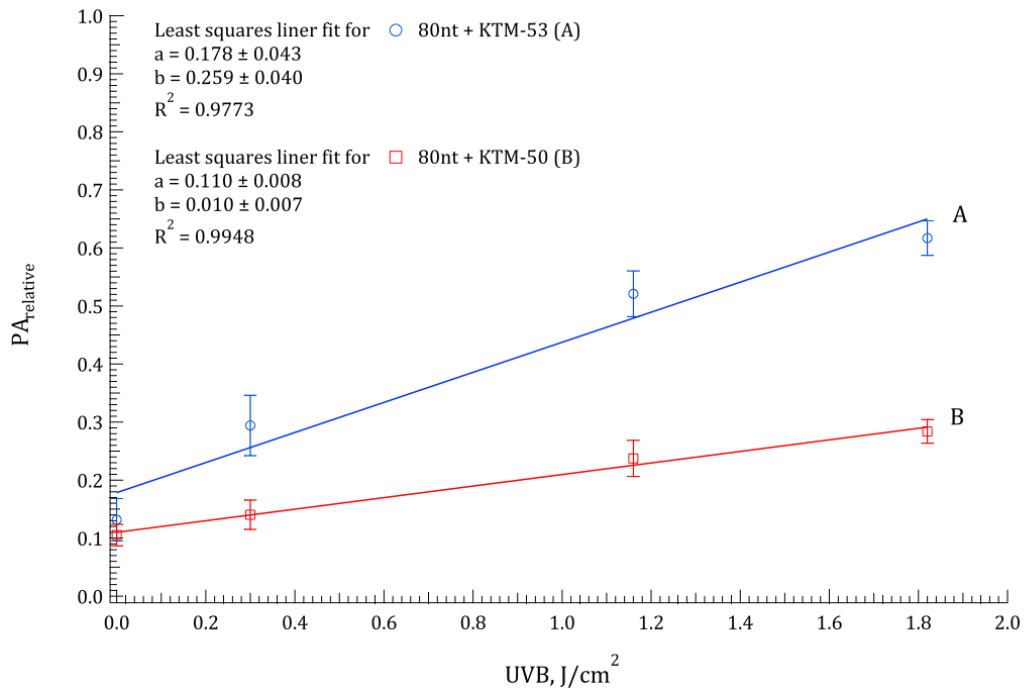
Figure 2.5. Linear range of the dose response for CPD (A) and 64PP (B) lesions formed in 80nt DNA library irradiated at low UVB doses

Each data point represents the mean value and the error bars represent ± standard deviation from a minimum of three independent experiments.

2.3.2. Detection of the CPD and 64PP lesions in UVC irradiated 80nt DNA library

UVC light is known to generate mainly CPDs rather than 64PPs in DNA samples [62-64]. The 80nt DNA library was irradiated at different UVC doses and the formation of both CPDs and 64PPs was monitored using CE-LIF immunoassay. Figure 2.6 shows example electropherograms obtained from these experiments.

The fluorescent intensity of the Ab*-DNA peak, representing the complex of the antibody with UV lesions in DNA, increases with increasing UVC radiation (Figure 2.6). Our UVC lamps have higher power than the UVB lamps. For the same duration of exposure, the doses of UVC were higher than the doses of UVB used in the previous experiments.

Figure 2.7 and Figure 2.8 show relative amounts of CPD and 64PP as a function of UVC doses. These results show an increase in the signal response at the lower doses (up to 10 J/cm^2) and then a decrease at doses > 30 J/cm^2. It is also noticeable that the decrease happened at the same UVC dose for the both the CPD and 64PP lesions. Thus most likely, the same process caused the decrease in the lesions at the higher UVC doses. UVC lamps have a small percentage of UVB spectrum. Thus it is unlikely that the decrease of 64PP is due to photochemical conversion into its Dewar isomers. Also, CPD does not undergo known non-enzymatic photochemical conversion.
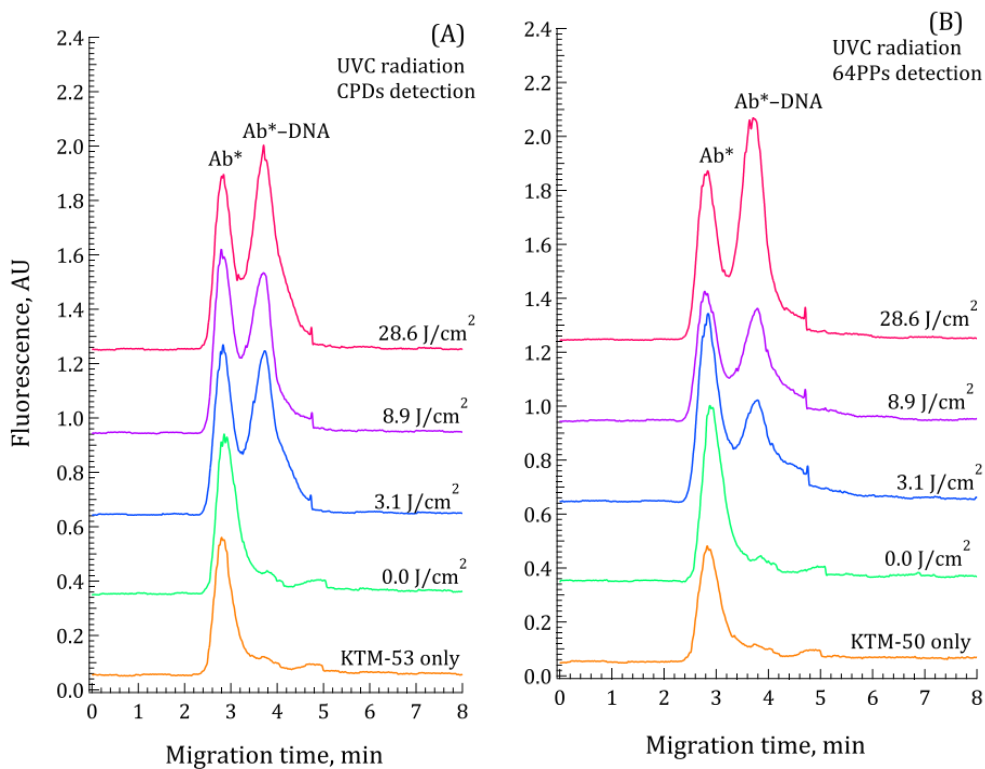
Figure 2.6. Electropherograms from CE-LIF immunoassay of CPD (A) and 64PP (B) in UVC-irradiated 80nt DNA library

The peak labeled Ab*-DNA represents the ternary complex between the DNA lesions (CPD or 64PP) and the antibody recognizing the specific lesion.

The peak denoted with Ab* represents the excess fluorescent secondary antibody fragment F_{ab} (*F_{ab}) and its complex (*F_{ab}-Ab) with the primary antibody.

It is well known that UV light produces UV lesions in DNA. In addition, UV light also causes in the formation of single and double strand breaks (SSB and DSB respectively) in DNA [73, 74]. In [73] it was shown that UVC light is ~4.2 and 5.7 times more effective than UVB light in the formation of SSB and DSB, respectively. In this research, plasmids were studied using AFM. Based on the DNA being relaxed or linear, the percentage of SSB (relaxed DNA) and DSB (linear DNA) was calculated. Half-relaxation and half-linearization for plasmids irradiated by UVB light occurred at 2.8 J/cm^2 and 38 J/cm^2 respectively. While half-relaxation and half-linearization of plasmids irradiated by UVC light occurred at 0.66 J/cm^2 and 6.7 J/cm^2 respectively.

We have observed the decrease in UV-response for UVC irradiated 80nt DNA library at doses > 20 J/cm^2 (Figure 2.7). Consistent with previous observations on the SSB and DSB formation [73. 74], our results on the lower CPD and 64PP formation after irradiation at UVC > 20 J/cm^2 could be partially due to the formation of strand breaks that could not be detected by this assay. Previous report [73] also observed that SSB and DSB induced by UV light are due to the formation of UV-induced free radicals, which means SSB and/or DSB do not necessarily happen at the UV damage site. The 80nt DNA is a fairly short molecule. Thus there is a higher probability of introducing SSB at sites where UV damage occurs.

Figure 2.8 shows the linear range of the response of formation of CPD and 64PP lesions *vs.* UVC dose. This linear range is later used to relate $PA_{relative}$ values to the number of UV lesions in DNA.
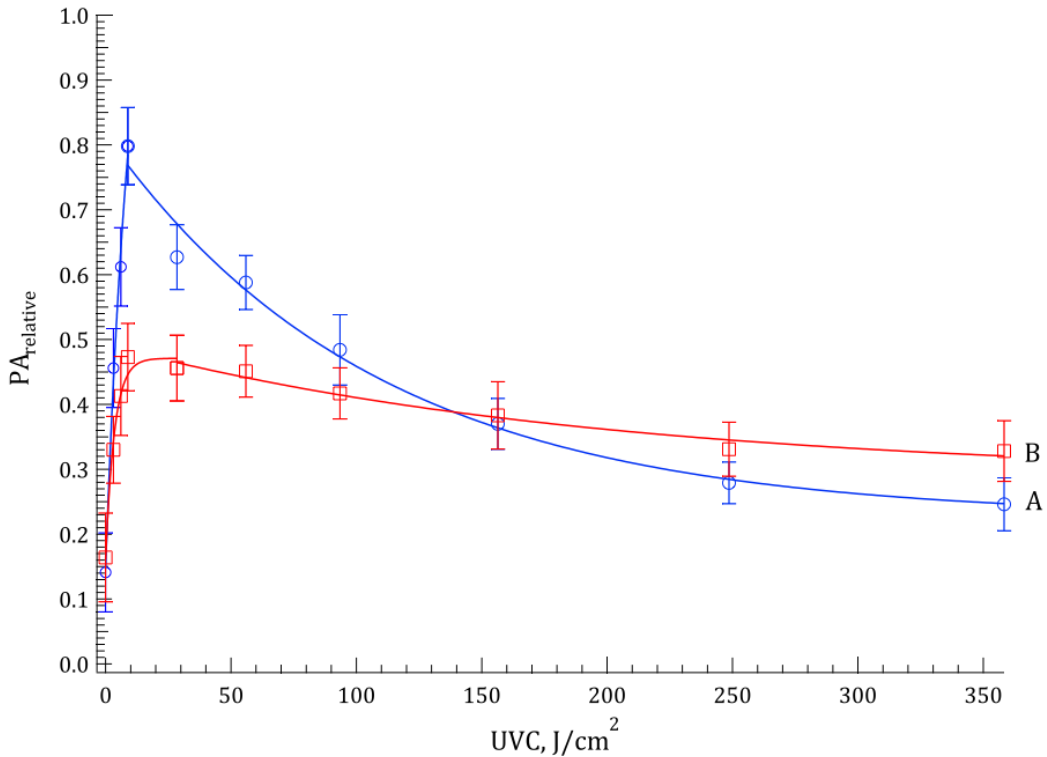
Figure 2.7. Dose response for CPD (A) and 64PP (B) lesions formed in UVC-irradiated 80nt DNA library irradiated with a wide range of UVC doses

Each data point represents the mean value and the error bars represent ± standard deviation from a minimum of three independent experiments.

Note: the lines connecting data points serve to show trends. The lines were not generated from any data-fitting program.
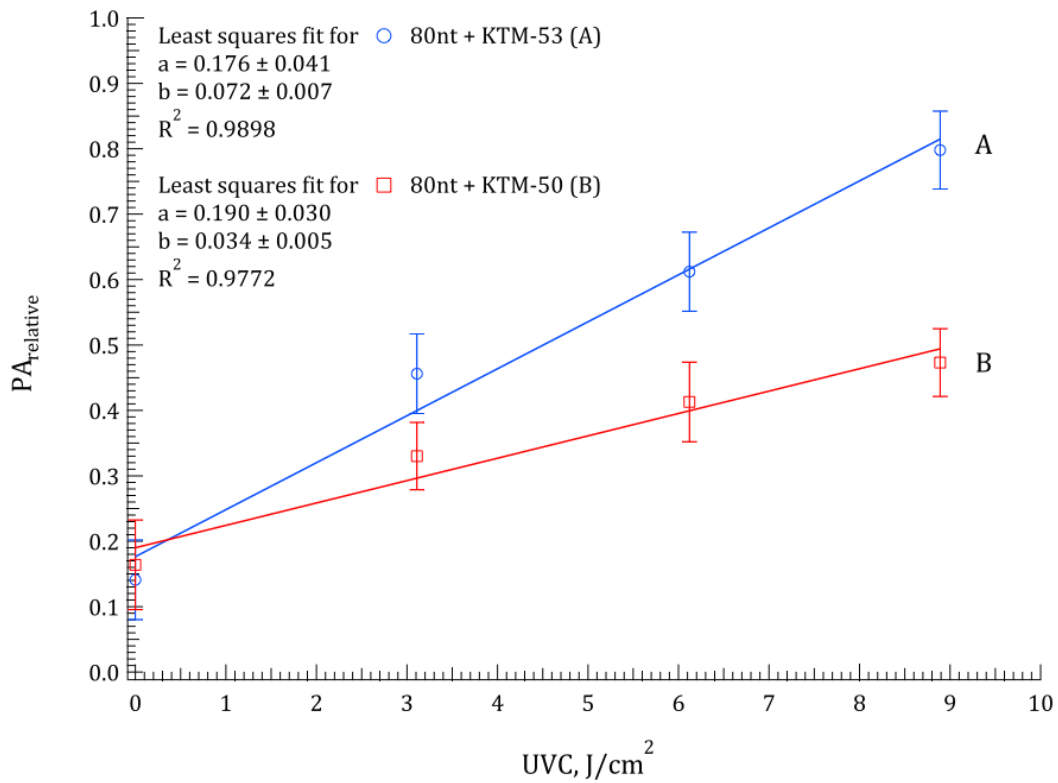
Figure 2.8. Linear range of the dose response for CPD (A) and 64PP (B) lesions formed in 80nt DNA library irradiated at low UVC doses

Each data point represents the mean value and the error bars represent ± standard deviation from a minimum of three independent experiments.

2.3.3. Detection of the CPD and 64PP lesions in UVB irradiated isolated CT- and HP-DNA

The isolated single-stranded human placenta DNA (HP-DNA) is a mixture of 530 – 830 nucleotides long molecules and the isolated single-stranded calf-thymus DNA (CT-DNA) is 50,000 nucleotides, which is the closest to extracted cellular DNA in length. These DNA samples represent examples of different sizes of DNA for the purpose of assay development.

Figure 2.9 shows electropherograms from the CE-LIF immunoassay for CPD lesions in UV irradiated HP-DNA and CT-DNA samples. The free zone electrophoresis resulted in separation of the Ab*-DNA complex from the excess Ab*. The resolution (R_S) between these two major species are 0.96 ± 0.10 for HP-DNA and R_s 1.11 ± 0.10 for CT-DNA. From electropherograms we see that increase in the UVB dose results in increase of the Ab*-DNA complex peak.
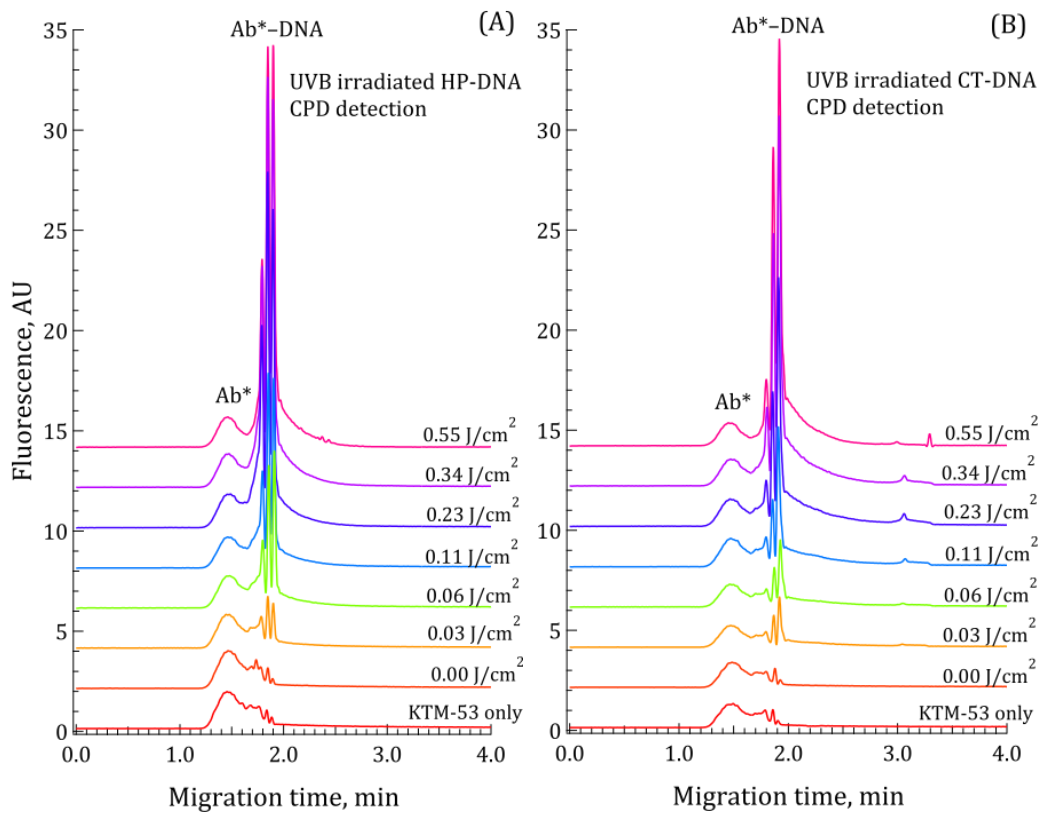
Figure 2.9. Electropherograms from the CE-LIF immunoassay of CPD in UVB irradiated HP-DNA (A) and CT-DNA (B) using fluorescently labeled KTM-53 (anti-CPD) antibody

Ab*: signal due to fluorescently labeled antibodies.

Ab*-DNA: signal due to the complex between the antibodies and the DNA containing CPD lesions.

As seen from the electropherograms in Figure 2.9, the signal due to the complex Ab*-DNA consists of multiple peaks. This is not surprising knowing that HP-DNA and CT-DNA samples contain DNA molecules of different lengths. The multiple peaks represent complexes formed between antibody and DNA molecules of different lengths. In order to analyze the signal we used the integration procedure to calculate the total peak area (area under all peaks) and then we used the Gaussian fit procedure to deconvolute the antibody peak. Thus, the peak area due to the complex is the difference between the total peak area and the peak area for Ab* (Appendix C). All integrations were done using the procedures in the IgorPro software (version 6.0).

Figure 2.10 shows the dose response curves as relative peak area (PA$_{relative}$) for the CPD lesions formed in HP-DNA and CT-DNA after UVB irradiation. As illustrated in Figure 2.11, there is a linear range between 0.0 and 0.1 J/cm^2. This linear range is later used to calculate the yield of CPD formation.
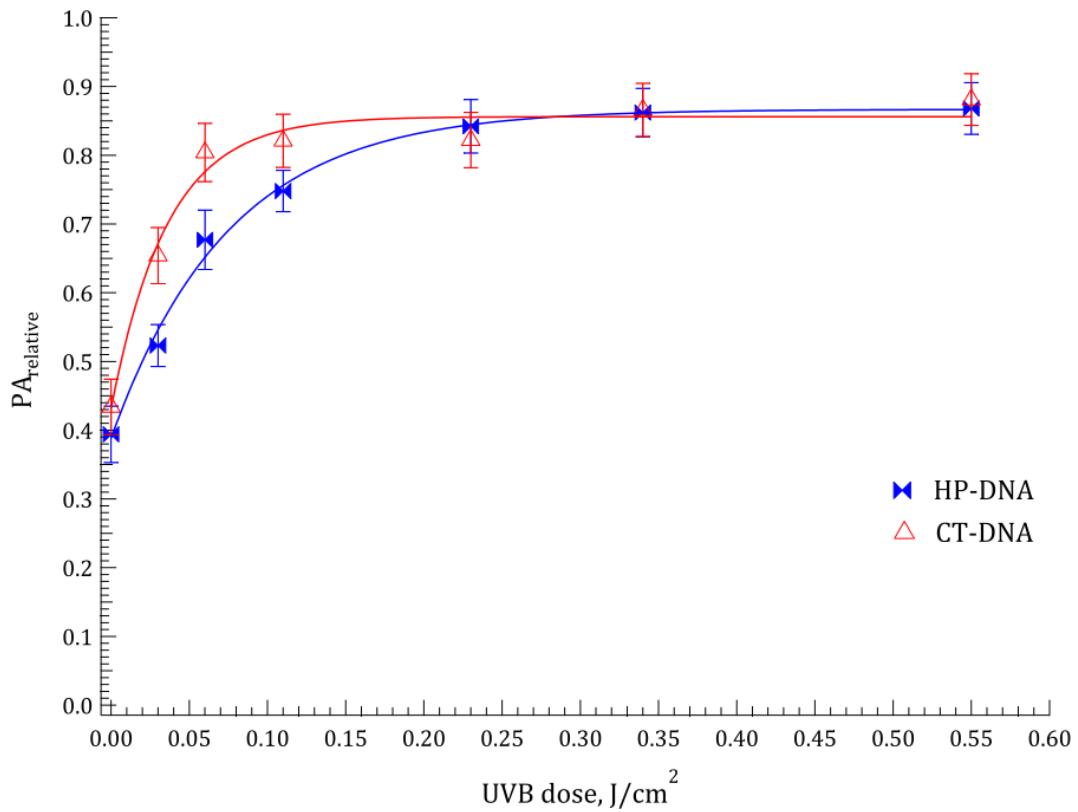
Figure 2.10. Dose response for CPD lesions formed in CT-DNA and HP-DNA after UVB radiation

Each data point represents the mean value and the error bars represent ± standard deviation from a minimum of three independent experiments.

Note: the lines connecting data points serve to show trends. The lines were not generated from any data-fitting program.
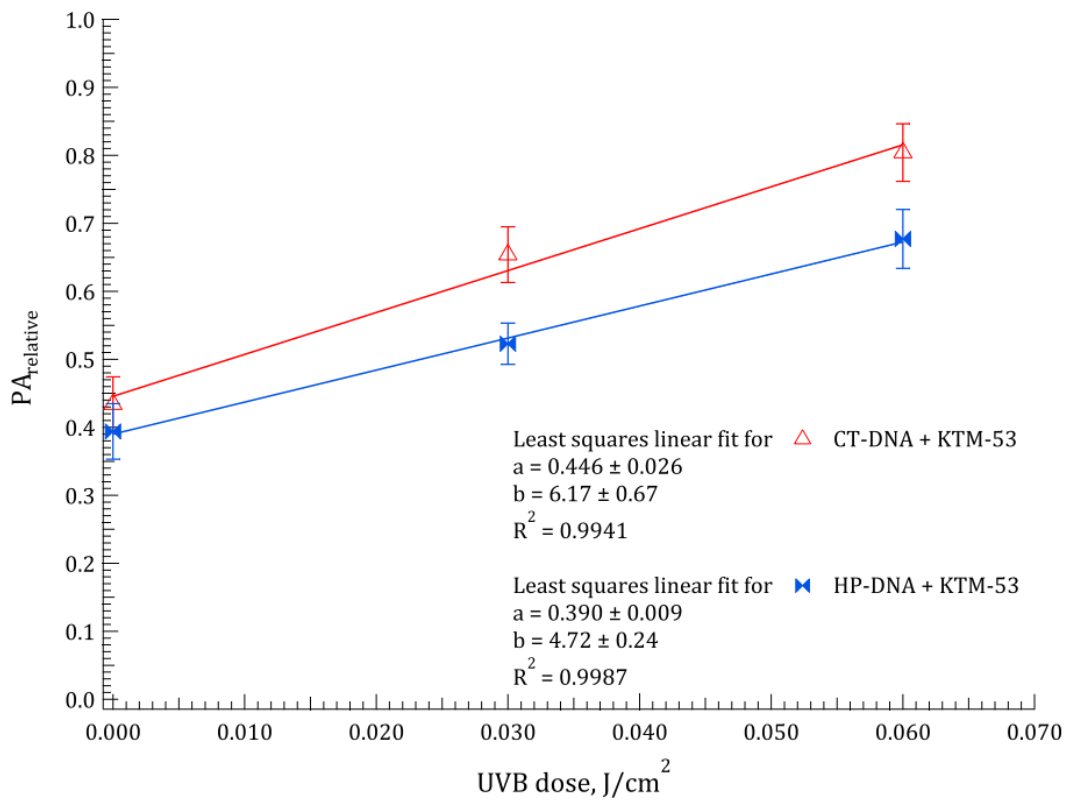
Figure 2.11. Linear dose response range for CPD lesions formed in CT-DNA and HP-DNA after UVB radiation

Each data point represents the mean value and the error bars represent ± standard deviation from a minimum of three independent experiments.

The 64PP lesions were also detected in UVB irradiated HP-DNA and CT-DNA samples. Figure 2.12 shows the electropherograms from the CE-LIF analyses of 64PP in HP-DNA and CT-DNA. Both electropherograms from the analyses of the control DNA (DNA not irradiated with UVB) showed the presence of the Ab*-DNA complex. There are several possible reasons for this: (i) KTM-50 antibody has some non-specific binding; and (ii) background 64PP lesions were already present in the DNA. The background DNA lesions could be introduced during the extraction and purification of DNA.

In experiments with cells, the analysis of the control cellular DNA also resulted in a high signal due to the Ab*-DNA complex (Chapter 4). The UV dose present in laboratory rooms was minimum for both UVB and UVC light. The only time when the control DNA samples were exposed to UV light was during the measurements of DNA concentrations by absorption when the incident light was at 260 nm. This exposure would not be significant because we did not see a very high background from the control 80nt DNA library samples (Figure 2.3).

Even though monoclonal antibodies have specific binding to certain damage this does not mean they cannot bind to other antigens. Thus it is possible that KTM-50 cross-reacts with other compounds present in the extracted DNA. As a result non-specific ternary complex is detected by the CE-LIF. This is probably a reason for the high background from the control DNA samples.
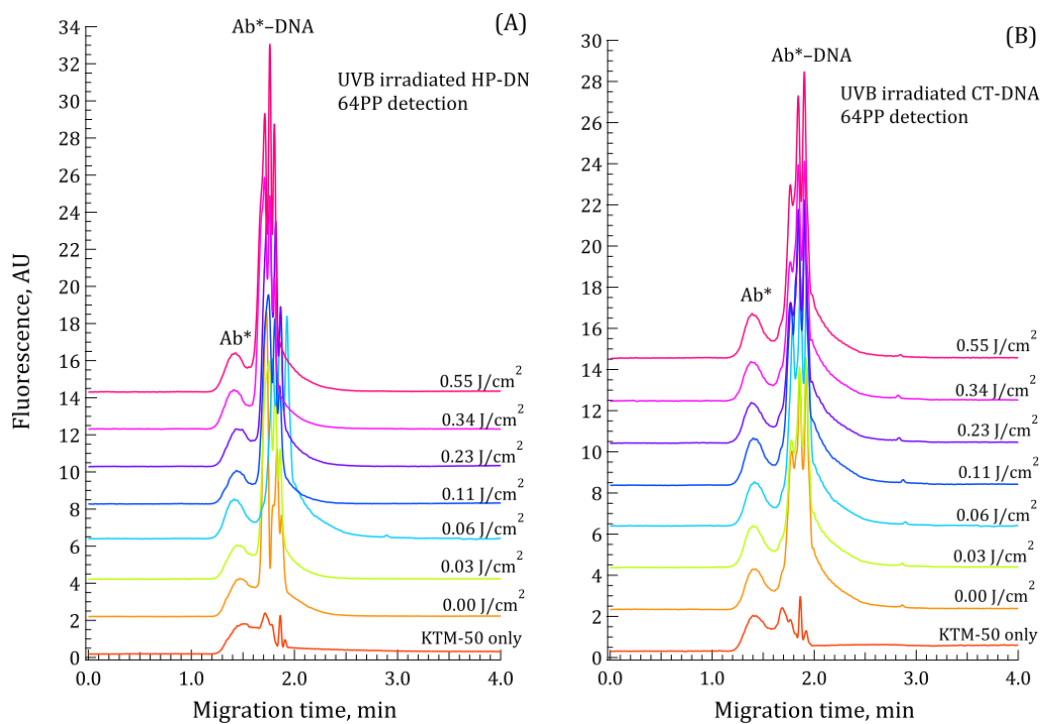
Figure 2.12. Electropherograms from the CE-LIF immunoassay of 64PP in UVB-irradiated HP-DNA (A) and CT-DNA (B) using fluorescently labeled KTM-50 (anti-64PP) antibody

Ab*: signal due to fluorescently labeled antibodies.

Ab*-DNA: signal due to the complex between the antibodies and the DNA containing 64PP lesions.

The reasons why the amount of 64PP was unchanged with increased UV dose (Figure 2.13) are not clear. Possibilities include the insufficient amount of monoclonal antibodies present in the sample. Several attempts were made to reduce the high background for 64PPs. One of these attempts was the use of a different antibody for 64PP lesions.
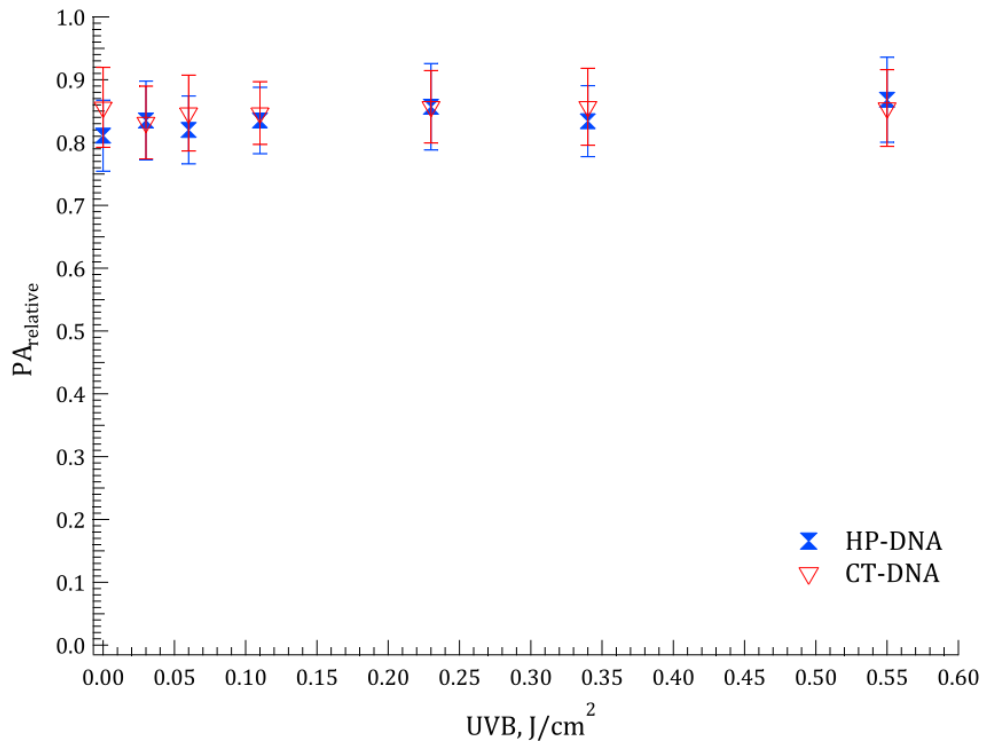
Figure 2.13. Dose response of 64PP lesions formed in HP-DNA and CT-DNA after UVB radiation (KTM-50 antibody used)

Each data point represents the mean value and the error bars represent ± standard deviation from a minimum of three independent experiments.

2.3.4. Comparison of different antibodies used for the detection of 64PP lesions in DNA samples

A different clone of a monoclonal anti-64PP antibody (C3B6, Trevigen®) was used to detect 64PP lesions in the HP-DNA and CT-DNA samples. Figure 2.14 shows electropherograms from the CE-LIF immunoassay of 64PP in HP-DNA and CT-DNA using the C3B6 antibody. Figure 2.15 shows the relative peak area as a function of the UVB dose. These results show that the high background remains in the control DNA samples.

These results support the possibility of non-specific binding of the two anti-64PP antibodies to DNA and/or other matrix in the samples. There was no other specific antibody against 64PP available at that time. Therefore, the subsequent experiments were focused on the determination of CPD lesions in DNA samples. The detection of 64PP was shown for the purpose of comparison and for depicting remaining challenges.

Note: after completing the work described in this chapter another monoclonal anti-64PP antibody became available (64M2 clone, Cosmo Bio Co. Ltd). However use of this antibody to detect 64PP lesions in cellular DNA did not show any improvement in the background signal for the control samples.
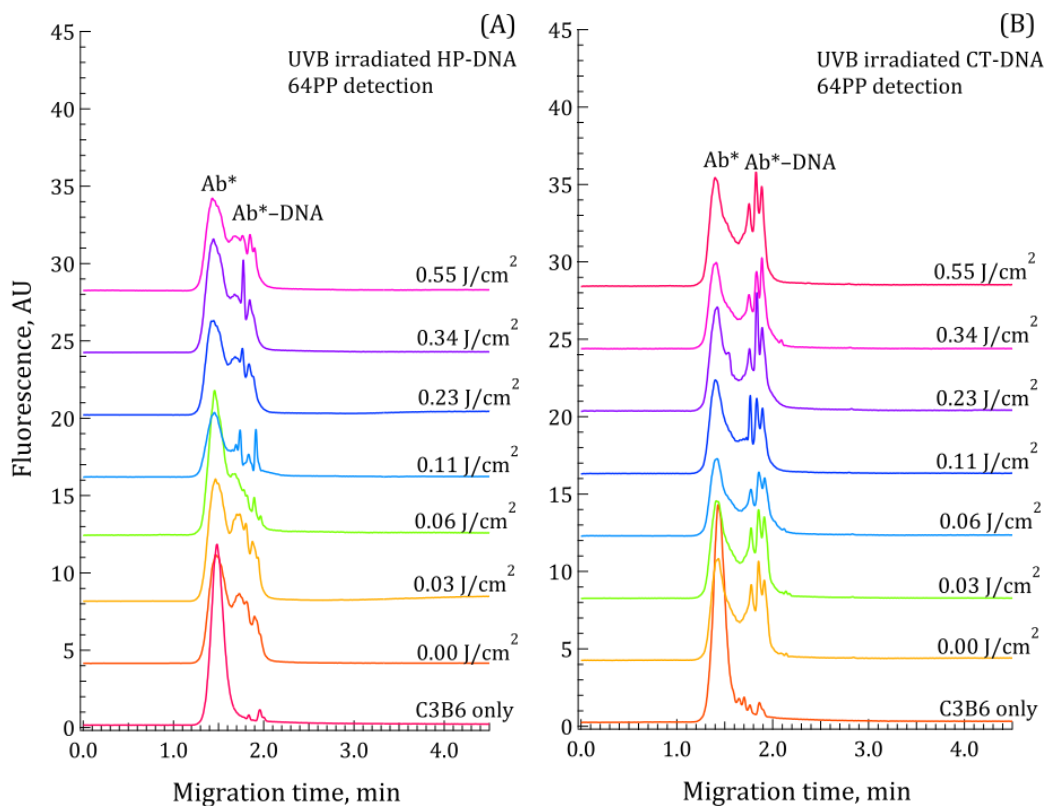
Figure 2.14. Electropherograms from CE-LIF immunoassay of 64PP in UVB-irradiated HP-DNA (A) and CT-DNA (B) using fluorescently labeled C3B6 (anti-64PP) antibody

Ab*: signal due to fluorescently labeled antibodies.

Ab*-DNA: signal due to the complex between the antibodies and the DNA containing 64PP lesions.
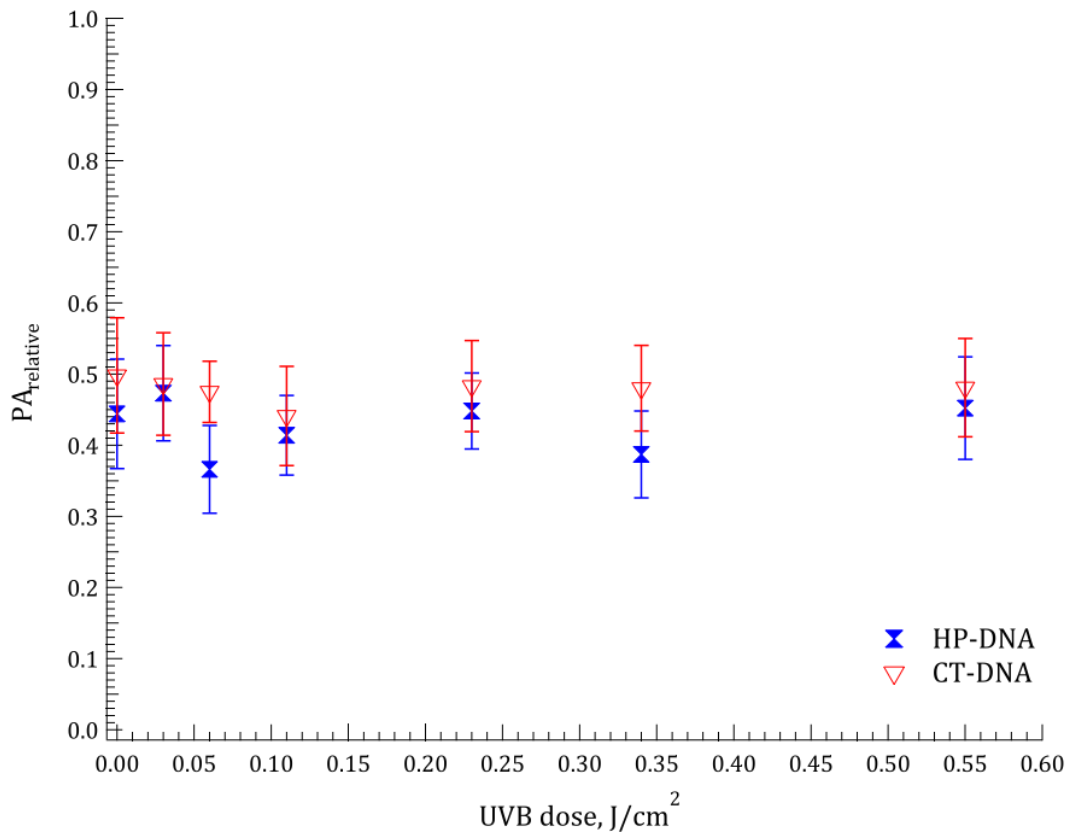
Figure 2.15. Dose response of 64PP lesions formed in HP-DNA and CT-DNA after UVB radiation (C3B6 antibody used)

Each data point represents the mean value and the error bars represent ± standard deviation from a minimum of three independent experiments.

2.4. Conclusions

The immunoassay combining capillary electrophoresis and laser induced fluorescence (CE-LIF) is able to detect CPD lesions in short oligonucleotides (80nt DNA library), isolated single-stranded human placenta DNA (530 – 830 basses long) and single-stranded calf-thymus DNA (~50,000 bases long) that are irradiated with varying doses of UVB and UVC. Another major UV-induced lesion, 64PP can be detected in UVB or UVC irradiated oligonucleotides (80nt DNA library). But detection of 64PP lesions in HP-DNA and CT-DNA was hampered by high background signals from the DNA samples.

At UVB doses greater than 5 J/cm^2 the amount of 64PPs lesions decreased significantly, which is most likely due to the photochemical conversion of 64PPs into their Dewar isomers. No decrease in CPD lesions was detected at the equivalent UVB doses. A decrease in UV photoproducts was noticeable in UVC irradiated 80nt DNA library at UVC doses > 25 J/cm^2. The decrease in both UV lesions was probably due to the UV–induced single strand breaks.

The CE-LIF immunoassay described in this chapter has shown promise for the detection of trace amounts of CPD lesions caused by UVB and UVC radiation. The subsequent research will extend to quantitation and application to the analysis of cellular DNA.

2.5. References

1. J.W. Jorgenson and K.D. Lukacs (1982), Zone electrophoresis in open-tubular glass capillaries, Anal. Chem., *53*, 1298-1302.

2. J.W. Jorgenson and K.D. Lukacs (1983), Capillary zone electrophoresis, Science, *222*, 266-272.

3. S. Terabe, K. Otsuka, K. Ichikawa, A. Tsuchiya and T. Ando (1984), Electrokinetic separations with micellar solutions and open-tubular capillaries, Anal. Chem., *56,* 111-113.

4. S. Terabe (1989), Electrokinetic chromatography: an interface between electrophoresis and chromatography, Trends Anal. Chem., *8*, 129-134.

5. Camilleri, P. Ed. *Capillary electrophoresis, theory and practice.* CRC Press: Boca Raton. 1998.

6. Landers, J.P. Ed. *Handbook of capillary electrophoresis.* CRC Press: Boca Raton. 1997.

7. Y.F. Cheng and N.J. Dovichi (1988), Subattomole amino acid analysis by capillary zone electrophoresis and laser-induced fluorescence, Science, *242*, 562-564.

8. B.B. Haab and R.A. Mathies (1995), Single molecule fluorescence burst detection of DNA fragments separated by capillary electrophoresis, Anal. Chem., *67*, 3253-3260.

9. S. Nie, D.T. Chiu, R.N. Zare (1994), Probing individual molecules with confocal fluorescence microscopy, Science, *266,* 1018-1021.

10. D.Y. Chen and N.J. Dovichi (1996), Single-molecule detection in capillary electrophoresis: molecular shot noise as a fundamental limit to chemical analysis, Anal. Chem., *68*, 690-696.

11. R.A. Keller, W.P. Ambrose, A.A. Arias, H. Cai, S.R. Emory, P.M. Goodwin and J.H. Jett (2002), Analytical applications of single-molecule detection, Anal. Chem., *74*, 316A-324A.

12. A.R. Eder, J.S. Chen and E.A. Arriaga (2006), Separation of doxorubicin and doxorubicinol by cyclodextrin-modified micellar electrokinetic capillary chromatography, Electrophoresis, *27*, 3263-3270.

13. R.K. Mosing, S.D. Mendonsa and M.T. Bowser (2005), Capillary electrophoresis-SELEX selection of aptamers with affinity for HIV-1 reverse transcriptase, Anal. Chem., *77*, 6107-6112.

14. S.D. Mendonsa and M.T. Bowser (2005), In vitro selection of aptamers with affinity for neuropeptide Y using capillary electrophoresis, J. Am. Chem. Soc., *127*, 9382-9383.

15. J.M.A. Gavina, R. Das and P. Britz-McKibbin (2006), Dynamic unfolding of a regulatory subunit of cAMP-dependent protein kinase by capillary electrophoresis: Impact of cAMP dissociation on protein stability, Electrophoresis, *27*, 4196-4204.

16. G. Seguí-Lines, J.M.A. Gavina, J.C. D'Amaral and P. Britz-McKibbin (2007), High-throughput screening of holoprotein conformational stability by dynamic ligand exchange-affinity capillary electrophoresis, Analyst, *132*, 741-744.

17. C. Galbusera, M. Thachuk, E. De Lorenzi and D.D.Y. Chen (2002), Affinity capillary electrophoresis using a low-concentration additive with the consideration of relative mobilities, Anal. Chem., *74,* 1903-1914.

18. N. Fang and D.D.Y. Chen (2006), Behavior of interacting species in capillary electrophoresis described by mass transfer equation, Anal. Chem., *78*, 1832-1840.

19. S.B. Cheng, C.D. Skinner, J. Taylor, S. Attiya, W.E. Lee, G. Picelli and D.J. Harrison, Anal. Chem., *73*, 1472-1479.

20. S. Attiya, T. Dickinson-Laing, J. Cesarz, R.D. Giese, W.E. Lee, D. Mah and D.J. Harrison (2002), Affinity protection chromatography for efficient labeling of antibodies for use in affinity capillary electrophoresis, Electrophoresis, *23*, 750-758.

21. N.H.H. Heegaard, S. Nilsson and N.A. Guzman (1998), Affinity capillary electrophoresis: important application areas and some recent developments, J. Chromatogr. B, *715*, 29-54.

22. N.H.H. Heegaard, P. Roepstorff, S.G. Melberg and M.H. Nissen (2002) Cleaved β_2-microglobulin partially attains a conformation that has amyloidogenic features, J. Biol. Chem., *277*, 11184-11189.

23. C. Schou and N.H.H. Heegaard (2006), Recent applications of affinity interactions in capillary electrophoresis, Electrophoresis, *27*, 44-59.

24. K. Shimura and B.L. Karger (1994), Affinity probe capillary electrophoresis: analysis of recombinant human growth hormone with a fluorescent labeled antibody fragment, Anal. Chem., *66*, 9-15.

25. F.T. Hafner, R.A. Kautz, B.L. Iverson, R.C. Tim and B.L. Karger (2000), Noncompetitive immunoassay of small analytes at the femtomolar level by affinity probe capillary electrophoresis: direct analysis of digoxin using a uniform-labeled scFv immunoreagent, Anal. Chem., *72*, 5779-5786.

26. N.M. Schultz and R.T. Kennedy (1993), Rapid immunoassays using capillary electrophoresis with fluorescence detection, Anal. Chem., *65*, 3161-3165.

27. L. Tao and R.T. Kennedy (1996), On-line competitive immunoassay for insulin based on capillary electrophoresis with laser-induced fluorescence detection, Anal. Chem., *68,* 3899-3906.

28. Q. Deng, I. German, D. Buchanan and R.T. Kennedy (2001), Retention and separation of adenosine and analogues by affinity chromatography with an aptamer stationary phase, Anal. Chem., *73*, 5415-5421.

29. P. Yang, R.J. Whelan, Y. Mao, A. W.-M. Lee, C. Carter-Su and R.T. Kennedy (2007), Multiplexed detection of protein-peptide interaction and inhibition using capillary electrophoresis, Anal. Chem., *79*, 1690-1695.

30. A. El-Shafey, H. Zhong, G, Jones and I.S. Krull (2002), Application of affinity capillary electrophoresis for the determination of binding and thermodynamic constants of enediynes with bovine serum albumin, Electrophoresis, *23*, 945-950.

31. A. Chan and U.J. Krull (2006), Capillary electrophoresis for capture and concentrating of target nucleic acids by affinity gels modified to contain single-stranded nucleic acid probes, Anal. Chim. Acta, *578*, 31-42.

32. M. Berezovski, A. Drabovich, S.M. Krylova, M. Musheev, V. Okhonin, A. Petrov and S.N. Krylov (2005), Nonequilibrium capillary electrophoresis of equilibrium mixtures: A universal tool for development of aptamers, J. Am. Chem. Soc., *127,* 3165-3171.

33. A.P. Drabovich, V. Okhonin, M. Berezovski and S.N. Krylov (2007), Smart aptamers facilitate multi-probe affinity analysis of proteins with ultra-wide dynamic range of measured concentrations, J. Am. Chem. Soc., *129*, 7260-7261.

34. Q.-H. Wan and X.C. Le (1999) Fluorescence polarization studies of affinity interactions in capillary electrophoresis, Anal. Chem*., 71*, 4183-4189.

35. Q.-H. Wan and X.C. Le (2000), Studies of protein-DNA interactions by capillary electrophoresis laser induced fluorescence polarization, Anal. Chem*., 72*, 5583-5589.

36. V. Pavski and X.C. Le (2001), Detection of human immunodeficiency virus type 1 reverse transcriptase using aptamers as probes in affinity capillary electrophoresis, Anal. Chem., *73,* 6070-6076.

37. V. Pavski and X.C. Le (2003) Ultrasensitive protein-DNA binding assays, Curr. Opin. Biotechnol., *14*, 65-73.

38. X.C. Le, V. Pavski and H. Wang (2005), Affinity recognition, capillary electrophoresis and laser induced fluorescence polarization for ultrasensitive bioanalysis, Can. J. Chem., *83*, 185-194.

39. R.B. Kotia, L. Li and L.B. McGown (2000), Separation of nontarget compounds by DNA aptamers, Anal. Chem., *72,* 827-831.

40. J.R. Cole, L.W. Dick Jr., E.J. Morgan and L.B. McGown (2007), Affinity capture and detection of immunoglobulin E in human serum using an aptamer-modified surface in matrix-assisted laser desorption/ionization mass spectrometry, Anal. Chem., *79,* 273-279.

41. M. Hong, H. Soini and M.V. Novotny (2000), Affinity capillary electrophoretic studies of complexation between dextrin oligomers and polyiodides, Electrophoresis, *21*, 1513-1520.

42. T. Bo and J. Pawliszyn (2006), Characterization of phospholipid-protein interactions by capillary isoelectric focusing with whole-column imaging detection, Anal. Biochem., *350*, 91-98.

43. Z. Liu, A.P. Drabovich, S.N. Krylov and J. Pawliszyn (2007), Dynamic kinetic capillary isoelectric focusing: A powerful tool for studying protein-DNA interactions, Anal. Chem., *79*, 1097-1100.

44. M. De Frutos, S.K. Paliwal and F.E. Regnier (1996), Analytical immunology, Methods Enzymol., *270*, 82-101.

45. H. Mirzaei and F. Regnier (2005), Affinity chromatographic selection of carbohydrated proteins followed by identification of oxidation sites using tandem mass spectrometry, Anal. Chem., *77*, 2386-2392.

46. Y.-H. Chu, L.Z. Avila, J. Gao and G.M. Whitesides (1995), Affinity Capillary Electrophoresis, Acc. Chem. Res., *28*, 461-468.

47. J. Rao, J. Lahiri, L. Isaacs, R.M. Weis and G.M. Whitesides (1998), A trivalent system from vancomycin·D-ala-D-ala with higher affinity than avidin·biotin, Science*, 280*, 708-711.

48. H. Wang, J. Xing, W. Tan, M. Lam, T. Carnelley, M. Weinfeld and X.C. Le (2002), Binding stoichiometry of DNA adducts with antibody studied by capillary electrophoresis and laser-induced fluorescence, Anal. Chem.**, *74*, 3714-3719.

49. H. Wang, M. Lu, M. Weinfeld and X.C. Le (2003), Enhancement of immunocomplex detection and application to assays for DNA adduct of benzo[a]pyrene, Anal. Chem., *75*, 247-254.

50. H. Wang, M. Lu and X.C. Le (2005) DNA-driven focusing for protein-DNA binding assays using capillary electrophoresis, Anal. Chem.*, 77,* 4985-4990.

51. X.C. Le, J.Z. Xing, J. Lee, S.A. Leadon and M. Weinfeld (1998), Inducible repair of thymine glycol detected by an ultrasensitive assay for DNA damage, Science, *280*, 1066-1069.

52. J.Z. Xing, T. Carnelley, J. Lee, W.P. Watson, E. Booth, M. Weinfeld and X.C. Le (2000), Assay for DNA damage using immunochemical recognition and capillary electrophoresis. In Mitchelson KR, Cheng J, eds. Capillary electrophoresis of nucleic acids, vol. 1: Introduction to the capillary electrophoresis of nucleic acids. Methods in Molecular Biology, *162*, Humana Press, NY, 419-428.

53. W.G. Tan, T.J. Carnelley, P. Murphy, H. Wang, J. Lee, S. Barker, M. Weinfeld and X.C. Le (2001), Detection of DNA adducts of benzo[a]pyrene using immunoelectrophoresis with laser-induced fluorescence analysis of A549 cells, J. Chromatogr. A, *924*, 377-386.

54. H.L. Wang, M.L. Lu, J. Lee, M. Weinfeld and X.C. Le (2003), Immunoassay using capillary electrophoresis laser induced fluorescence for DNA adducts. Anal Chim Acta, *500*, 13-20.

55. T.J. Carnelley, S. Barker, H. Wang, W.G. Tan, M. Weinfeld and X.C. Le (2001), Synthesis, characterization and application of a fluorescent probe of DNA damage, Chem. Res. Toxicol., *14*, 1513-1522.

56. Information and protocol was last accessed on November 26, 2010
www.invitrogen.com

57. Information and protocol was last accessed on November 26, 2010
www.promega.com

58. Information and protocol was last accessed on November 26, 2010
www.amershambiosciences.com

59. Zenon® Alexa Fluor® labeling kit protocol, Molecular Probes, 2007.

60. I.D. Podmore, M.S. Cooke, K.E. Herbert and J. Lunec (1996), Quantitative determination of cyclobutane thymine dimers in DNA by stable isotope-dilution mass spectrometry, Photochem. Photobiol., *64*, 310-315.

61. T. Douki, M. Court, S. Sauvaigo, F. Odin and J. Cadet (2000), Formation of the main UV-induced thymine dimeric lesions within isolated and cellular DNA as measured by high performance liquid chromatography-tandem mass spectrometry, J. Biol. Chem, *275*, 11678-11685.

62. T. Douki, T. Zalizniak and J. Cadet (1997), Far-UV-Induced dimeric photoproducts in short oligonucleotides: sequence effects, Photochem. Photobiol., *66*, 171-179.

63. D.L. Mitchell (1988), The relative cytotoxicity of (6-4) photoproducts and cyclobutane dimers in mammalian cells, Photochem. Photobiol., *48*, 51-57.

64. T. Douki and J. Cadet (1992), Far-UV photochemistry and photosensitization of 2'-deoxycytidylyl-(3'-5')-thymidine: isolation and characterization of the main photoproducts, J. Photochem. Photobiol. B: Biol., *15*, 199-213.

65. J. Moan and M.J. Peak (1989), Effects of UV radiation on cells, J. Photochem. Photobiol. B: Biol., *4*, 21-34.

66. G.L. Chan, M.J. Peak, J.G. Peak and W.A. Haseltine (1986), Action spectrum for the formation of endonuclease sensitive sites and (6-4) photoproducts induced in a DNA fragment by ultraviolet radiation, Int. J. Radiat. Biol., *50*, 640-648.

67. M.J. Peak, J.G. Peak and B.A. Carnes (1987), Induction of direct and indirect single-strand breaks in human call DNA by far- and near-ultraviolet radiations: Action spectrum and mechanics, Photochem. Photobiol., *45*, 381-387.

68. H.C. Enninga, R.T.L. Groenendijk, A.R. Filon, A.A. van Zelland and J.W.I.M. Simons (1986), The wavelength dependence of UV-induced pyrimidine dimer formation, cell killing and mutation induction in human diploid skin fibroblasts, Carcinogenesis, *7*, 1829-1836.

69. M.H. Patrick (1977), Studies on thymine-derived UV photoproducts in DNA. I. Formation and biological role of pyrimidine adducts in DNA, Photochem. Photobiol., *25*, 357-372.

70. J.-S. Taylor and M.P. Cohrs (1987), DNA, light and Dewar pyrimidones: The structure and biological significance to TpT_3, J. Am. Chem. Soc. *109*, 2834-2835.

71. J.-S. Taylor, D.S. Garrett and M.P. Cohrs (1988), Solution-state structure of the Dewar photoproduct of thymidylyl-(3'→5')-thymidine, Biochemistry *27*, 7206-7215.

72. F. Gaecés and C.A. Dávila (1982), Alterations in DNA irradiated with ultraviolet radiation-I. The formation process of cyclobutylpyrimidine dimers : cross sections, action spectra and quantum yields, Photochem. Photobiol., *35*, 9-16.

73. Y. Jiang, C. Ke, P.A. Mieczkowski and P.E. Marszalek (2007), Detecting ultraviolet damage in single DNA Molecules by atomic force microscopy, Biophysical Journal, *93*, 1758-1767.

74. M.H. Lankinen, L.M. Vilpo and J.A. Vilpo (1996), UV- and γ-irradiation-induced DNA single-strand breaks and their repair in human blood granulocytes and lymphocytes, Mutat. Res., *352*, 31-38.

75. C.L.A. Hamula, H. Zhang, L.L. Guan, X.-F. Li and X.C. Le (2008), Selection of aptamers against live bacterial cells, Anal. Chem., *80*, 7812-7819.

Chapter Three

Calibration and quantification of UV lesions
in DNA samples

3.1. Introduction

Chapter 2 describes the development of a new CE-LIF immunoassay and its feasibility for the direct detection of UV-induced lesions. The method eliminates the need for excessive digestion of DNA, a common requirement of many other methods [1-7]. The CE-LIF immunoassay involves a simple incubation (typically 30 minutes) of the DNA sample with the antibodies, followed by the CE-LIF analysis of the incubation mixture.

The relative peak areas of the Ab*-DNA complex provided information on the relative amounts of DNA lesions in DNA samples. This information can be useful for a range of meaningful studies, e.g. comparing the relative amounts of DNA lesions between a control and the various treatments of DNA and/or cells. Such studies are indeed useful when assessing sensitivity of various cells to UV irradiation and studying DNA repair kinetics (removal of DNA damage over time). However, many other studies require the determination of the concentration of DNA lesions in a given sample. Therefore, there is a need to calibrate and quantify specific DNA lesions. The objective of this chapter is to develop a calibration method and to apply the calibration to the quantification of DNA lesions.

3.2. Experimental

3.2.1. Reagents

Tris-glycine buffer solutions (TG, 25 mM Tris and 192 mM Glycine) were prepared from 10× TG buffer (Bio-Rad Laboratories, Hercules, CA, USA) by diluting with 18.2 MΩ distilled deionized water (DDW) from a Milli-Q Gradient Water System (Millipore, Nepean, ON, Canada). The pH of TG buffer for incubation was adjusted to 7.5 and the pH of the TG buffer for CE separation was 8.3.

The single-stranded 16-nucleotide standards (16mer) containing a single CPD (CPD-16mer) or 64PP (64PP-16mer) lesion were synthesized by the Synthetic Organic Chemistry Core Lab (University of Texas Medical Branch, USA). The 16mer had the following sequence: 5'-CCCA**TT**ATGCATAACC-3'. Single UV lesion was introduced into the 16mer via photolysis (unfortunately, conditions of this reaction are not known). Products were purified using HPLC and characterized with MS. Results of the purification and characterization are shown in Appendix B. Purified and lyophilized products, shipped to our lab, were dissolved in 1 mL of DDW. The final concentration of oligonucleotides in the solutions was measured at 260 nm using a SmartSpec™ 3000 spectrometer (Bio-Rad Laboratories, Cambridge, MA). Smaller aliquots were stored in a -20°C freezer. All samples were kept in the dark to prevent possible photoreverse reactions [8-10].

Monoclonal mouse anti-thymine dimer antibody (clone KTM-53, IgG_1 type) and anti-(6-4) photoproducts antibody (clone KTM-50, IgG_1 type) were purchased from Kamiya Biomedical Company (Seattle, WA, USA). Goat anti-mouse F_{ab} fragment (*F_{ab}) supplied in a Zenon® Alexa Flour® 546 (λ_{ex} = 556 nm, λ_{em} = 573 nm) mouse IgG_1-labeling kit (Molecular Probes, Eugene, OR, USA) was used as a secondary antibody to fluorescently label KTM-53.

3.2.2. Detection of CPDs and 64PPs in 16mer standards

The non-competitive CE-LIF based immunoassay (described in Chapter 2) was used to detect CPD and 64PP lesions. The primary anti-CPD (KTM-53) and anti-64PP (KTM-50) antibodies were labeled (Ab*) using the Zenon® mouse IgG labeling kit which included fluorescently labeled goat F_{ab} fragment selective for the F_c portion of the mouse IgG_1. The fluorescent label conjugated to F_{ab} fragment is an Alexa Fluor® 546 dye.

After formation of the monoclonal antibody and *F_{ab} conjugates (Ab*), the "master mix" was added to DNA samples (e.g. 16mer) and solutions were incubated for 20 minutes at room temperature prior to the CE-LIF separation and detection. The incubation buffer was 1×TG buffer (25 mM Tris and 192 mM Glycine) at pH 7.5. Electrokinetic injection into the capillary (20 µm i.d., 30 – 32 cm long) was accomplished by applying an injection electric field of 500 V/cm for 5 s. Separation was carried out at room temperature with 1×TG running buffer, pH 8.3, at an electric field of 400 V/cm. The capillary was washed after every injection with 20 mM NaOH, DDW and 1×TG, pH 8.3, at

least 3 minutes for each wash step.

3.3. Results and Discussion

In order to calibrate the non-competitive CE-LIF immunoassay, the 16nt oligonucleotide standards (16mer) containing a single lesion (either CPD or 64PP) were custom synthesized. The designed sequence of the 16mer (5'-CCCA**TT**ATGCATAACC-3') allowed for the preferential formation of the UV lesions at the T-T bases. The formation of UV lesions at the C-C bases is minimum to none [1-2, 11]. The two standards were: CPD-16mer (5'-CCCA**T**◇**T**ATGCATAACC-3') and 64PP-16mer (5'-CCCA**T(64)T**ATGCATAACC-3'). Having one lesion per molecule allowed the calibration of the method based upon the fluorescent signal response *vs.* number of lesions present in the sample. As mentioned earlier (Chapter 2) the fluorescent signal obtained by LIF detection was analyzed as the relative peak area - which was calculated as the ratio of peak area of the complex signal over the total peak area of all fluorescent species.

Calibration curves of relative peak area *vs.* number of lesions per 10^3 nucleotides were plotted and later used to measure UV lesions in UV irradiated samples.

Prior to method calibration, the complex formation between monoclonal antibodies KTM-53 and KTM-50 with the 16mer standards was

studied. Figure 3.1 shows the electropherograms used to study the binding of KTM-53 antibody with 16mer standards and Figure 3.2 shows the electropherograms used to study the binding of KTM-50 antibody with 16mer standards.

Under the free zone CE separation conditions (pH 8.3) we use, the antibodies (*F_{ab}, Ab and Ab*) migrate first to the LIF detector at the cathode end. The binding of the 16mer oligonucleotides to the antibodies contributes negative charges and ~5 kDa mass to the complex. As a result, the complex formed by the antibody and DNA migrates at a slower mobility. Migration time of *F_{ab} labeled KTM-53 is around 1.9 minutes whereas the migration time of the complex formed between *F_{ab} labeled KTM-53 and the CPD-16mer is around 2.1 min. The small shift in migration time is due to the difference in charge-to-mass ratio between the antibody and the complex of antibody with CPD-16mer or 64PP-16mer.

To support the identification of the second peak as the complex, we varied the concentration of 16mer standards while keeping the concentration of antibody constant and analyzed these mixtures. As expected, the signal intensity of the second peak increases with the increase of the CPD-16mer concentrations (Figure 3.3).
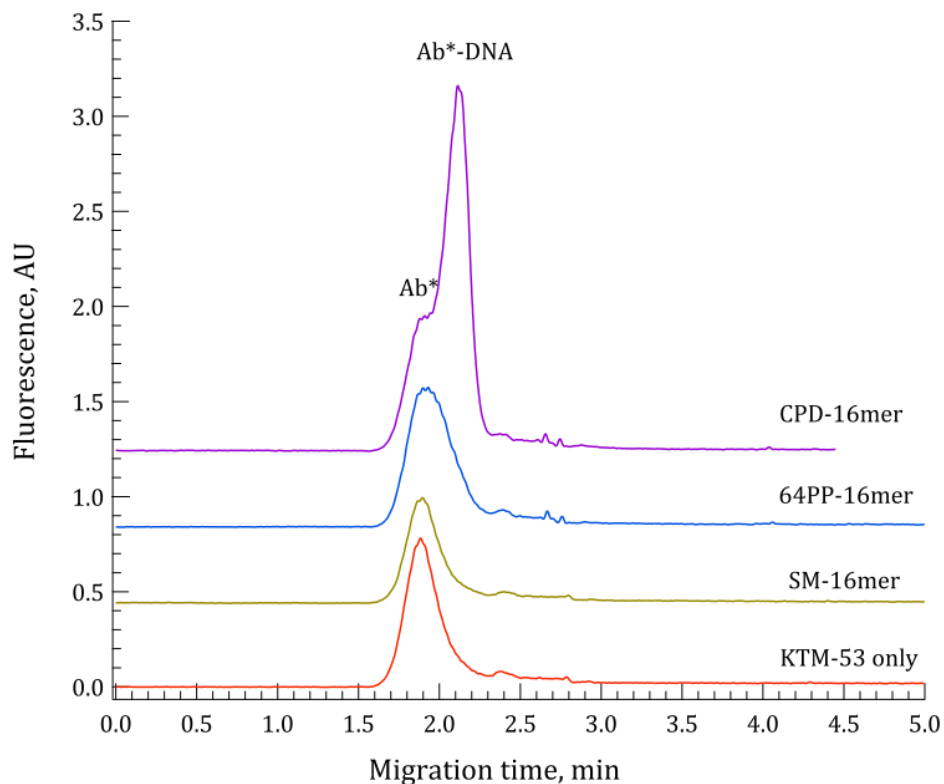
Figure 3.1. Electropherograms obtained from the CE-LIF analyses of incubation solutions containing antibody KTM-53 and the 16mer standards

Peak Ab* represents the unbound fluorescent $*F_{ab}$ and the complex of $*F_{ab}$ with KTM-53.

Peak Ab*-DNA represents complex formed between the antibodies and CPD lesions in the 16mer.

The four electropherograms from top to bottom represent the analysis of CPD-16mer standard, 64PP-16mer standard, the control 16mer (no UV lesion) and the blank (no oligonucleotide).

All the four incubation solutions contained the fluorescently labeled secondary antibody ($*F_{ab}$) and the primary antibody to CPD (monoclonal KTM-53).
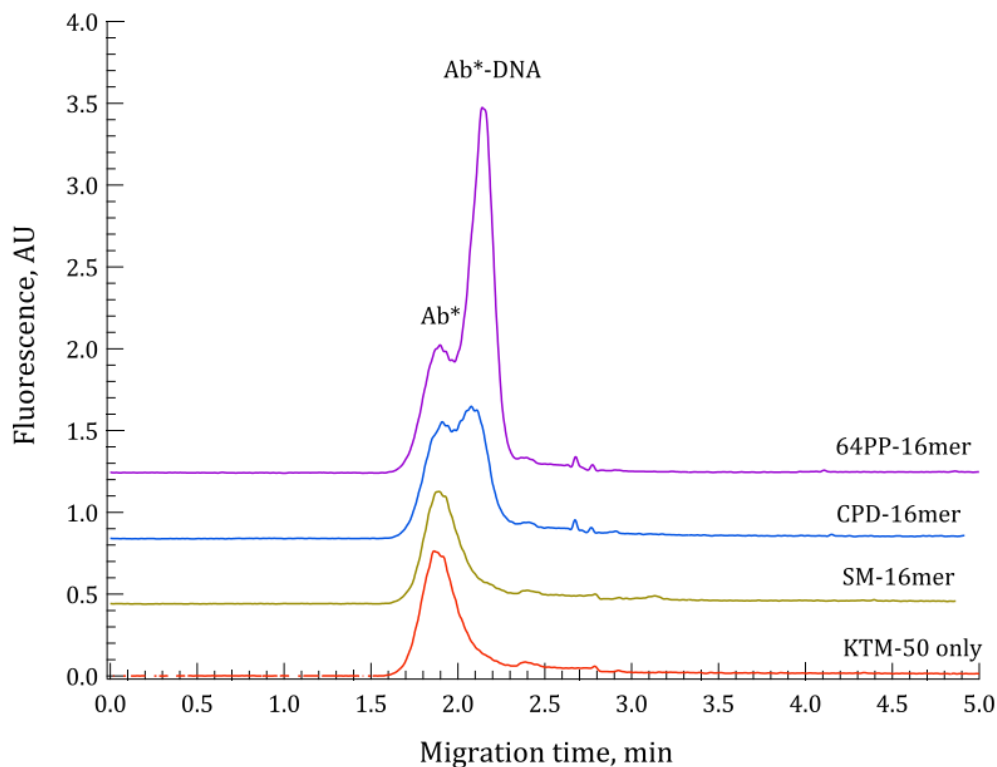
Figure 3.2. Electropherograms obtained from the CE-LIF analyses of incubation solutions containing antibody KTM-50 and the 16mer standards

Peak Ab* represents the unbound fluorescent $*F_{ab}$ and the complex of $*F_{ab}$ with KTM-50

Peak Ab*-DNA represents complex formed between the antibodies and 64PP lesions in the 16mer.

The four electropherograms from top to bottom represent the analysis of 64PP-16mer standard, CPD-16mer standard, the control 16mer (no UV lesion) and the blank (no oligonucleotide).

All the four incubation solutions contained the fluorescently labeled secondary antibody ($*F_{ab}$) and the primary antibody to 64PP (monoclonal KTM-50).
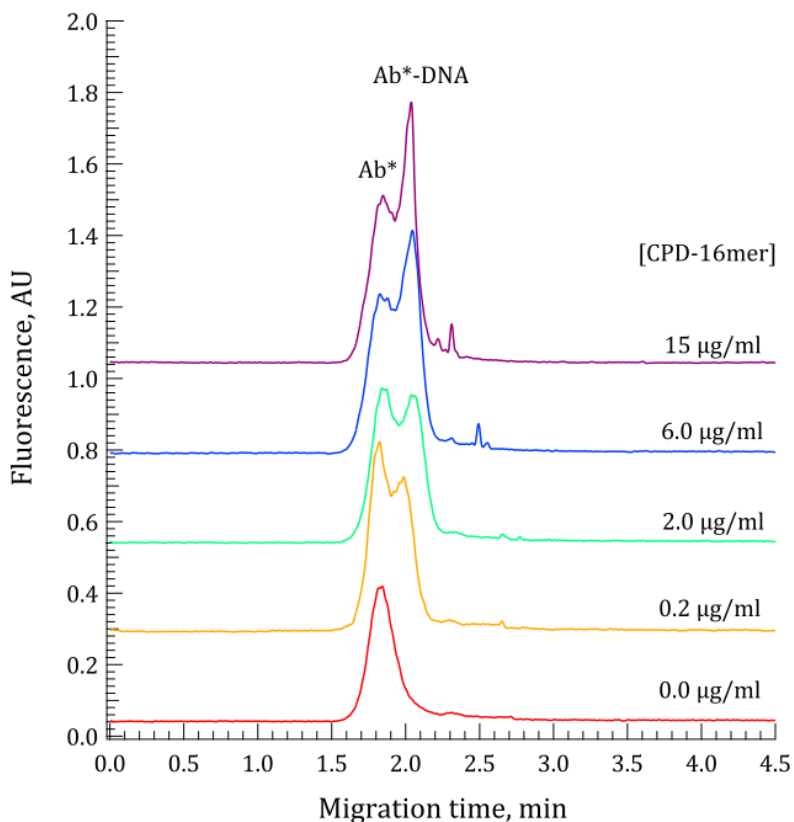
Figure 3.3. Representative CE-LIF electropherograms obtained from the analyses of CPD-16mer at different concentrations of CPD-16mer

Peak Ab* represents the unbound antibodies (*F_{ab} and fluorescently labeled KTM-53).

Peak Ab*-DNA represents the complex formed between the antibodies and CPD lesions in the 16mer.

3.3.1. Calibration for CPD photoproducts using the CPD-16mer standard

In this experiment the concentration of the CPD-16mer was varied from 0.0 to 15 µg/ml while the concentration of KTM-53 was kept constant at 2 µg/ml. Representative CE-LIF electropherograms are shown in Figure 3.3. As one can see, the signal due to Ab*-DNA peak rose with an increase of CPD-16mer concentration; this was expected since higher CPD-16mer concentrations would mean more CPD lesions detected by the antibody.

In order to control for variations and make comparison between different experiments, relative peak areas were employed. Relative peak area ($PA_{relative}$) is the ratio of the peak area for the complex over the total peak area of all fluorescent species (*F_{ab}, Ab* and Ab*-DNA) for the antibody (PA_{cmplx}/PA_{total}). This ratio helps eliminate any changes related to the fluorescence signal fluctuations that may occur.

The IgorPro software (version 6.12, WaveMetrics Inc., Lake Oswego, OR, USA) was used to integrate peaks from the electropherograms. The peak areas were used to calculate PA relative ($PA_{relative} = PA_{cmplx}/PA_{total}$). Therefore we were able to obtain calibrations between $PA_{relative}$ and the concentrations of CPD-16mer.

Knowing that concentration is related to the number of CPD lesions, we can derive the relationship between $PA_{relative}$ and the number of CPD lesions detected (#CPD lesions). Obtaining the information on the number of

CPD lesions requires the volume of samples injected into the capillary.

The volume of the injected sample can be calculated using the following equation:

$$V_{injected}(mL) = \left(\frac{L_D}{t_R \cdot V}\right) \cdot V_{inj} \cdot t_{inj} \cdot \pi \cdot r^2 \qquad \text{(eq. 3-1)}$$

Where: $V_{injected}$ – volume of sample injected (cm^3);

L_D – length of the capillary to the detector (cm);

t_R – migration time of the species (s);

V – voltage of the run (kV);

V_{inj} – injection voltage (kV);

t_{inj} – injection time (s);

πr^2 – internal cross section area (cm^2) of the capillary having an internal radius r.

The relevant conditions of the experiment were: L_D = 30 cm (20 µm i.d.); t_R = 2 minutes = 120 s; V = 15 kV; V_{inj} = 20 kV; t_{inj} = 5 s; r^2 = 1×10^{-6} cm^2. Thus $V_{injected}$ = 2.09×10^{-5} cm^3 = 5.24×10^{-6} mL $\approx$ 5 nL.

The number of molecules injected into the capillary can be calculated using the following equation:

$$N_{molecules} = C\left(\frac{\mu g}{mL}\right) \cdot 10^{-6}\left(\frac{g}{\mu g}\right) \cdot V_{injected}(mL) \cdot \frac{1}{MW}\left(\frac{mol}{g}\right) \cdot 6.022 \times 10^{23}\left(\frac{molecules}{mol}\right)$$
$$\text{(eq. 3-2)}$$

Knowing the concentrations of KTM-53 (2 µg/ml) and CPD-16mer (0 – 15 µg/ml) used in the experiments and using molecular weights for KTM-

53 and CPD-16mer ($MW_{(Ab)} \approx 150$ kDa = 150,000 g/mol and $MW_{(CPD-16mer)}$ = 4947.1 g/mol respectively), we can calculate the number of molecules injected into the capillary. The number of CPD lesions in CPD-16mer is identical to the number of CPD-16mer molecules (one lesion per molecule). For proper calibration we are also interested in the ratio of CPD lesions to the antibody KTM-53 molecules (ratio #CPD lesions/#KTM-53). This ratio helps to distinguish between results in which all CPD lesions could be detected *vs.* results wherein not enough antibody molecules were present to detect all CPD lesions. Since one antibody molecule is capable of binding a maximum of two antigens, a ratio of #CPD lesions/#KTM-53 smaller than or equal to 2 is appropriate.

A

Figure 3.4 shows $PA_{relative}$ *vs.* the concentration of CPD-16mer and $PA_{relative}$ *vs.* the ratio of #CPD lesions/KTM-53. Thus we can clearly see the region where the ratio #CPD lesions/KTM-53 is equal or less than 2.
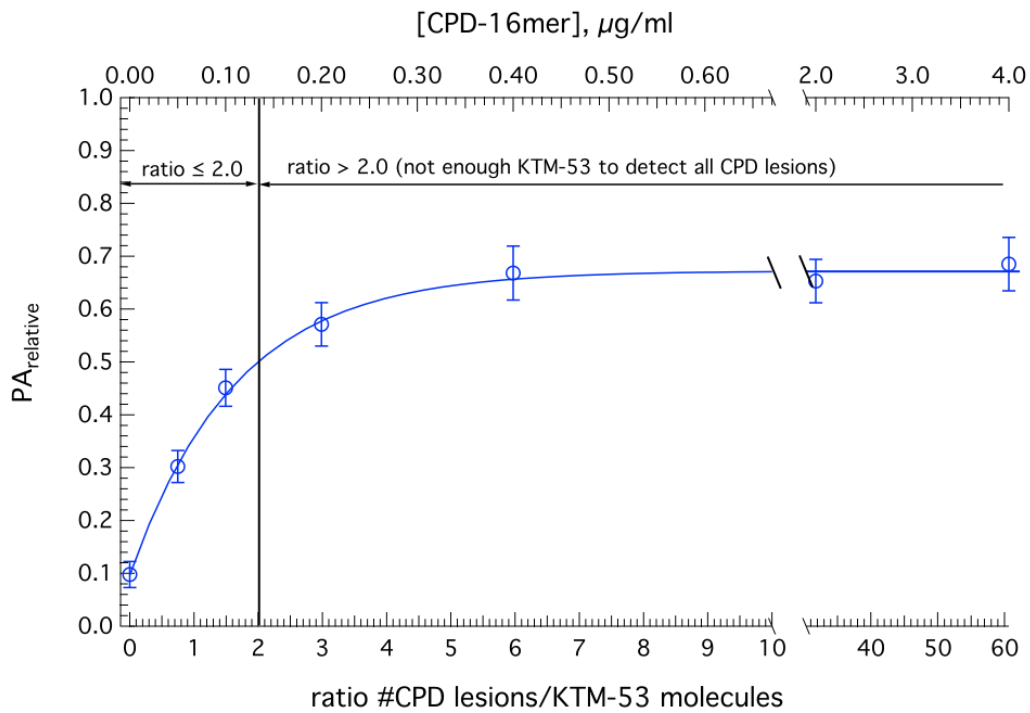
Figure 3.4. Relative intensity of the Ab*-DNA complex peak as a function of the concentration of the CPD-16mer and the ratio of the CPD lesions over the antibody

Top axis represents the concentration of CPD-16mer in the incubation solutions

Bottom axis represents the ratio of the number of CPD lesions over the antibody molecules present in the sample solutions

Each data point represents the mean value and the error bars represent ± standard deviation from a minimum of three independent experiments.

Note: the lines connecting data points serve to show trends. The lines were not generated from any data-fitting program.
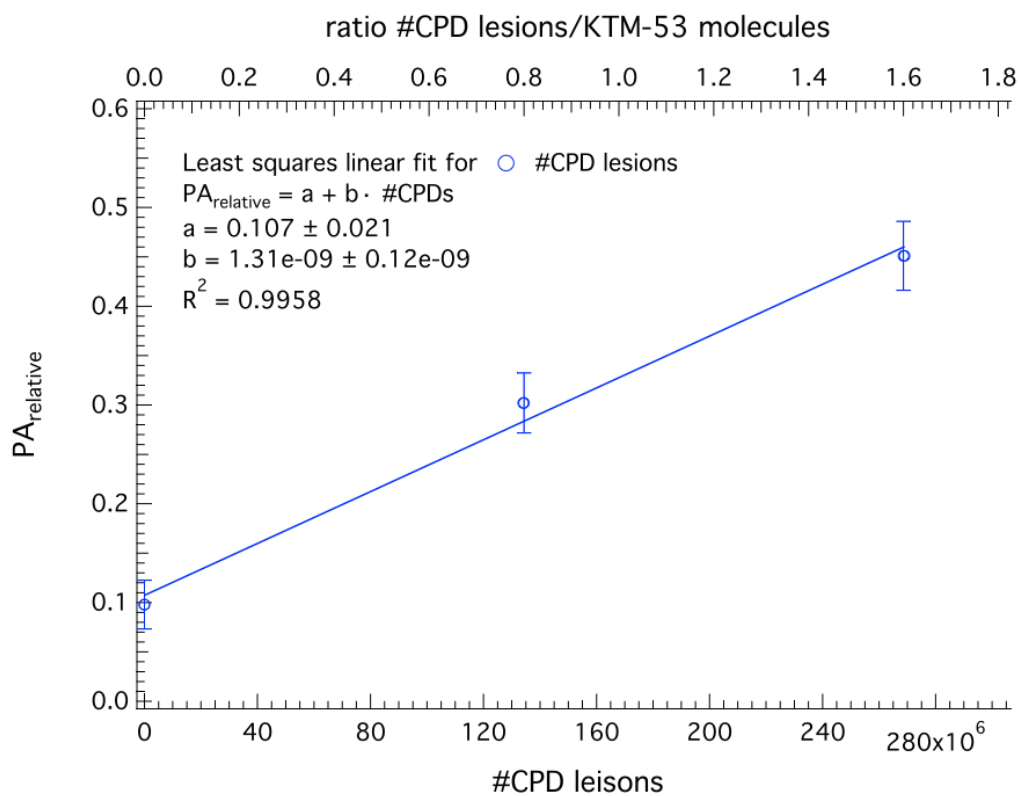
Figure 3.5. A calibration curve showing the relationship between signal response (PA$_{relative}$) and #CPD lesions

Each data point represents the mean value and the error bars represent ± standard deviation from a minimum of three independent experiments.

Within the appropriate region of the #CPD lesions/KTM-53 ratios ($\leq$ 2) the number of CPD lesions could be calculated since in all our experiments a constant amount of KTM-53 was maintained. Figure 3.5 shows the relationship between $PA_{relative}$ *vs.* the number of CPD lesions (#CPD lesions) detected and $PA_{relative}$ *vs.* the ratio of #CPD lesions/KTM-53 for the ratio region below 2. As expected this relationship is linear. The linear calibration between $PA_{relative}$ and #CPD lesions is subsequently used to determine quantitative amounts of CPD lesions in isolated DNA and cellular DNA samples.

3.3.2. Calibration for 64PP photoproducts using the 64PP-16mer standard

Figure 3.2 shows that both the 64PP-16mer and CPD-16mer formed a complex with the anti-64PP monoclonal antibody (KTM-50). The binding of KTM-50 with CPD-16mer was unexpected. There could be several possible reasons: (i) non-specific binding of KTM50 to the CPD lesions (although the manufacturer states that KTM-50 binds only to 64PP); (ii) CPD-16mer had some impurities of 64PP-16mer; or (iii) the 64PP-16mer binds to the fluorescent antibody fragment $^*F_{ab}$. The purification results, provided by the Synthetic Organic Chemistry Core Lab, suggest that all of the 16mer standards had few impurities (Appendix B), therefore the second reason is unlikely. Analysis of an incubation solution containing the *Fab and the 64PP-16mer did not show formation of a complex. Thus we may rule out the

third possibility. It is more likely that the KTM-50 antibody could cross-react with CPD lesions and/or other antigens.

In plotting the calibration curve of $PA_{relative}$ *vs.* 64PP lesions, this non-specific binding did not affect the calibration curve since the 64PP-16mer standard was free of CPD-16mer. However, non-specific binding of KDM-50 is an issue when detecting 64PP in real DNA samples that may contain both lesions. Thus the non-specific binding must be accounted for. By comparing signal from pure 64PP-16mer, CPD-16mer and mixtures of 64PP-16mer and CPD-16mer of differing concentrations, we were able to determine that binding of KTM-50 to the CPD-16mer corresponded to approximately 30% of the complex signal from equivalent amount of 64PP. Additional experiments would be needed to support the latter results. Experiments could include the use of the *E.coli* photoreverse enzyme to remove CPD followed by the repeated CE-LIF analyses with anti-64PP antibody.

Figure 3.6 shows representative electropherograms for samples with different 64PP-16mer concentrations. Similar to the results for the CPD-16mer, $*F_{ab}$ labeled KTM-50 migrates at earlier times, around 1.9 min and the ternary complex formed between the 64PP-16mer and $*F_{ab}$ labeled KTM-50 migrates at around 2.1 min. This small difference in migration times is due to the difference in the charge-to-mass ratio between the antibody and the complex of antibody with the 64PP-16mer. The IgorPro software was used to integrate peaks from the electropherograms. Results of such integration

provided information needed for the calibration between the relative peak areas ($PA_{relative}$) and the concentration of 64PP-16mer.

The relationship between $PA_{relative}$ and the concentration of 64PP-16mer is shown in Figure 3.7, in which the ratio of the number of 64PP lesions to the number of KTM-50 molecules (ratio #64PP lesions/#KTM-50) is plotted. We use the region of the ratio #64PP/#KTM-50 smaller than or equal to 2 for quantitative analysis. Given that one monoclonal antibody binds to a maximum of two lesions, two-fold molar excess of the antibody over the 64PP provides sufficient amount of the antibody to bind with all of the 64PP lesions.
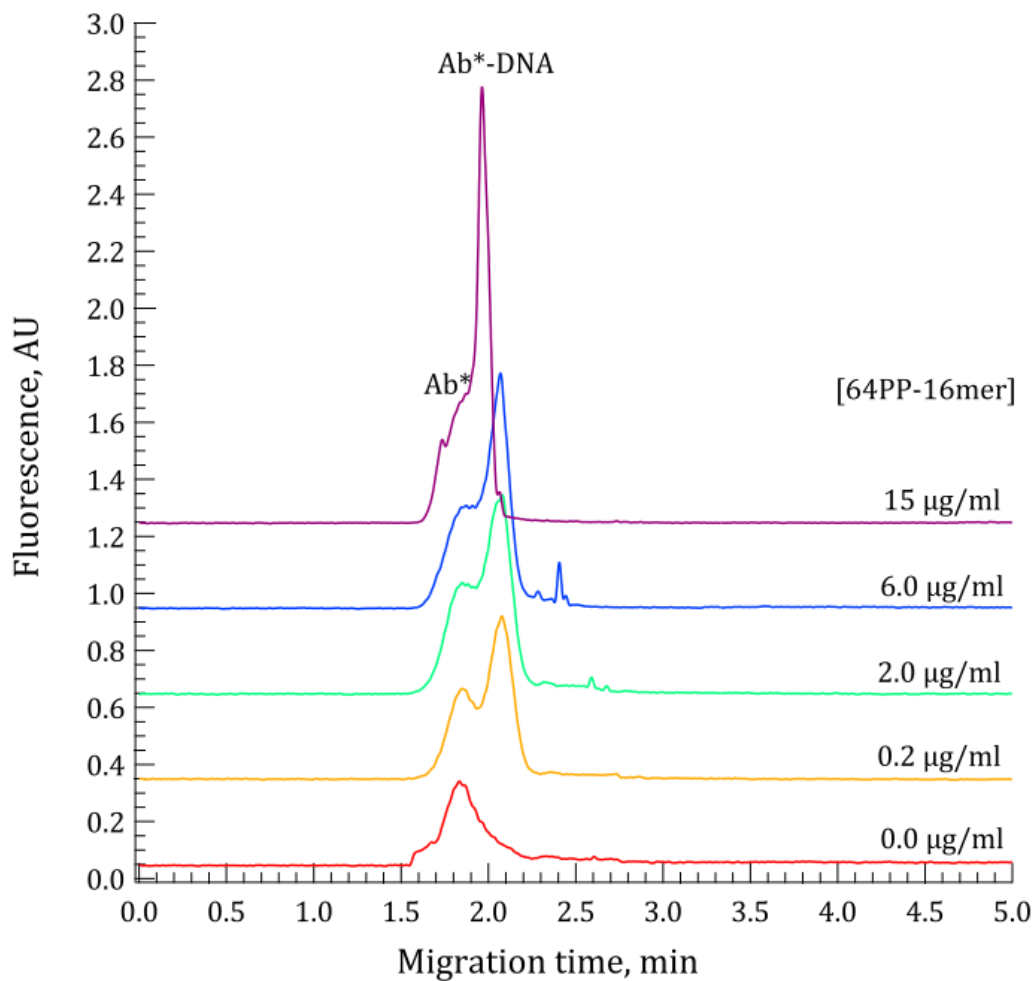
Figure 3.6. Representative CE-LIF electropherograms obtained from the analyses of 64PP-16mer at different concentrations

Peak Ab* represents the unbound antibodies (*Fab and fluorescently labeled KTM-50).

Peak Ab*-DNA represents the complex formed between the antibodies and CPD lesions in the 16mer.
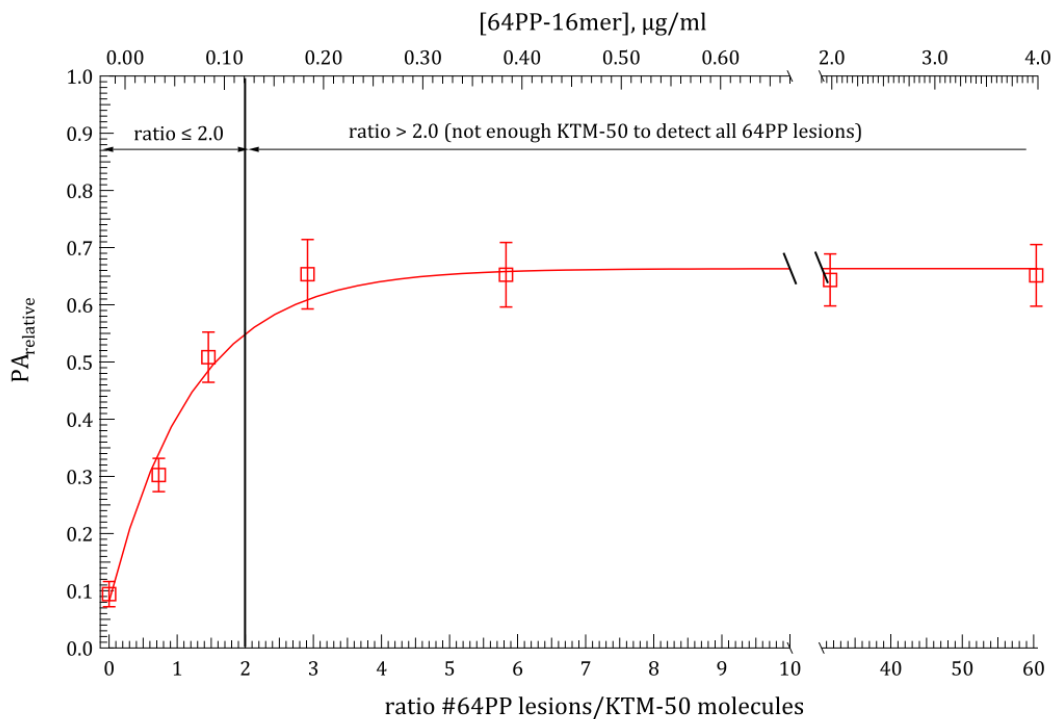
Figure 3.7. Relative intensity of the Ab*-DNA complex peak as a function of the concentration of the 64PP-16mer and the ratio of the 64PP lesions over the antibody

Top axis represents the concentration of 64PP-16mer in the incubation solutions

Bottom axis represents the ratio of the number of 64PP lesions over the antibody molecules present in the sample solutions

Each data point represents the mean value and the error bars represent ± standard deviation from a minimum of three independent experiments.

Note: the lines connecting data points serve to show trends. The lines were not generated from any data-fitting program.

Figure 3.8 shows a calibration curve between the signal response and the number of 64PP lesions. The calibration was linear which could be potentially used to determine the amount of 64PP lesions in UV-irradiated DNA samples, provided that the issue of non-specific binding by the monoclonal KTM-50 antibody could be dealt with.

Figure 3.9 shows calibration curves for both CPD and 64PP lesions in the 16mer oligonucleotide standards. Application of these calibrations to determine such DNA lesions in other DNA samples of different size assumes that the fluorescent intensities of the antibody complex to DNA of different sizes are consistent. In principle, the same number of fluorescent molecules in the complex should give the same intensity of fluorescence under identical experimental conditions. However, the size of DNA could change the fluorescent yield of the bound fluorescent antibody. Thus the use of a small oligonucleotide standard for the calibration could involve errors. We recognize this potential error in quantitative measurements while facing the common challenge of producing a longer DNA standard containing UV damage.
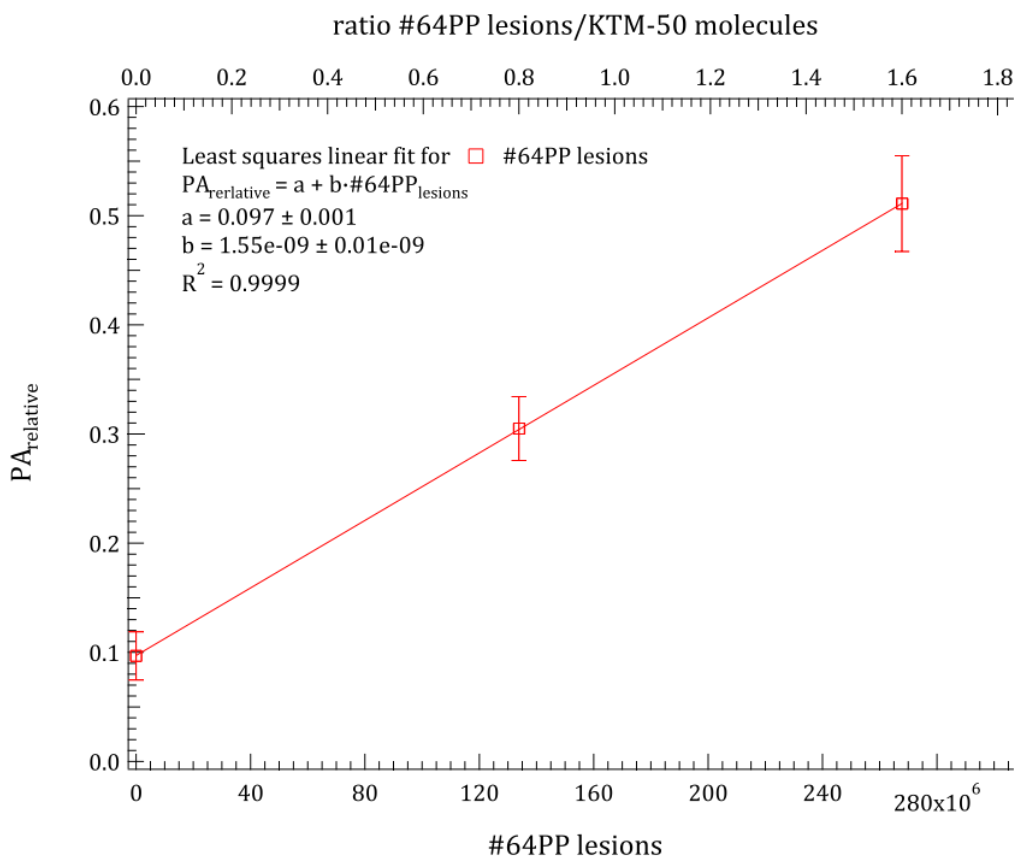
Figure 3.8. A calibration curve showing the relationship between signal response (PA$_{relative}$) and #64PP lesions

Each data point represents the mean value and the error bars represent ± standard deviation from a minimum of three independent experiments.

Figure 3.9. Calibration curves for the CPD-16mer and 64PP-16mer

Each data point represents the mean value and the error bars represent ± standard deviation from a minimum of three independent experiments.

3.4. Quantification of UV lesions in DNA samples

Having achieved calibrations using the CPD-16mer and 64PP-16mer standards, we further extended the previous experiments (Chapter 2) on the relative peak areas ($PA_{relative}$) to the determination of the amounts of DNA lesions. Results from the determination of the CPDs and 64PPs in UV-irradiated DNA library (80nt), human placenta DNA (HP-DNA) and calf-thymus DNA (CT-DNA) are summarized here.

3.4.1. Quantification of CPD and 64PP lesions in 80-nt DNA library irradiated with UVB and UVC light

Figure 3.10 and 3.11 summarize dose-dependent response from the analyses of the DNA sample (80nt DNA library) after irradiation with different doses of UVB light (Figure 3.10) and UVC light (Figure 3.11). The UVB and UVC dose ranges were chosen based on the previous experiments (Figures 2.5 and 2.8) where the responses were linearly increasing with the increases in the radiation doses. The number of UV lesions in each sample was obtained from the CE-LIF immunoassay (see Figures 2.5 and 2.8), integration of relative peak areas ($PA_{relative}$) and calibration against the standards (Figure 3.9).

Knowing the size of the DNA (80 bases), the number of DNA lesions in the sample (Figure 3.10 and 3.11) and the amount of sample injected for CE-

LIF analysis, we are able to obtain the information on the number of lesions per 1000 nucleotides.
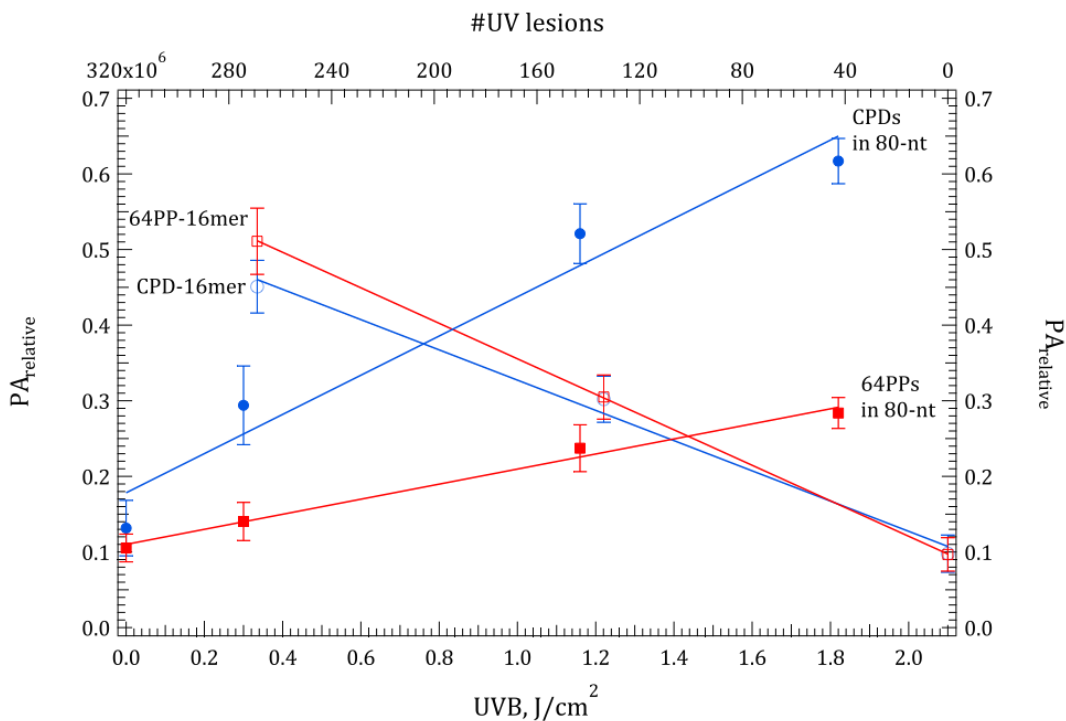
Figure 3.10. Quantification of CPDs and 64PPs in 80-nt DNA library irradiated with varying doses of UVB

$PA_{relative}$ (left) *vs.* UVB, J/cm^2 (bottom): dose response for CPDs (●) and 64PPs (■) in 80nt DNA library.

$PA_{relative}$ (right) *vs.* # UV lesions (top): damage response for CPD-16mer (○) and 64PP-16mer (□).

Each data point represents the mean value and the error bars represent ± standard deviation from a minimum of three independent experiments.
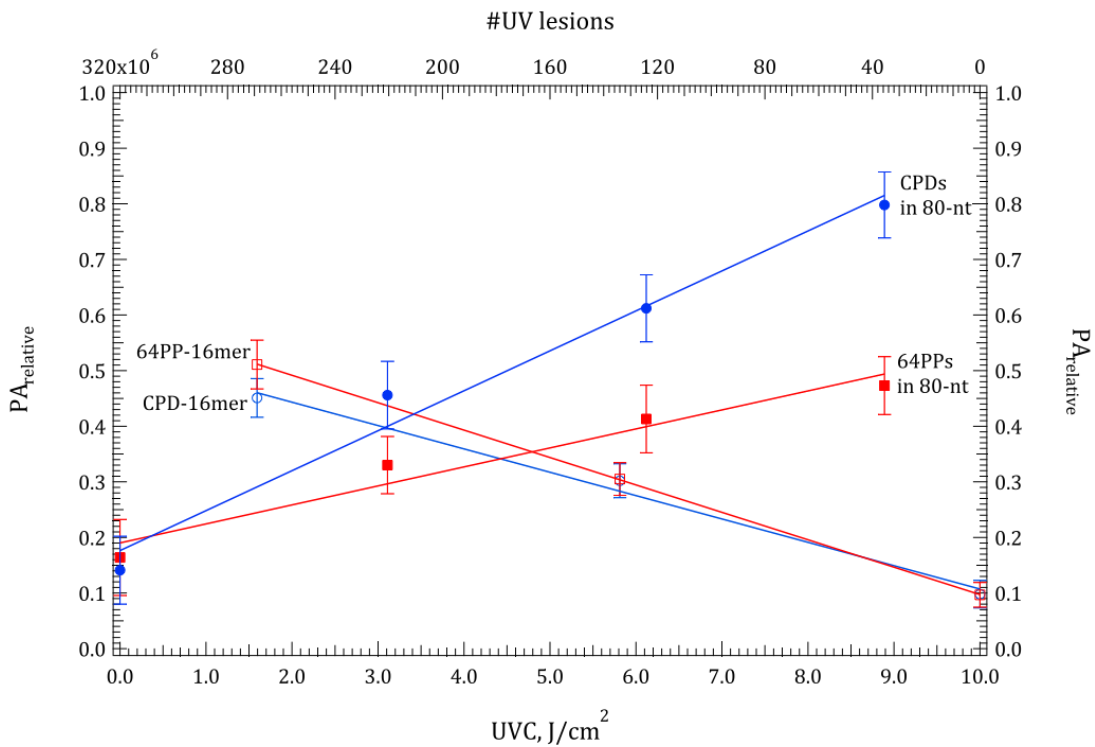
Figure 3.11 Quantification of CPDs and 64PPs in 80-nt DNA library irradiated with different doses of UVC

$PA_{relative}$ (left) *vs.* UVB, J/cm² (bottom): dose response for CPDs (●) and 64PPs (■) in 80nt DNA library.

$PA_{relative}$ (right) *vs.* # UV lesions (top): damage response for CPD-16mer (○) and 64PP-16mer (□).

Each data point represents the mean value and the error bars represent ± standard deviation from a minimum of three independent experiments.

Figures 3.12 and 3.13 show the results as #UV lesions per 10^3nt following irradiation of the DNA with UVB and UVC, respectively. These results also provide the yield of formation of the UV lesions as #UV lesions per10^3nt per J/cm^2.
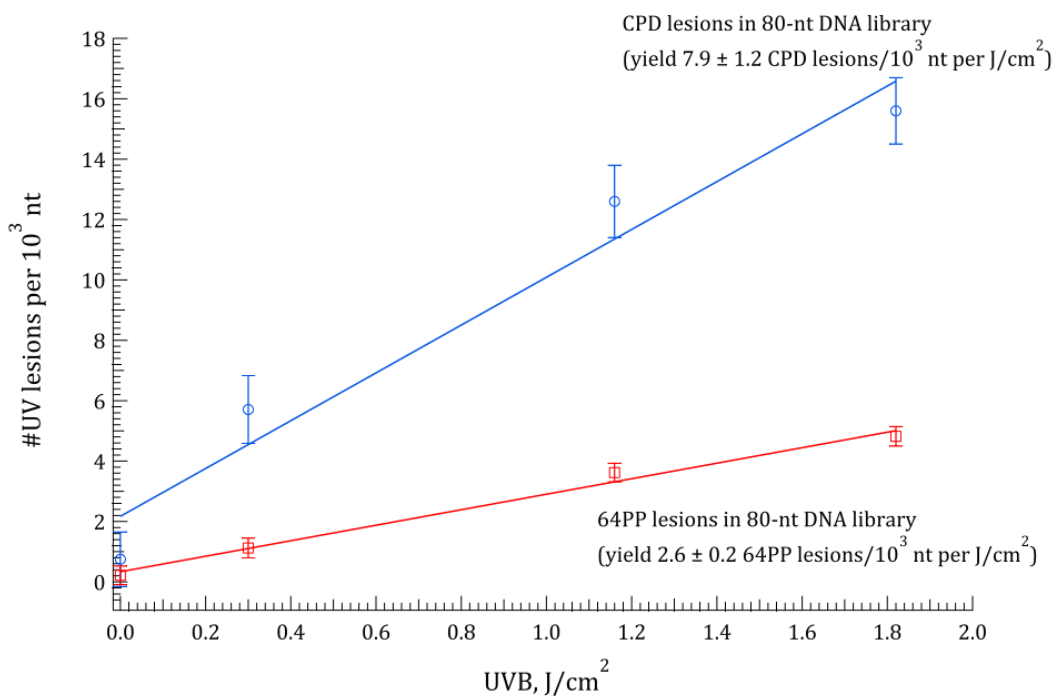
Figure 3.12. Yield of formation of CPD and 64PP lesions following irradiation of an 80nt DNA library with UVB

Each data point represents the mean value and the error bars represent ± standard deviation from a minimum of three independent experiments.
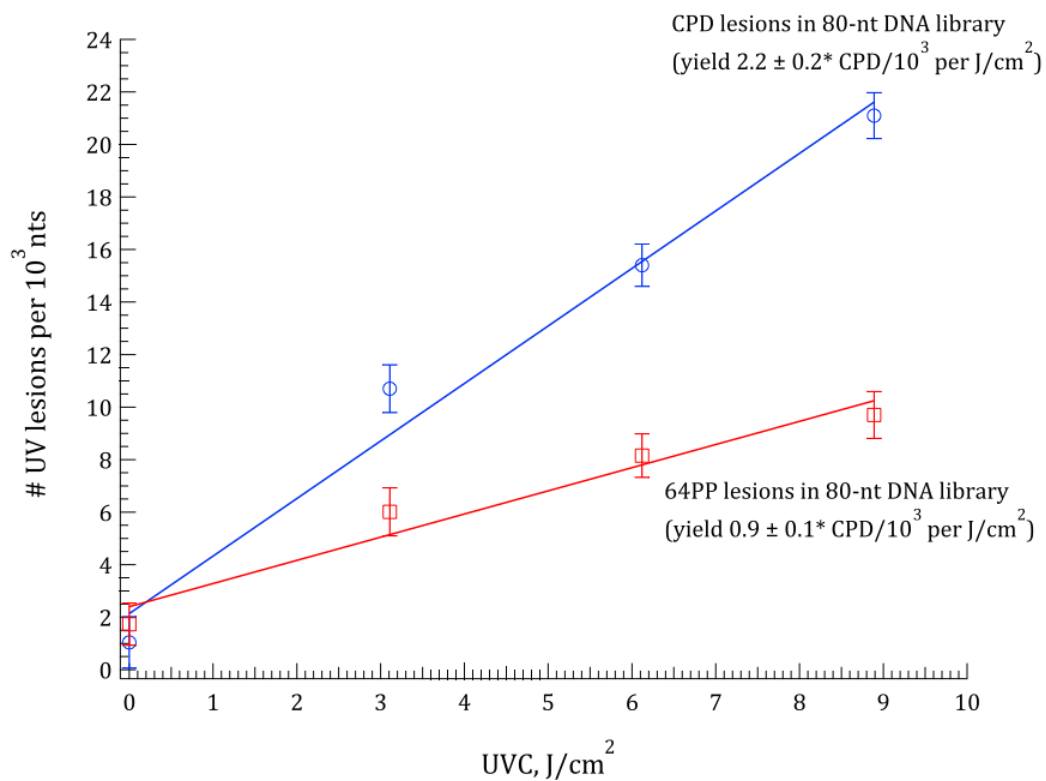
Figure 3.13. Yield of formation of CPD and 64PP lesions following irradiation of an 80nt DNA library with UVC

Each data point represents the mean value and the error bars represent ± standard deviation from a minimum of three independent experiments.

(*) – standard deviation of the slope.

Table 3.1 summarizes the yield of formation of CPD and 64PP in 80nt DNA library irradiated with either UVB or UVC light. Approximately 3× more CPD lesions are formed than 64PP lesions in UVB irradiated 80nt DNA library. Approximately 3.5× more CPD lesions are formed in the case of UVB radiation compared to UVC radiation. These results are in general accordance with the previously reported findings [12, 13].

Table 3.1. Yield of formation of CPD and 64PP in UV irradiated 80nt DNA library

Type of UV light	Yield of formation of UV lesions (#lesions per 10^3 nt per J/cm^2)	
	CPDs	64PPs
UVB	7.9 ± 1.2*	2.6 ± 0.2*
UVC	2.2 ± 0.2*	0.9 ± 0.1*

(*) – standard deviation of the slope

In [12, 13] the action spectra for CPDs and 64PPs were determined. These spectra show the amount of UV lesions vs. wavelength of UV light between 265 and 313 nm. For normal human skin fibroblasts the spectra showed higher formation of CPD lesions compared to 64PP. The level for 64PP was at least 2-3 times lower than that observed for CPDs in cells exposed to 313 nm. The rate of formation of 64PP decreased significantly at wavelengths of UV > 310 nm, which was due to photoconversion of 64PP to

its Dewar isomers [13, 14]. Studies of action spectra for CPD photoproducts showed the maximum yield of formation near 300 nm and then rapid decrease at both longer and shorter wavelengths. Therefore results obtained from our experiments for 80nt DNA library agree nicely with findings reported earlier [13-15].

3.4.2. Quantification of CPD lesions in HP-DNA and CT-DNA irradiated with UVB light

The doses that produced a linear dose-response in Figure 2.11 were used to determine the yield of the formation of CPD lesions after the HP-DNA and CT-DNA samples were UVB irradiated. Figure 3.14 shows the dose-response relationship expressed as the relative peak areas (PArelative) vs. the UVB dose and PA relative vs the number of CPDs. Figure 3.15 shows the number of CPD lesions (#CPD lesions) per 10^3 nt in the HP-DNA and CT-DNA after irradiation with the different doses of UVB.
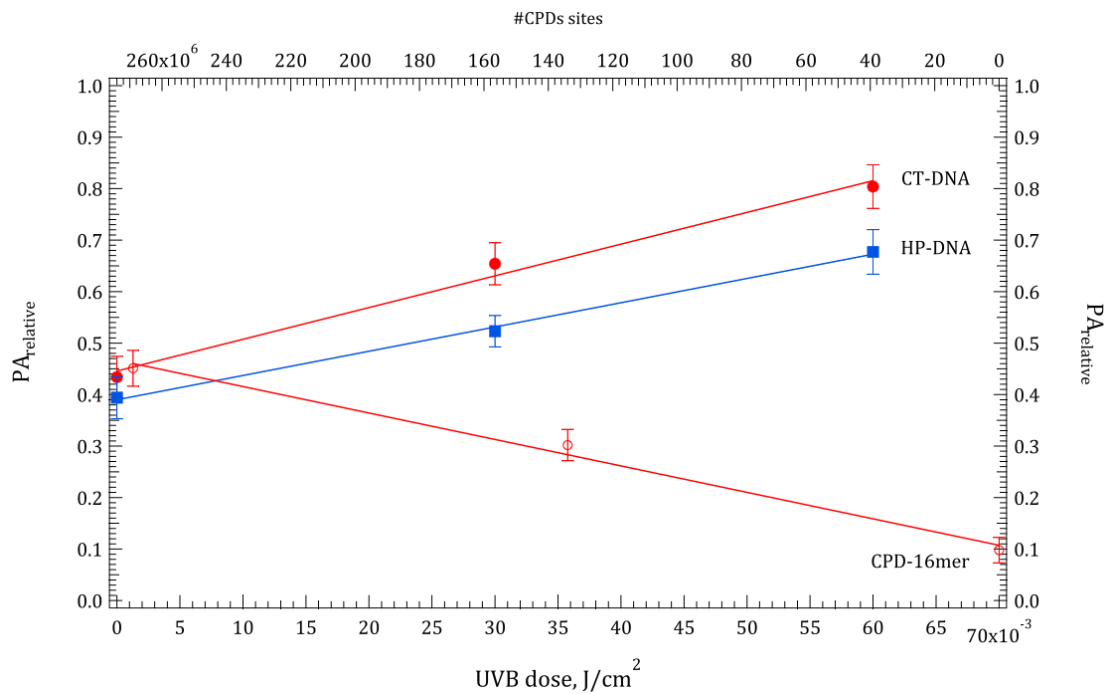
Figure 3.14. Quantification of CPD lesions in UVB irradiated HP-DNA and CT-DNA samples

$PA_{relative}$ (left) *vs.* UVB, J/cm² (bottom): dose response for CPDs in HP-DNA (■) and CT-DNA (●).

$PA_{relative}$ (right) *vs.* # UV lesions (top): damage response for CPD-16mer (○).

Each data point represents the mean value and the error bars represent ± standard deviation from a minimum of three independent experiments
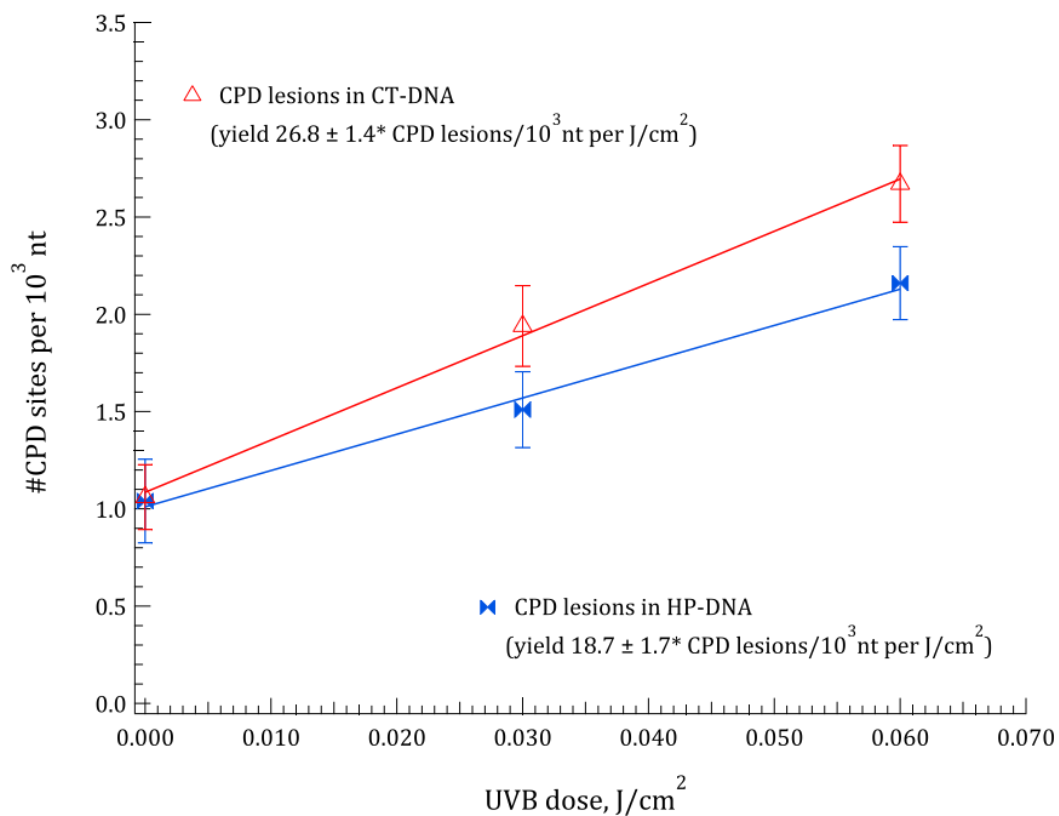
Figure 3.15. Yield of formation of CPD lesions in UVB irradiated CT-DNA and HP-DNA samples

Each data point represents the mean value and the error bars represent ± standard deviation from a minimum of three independent experiments.
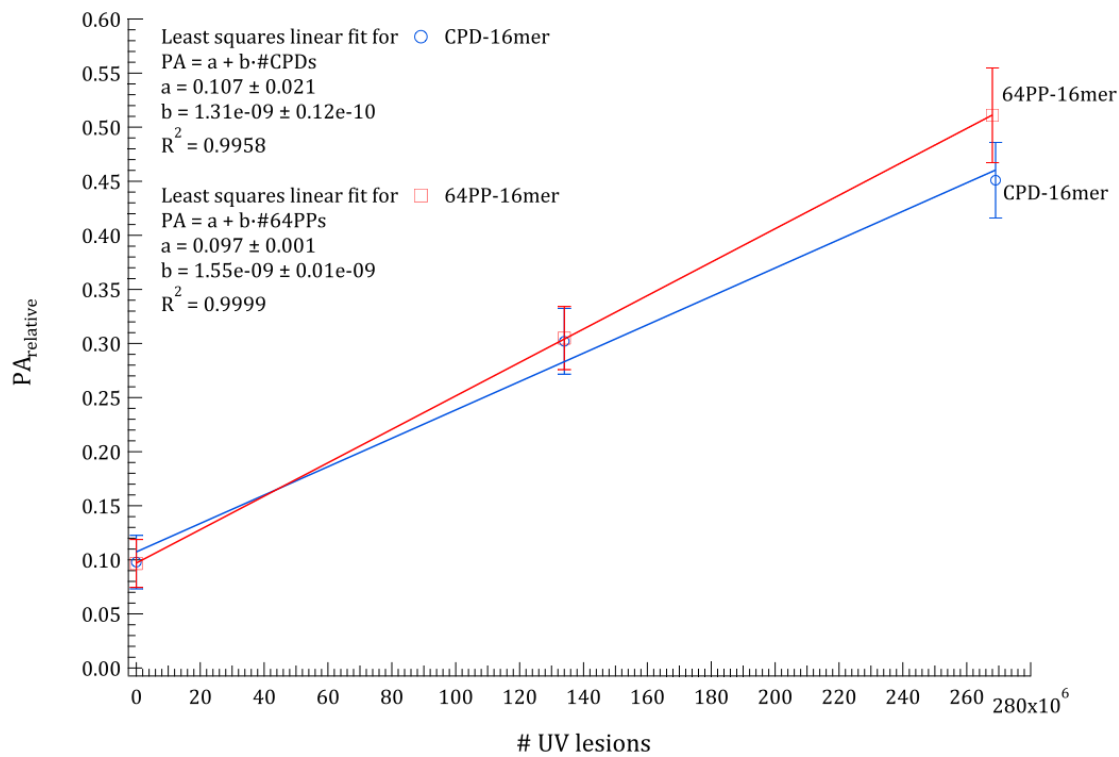
(*) – standard deviation of the slope.

3.4.3 Comparison of yield for CPD lesions produced in DNA of differing lengths after UVB irradiation

Table 3.2 summarizes the yields of formation of CPD lesions in the three samples. For these three DNA samples the yield of formation of CPDs increases with increase in DNA length (Figure 3.16).

Reasons for the higher yield of CPD formation in the larger DNA among these DNA samples are not known. However, the pyrimidine tracts are preferential sites for dimer formations [16, 17] and longer DNA molecules might have higher frequencies of pyrimidine tracts. Thus having more pyrimidine tracts in the longer DNA samples may be a plausible explanation why the yield of formation for CPDs increases with the DNA lengths.

Table 3.2. Comparison of yield of formation of CPD lesions between three DNA samples irradiated by UVB light

DNA sample	Length of the DNA, bases	Yield #CPD lesions per 10^3nt per J/cm^2
80nt DNA library	80	7.9 ± 1.2*
ss HP-DNA	530-830	18.7 ± 1.7*
ss CT-DNA	50,000	26.8 ± 1.4*

(*) – standard deviation of the slope.
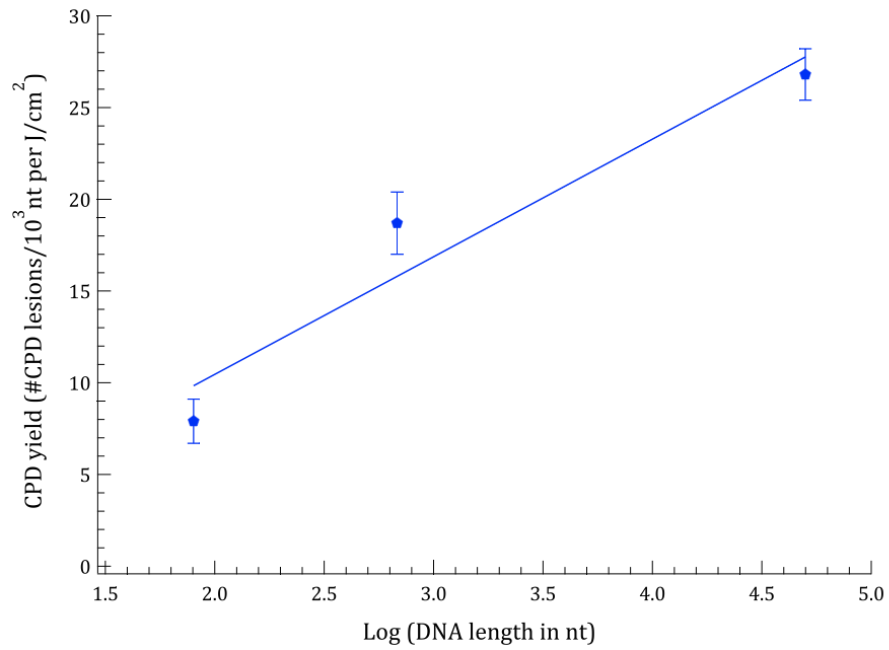
Figure 3.16. A relationship between log (DNA length) and the yield of formation of CPD lesions in UVB irradiated DNA samples

Each data point represents the mean value and the error bars represent ± standard deviation from a minimum of three independent experiments

3.5. Conclusions

A calibration method was developed for the determination of UV-induced DNA lesions using CPD-16mer and 64PP-16mer as standards. Application of this calibration method enables the quantification of the number of CPD and 64PP lesions in the DNA samples. A note of caution is that the small oligonucleotide standards may not represent the larger DNA. Larger DNA standard with well defined quantitative amounts of DNA lesions are difficult to produce. Our work described here is a viable option.

The calibration method was also applied to the quantification of UV lesions in three types of DNA samples of different sizes. Yields of formation of CPD in UVB-irradiated 80-nt DNA library was 7.9 ± 1.3 per 10^3 nt per J/cm^2 and in UVC-irradiated 80-nt DNA library was 2.2 ± 0.2. The yields of 64PP formation in UVB-irradiated 80-nt DNA library was 2.6 ± 0.3 and in UVC-irradiated 80-nt DNA library was 0.9 ± 0.1 lesions per 10^3 nt per J/cm^2. The 3 – 4 fold more CPD than 64PP, induced by the same doses of UV radiation, is consistent with literature reports. Yields of formation of CPD lesions were also determined in UVB-irradiated HP-DNA (18.7 ± 1.7 lesions per 10^3 nt per J/cm^2) and CT-DNA (26.8 ± 1.4 lesions per 10^3 nt per J/cm^2).

3.6. References

1. T. Douki, M. Court, S. Sauvaigo, F. Odin and J. Cadet (2000), Formation of the main UV-induced thymine dimeric lesions within isolated and cellular DNA as measured by high performance liquid chromatography-tandem mass spectrometry, J. Biol. Chem, *275*, 11678-11685.

2. T. Douki and J. Cadet (2001), Individual determination of the yield of the main UV-induced dimeric pyrimidine photoproducts in DNA suggests a high mutagenicity of CC photolesions, Biochemistry, *40*, 2495-2501.

3. T. Douki, L. Voituriez and J.Cadet (1995), Measurement of pyrimidine (6-4) pyrimidine photoproducts in DNA by a mild acidic hydrolysis-HPLC fluorescence assay, Chem. Res. Toxicol., *8*, 244-253

4. M. Liuzzi, M. Weinfeld and M.C. Paterson (1989), Enzymatic analysis of isomeric trithymidylates containing ultravioles light-induced cyclobutane pyrimidine dimers. I. Nuclease P1-mediated hydrolysis of the intradimer phosphodiester linkage, J. Biol. Chem, *264*, 6355-6363.

5. M. Weinfeld, M. Liuzzi and M.C. Paterson (1989), Enzymatic analysis of isomeric trithymidylates containing ultravioles light-induced cyclobutane pyrimidine dimers. II. Phosphorylation by phage T4 polynucleotide kinase, J. Biol. Chem, *264*, 6364-6370.

6. V.J. Bykov and K. Hemminki (1995), UV-induced photoproducts in human skin explants analyzed by TLC and HPLC-radioactivity detection, *16*, Carcinogenesis, 3015-3019.

7. T. Douki and J. Cadet (2003), Formation of the spore photoproduct and other dimeric lesions between adjacent pyrimidines in UVC-irradiated dry DNA, Photochem. Photobiol. Sci., *2*, 433-436.

8. J.-S. Taylor and M.P. Cohrs (1987), DNA, light and Dewar pyrimidones: The structure and biological significance to TpT_3, J. Am. Chem. Soc. *109*, 2834-2835.

9. J.-S. Taylor, D.S. Garrett and M.P. Cohrs (1988), Solution-state structure of the Dewar photoproduct of thymidylyl-(3'→5')-thymidine, Biochemistry *27*, 7206-7215.

10. F. Gaecés and C.A. Dávila (1982), Alterations in DNA irradiated with ultraviolet radiation-I. The formation process of cyclobutylpyrimidine dimers : cross sections, action spectra and quantum yields, Photochem. Photobiol., *35*, 9-16.

11. G.P. Pfeifer (1997), Formation and processing of UV photoproducts: effect of DNA sequence and chromatin environment, Photochem. Photobiol, *65*, 270-283.

12. B.S. Rosenstein and D.L. Mitchell (1987) Action spectra for the induction of pyrimidine (6-4) pyrimidone photoproducts and cyclobutane pyrimidine dimers in normal human skin fibroblasts, Photochem. Photobiol., *45*, 775-780.

13. D.L. Mitchell and B.S. Rosenstein (1987), The use of specific radioimmunoassay to determine action spectra for thephotolysis of (6-4) photoproducts, Photochem. Photobiol., *45*, 781-786.

14. S.E. Freeman, H. Hacham, R.W. Gange, D.J. Maytum, J.C. Sutherland and B.M. Sutherland (1989), Wavelength dependence of pyrimidine dimer formation in DNA of human skin irradiated in situ with ultraviol light, Proc. Natl. Acad. Sci. U.S.A, *86*, 5605-5609.

15. H.C. Birnboim (1975), Ultraviolet-induced pyrimidine dimers in long pyrimidine tracts from L-cell DNA, Photochem. Photobiol., *22*, 71-73

16. J. Texter (1992), Quantum yield for preferential photodimerization in long pyrimidine tracts, Biopolymers, *32*, 53-59.

17. N. Ramakrishnan and D.S. Pradhan (1979), Occurrence of pyrimidine-rich tracts in ascites tumor DNA and the formation of UV induced thymine dimers, Photochem. Photobiol., *29*, 539-542.

Chapter Four

Application of the non-competitive CE-LIF immunoassay
to determine the formation of CPD and 64PP lesions
in CRL-2522 cells

4.1. Introduction

UV light is one of the most studied damaging agents to DNA. Exposure of cells to UV radiation is the best known model for studying the behavior of cells in the presence of biological and environmental damage [1. 2]. The acute effects of UV radiation are: DNA damage, protein crosslinking and the peroxidation of lipids - all of which lead to sunburns, erythema and immunosuppresion. Prolonged and/or repeated exposure to UV light results in photoaging and potentially skin cancer [3].

UVB radiation is known to primarily induce CPD and 64PP lesions [4-6]. Both photolesions are sequence specific and occur in runs of tandemly located pyrimidine residues [7-9], which often become the UV-induced DNA damage and mutation site. In addition to CPDs and 64PPs, UV radiation also induces many other types of DNA lesions such as cytosine photohydrates, purine photoproducts and single-strand breaks (SSB) in DNA. UVA, on the other hand, is known to cause indirect DNA damage by producing reactive oxygen radicals and other reactive short-lived molecules which result in

SSBs, DNA-protein crosslinks, etc. [3]. Due to the complexity and wide-ranging effects of UV radiation on living organisms, it comes as no surprise that so many projects have been devoted to the understanding and ongoing research in this field. Addressing a wide range of questions and testing different hypotheses related to DNA damage require various analytical methods. The desirable attributes of these methods may include sensitivity, specificity, ease of operation and applicability to particular samples and/or areas of research.

This chapter outlines an application of the newly developed CE-LIF immunoassay to detect and quantify CPD-lesions in DNA extracted from UVB irradiated human fibroblasts cells at environmentally relative UV doses.

4.2. Experimental

4.2.1. Reagents

Tris-glycine buffer solutions (TG, 25 mM Tris and 192 mM Glycine) were prepared from $10\times$ TG buffer (Bio-Rad Laboratories, Hercules, CA, USA) by dilution with 18.2 MΩ distilled deionized water (DDW) from a Milli-Q Gradient Water System (Millipore, Nepean, ON, Canada). The pH of TG buffer for incubation was 7.5 and the pH of the TG buffer for CE separation was 8.3. The monoclonal mouse anti-thymine dimer antibody (clone KTM-53, IgG_1

type) and mouse anti-(6-4) photodimer antibody (clone KTM-50, IgG_1 type) were purchased from Kamiya Biomedical Company (Seattle, WA, USA). Goat anti-mouse F_{ab} fragment (*Fab) supplied in a Zenon® Alexa Flour® 546 (λ_{ex} = 556 nm, λ_{em} = 573 nm) mouse IgG_1-labeling kit (Molecular Probes, Eugene, OR, USA) was used as a secondary antibody to fluorescently label antibodies.

(±)-r-7,t-8-Dihydroxy-t-9,10-epoxy-7,8,9,10-tetrahydro-benzo(a)pyrene (BPDE) was supplied by the National Cancer Institute Chemical Carcinogen Reference Standard Repository (Midwest Research Institute, Kansas city, MO, USA). A stock solution of BPDE was freshly prepared in anhydrous tetrahydrofuran (THF) (>99.9 % purity, Sigma-Aldrich, St. Louis, MO, USA) before each use. Monoclonal mouse anti-BPDE antibody (clone 8E11, isotype IgG_1) was purchased from Trevigen® Inc. (Gaithersburg, MD, USA).

4.2.2. Cell culture

Human normal fibroblast CRL-2522 cells were obtained from the American Type Culture Collection (ATCC, Rockville, MD, USA). Cells were cultivated in ATCC-formulated Eagle's Minimum Essential Medium supplemented with 10% fetal bovine serum (ATCC, Manassas, VA, USA). Cells were seeded into 60-mm dishes at 1×10^5 – 2×10^5 cells/dish and incubated at 37 ˚C in humidified air with 5% CO_2. Cells were UVB or UVC irradiated at about 90% confluence.

4.2.3. UV irradiation

CRL-2522 cells were irradiated in a UV chamber with overhead UVB (λ_{max} = 315 nm) and UVC (λ_{max} = 254 nm) lamps (Luzchem Research Ltd., Ottawa, ON, Canada). UV doses were measured using a UVX digital radiometer with either UVB sensor (UVX-31, 310 nm, UVP Inc., Upland, CA, USA) or UVC sensor (UVX-25, 254 nm, UVP Inc., Upland, CA, USA) in mW/cm^2 and later recalculated into J/cm^2 based on different irradiation times. Culture medium for CRL-2522 cells was renewed one day prior to irradiation. On the day of irradiation, growth medium was removed and CRL-2522 cells were washed with 1× PBS solution (phosphate-buffered saline, Invitrogen™) twice and then placed into the UV chamber. CRL-2522 cells were covered by 1 ml of 1× PBS during UV-irradiation. Cells could not be irradiated in the growth medium because it contained phenol red, which absorbs UV light.

4.2.4. DNA isolation

Two types of DNA isolation were performed. Initially, immediately after UVB irradiation, cells were washed once with 1× PBS and lyzed with DNAzol reagent (Invitrogen™ Life Technologies, Carlsbad, CA, USA). Then genomic DNA was extracted using ethanol precipitation. Concentrations of extracted DNA from CRL-2522 cells (CRL-DNA) were measured using a SmartSpec 3000 spectrometer (Bio-Rad Laboratories, Cambridge, MA, USA) at 260 nm and 280 nm. Measurements of the absorption ratios A_{260}/A_{280} of the isolated DNA were 1.4 - 1.6, suggesting the presence of proteins. Since the

isolation of cellular DNA with DNAzol reagent did not have a separate step to allow removal of cellular proteins, we used the Trevigen® genomic DNA isolation kit (Gaithersburg, MD, USA) in our later experiments. Before DNA isolation with the Trevigen® kit and immediately after UVB radiation, CRL-2522 cells were washed once with 1× PBS and trypsinized using 0.25% Trypsin-EDTA solution (Invitrogen™ Life Technologies). Cells were harvested into 1 mL microcentrifuge tubes and DNA from the harvested cells was extracted by following the procedure provided in the Trevigen® isolation kit. Concentrations of CRL-DNA were measured at 260 nm and 280 nm and purity of isolated DNA (A_{260}/A_{280}) was 1.8 - 2.0, which is considered to be protein-free. All results described in this chapter correspond to experiments with cellular DNA isolated using the Trevigen® kit.

4.2.5. Detection of CPDs in DNA using CE-LIF immunoassay

To detect UV-photoproducts in DNA samples, we applied the previously described CE-LIF-based immunoassay (Chapter 2). The basis of this immunoassay is non-competitive interactions between the DNA lesions and monoclonal antibody (Ab*), which is labeled by fluorescently labeled secondary antibody. LIF detects CE separated Ab* and [Ab*-DNA] complexes. Typically DNA from UVB irradiated CRL-2522 cells was denatured in the incubation buffer (1x TG buffer, pH 7.5) prior to antibody addition. DNA was denatured for 10 minutes in a water bath at 95°C and put on ice immediately after heating to prevent the DNA from reannealing. Denaturation was

necessary because the antibodies (clone KTM-53 and KTM-50) have higher binding affinity to lesions in the single stranded DNA. Addition of *h*IgG helped to stabilize the antibody and Ab*-DNA complexes and to minimize non-specific binding to Ab*. After addition of Ab* to DNA samples, mixtures were incubated for 20 minutes at room temperature. Then samples were electrokinetically injected into the capillary by applying an electric field of 500 V/cm for 5 sec. Separation was carried out at room temperature with a separation buffer of 1×TG buffer, pH 8.3, at an electric field of 500 V/cm. The capillary was washed after every injection with 20 mM NaOH, distilled deionized water and separation buffer for at least 3 minutes for each wash step.

4.2.6. Detection of CPDs in DNA using ^{32}P-postlabeling

[32]P-postlabeling was performed as described previously [31, 32]. Briefly, 5 μg DNA from the CRL-2522 cells were digested overnight at 37 °C with the digestion mixture composed of snake venom phosphodiesterase (SVPD, 0.02 units), shrimp alkaline phosphatase (SAP, 0.2 units), DNAse I (0.2 units), $MgCl_2$ (24 mM) and 10 mM TRIS·HCl. Then proteins were removed by precipitation from ice-cold ethanol. The recovered supernatant containing the DNA was taken to dryness and then re-dissolved in 50 μl of water. To remove residual phosphatase activity, solutions were incubated at 100 °C for 5 minutes and stored at -20 °C. Digested DNA (5 μl) was enzymatically phosphorylated in 5 μl of kinase mix (10 units polynucleotide

kinase (PNK) in kinase buffer, 0.5 μl γ-^{32}P-ATP and water). After incubation for 1 hour at 37 °C, the excess ATP was removed with dT$_{16}$ and 2.5 units PNK. Samples were incubated for another 30 minutes at 37 °C. The products were analyzed using 20% urea – acrylamide gel and radiolabeled products were visualized by autoradiography.

4.2.7. BPDE treatment of UVB-irradiated CRL-2522 cells

CRL-2522 cells were exposed to 0.00 or 0.12 J/cm^2 UVB light as described above. After UVB radiation, cells were washed with 1×PBS twice and then incubated in the growth medium with or without BPDE for 35 min. Concentrations of BPDE in the medium were 0, 1 and 2 μM. After a designated period of incubation, cells were washed twice with 1×PBS and trypsinized using 0.25% Trypsin-EDTA solution (Invitrogen™ Life Technologies). Cells were harvested into 1 mL microcentrifuge tubes and DNA was extracted by following the procedure provided in the Trevigen® isolation kit. Concentrations of the cellular DNA were measured at 260 nm and 280 nm and purity of isolated DNA was assessed by measuring A$_{260}$/A$_{280}$. The ratio of A$_{260}$/A$_{280}$ was 1.8 - 2.0, which is considered to be protein-free. Extracted DNA was tested for the presence of BPDE adducts.

CRL-2522 cells were also initially exposed to BPDE in the growth medium for 35 min and then exposed to UVB light. Concentrations of BPDE in the growth medium and UVB doses used were the same as mentioned above.

Extracted DNA (see above) was analyzed for the presence of CPD photoproducts.

4.2.8. Detection of BPDE-adducts in cellular DNA

A modified CE-LIF immunoassay was used to detect BPDE-adducts in cells [10- 13]. An aliquot of DNA was heat-denatured at 95 °C for 10 minutes and then put on ice to prevent reannealing of DNA. Denatured DNA was incubated with anti-BPDE antibody and incubated at room temperature for 30 minutes. CE separation conditions were the same as for detection of UV lesions described above.

4.3. Results and Discussion

Previous chapters outlined the development of the assay for detection and measurement of CPD and 64PP photoproducts in UVB irradiated isolated DNA. The main focus was detection of CPDs formed after UVB radiation at environmentally relevant doses (< 0.3 J/cm^2). Here the results of detection and measurements of CPD lesions in UV irradiated cultured CRL-2522 cells are presented.

4.3.1. Detection of CPD and 64PP lesions in DNA extracted from UVB irradiated CRL-2522 cells

Figure 4.1 shows a series of electropherograms from the CE-LIF

immunoassay of cellular DNA extracted from CRL-2522 cells that were irradiated at UVB doses between 0.0 and 0.3 J/cm^2. These doses were chosen based on the daily average exposure of Canadians in Edmonton, AB [52, 53]. Figure 4.1 shows that at higher UVB doses, the complex peak (Ab*-DNA) significantly broadens and partially shifts from a migration time of ~2.2 minutes towards a shorter migration time of ~1.4 min. A similar pattern for the complex Ab*-DNA was observed for cells irradiated at higher doses in repeat experiments (results not shown).

UVB-radiation induces both single and double strand breaks (SSBs and DSBs) in DNA [14]. A CPD is a major source of UV-induced DNA breaks [15]. Jiang *et al.* [16] detected SSBs and DSBs in supercoiled plasmid DNA using AFM imaging and showed that SSBs (relaxed plasmid) mainly formed at much lower UVB doses than DSBs (linear plasmid). Even though research in [16] has been conducted at higher UVB doses than those used in this study (0 – 60 J/cm^2), a slightly different configuration in plasmids was noticed at 0.14 J/cm^2. Jiang *et al.* [16] assumed this was due to background of damaged DNA in the chosen sample. Working at low UVB doses (0 - 0.3 J/cm^2), we most likely did not induce DSBs but probably did induce SSBs. The shift of the complex peak toward shorter migration times suggests the complex formation between the antibody and shorter DNA. Since we denatured the DNA prior to its incubation with $*F_{ab}$-KTM-53, we realized that denaturing may have created shorter DNA only if breaks were present. Therefore the results from the CE-LIF-based immunoassay also indicate the presence of

UVB-induced SSBs and our findings are consistent with results from the literature [14 - 16].
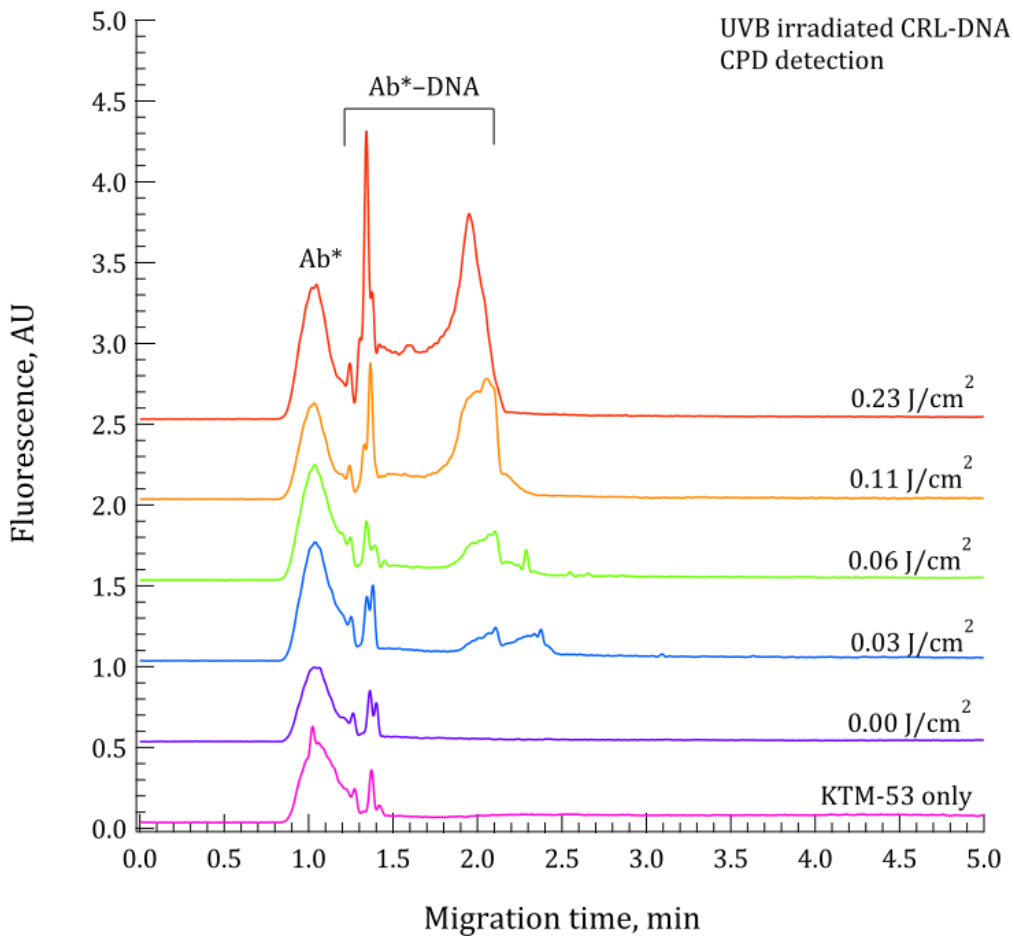
Figure 4.1. Representative electropherograms from CE-LIF immunoassay for CPD in DNA of UVB irradiated CRL-2522 cells

Peak Ab* shows the signal from antibodies.

Peak Ab*-DNA shows the signal from complex formed between the antibodies and CPD lesions in the DNA of CRL-2522 cells.

Figure 4.2 shows electropherograms corresponding to the detection of 64PP in UVB irradiated cells. The behavior of the electropherograms is similar to those for CPD detection. The complex peak also shifts slightly towards shorter migration times with the increase in UVB dose. The main difference between the CPD and 64PP electropherograms is a high background for the control sample when detecting 64PPs. These results are similar to those observed for HP-DNA and CT-DNA samples (Figure 2.12).

Figure 4.3 shows dose response results obtained from Figures 4.1 and 4.2. The dose response once again shows a much higher background signal for 64PP compared to CPD in the un-irradiated control sample. Although the high background signal from the assay for 64PP makes determination of 64PP in the cellular DNA unreliable, the data are shown here for comparison. The main focus here is on the assay for CPD in treated cells.
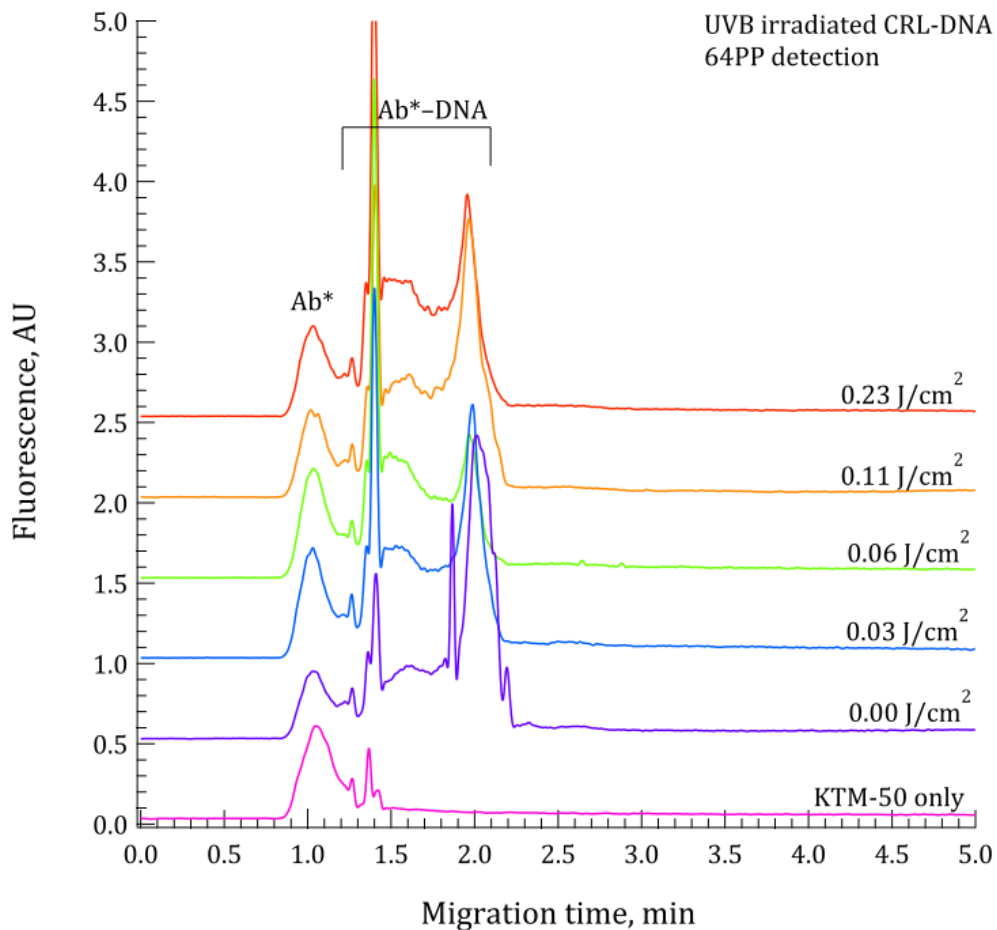
Figure 4.2. Representative electropherograms from CE-LIF immunoassay for 64PP in DNA of UVB-irradiated CRL-2522 cells

Peak Ab* shows the signal from antibodies.

Peak Ab*-DNA shows the signal from complex formed between the antibodies and 64PP lesions in the DNA of CRL-2522 cells.
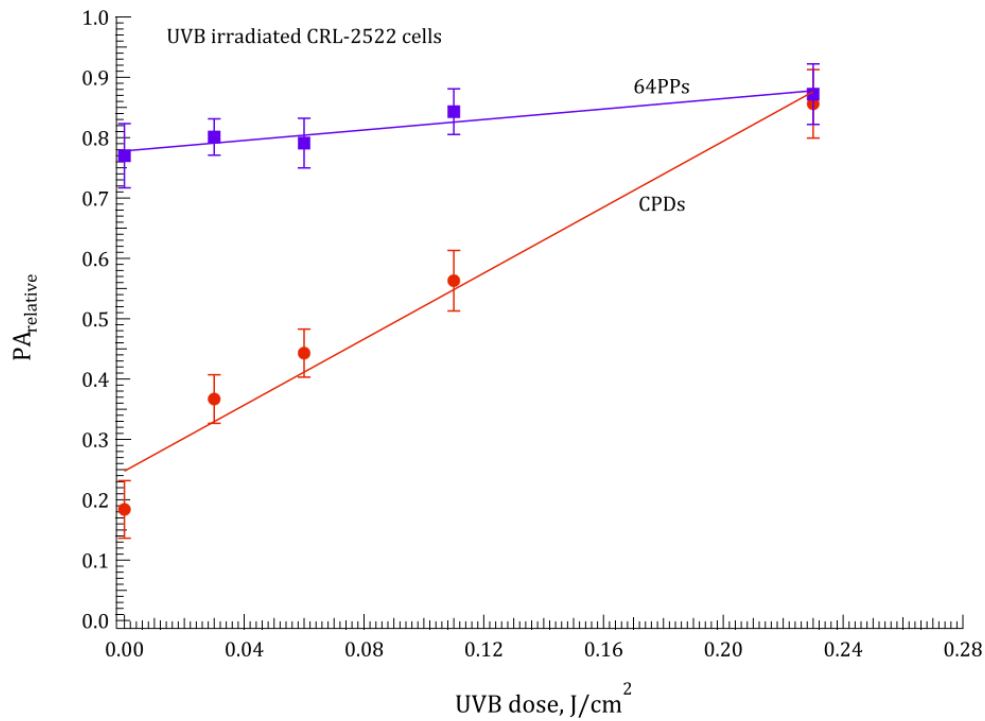
Figure 4.3. Dose response for CPD and 64PP in DNA extracted from UVB irradiated CRL-2522 cells

CPDs: dose response for CPD photoproducts
64PPs: dose response for 64PP photoproducts

Each data point represents the mean value and the error bars represent ± standard deviation from a minimum of three independent experiments done with at least two independent series of cells.

4.3.2. Quantification of CPD and 64PP lesions in UVB-irradiated CRL-2522

The calibration method described earlier (Chapter 3) was used to quantify the number of CPD lesions per 10^3 nt formed in cellular DNA as well as the yield of formation of these photoproducts. Similar calculations were performed to quantify 64PP while caution is noted due to the high background when measuring 64PP lesions.

Figure 4.4 illustrates the dose response for both CPDs and 64PPs as the number of UV-induced lesions (#UV lesions) per 10^3 nt *vs.* UVB dose. The slope of the curves is the yield of formation of CPD and 64PP photoproducts. As we can see, the yield of formation for CPD photoproducts is higher than that for 64PP (0.5 ± 0.1) in DNA extracted from UVB-irradiated CRL-2522 cells. These results (of more CPDs produced than 64PPs) are consistent with previously reported results [16, 17].

The yield of CPD formation in the cellular DNA of the CRL-2522 cells (3.6 ± 0.4 lesions per 10^3 nt per J/cm^2, Figure 4.4) is approximately 7 times lower than that in the naked calf-thymus DNA (26.8 ± 1.4 lesions per 10^3 nt per J/cm^2, Figure 3.15). The lower yield of CPD formation in the cells than in the naked DNA is consistent with the fact that the cellular DNA is protected by other cellular components.
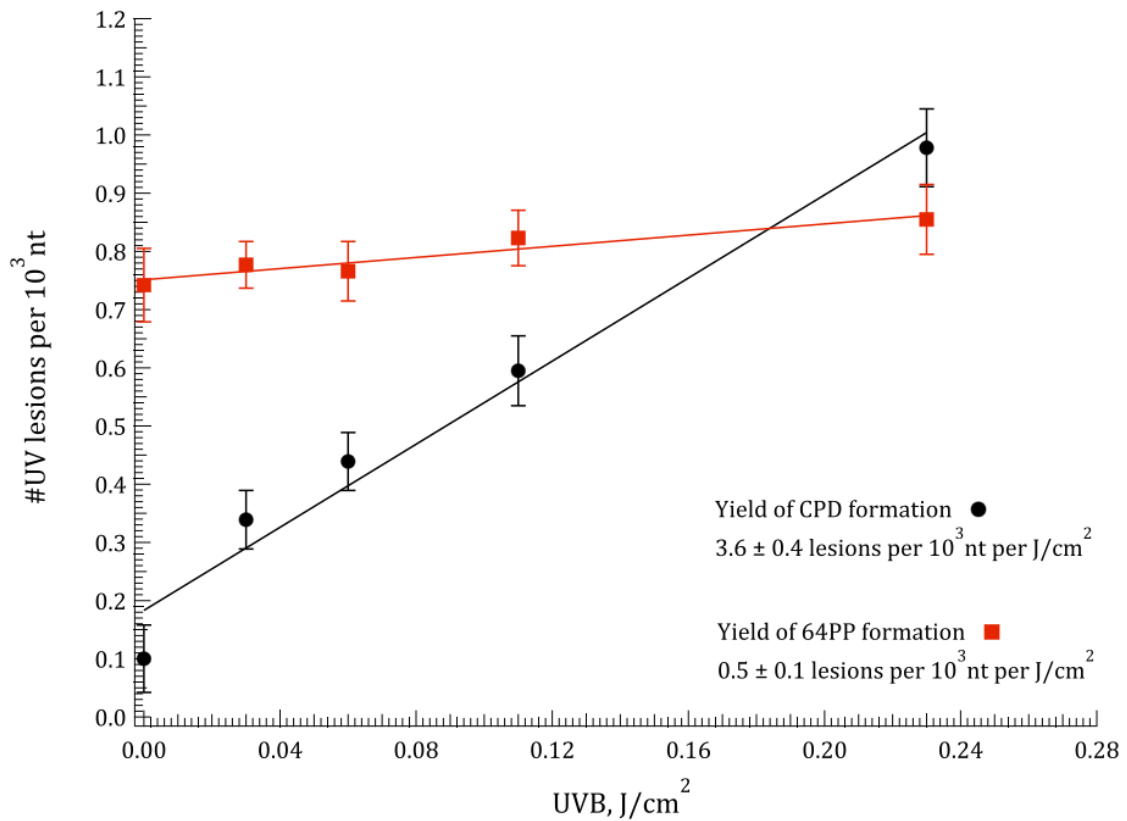
Figure 4.4. Yield of formation of CPD and 64PP in DNA extracted from UVB irradiated CRL-2522 cells

Yield of CPD formation calculated from experimental results

Yield of 64PP formation calculated from experimental results

Each data point represents the mean value and the error bars represent ± standard deviation from a minimum of three independent experiments done with at least two independent series of cells.

Table 4.1 compares the yield of CPD formation obtained in this work with those reported in the literature. These results fall within the same order of magnitude. However, there are noticeable differences between the cell types and the type of CPD measured. These differences between our results and the literature values may be attributed to: the source of irradiation; different DNA sequences in different cells; and differing experimental conditions. Different sources of UV light (e.g. different brands, filters used, etc.) may noticeably affect the formation of UV damage as illustrated by the UV damaging spectra for DNA [21-23]. Also the amount and type of UV-lesions is sequence dependent. Therefore the differences in DNA sequence may also contribute to the varying yields of CPD formation. Lastly, in [16] different yields of formation were reported for the same cells irradiated under the same conditions (Table 4.1), with the exception that the number of cells per cm^2 exposed to UV light was varied (same number of cells were placed in two differently sized Petri dishes). Cells of higher density resulted in a lower yield of CPD formation. The density of cells in our experiments was lower than that used in [16]. Thus slightly higher yields of formation of CPD could be expected.

Table 4.1. Yield of formation of CPD photoproducts[‡] (lesions per 10^3 nt per J/cm^2) formed in DNA after UVB irradiation of cells

Sample type	Dose range	Type of CPD	Yield of CPDs	Method used
Human CRL-2522 cells [this work]	0.0 – 0.25 J/cm^2	all	3.6 ± 0.4	CE-LIF
Human THP1 cells [18]	0.0 – 0.10 J/cm^2	all	5.5	HPLC-MS/MS
Human THP1 cells [16]	0.0 – 0.06 J/cm^2	TT	3.1* 0.8**	HPLC-MS/MS
Human dermal fibroblasts [18]	0.0 – 0.13 J/cm^2	TT and CT	4.85	HPLC-MS/MS
CHO cells [19]	0.0 – 0.10 J/cm^2	all	2.0	Immunodot-blot
Skin [20]	0.0 – 0.20 J/cm^2	all	0.52 ± 0.08 11.3 ± 1.8	HPLC-MS/MS
Keratinosytes cultured from skin [20]				

(‡) - units for the yield in the original papers were changed to lesions per 10^3 nt per J/cm^2

(*) - yield measured for UVB radiated cells with density of 1×10^6 cells per cm^2

(**) - yield measured for UVB radiated cell with density of 6×10^6 cells per cm^2

Note: numbers in brackets indicate the cited references.

4.3.3 Detection limits of the method toward CPD detection in DNA

The detection limits were determined from a series of experiments: (i) CPDs were detected in DNA extracted from irradiated cells at different UVB doses; (ii) CPDs were analyzed in the samples of different DNA concentrations. The concentrations of DNA varied form 5 µg/mL to 25 µg/mL. Figure 4.5 shows the curves used to estimate the detection limits using different DNA concentrations. The definition for detection limits used for this assay was defined as the sum of the average of the $PA_{relative}$ for the control samples (cells not UV-irradiated) plus three standard deviations (3σ) from the control sample runs [54]. The lower dotted line on the graph represents the $PA_{relative}$ for the control CRL-DNA. The upper dotted line is the average of $PA_{relative}$ for the control samples plus three standard deviations (3σ) obtained from a minimum of three $PA_{relative}$ results for the control samples. The dotted upper trace is the estimated detection limits of the method.

Table 4.2 summarizes the results of the minimum UVB dose at which CPD photoproducts could be reliably detected, which corresponded to ~0.2 fmol of CPD lesions detected in the capillary.
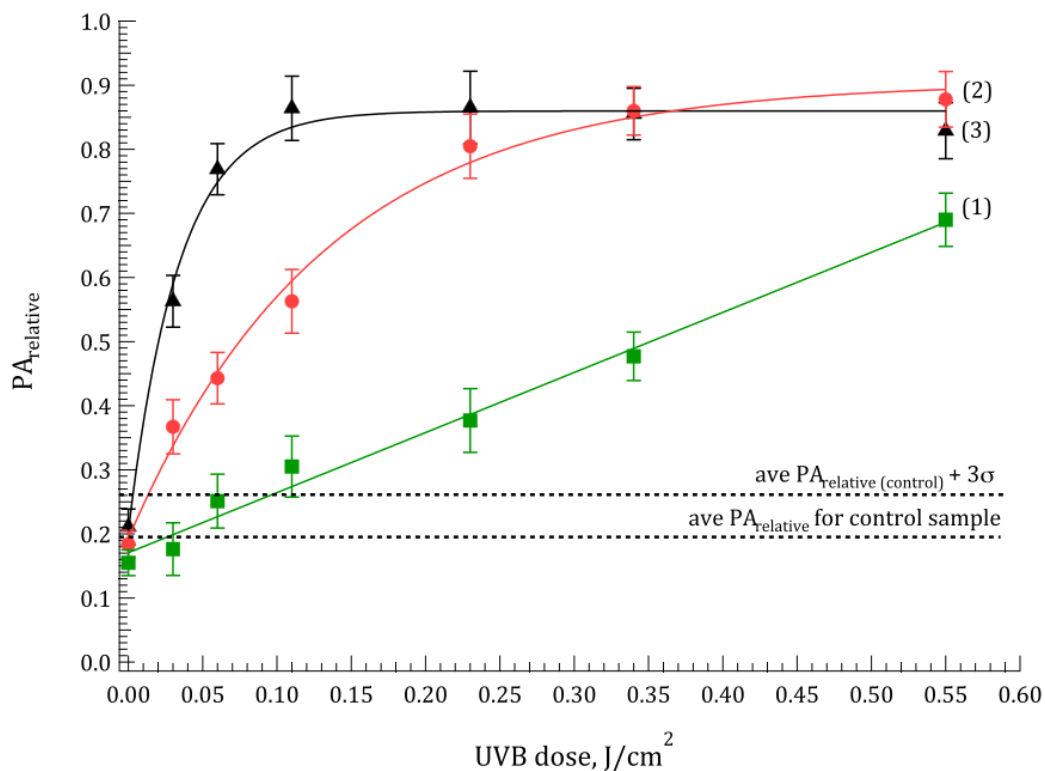
Figure 4.5. Dose response curves for CPD lesions in DNA from UVB-irradiated CRL-2522 cells. Different DNA concentrations were used for the CE-LIF immunoassay*

(1) – [DNA] = 5 µg/ml; (2) – [DNA] = 10 µg/ml; (3) – [DNA] = 25 µg/ml

(*) – concentrations of DNA in the sample vials

Intersection between upper dotted line and the curve represents the minimum UVB dose where CPDs lesions were detected.

Each data point represents the mean value and the error bars represent ± standard deviation from a minimum of three independent experiments done with at least two independent series of cells.

Note: the lines connecting data points serve to show trends. The lines were not generated from any data-fitting program.

Table 4.2. Minimum UVB dose needed to detect CPDs in cellular DNA of CRL-2522 cells when different DNA concentrations were used for CE-LIF immunoassay

Concentration of DNA in the sample (µg/mL)	UVB dose, J/cm²	Amount of CPD*
5	>0.10	
10	0.02	0.2 fmol
25	< 0.01	

(*) Minimum reliably detected amount of CPD lesions. This value was calculated using the calibration method described in Chapter 2.

$PA_{relative}$ used was the average of $PA_{relative}$ plus three standard deviations (3σ) from the control samples.

1 fmol = 10^{-15} mol.

To estimate the minimum amount of DNA with detectable CPD lesions using the CE-LIF immunoassay, the concentration of DNA in the sample vial was recalculated to the amount of DNA injected into the capillary. Figure 4.6 illustrates how minimum amounts of DNA, extracted from the UVB-irradiated cells, were obtained. Similar to Figure 4.5, the lower dotted line in Figure 4.6 represents the $PA_{relative}$ for the control sample and the upper dotted line represents the average $PA_{relative}$ for the control sample plus three standard deviations (3σ) obtained from a minimum of three $PA_{relative}$ results for the control samples.
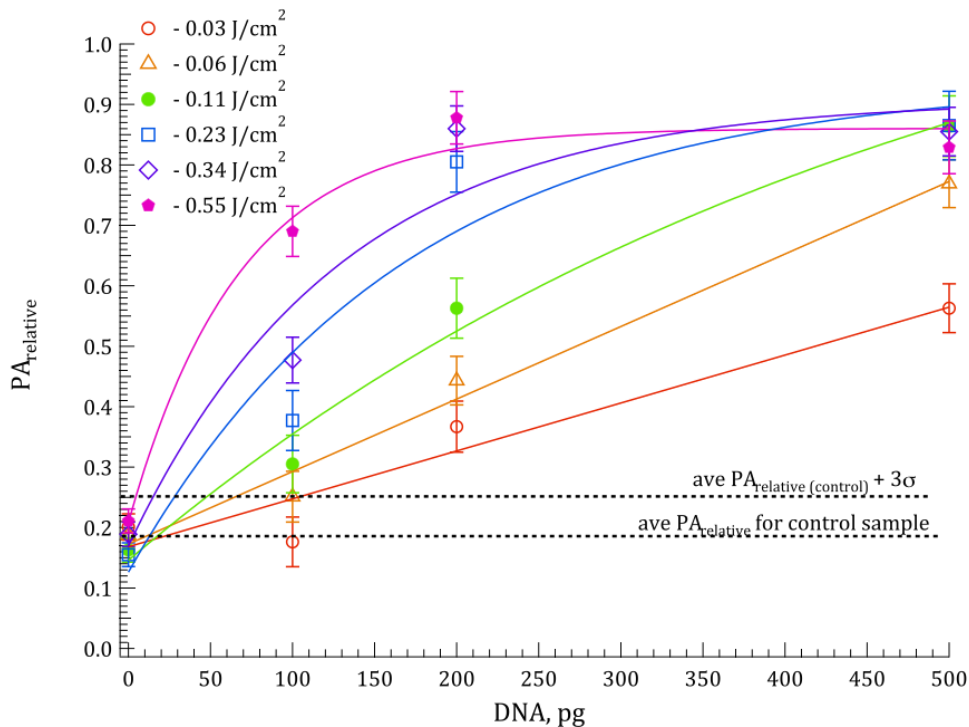
Figure 4.6. Concentration curves for CPD lesions in DNA from UVB-irradiated CRL-2522 cells. DNA samples corresponding to different UVB dose irradiation were used for the CE-LIF immunoassay

Intersection between upper dotted line and the curve represents the minimum amount of CRL-DNA where CPDs lesions were detected.

Each data point represents the mean value and the error bars represent ± standard deviation from a minimum of three independent experiments done with at least two independent series of cells.

Note: the lines connecting data points serve to show trends. The lines were not generated from any data-fitting program.

Table 4.3 shows the summary of data corresponding to the minimum amount of DNA and UVB doses at which CPD lesions were reliably detected. It is clear that detection limits for this method are dependent upon the dose of UV light. Using CE-LIF immunoassay, CPD photoproducts in UVB irradiated cells at the environmentally relevant doses can be detected at 3 – 10 attomol levels of DNA. The detection limits for this method are significantly lower (15 – 100 pg of DNA) than those for other immunoassays (1 – 10 ng of DNA).

Table 4.3. Minimum amount of cellular DNA of UVB-irradiated CRL-2522 cells in which CPD lesions were detected using CE-LIF immunoassay

UVB dose (J/cm²)	Mass DNA* (pg)	Amount of DNA (attomoles**)
0.03	100	3
0.06	70	2
0.11	50	1.5
0.23	30	0.9
0.34+	< 15	< 0.4

(*) Mass of injected DNA in the capillary. It is calculated based on the DNA concentration in the sample and injection conditions (time and voltage).

(**) Calculated knowing the mass of DNA in the capillary and using an approximate length of DNA as 150,000 bases (1 attomole = 10^{-18} mole)

Table 4.4 shows the summary of reported detection limits (minimum amount of detected CPD lesions) for different methods used to detect CPD lesions. The detection limits for our developed CE-LIF immunoassay compare favorably to those reported in the literature [24-30]. Importantly, our CE-LIF immunoassay has achieved this detection limit, while using 10 times less DNA than these other methods require. The minimum doses of UV radiation required to produce detectable CPD is also lower for the CE-LIF immunoassay than for these other assays [24-30].

Table 4.4. Comparison of various techniques used to detect CPD lesions in UV-irradiated DNA samples*

Technique	DNA type	Sensitivity (fmol[‡] of CPDs)	Reference
[32]P-postlabeling	isolated DNA	low fmol range	[24, 25]
ELISA	cellular DNA	0.9 fmol	[26]
alkaline gel electrophoresis	cellular DNA	tenths of fmol	[27]
GC-MS	isolated DNA	20 – 50 fmol	[28]
voltammetry	plasmid DNA	low fmol	[29]
HPLC-MS/MS	isolated and cellular DNA	low tenth of fmol	[30]
CE-LIF immunoassay	isolated and cellular DNA	< 0.5 fmol	This work

(*) table partially adopted from [29]

(‡) 1 fmol = 10^{-15} mol

4.3.4. ^{32}P-postlabeling assay

[32]P-postlabeling assays have been used earlier for detection of CPD and 64PP in UV irradiated DNA [31, 32]. Thus we used this assay to measure CPD photoproducts in DNA extracted from UVB-irradiated CRL-2522 cells.

Briefly, CRL-DNA samples were digested with the digestion mixture overnight at 37 °C. Then proteins were removed by precipitation from ice-cold ethanol. The recovered DNA was taken to dryness, re-dissolved in water and incubated at 100 °C for 5 minutes to remove residual phosphatase activity. Digested DNA was then enzymatically phosphorylated to introduce ^{32}P using γ-^{32}P-ATP. The products were analyzed using 20% urea – acrylamide gel and radiolabeled products were visualized by autoradiography. Figure 4.7 shows an example of an autoradiogram of the gel.

dT$_{16}$ 0.0   0.04   0.08   0.16   0.24   0.25   0.33   J/cm^2

dT$_{16}$

UV-damage

ATP

ATP products
hydrolyzed
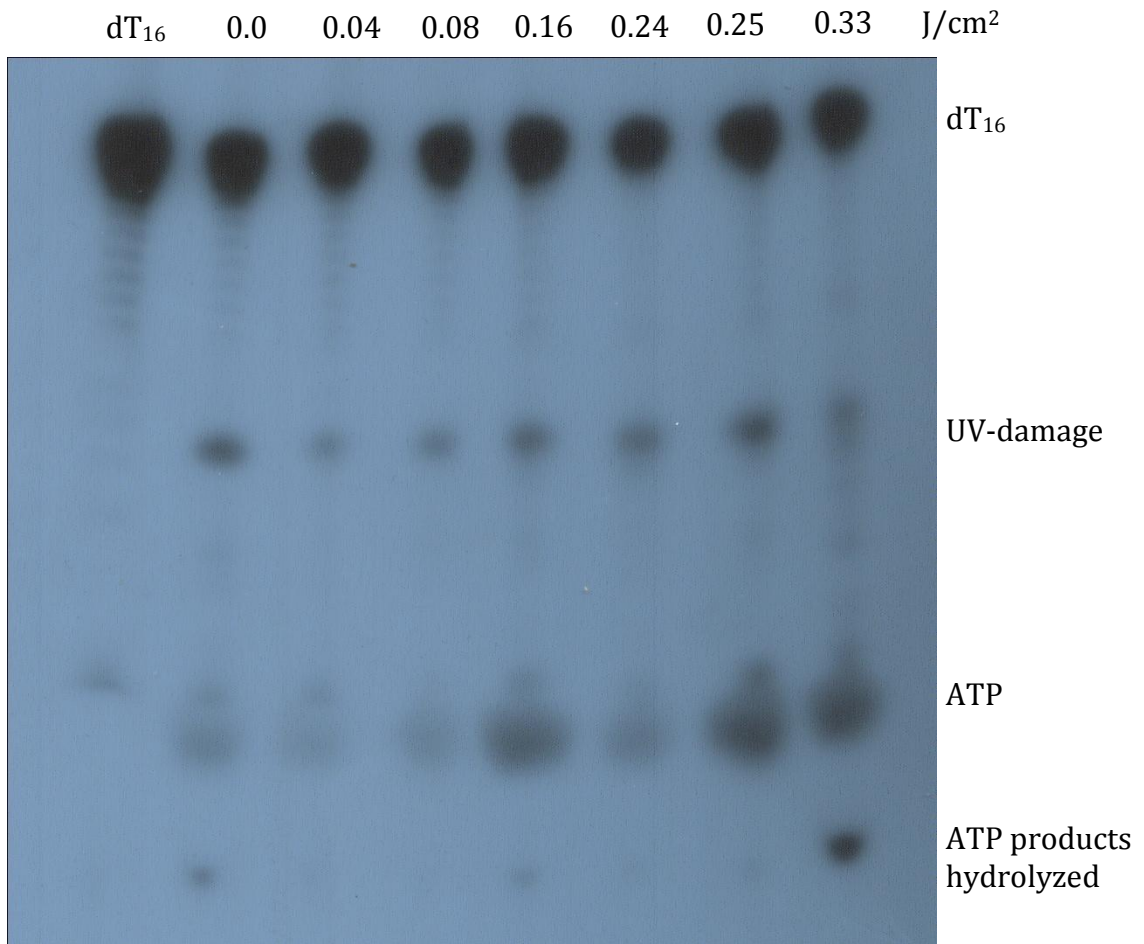
Figure 4.7. Autoradiogram of a polyacrylamide gel showing the ^{32}P-labeled products from cellular DNA of UVB-irradiated CRL-2522 cells

The same DNA samples were analyzed using CE-LIF.

In the autoradiogram the UV-damage bands have the same intensity throughout the samples, which is similar to the background. The same samples were analyzed using CE-LIF immunoassay and gave good damage response to CPD-products (Figure 4.4). The amount of DNA visualized by autoradiogram was 7 ng, which is higher than the minimum amount of DNA used in the CE-LIF immunoassay (Table 4.3). Either the amount of DNA used in the ^{32}P-postlabeling was too low or the amount of CPD lesions was below the detection limits of the ^{32}P-postlabeling method to pick up the difference in the radioactive signal from the background.

To ensure the detection of CPD lesions produced by UVB radiation of low doses, oligo dT$_3$ was UVB irradiated. ^{32}P-postlabeling was used to measure CPD photoproducts in UVB-irradiated poly-dT$_3$ (autoradiogram is not shown). The dose response was measured using the relative radioactivity counts (Figure 4.8). At doses lower than 0.4 J/cm^2, the signal is very similar to the background. Using the CE-LIF immunoassay, however, we are able to detect CPD in both naked and cellular DNA following radiation of the DNA or cells at the doses below 0.3 J/cm^2 (Figure 3.15 and Figure 4.4). From our experiments, CPD formation in naked CT-DNA (yield = 26.8 ± 1.4 CPDs per 10^{3}nt per J/cm^2) is 7 times higher than the formation of CPD lesions in cellular DNA (yield = 3.6 ± 0.4 CPDs per 10^{3}nt per J/cm^2). It is clear that CE-LIF immunoassay was much more sensitive for CPD detection in the same type of DNA samples compared to ^{32}P-postlabeling. However, it does not

144

mean that ^{32}P-postlabeling cannot be highly sensitive toward detection of other DNA adducts [33, 34].
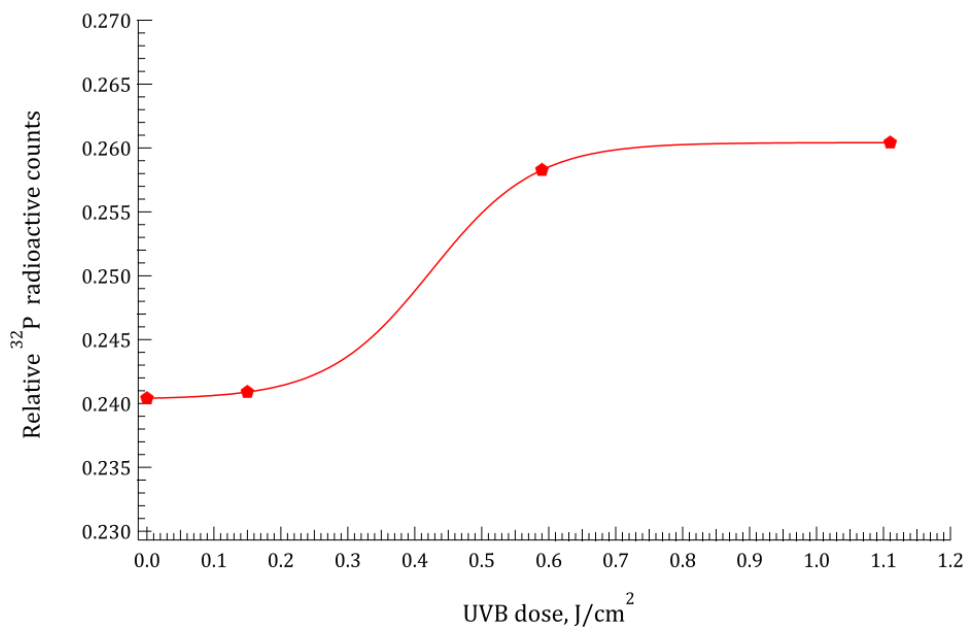
Figure 4.8. Dose response of CPD photoproducts in poly-dT$_3$ exposed to low UVB doses

Relative ^{32}P radioactive counts were calculated as a ratio of counts from the bands cut out of the gel (at a specific UVB dose) over the total radioactive counts from all bands cut out of the gel.

Note: the lines connecting data points serve to show trends. The lines were not generated from any data-fitting program.

4.4. Combined exposure of CRL-2522 cells to BPDE and UV light

DNA exposure to damaging reagents usually leads to the formation of adducts that are repaired by the cells [35]. Unrepaired adducts may introduce mutations during DNA replication. The type of induced mutations depends on many factors, such as the nature of the induced damage, efficiency of repair of the damage, the sequence where the damage occurred, etc. [36-38]. In many cases, exposure occurs as a complex combination of mutagens. Limited research has been done in the area of combinations of mutagens. For example, the combined exposures to UV light were mostly studied in Salmonella [39]. It is also possible that the damage and mutation induction by a specific agent can be altered in the presence of another agent. For instance, it has been demonstrated that N-nitrosodialkylamines are activated by irradiation with near UV light (UVA, 320 – 400 nm) causing increased mutations in DNA [40, 41].

Benzo[a]pyrene diol epoxide (BPDE) is carcinogenic and a metabolite of benzo[a]pyrene (B[a]P) in humans. B[a]P is a polycyclic aromatic hydrocarbon (PAH) and is commonly found in cigarette smoke, burnt food and smoke from the burning of fossil fuels. BPDE covalently binds to DNA at guanines and is known to induce mutagenicity and carcinogenicity [42-45].

UV light is a known mutagen and carcinogen as well [46-48] due to formation of CPD and 64PP lesions that induce GC→AT transitions.

Studies of the combined effect of PAH and UV exposure in aquatic organisms [49, 50] suggest that these two factors may have a combined toxic effect. Thus the combination of UV-light and PAH may be harmful for people working in an environment where they can be exposed to both factors, e.g. road maintenance workers.

A few papers reported on the mutation spectra from the combination of BPDE and UV light [50, 51]. In these studies, the mutation frequency in DNA exposed to BPDE + UV was higher than the mutation frequency in DNA exposed to BPDE alone or UV alone. BPDE + UV exposed DNA displayed the presence of both UV signature mutations (mainly GC $\rightarrow$ AT transitions) and BPDE signature mutations (mainly GC $\rightarrow$ TA transversions). Since results in [50] showed significant absolute increase in BPDE signature transversions, but not an absolute increase in UV photolesions, two possible reasons have been suggested: (i) the BPDE adducts are photoactivated to more mutagenic lesions; or (ii) the presence of UV-induced lesions enhanced the mutagenicity of the BPDE adducts. Reference [51] showed that the BPDE mutagenicity is enhanced in the presence of the UV-induced lesions. Results of this work led us to hypothesize that enhanced mutagenicity of BPDE adducts could be due to increased amounts of either BPDE adducts or UV-lesions in DNA. In a preliminary study to test this hypothesis we applied our newly developed

CE-LIF immunoassay to monitor whether the amounts of both lesions change in the presence of both agents.

Two sets of combination treatment were carried out. In the first set of experiments CRL-2522 cells were incubated in the growth medium with BPDE (0 – 2 μM) for 35 min and then UVB irradiated (0.00 J/cm^2 and 0.12 J/cm^2). Figure 4.9 shows the CPD detection in DNA extracted from treated CRL-2522 cells. In the second set of experiments, CRL-2522 cells were UVB irradiated (0.00 J/cm^2 and 0.12 J/cm^2) first and then incubated in the growth medium with BPDE (0 – 2 μM) for 35 min. Figure 4.10 shows the BPDE adducts detection in DNA extracted from these treated CRL-2522 cells. From Figure 4.9 we see that CPDs increase with an increase of the UVB dose, but the presence of the BPDE in the growth medium did not affect the amount of photoproducts formed. Figure 4.10 shows an increase in the formation of BPDE adducts with increase in the concentration of BPDE in the growth medium. However, the irradiation of the cells with UVB did not significantly change the amount of BPDE adducts in the DNA. These results suggest that increase in mutagenicity of BPDE adducts in cells that underwent combined treatment of BPDE and UVB radiation, is more likely due to formation of both types of DNA damage (BPDE-DNA adducts and UV lesions) and was less likely due to the enhanced formation of one type of damage by the other type of treatment.
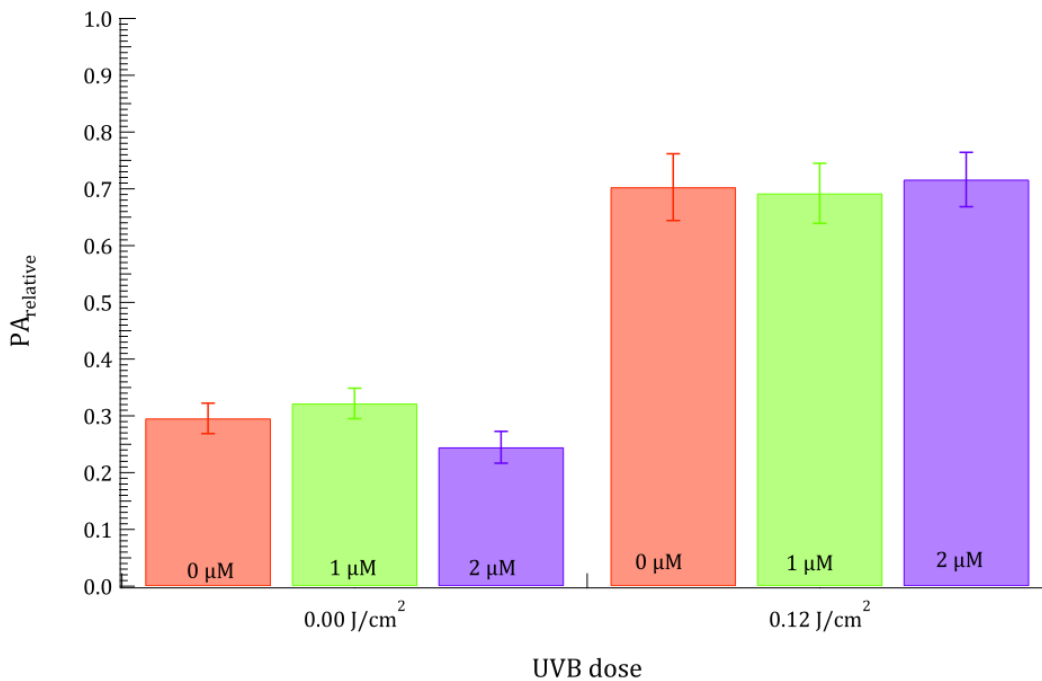
Figure 4.9. Detection of CPD photoproducts in DNA extracted from BPDE exposed and UVB irradiated CRL-2522 cells

BPDE concentration in MEM was 0, 1 and 2 μM;

UVB exposure was 0.00 and 0.12 J/cm^2.

CRL-2522 cells were exposed to BPDE in the growth medium for 35 minutes and then UVB-irradiated.

Each bar point represents the mean value and the error bars represent $\pm$ one standard deviation from a minimum of three independent experiments done with at least two independent series of cells.
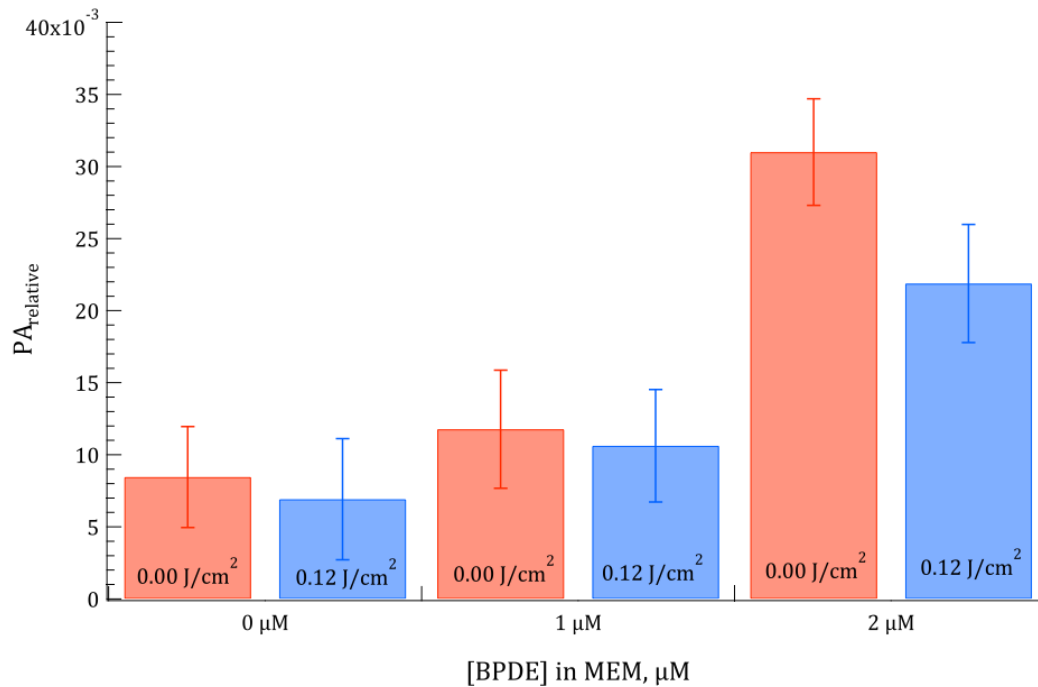
Figure 4.10. Detection of BPDE-DNA adducts in DNA extracted from UVB irradiated and BPDE-exposed CRL-2522 cells

BPDE concentration in MEM was 0, 1 and 2 μM;
UVB exposure was 0.00 and 0.12 J/cm^2.

CRL-2522 cells were UVB-irradiated first and then exposed to BPDE in the growth medium for 35 minutes.

Each bar point represents the mean value and the error bars represent $\pm$ one standard deviation from a minimum of three independent experiments done with at least two independent series of cells.

4.5. Conclusions

Using our CE-LIF based immunoassay, we successfully determined CPD lesions in CRL-2522 cells after UVB radiation at low doses (< 0.3 J/cm^2) relevant to environmental exposure.

The CE-LIF assay was also shown to be applicable for studies that involve the combined effects of two DNA-damaging agents, UV light and BPDE. The BPDE adducts and UV lesions were measured in CRL-255 cells after the combined exposure to both agents. Comparison of results between non-combined and combined exposures did not show significant differences between formation of BPDE adducts and UV lesions in cells.

[32]P-postlabeling experiments were not sensitive enough to measure CPD lesions in our samples. The detectable limit of our CE-LIF assay was ~0.2 fmol, which compares favorably with other methods [26-32] and our assay requires 10 times less DNA.

The yield of CPD formation in UVB-irradiated CRL-2522 cells was 3.6 ± 0.4 lesions per 10^3 nt per J/cm^2. This is about 7 times lower than that for the naked CT-DNA (yield 26.8 ± 1.4 CPD per 10^3 nt per J/cm^2). These results are consistent with previous understanding of the protection of DNA afforded by cells.

Yield of formation for CPD lesions was found to be ~2.5× higher than the yield of formation for 64PP lesions, which is consistent with previous

results [16, 17]. The determination of 64PP lesions in the cellular DNA using the CE-LIF immunoassay is considered preliminary because of the high background from the cellular DNA of the un-irradiated cells. This problem must be dealt with before quantitative measurements of 64PP lesions can be performed.

4.6. References

1. C.S. Cochell and G. Horneck (2001), The history of the UV radiation climate of the earth-theoretical and space-based observations, Photochem. Photbiol., *73*, 447-451.

2. E.C. Friedberg, Correcting the blueprints of life: a historical account of the discovery of DNA repair mechanisms, Cold Spring Harbor Laboratory Press, Plainview, NY, 1997.

3. V.O. Melnikova and H.N. Ananthaswamy (2005), Cellular and molecular events leading to the development of skin cancer, Mutat. Res., *571*, 91-106

4. R.B. Setlow and W.L. Carrier (1966), Pyrimidine dimers in ultraviolet irradiated DNA's, J. Mol. Biol., *17*, 237-254.

5. D.L. Mitchell (1988), The relative cytotoxicity of (6-4) photoproducts and cyclobutane dimers in mammalian cells, Photochem. Photobiol., *48*, 51-57

6. D.L. Mitchell and R.S. Nair (1989), The biology of the 6-4 photoproducts, Photochem. Photobiol., *49*, 805-819.

7. E. Sage (1993), Distribution and repair of photolesions in DNA: genetic consequences and the role of sequence context, Photochem. Photobiol., *57*, 163-174.

8. D.E. Brash (1988), UV mutagenic photoproduct in Escherichia coli and human cells: a molecular genetics perspective on human skin cnacer, Photochem. Photbiol., *48*, 59-66.

9. D.L. Mitchell, J. Jen and J.E. Cleaver (1992), Sequence specificity of cyclobutane pyrimidine dimers in DNA treated with solar (ultraviolet B) radiation, Nucleic Acid Res., 20, 225-229.

10. X.C. Le, J.Z. Xing, J. Lee, S.A. Leadon and M. Weinfeld (1998), Inducable repair of thymine glycol detected by an ultrasensitive assay for DNA damage, Science, *280*, 1066-1069.

11. H. Wang, M. Lu, N. Mei, J. Lee, M. Weinfeld and X.C. Le (2003), Immunoassays using capillary electrophoresis laser induced fluorescence détection for DNA adducts, Anal. Chim. Acta, *500*, 13-20.

12. S. Shen, J. Lee, X. Sun, H. Wang, M. Weinfeld and X.C. Le (2006), Elevation of cellular BPDE uptake by human cells: A possible factor contributing to co-carcinogenicity by arsenite, Environ. Health Perspectives, *114*, 1832-1837.

13. S. Shen, Arsenic effects on the formation and repair of benzo(a)pyrene diol epoxide-DNA adducts, Ph.D. thesis, Edmonton, AB, 2006.

14. Y. Jiang, C. Ke, P.A. Mieczkowski and P.E. Marszalek (2007), Detecting ultraviolet damage in single DNA Molecules by atomic force microscopy, Biophysical Journal, *93*, 1758-1767.

15. G.A. Garinis, J.R. Mitchell, M.J. Moorhouse, K. Hanada, H. de Waard, D. Vandeputte, J. Jans, K. Brand, M. Smid, P. van der Spek, J.H.-J. Hoeijmakers, R. Kanaar and G.T.-J. van der Horst (2005), Transcriptome analysis reveals cyclobutane pyrimidine dimers as a major source of UV-induced DNA breaks, The EMBO J., *24*, 3952-3962.

16. T. Douki, M. Court, S. Sauvaigo, F. Odin and J. Cadet (2000), Formation of the main UV-induced thymine dimeric lesions within isolated and cellular DNA as measured by high performance liquid chromatography-tandem mass spectrometry, J. Biol. Chem, *275*, 11678-11685.

17. T. Douki and J. Cadet (2001), Individual determination of the yield of the main UV-induced dimeric pyrimidine photoproducts in DNA suggests a high mutagenicity of CC photolesions, Biochemistry, *40*, 2495-2501.

18. S. Courdavault, C. Baudouin, S. Sauvaigo, A. Mouret, S. Candéias, M. Charveron, A. Favier, J. Cadet and T. Douki, (2004), Unrepaired cyclobutane pyrimidine dimers do not prevent proliferation of UV-B-irradiated cultured human fibroblasts, Photochem. Photobiol., *79*, 145-151.

19. D. Perdiz, P. Gróf, M. Mezzina, O. Nikaido, E. Moustacchi and E. Sage, (2000), Distribution and repair of bipyrimidine photoproducts in solar UV-irradiated mammalian cells, J. Biol. Chem., 275, 26732-26742.

20. S. Mouret, C. Baudouin, M. Charveron, A. Favier, J. Cadet and T. Douki (2006), Cyclobutane pyrimidine dimers are predominant DNA lesions in whole human skin exposed to UVA radiation, Proc. Natl. Acad. Sci., *103*, 13765-13770.

21. D.L. Mitchell and B.S. Rosenstein (1987), The use of specific radioimmunoassay to determine action spectra for thephotolysis of (6-4) photoproducts, Photochem. Photobiol., *45*, 781-786.

22. S.E. Freeman, H. Hacham, R.W. Gange, D.J. Maytum, J.C. Sutherland and B.M. Sutherland (1989), Wavelength dependence of pyrimidine dimer formation in DNA of human skin irradiated in situ with ultraviolet light, Proc. Natl. Acad. Sci. U.S.A., *86*, 5605-5609.

23. H.C. Birnboim (1975), Ultraviolet-induced pyrimidine dimers in long pyrimidine tracts from L-cell DNA, Photochem. Photobiol., *22*, 71-73.

24. V.J. Bykov, R. Kumar, A. Forsti and K. Hemminki (1995), Analysis of UV-induced DNA photoproducts by ^{32}P-postlabeling, Carcinogenesis, *16*, 113-118

25. V.J. Bykov and K. Hemminki (1995), UV-induced photoproducts in human skin explants analyzed by TLC and HPLC-radioactivity detection, Carcinogenesis, *16*, 3015-3019.

26. M.S. Cooke, I.D. Podmore, N. Mistry, M.D. Evans, K.E. Herbert, H.R. Griffiths and J. Lunec (2003), Immunochemical detection of UV-induced DNA damage and repair, J. Immunol. Methods, *280*, 125-133.

27. S.E. Freeman, A.B. Blackett, D.C. Monteleone, R.B. Setlow, B.M. Sutherland and J.C. Sutherland (1986), Quantitation of radiation-, chemical-, or enzyme-induced single strand breaks in nonradioactive DNA by alkaline gel electrophoresis: Application to pyrimidine dimers, Anal. Biochem., *158*, 119-129.

28. I.D. Podmore, M.S. Cooke, K.E. Herbert and J. Lunec (1996), Quantitative determination of cyclobutane thymine dimers in DNA by stable isotope-dilution mass spectrometry, Photochem. Photobiol., *64*, 310-315.

29. K. Cahová-Kuchaříková, M. Fojta, T. Mozga and E. Paleček (2005), Use of DNA-repair enzymes in electrochemical detection of damage to DNA bases in vitro and in cells, Anal. Chem., *77*, 2920-2927.

30. X. Liu and M.J. Smerdon (1995), A slot blot method for detection of ultraviolet photoproducts in DNA, Anal. Biochem., *229*, 323-328.

31. M. Liuzzi, M. Weinfeld and M.C. Paterson, (1989), Enzymatic analysis of isomeric trithymidylates containing ultraviolet light-induced cyclobutane pyrimidine dimers. I. Nuclease P1-mediated hydrolysis of the intradimer phosphodiester linkage, J. Biol. Chem., *264*, 6355-6363.

32. M. Weinfeld, M. Liuzzi and M.C. Paterson, (1989), Enzymatic analysis of isomeric trithymidylates containing ultraviolet light-induced cyclobutane pyrimidine dimers. II. Phosphorylation by phage T4 polynucleotide kinase, J. Biol. Chem., *264*, 6364-6370.

33. M. Stiborova, M. Rupertova, P. Hodek, E. Frei and H.H. Schmeiser (2004), Monitoring of DNA adducts in humans and ^{32}P-postlabeling methods, Collect. Czech. Chem. Commun., *69*, 476-498.

34. X.Sun, J. Nair and H. Bartsch (2004), A modified immuno-enriched ^{32}P-postlabeling method for analyzing the malondialdehyde-deoxyguanosine adduct, 3-(2-deoxy-β-D-erythro-pentofuranosyl)-pyrimido[1,2-α]purin-10(^{3}H)one in human tissue samples, Chem. Res. Toxicol., *17*, 268-272.

35. E.C. Freidberg, G.C. Walker and W. Siede (1995), DNA repair and mutagenesis, ASM Press, Washington, D.C.

36. C.A.H. Bigger, I. Ponten, J.E. Page and A. Dipple (2000), Mutational spectra for polycyclic aromatic hydrocarbons in the *supF* target gene, Mutat. Res., *450*, 75-93.

37. D.D. Levy, A.D. Magee and M.M. Seidman (1996), Single nucleotide positions have proximal and distal influence on UV mutation hotspots and coldspots, J. Mol. Biol., *258*, 251-260.

38. K.-Y. Seo, S.A. Jelinsky and E.L. Loechker (2000), Factors that influence the mutagenic patterns of DNA adducts from carcinogens, Mutat. Res*., 463*, 215-246.

39. D.M. DeMarini (1998), Mutation spectra of complex mixtures. Mutat. Res., *411,* 11-18.

40. S. Arimoto-Kobayashi, K. Kaji, G.M.A. Sweetman and H. Hayatsu (1997), Mutation and formation of methyl- and hyfroxylguanine adducts in DNA caused by N-nitrosodimethylamine and N-

nitrosodiethylamine with UVA irradiation, Carcinogenesis, *18*, 2429-2433.

41. S. Arimoto-Kobayashi, B.M. Tracey, M. Asao, H. Hayatsu and P.B. Farmer (1999), Mutation and DNA modifications in Salmonella exposed to N-nitrosodimethylamine under UVA- and sunlight-irradiation, Mutat. Res., *444*, 413-419.

42. I.B. Weinstein, A.M. Jeffrey, K.W. Jennette, S.H. Blobstein, R.G. Harris, H. Autrup, H. Kasai and K. Nakanishi (1976), Benzo[a]pyrene diol epoxides as intermediates in nucleic acid binding in vitro and in vivo, Science, *193,* 592-595.

43. D. Pruess-Schwartz, W.M. Baird, H. Yagi, D.M. Jerina, M.A. Pigott and A. Dipple, (1987) Stereochemical specificity in the metabolic activation of benzo[a]phenanthrene to metabolites that covalently bind to DNA in rodent embryo cell cultures, Cancer Res., *47*, 4032-4037.

44. M.K. Buening, P.G. Wislocki, W. Levin, H. Yagi, D.R. Thakker, H. Akagi, M. Koreeda, D.M. Jerina and A.H. Conney (1978), Tumorigenicity of the optical enantiomers of the diastereomeric benzo[a]pyrene 7,8-diol-9.10-epoxides in newborn mice: exceptional activity of (+)-7β,8α-dihydroxy-9α,10α-epoxy-7,8,9,10-tetrahydrobenzo[a]pyrene, Proc. Natl. Acad. Sci. U.S.A, *75*, 5358-5361.

45. J.-H. Yoon, L.E. Smith, Z. Feng, M.-S. Tang, C.-S. Lee and G.P. Pfeifer (2001), Methylated CpG dinucleotides are the preferential targets for G-to-T transversion mutations induced by benzo[a]pyrene diol epoxide in mammalian cells: similarities with the *p53* mutation spectrum in smoking-associated lung cancers, Cancer Res., *61*, 7110-7117.

46. D.E. Brash and W.A. Haseltine (1982), UV-induced mutation hotspots occur at DNA damage hot spots, Nature, *298*, 189-192.

47. A. Vink and L. Rosa (2001), Biological consequences of cyclobutane pyrimidine dimers, J. Photochem. Photobiol. B: Biology, *65*, 101-104.

48. R. Drouin and J.-P. Therrien (1997), UVB-induced cyclobutane pyrimidine dimer frequency correlates with skin cancer mutational hotspots in p53, Photochem. Photobiol., *66*, 719-726.

49. B.L. Boese, R.J. Ozretich, J.O. Lamberson, F.A. Cole, R.C. Swartz and S.P. Ferraro (2000), Phototoxic evaluation of marine sediments collected from PAH-contaminated site, Arch. Environ. Contam. Toxicol., *38*, 274-282.

50. M.N. Routledge, K.I.E. McLuckie, G.D.D. Jones, P.B. Farmer and E.A. Martin (2001), Presence of benzo[a]pyrene diol epoxide adducts in target DNA leads to an increase in UV-induced DNA single strand breaks and *supF* gene mutations, Carcinogenesis, *22*, 1231-1238.

51. K.I.E. McLuckie, M. Gaskell, P.B. Farmer, E.A. Martin, G.D.D. Jones and M.N. Routledge (2004), Effects of the order of exposure to a binary mixture of mutagenes on the induced mutation spectra in the *supF* gene, Mutagenesis, *19*, 137-141.

52. Environment Canada. Weather and Meteorology (last access was on February 1, 2011):
http://www.ec.gc.ca/uv/default.asp?lang=En&n=C74058DD-1

53. Tropospheric Emission Monitoring Internet Service (TEMIS), last access was on February 17, 2011:
http://www.temis.nl/uvradiation/

54. N.M. Schultz and R.T. Kennedy (1993), Rapid immunoassays using capillary electrophoresis with fluorescence detection, Anal. Chem., *65*, 3161-3165.

Chapter Five

Synthesis and characterization of a longer CPD-oligonucleotide standard

5.1. Introduction

Previous chapters described the development and successful application of a non-competitive CE-LIF assay for CPD photoproducts in isolated DNA and in CRL-2522 cells irradiated with environmentally relevant UVB doses. Using this method we were also able to find the yield of formation of CPD photoproducts in DNA using the derived calibration curves. Calibration of the method was based on the relation of $PA_{relative}$ for the complex and the number of CPD lesions found in CPD-16mer standard. A disadvantage of this method is incomplete separation of a complex peak from an antibody peak. The integration of overlapping peaks is not ideal for the quantitative analysis. To ensure more accurate integrations, special adjustments to the experimental conditions have to be performed. Unfortunately, varying adjustments in experimental conditions did not allow us to separate peaks completely (Appendix A). However a fluorescent standard, with a known amount of UV-lesions, can be used to validate the calibration of the developed non-competitive method. The advantage of having a fluorescently labeled standard is its versatile application throughout different research projects. For instance this standard can also be used to

study interactions between DNA damage and nucleotide excision repair (NER) proteins, or it may be used as a probe towards screening antibodies, etc.

In this chapter the synthesis and some characterization of fluorescently labeled standards are described.

5.2. Experimental

5.2.1. Reagents

Tris-glycine buffer solutions (TG, 25 mM Tris and 192 mM Glycine) were prepared from 10× TG buffer (Bio-Rad Laboratories, Hercules, CA, USA) by diluting with 18.2 MΩ distilled deionized water (DDW) from a Milli-Q Gradient Water System (Millipore, Nepean, ON, Canada). The pH of TG buffer for incubation was adjusted to 7.5 and the pH of the TG buffer for CE separation was 8.3.

The single-stranded 26-nucleotide long standard (26mer) with a single CPD lesion (CPD-26mer) was synthesized by the Synthetic Organic Chemistry Core Lab (University of Texas Medical Branch, USA). CPD-26mer standard had the following sequence: 5'-ACGCACGTACGA**T◇T**AGGTACGTGCGT-3'. The CPD-26mer was dissolved in 1 mL of DDW and the final concentration was measured at 260 nm using a

SmartSpec™ 3000 spectrometer (Bio-Rad Laboratories, Cambridge, MA). Smaller aliquots were stored in a -20°C freezer. All samples were also kept in the dark to prevent possible photoconversion and degradation [4-6]. Oligonucleotides (oligos) used in the ligation were synthesized by Integrated DNA Technologies (IDT, Corarville, IA, USA). Two of the oligos were fluorescently labeled at either the 5'- or 3'-end with 546-AlexaFluor® and purified by reversed-phase HPLC (Section 5.2.3). The T4 phage DNA ligation kit was purchased from Invitrogen™ Co. (Carlsbad, CA, USA).

Monoclonal anti-CPD antibody (clone TDM-2, IgG_2 type) was purchased from Cosmo Bio Co., Ltd. (Tokyo, Japan).

Acetonitrile (ACN) and tetraethylammonium acetate (TEAA) used for the mobile phase in HPLC analysis were of analytical grade and provided by Sigma-Aldrich (Oakville, ON, Canada).

5.2.2 Instrumentation

Neutral polyacrylamide gel electrophoresis used in purification of the ligation products was powered by a Bio-Rad general power supply (Hercules, CA, USA). HPLC purification was done using an Agilent 1100 HPLC system with UV-vis detector (Mississauga, ON). The laboratory-built capillary electrophoresis laser induced fluorescence (CE-LIF) system was used to detect CPD lesions in DNA standards. This system is described in detail in Chapter 2.

5.2.3. HPLC analyses of fluorescently labeled standards

Fluorescently labeled CPD*-16mer was purified using reversed-phase HPLC (Jupiter column, XS C18, 4 µm, 50×4.6 mm, Phenomenex, USA). Separation was performed at ambient temperature using a mobile phase gradient (Table 5.1). Mobile phase A: 5% acetonitrile + 95% 0.05M TEAA, pH 7.0. Mobile phase B: 95% acetonitrile + 5% 0.05M TEAA, pH 7.0.

Table 5.1. Gradient of the mobile phase used to purify CPD*-16mer

Time, min	% Mobile phase B	Flow, ml/min
0.00	5	1.00
35.0	35	1.00
50.0	65	1.00

The fluorescent CPD*-90mer was purified using reversed-phase HPLC (XTerra column, XS C18, 2.5 µm, 50×4.5 mm, Waters, Canada). Separation was performed at ambient temperature using mobile phase gradient (Table 5.2). To purify the CPD*-90mer, the mobile phase was slightly modified from that suggested by Waters for separation of fluorescently labeled oligonucleotides. Mobile phase A: 5% acetonitrile + 95% 0.1M TEAA, pH 7.0. Mobile phase B: 30% acetonitrile + 70% 0.1M TEAA, pH 7.0 Mobile phase C: 100% acetonitrile.

Table 5.2. Gradient of the mobile phase used to analyze and purify DNA ligation products

Time, min	% Mobile phase B	Flow, ml/min
0.00	0	0.75
0.50	0	0.75
7.50	50	0.75
7.51	50	1.00
15.0	100	1.00
20.0	100	1.00
30.0	mobile phase C	1.00
30.1	mobile phase C	1.50
keep flushing the column for ~5 min		

5.2.4. Detection of CPD damage in DNA standards

CE-LIF based immunoassay was used to detect CPD lesions in DNA standards (CPD*-16mer and CPD*-90mer). Fluorescently labeled CPD-standard (CPD*) was incubated with TDM-2 antibody. After CE separation, LIF was able to detect the unbound CPD* and its antibody complex: peak #1 was due to the labeled standard (longer migration times) and peak #2 was due to the complex formed between CPD* and TDM-2 antibody (shorter migration times).

5.3. Results and Discussion

5.3.1. Synthesis of the fluorescently labeled CPD*-16mer

A custom synthesized 16-nt oligonucleotide with a single CPD damage (CPD-16mer) was fluorescently labeled using terminal deoxynucleotidyl transferase (TdT) and ChromaTide Alexa Fluor® 546-14dUTP. TdT labels the 3'-end of the oligonucleotide (Figure 5.1). After the labeling, the CPD*-16mer was purified using reversed-phase HPLC. Eluted fractions were monitored at two wavelengths: 260 nm (DNA absorption) and 555 nm (max absorption for the 546-Alexa Fluor® dye).

Figure 5.2 shows the chromatogram of the CPD*-16mer with the indication of the collected fraction. This fraction was precipitated and concentrated using ethanol precipitation. Interaction with anti-CPD antibody (TDM-2) was used to characterize the purified product. Figure 5.3 shows representative electropherograms of complex formation between CPD*-16mer and the TDM-2 antibody. Figure 5.4 illustrates the kinetic curve plotted using data from the electropherograms. It is apparent that the binding between CPD*-16mer and the TDM-2 antibody was extremely slow which is quite unusual for the recognition of an antigen by an antibody. It should be mentioned that TDM-2 antibody was approximately 2 years old. Even though we were able to monitor the binding between the CPD*-16mer and the antibody, the yield of the labeling reaction was extremely small (<< 5%).

CPD-16mer

Alexa Fluor 546-14dUTP (*)

TdT

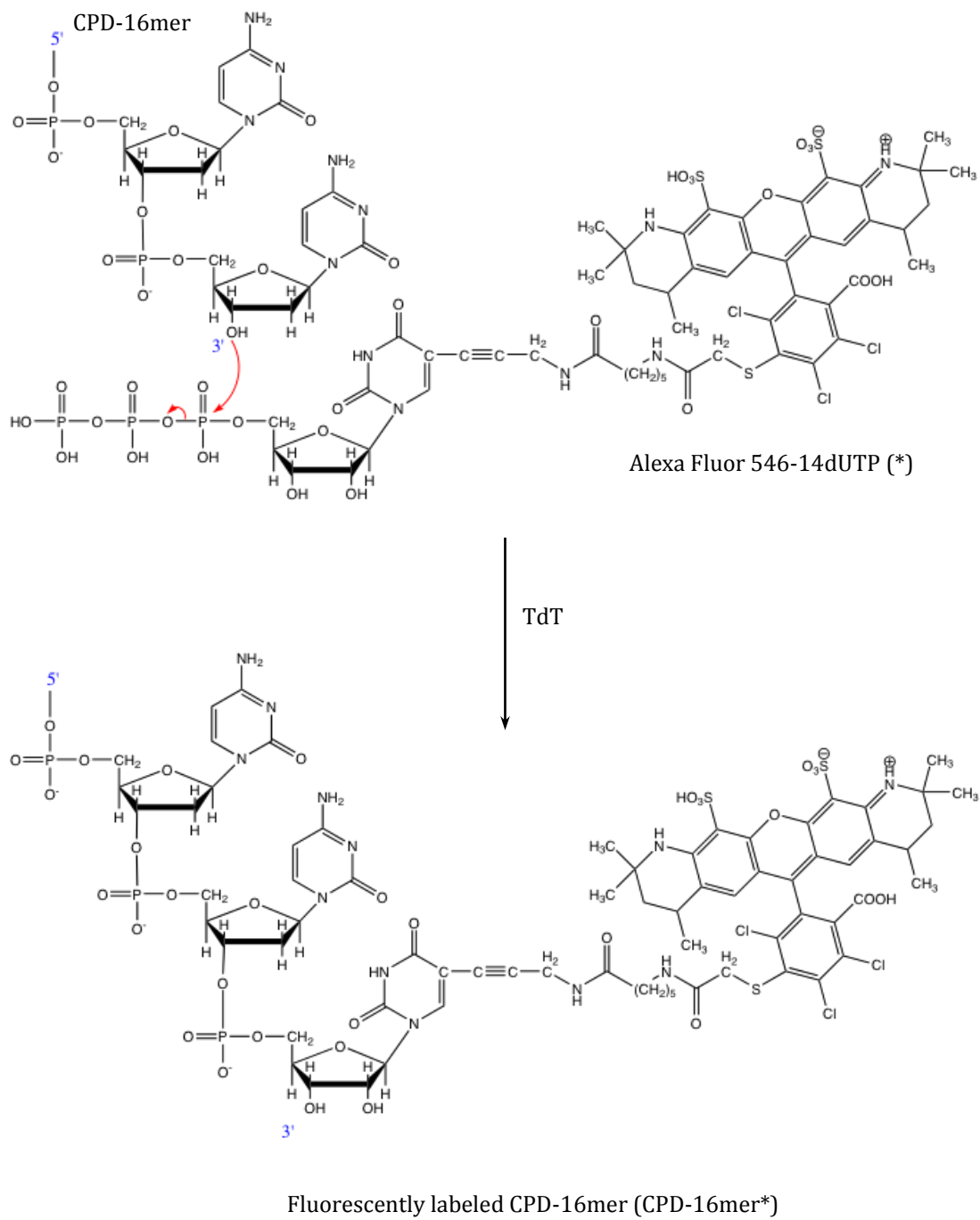Fluorescently labeled CPD-16mer (CPD-16mer*)

Figure 5.1. Enzymatic labeling of CPD-16mer using ChromaTide Alexa Fluor® 546-14dUTP
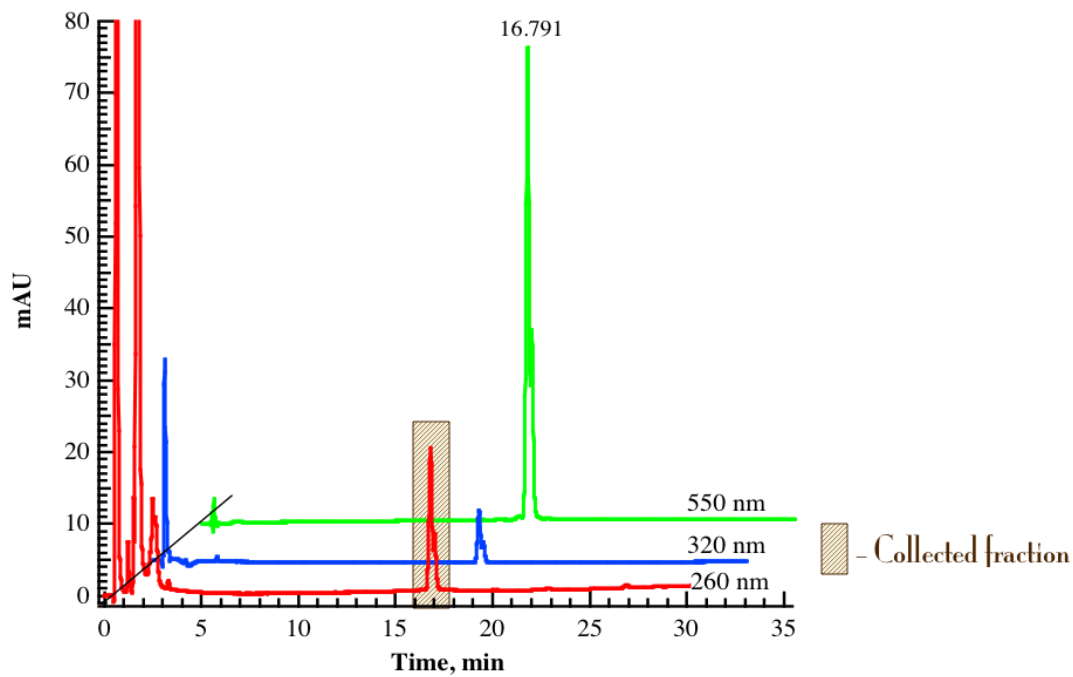
Figure 5.2. Chromatograms showing the separation of the fluorescent CPD-16mer* from the labeling reaction by-products

Fraction at 16.8 minutes was collected and considered to be CPD-16mer*. Shaded area represents the collected fraction.
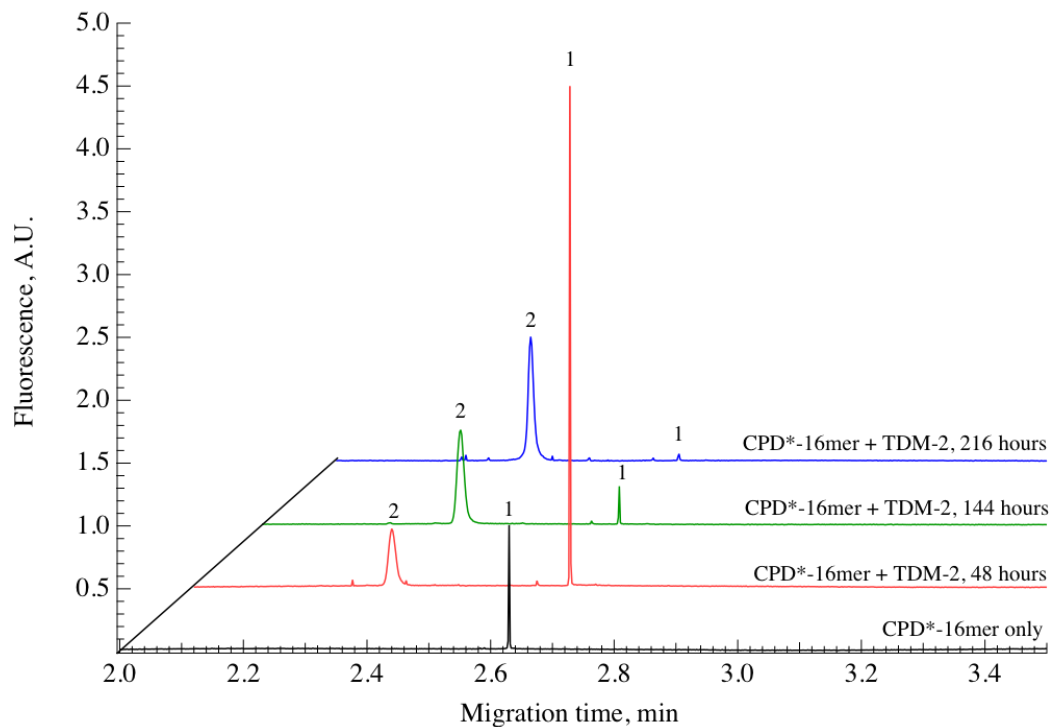
Figure 5.3. Representative electropherograms from CE-LIF immunoassay showing complex formation between CPD*-16mer and the TDM-2 antibody

Peak 1: CPD*-16mer; Peak 2: complex of TDM-2 and CPD*-16mer.

Figure 5.4. Kinetic curve based on the complex formation over time

Plotted using integration analysis of the electropherograms, examples of which are shown in Figure 5.6.

Each data point represents the mean value and the error bars represent ± standard deviation from a minimum of three independent.

Note: the lines connecting data points serve to show trends. The lines were not generated from any data-fitting program.

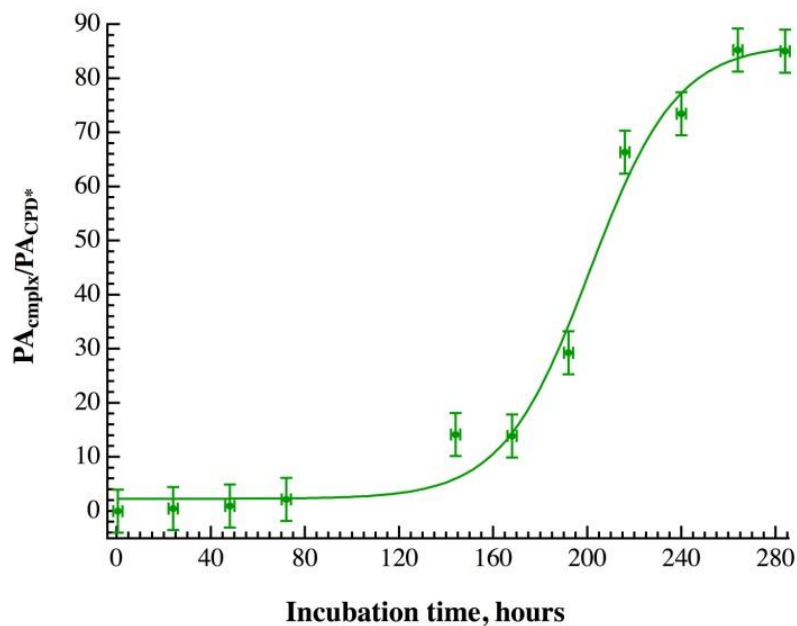CPD*-16mer can be used in the studies of protein recognition, or screening of antibodies, or in the binding studies, or even DNA repair studies. Nucleotide excision repair (NER) proteins, such as the UvrABC system, recognize and bind to a bulky DNA damage in an oligonucleotide of approximately 30 bases [8]. The 16mer containing a CPD lesion would be too short to bind to the UvrABC system. Thus the synthesis of a longer CPD-standard would be useful for DNA repair studies.

5.3.2. Design and synthesis of a 90mer oligonucleotide containing a single CPD (CPD-90mer*)

Synthesis of a longer oligonucleotide containing a single UV damage is challenging. Oligonucleotide with only one possible site for CPD damage must have high content of adenosine (A) and guanine (G). The longest stable nucleotide that could be used was a 26mer with the TT-site in the middle. The best way to synthesize the longer CPD-standard is through the ligation reaction. The 26mer containing a single CPD lesion (CPD-26mer) was employed to synthesize a longer CPD* standard.

The CPD-26mer had the following sequence (CPD site is underlined):

5'-A CGC ACG TAC GA**T◇T**AG GTA CGT GCG T-3'

Figure 5.5 shows the design and approach for the synthesis of a fluorescently labeled 90mer containing a single CPD lesion (CPD*-90mer). Briefly, six complementary overlapping oligonucleotides were annealed and

171

ligated to form a fluorescently labeled double stranded 90mer with a single CPD damage.
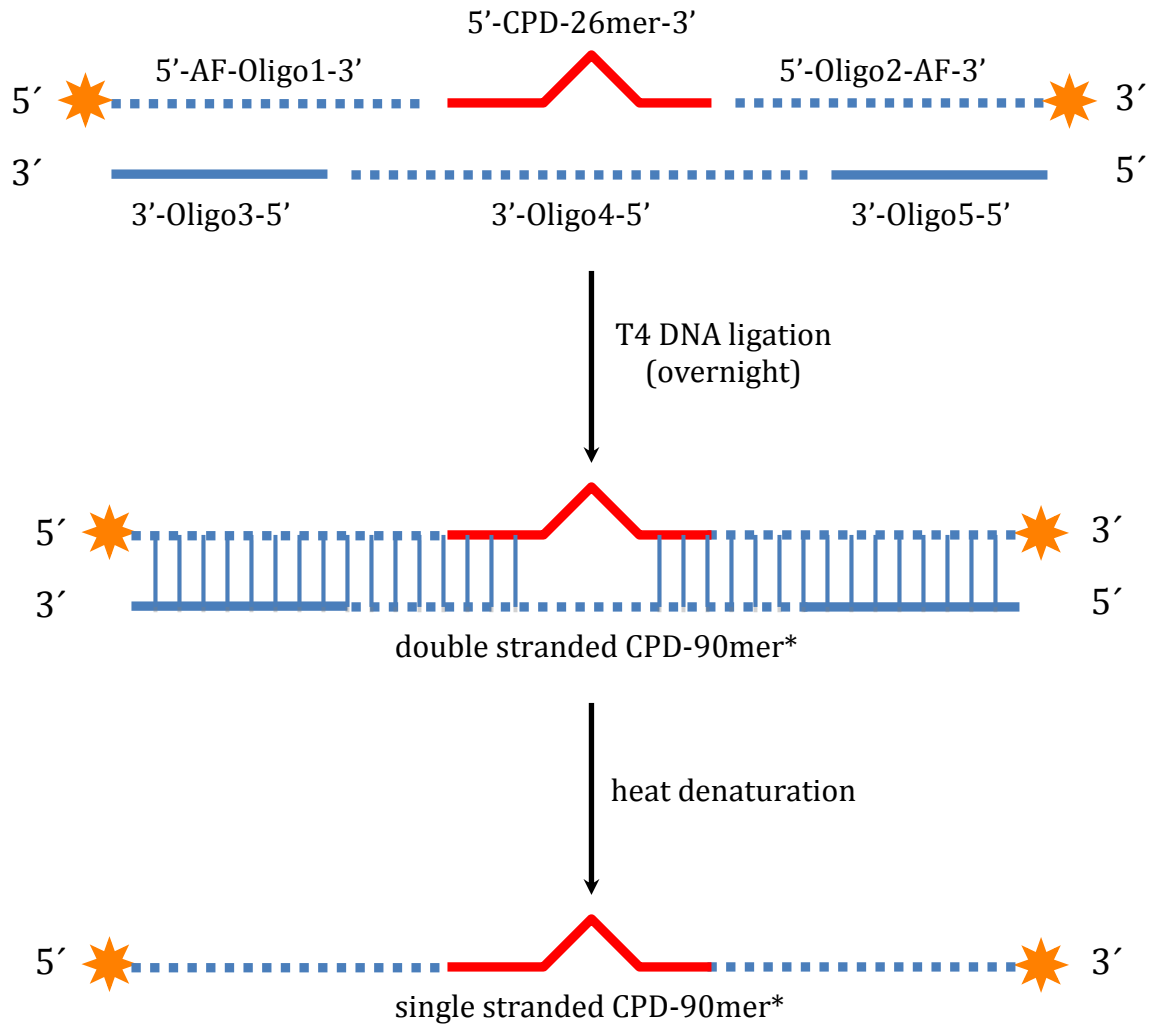

Figure 5.5. Diagram showing the design and synthesis of the fluorescent 90mer containing a single CPD lesion (CPD*-90mer)

The six oligonucleotides used in Figure 5.5 have the following sequences:

Oligo1 (32 nt) or 5'-AF-Oligo1-3': 5'-/5Alexa546N/-CCT AGC TAC CTC ACC ACT ACC ATA CTC GAG AT-3' (labeled at 5' with AlexaFluor- 546 dye)

Oligo2 (32 nt) or 5'-Oligo2-AF-3': 5'-GTC ATA TGC GGC CTC TGA CCT CGC TAG ATA CC-/3Alexa546N/-3' (labeled at 3' with AlexaFluor- 546 dye)

Oligo3 (23 nt) or 5'-Oligo3-3': 5'-ATG GTA GTG GTG AGG TAG CTA GG-3'

Oligo4 (44 nt) or 5'-Oligo4-3': 5'-GCA TAT GAC ACG CAC GTA CCT AAT CGT ACG TGC GTA TCT CGA GT-3'

Oligo5 (23 nt) or 5'-Oligo5-3': 5'-GGT ATC TAG CGA GGT CAG AGG CC-3'

CPD-26mer (26 nt) or 5'-CPD-26mer-3': 5'-A CGC ACG TAC GA**T T**AG GTA CGT GCG T-3'

Both oligo1 and oligo2 were fluorescently labeled. This served two purposes: (i) better detection of the ligation product since previous experiments showed that the yield of ligation was not high; and (ii) increase of the method sensitivity and increased detection limits when detecting CPD-damage in cellular DNA.

In order to perform the ligation, oligonucleotides had to be phosphorylated at the 5'-end, except fluorophore labeled oligonucleotides, which were already phosphorylated. After phosphorylation, all

oligonucleotides were ligated overnight at 37 °C. After ligation, products of the reaction were separated using neutral polyacrylamide gel electrophoresis (PAGE). Figure 5.6 shows the result of the PAGE separation.

The 5-µl load of the ligated products was used to visualize the separated bands. Bands that are highlighted with boxes are the ones with fluorescent 546-AlexaFluor® dye which is pink. Band #1 shows the fluorescently labeled ligation product that is slightly longer than 100 bp. Band #2 is between 70 and 80bp long and band #3 was visible only at higher concentrations and was around 30bp long. Bands that were cut out of the gel for further extraction of the standard were not visualized under UV light in order to eliminate unwanted formation of UV-photolesions in the standard. Band #3 represented the excess unreacted oligos 1 and 2, probably annealed to oligos 3 and 5 respectively. Choosing between bands #1 and #2 was difficult because both could have fluorescently labeled CPD-standard. Thus both bands were cut and DNA was extracted using the QIAEX II polyacrylamide gel extraction protocol [7]. After the extraction of products from the gel, eluted DNA standards were RP-HPLC purified.
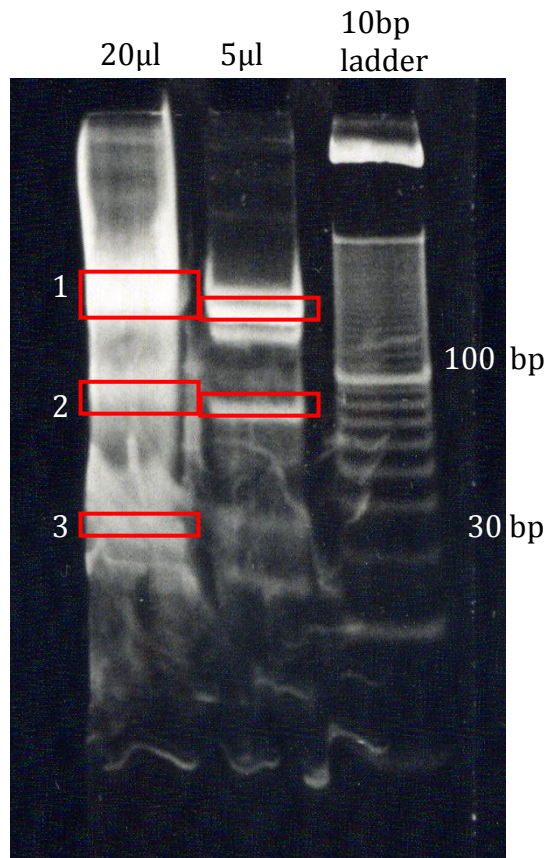
Figure 5.6. Neutral PAGE of the DNA ligation products and excess oligos

Bands are visualized using ethidium bromide dye.

"10bp ladder" shows the size of the DNA molecule

"5µl" and "20µl" are sizes of the loaded samples

Boxes highlight bands that had pink colour (fluorescent probe) under the natural light.

Band #1: product of ligation of > 100 bp long

Band #2: products of ligation of 70 – 80 bp long

Band #3: non-ligated oligo1 and oligo2 (32 nt long)

5.3.2. RP-HPLC analysis and purification of CPD-standard

The CPD-standard was purified using reversed-phase HPLC. Eluted fractions were monitored at 260 nm (DNA absorption) and 555 nm (max absorption for the 546-Alexa Fluor dye). Separation was performed at ambient temperature using the mobile phase gradient (see Table 5.2 in Experimental section).

Figure 5.7 shows chromatograms of DNA ligation products and starting oligonucleotides. Presence of the fluorescent label retained oligonucleotides longer, which can be seen from the comparison between elution of non-labeled oligonucleotide (Figure 5.7, trace "oligo2", peak (a)) with fluorescently labeled oligonucleotide (Figure 5.7, trace "oligo2", peak (b)). Both bands #1 and #2, which were cut from the neutral PAGE, were HPLC analyzed and purified. Figure 5.8 shows a magnified portion of the chromatograms for band #1 and band #2. Absorbance at 260 nm and 555 nm is shown as solid and dotted lines respectively. Comparison of the relative absorbance of nucleotides at 260 nm and absorbance of the dye at 555 nm provide support of formation of the ligated products. One molecule of the dye attached to the 32-nt oligo (ratio of the dye to nucleotides is 1:30) gives an absorbance ratio of approximately 1:2 based on the peak height ($A_{555}:A_{260}$). The ligated product is supposed to have two molecules of dye and 180-nt (double-stranded 90mer) or the ratio of the dye molecules to nucleotides

should be 1:90. Therefore, $A_{555}{:}A_{260}$ expected to be around 1:6, which is observed in the results for the band #1 ($A_{555}{:}A_{260} \approx 40{:}8$, Figure 5.8).
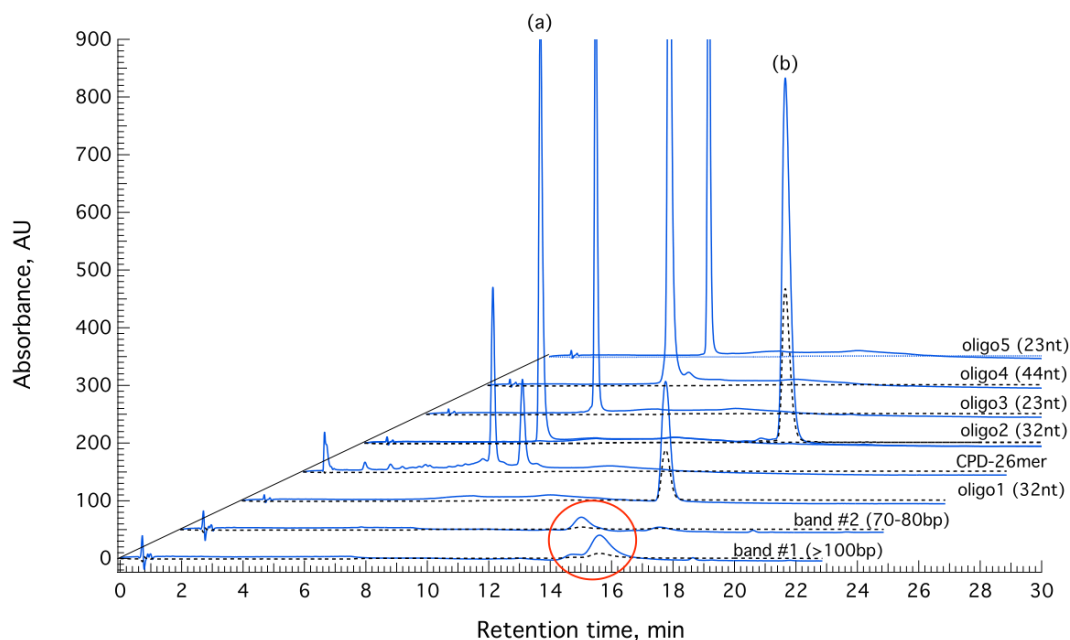

Figure 5.7. Chromatograms of the DNA ligation products and original oligonucleotides used in the ligation

Band #1 and #2 refer to neutral PAGE results.

All other traces refer to oligos used in the ligation.

Solid line – absorbance at 260 nm;

Dotted line – absorbance at 555 nm.

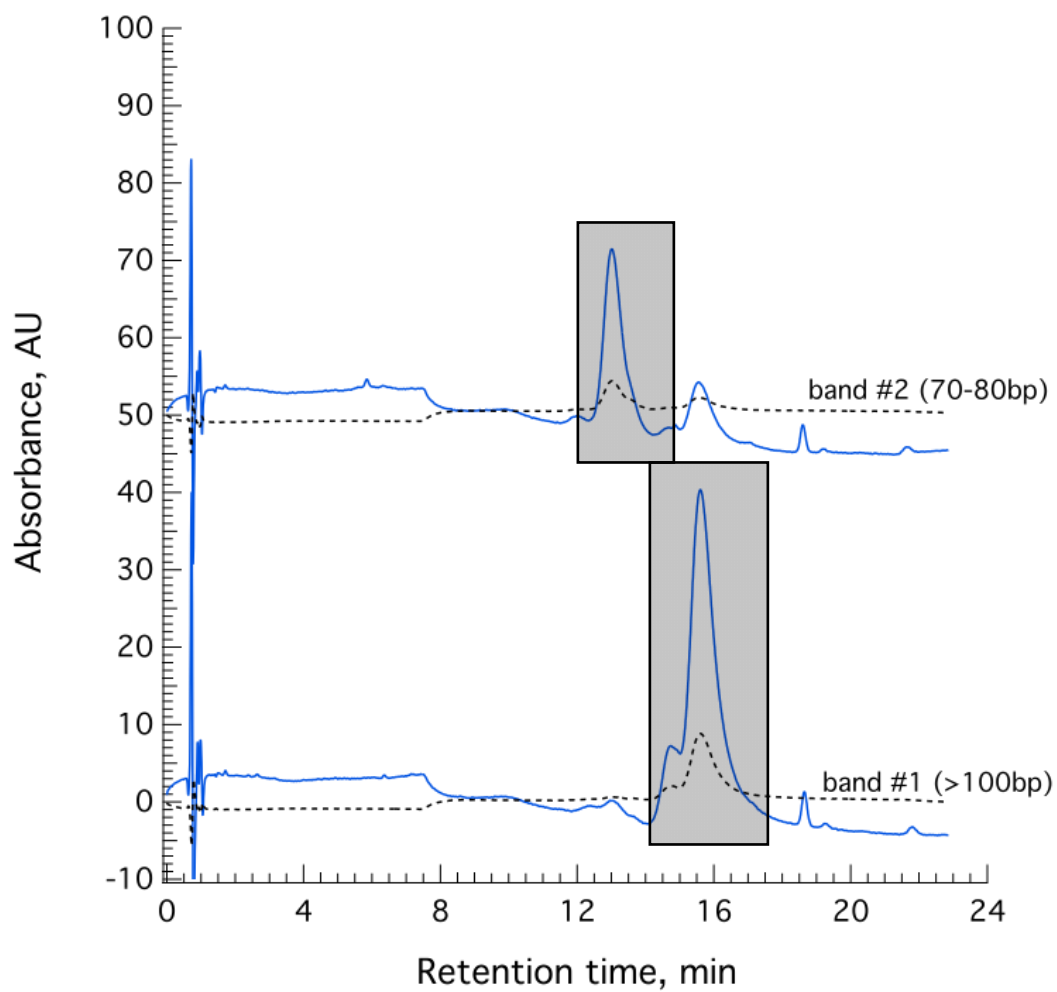Circle highlights the collected fractions of the products of the DNA ligation (see Figure 5.5)

Figure 5.8. Magnification of the fractions that were collected during RP-HPLC analysis of DNA ligation products (band #1 and band #2)

Boxed areas were collected for further salt purification and concentration of fluorescently labeled CPD –standard.

After the RP-HPLC purification, collected fractions were vacuum dried for future experiments. Dried pellets had a slightly pink coloration, which confirmed the presence of fluorescently labeled CPD-standards in the collected fractions.

5.3.3. Characterization of fluorescently labeled CPD-90mer standard using CE-LIF

To quickly characterize the ligation product, fluorescently labeled CPD-90mer standard (CPD*mer) was extracted from band #1 in the neutral PAGE (Figure 5.6). Interaction of CPD*-90mer with monoclonal anti-CPD antibody (TDM-2) was monitored using capillary electrophoresis laser-induced fluorescence. We should mention that this batch of TDM-2 was purchased shortly before these experiments. The competitive interaction of TDM-2 between CPD*-90mer and DNA extracted from UVB-irradiated CRL-2522 cells at 0.2 J/cm^2 was also monitored. Figure 5.9 shows electropherograms of sample solutions after 30 minutes incubation at 37 °C (Figure 5.9A) and after 5 days of incubation at 4 °C (Figure 5.9B). It is apparent that binding between TDM-2 antibody and CPD lesion in DNA is quite slow. PA$_{relative}$ of the possible complex peak (peak 2) was 4× higher for the 5-day incubation compared to 30-min incubation. The addition of CRL-DNA resulted in the decreased PA$_{relative}$ of complex peaks. Decrease was 3.3-fold the value of the PA$_{relative}$ after 30-min incubation. 5-day incubation resulted in the decrease of 1.4-fold the PA$_{relative}$. Decrease in the PA$_{relative}$

suggests competitive interactions of the antibody between CPD*-90mer standard and the cellular DNA. This implies the presence of CPD lesions in ligated CPD*-90mer standard.

When CRL-DNA replaces CPD*-90mer from the complex with TDM-2, the $PA_{relative}$ of the complex decreases (Figure 5.10). However, the value of $PA_{relative}$ for 5-day incubation was $10\times$ higher compared to 30-min incubation. This indicates that more CPD*-90mer was bound to TDM-2 after the 5-day incubation than after 30-min incubation. The change in the $PA_{relative}$ over time suggests that after 30-min incubation the competitive system did not reach complete equilibrium. For reproducible results equilibrium of the system had to be reached.
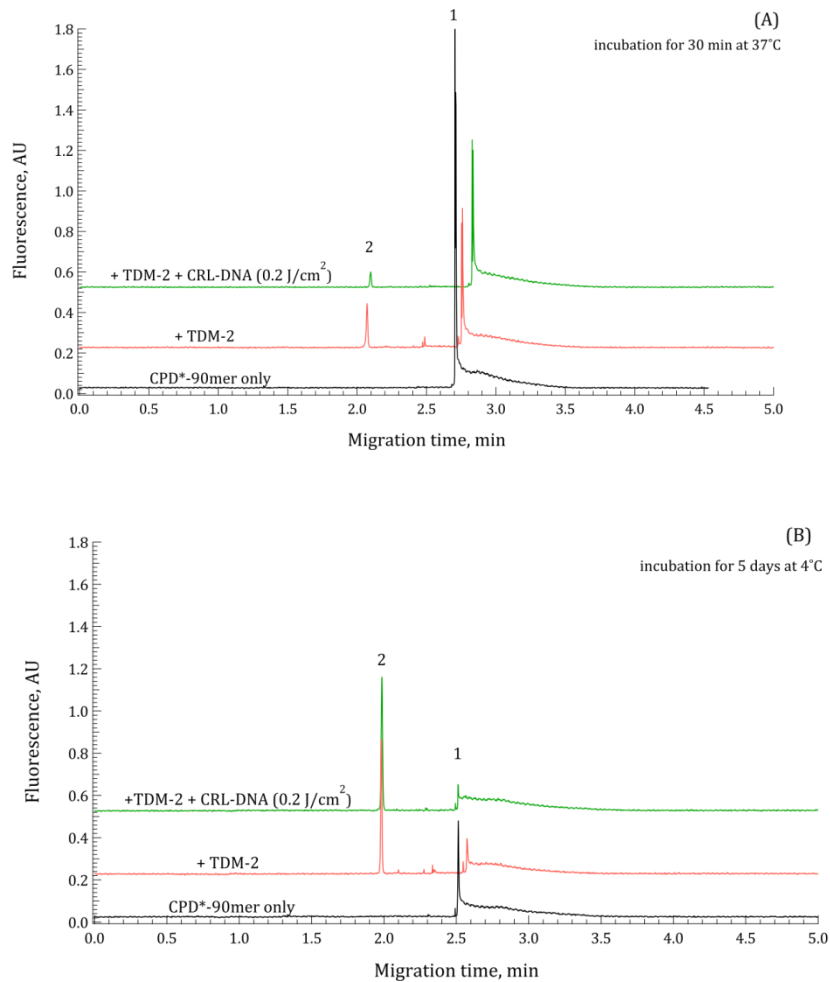
Figure 5.9. Electropherograms from the CE-LIF analyses of incubation mixtures designed for studying of interactions between CPD*-standard (CPD*-90mer) and TDM-2 antibody

(A): incubation of CPD*-std and TDM-2 for 30 minutes at 37 °C

(B): incubation of CPD*-std and TDM-2 for 5 days at 4 °C.

Peak 1: CPD*-standard signal

Peak 2: signal due to complex formed by CPD*-standard and TDM-2

Lower trace: CE-LIF for the CPD*-std only

Middle trace: CE-LIF for the mixture of CPD*-std and TDM-2

Upper trace: CE-LIF for the competitive interaction between CPD*-std and UVB-CRL-DNA for binding with TDM-2.
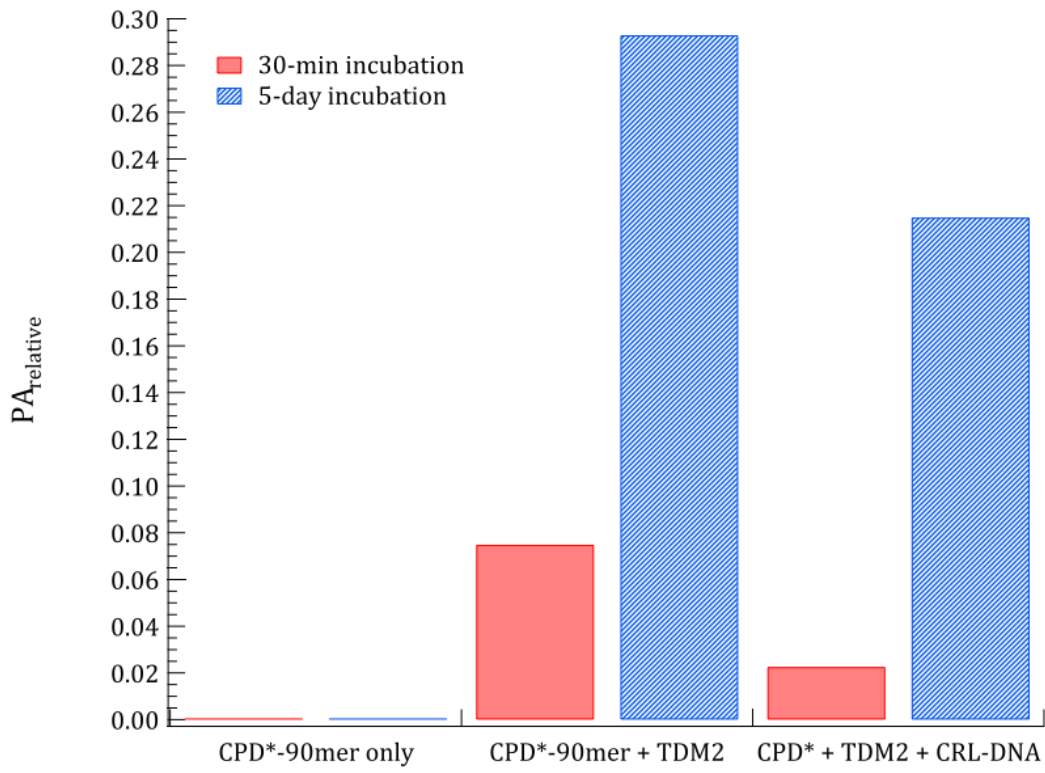
Figure 5.10. PA$_{relative}$ for complex peak for the samples with CPD-90mer* incubated at different times

5.4. Conclusions

A design for a longer fluorescently labeled CPD-standard was proposed. Fluorescently labeled CPD-90mer standard (CPD*-90mer) was synthesized using the ligation reaction and characterized tentatively using competitive CE-LIF immunoassay. Competitive interactions between CPD*-90mer and DNA extracted from UV-irradiated CRL-2522 cells (UV-CRL-DNA) showed the decrease in the complex peak by a factor of 3 in the samples incubated for 30 minutes at 37 °C.

The preliminary results show successful synthesis of fluorescently ligated product, which could be potentially used for future studies on binding of DNA and repair proteins.

The peak #2 (possible complex peak) on electropherograms suggests the binding between the fluorescently labeled standard and antibody. The decrease in the complex peak during competitive reaction supports binding competition between the labeled and non-labeled DNA. These results are preliminary. Further experiments with appropriate controls are needed to confirm the findings.

5.5. References

1. T.J. Carnelley, S. Barker, H. Wang, W.G. Tan, M. Weinfeld and X.C. Le, (2001) Synthesis, characterization and applications of fluorescent probe of DNA damage, Chem. Res. Toxicol., *14*, 1513-1522.

2. H. Wang, M. Lu, N. Mei, J. Lee, M. Weinfeld and X.C. Le, (2003), Immunoassays using capillary electrophoresis laser induced fluorescence detection for DNA adducts, Anal. Chim. Acta, *500*, 13-20.

3. W.G. Tan, T.J. Carnelley, P. Murphy, H. Wang, J. Lee, S. Barker, M. Weinfeld and X.C. Le (2001), Detection of DNA adducts of benzo[a]pyrene using immunoelectrophoresis with laser-induced fluorescence. Analysis of A549 cells, J. Chromatrogr. A, *924*, 377-386.

4. J.-S. Taylor and M.P. Cohrs (1987), DNA, light and Dewar pyrimidones: The structure and biological significance to TpT_3, J. Am. Chem. Soc. *109*, 2834-2835.

5. J.-S. Taylor, D.S. Garrett and M.P. Cohrs (1988), Solution-state structure of the Dewar photoproduct of thymidylyl-(3'→5')-thymidine, Biochemistry *27*, 7206-7215.

6. F. Gaecés and C.A. Dávila (1982), Alterations in DNA irradiated with ultraviolet radiation-I. The formation process of cyclobutylpyrimidine dimers : cross sections, action spectra and quantum yields, Photochem. Photobiol., *35*, 9-16.

7. Information and protocol was last accessed on April 11, 2011 www.invitrogen.com

8. E.C. Freidberg, G.C. Walker and W. Siede (1995), DNA repair and mutagenesis, ASM Press, Washington, D.C.

Chapter Six

Conclusions and Synthesis

6.1. Introduction

Lethal and mutagenic effects of UV radiation have been reported since 1928 [1]. However the implications of these findings for public health were ignored until the 1960-1980 when the incidence of skin cancer rose dramatically. Concerns arose with the depletion of the ozone layer, predicting probable increase in skin cancer (particularly nonmelanoma) as more UVB radiation reached the earth's surface. In fact, both melanoma and non-melanoma skin cancers are among the most deleterious effects of UV light [2].

Absorption of UV light by DNA molecules leads to photoinduced reactions in DNA bases, generating lesions referred to as photoproducts, among which the most common are cyclobutane pyrimidine dimers (CPDs) and (6-4) pyrimidine-pyrimidone photoproducts (64PPs) [3]. In addition, a third type of UV-induced photoproduct, called Dewar valence isomers (DewPPs), may be generated by photoisomeration of 64PPs by absorption of UVA irradiation (> 315 nm) [4, 5]. Although several studies have shown that the overall formation ratio between CPDs and 64PPs after UVC irradiation is approximately 3:1 [6], this is in fact related to the specific DNA sequence.

Depending on the task researchers are trying to accomplish, different techniques are required. Methods have been developed to study the formation of UV photoproducts, their behavior and effects on DNA and cells. Such methods include immuno-dot-blot assays [5, 7], radioactive labeling followed by gel electrophoresis on sequencing gels [8] combined with enzymatic reactions, immunocyto- and immunohistochemistry [9-11], high performance liquid chromatography coupled with mass spectrometry (HPLC-MS) [12-14], electrospray/tandem mass spectrometry (ES/MS) [15] and comet assays [16-18].

Because of the crucial roles of DNA damage in many biochemical processes, there is continued interest and need for more sensitive, specific, fast and simple methods for determination of specific DNA damage. The goal of this thesis research was to develop such a technique.

6.2. Advancement in knowledge

6.2.1. Chapter 2: Development of a CE-LIF immunoassay for detection of UV-induced DNA lesions

I have developed an immunoassay combined with capillary electrophoresis – laser induced fluorescence (CE-LIF). This assay is able to detect CPD lesions in short oligonucleotides (80-nt DNA library), human placenta DNA (HP-DNA, 530 – 830 bases long) and calf-thymus DNA (CT-DA,

~ 50,000 bases long) that are irradiated with a wide range of UVB and UVC doses.

I have also attempted to develop a similar method for the detection of another major UV-induced photoproduct, 64PP lesions, in UVB and UVC irradiated 80-nt DNA library, HP-DNA and CT-DNA. However, detection of 64PP lesions in HP-DNA and CT-DNA was hampered by a high background signal.

UVB-irradiation of 80-nt DNA library at the doses greater than 5 J/cm^2 resulted in significant decrease of 64PP. This is most likely due to photochemical conversion of 64PP into its Dewar isomers.

6.2.2. Chapter 3: Calibration and quantification of UV-induced lesions in DNA

I have developed a calibration method for the determination of CPD and 64PP photoproducts using CPD-16mer and 64PP-16mer as standards. Using the developed calibration method, I have quantified CPD and 64PP lesions in UVB-irradiated 80-nt DNA library (7.9 ± 1.2 CPD and 2.6 ± 0.3 64PP per 10^3 nt per J/cm^2) and in UVC-irradiated 80-nt DNA library (2.2 ± 0.2 CPD and 0.9 ± 0.1 64PP per 10^3 nt per J/cm^2). I have also determined the formation of CPD lesions in UVB-irradiated HP-DNA (18.7 ± 1.7 CPD lesions per 10^3 nt per J/cm^2) and CT-DNA (26.8 ± 1.4 CPD lesions per 10^3 nt per J/cm^2).

However, while using the developed calibration method, a caution that the short 16mer standards may not represent the larger DNA molecules has to be kept in mind.

6.2.3. Chapter 4: Application of the non-competitive CE-LIF immunoassay for detection and measurement of CPD-lesions in UVB-irradiated cells

I successfully applied the developed CE-LIF immunoassay to detect CPD lesions in DNA extracted from CRL-2522 cells irradiated with environmentally relevant UVB doses. I have determined that the detection limit of the CE-LIF immunoassay was ~0.2 fmol of CPD, which is in the low region of the detection limits reported for other techniques [11, 19-24]. I determined that ^{32}P-postlabeling method was not sensitive enough to measure CPD lesions in DNA extracted from UVB-irradiated CRL-2522 cells at doses < 0.3 J/cm^2.

For DNA extracted from UVB-irradiated CRL-2522 cells, the yield of the CPD formation was 3.6 ± 0.4 CPD lesions per 10^{3}nt per J/cm^2 which is about 7 times lower than the yield of the CPD formation in naked CT-DNA (26.8 ± 1.4 CPD lesions per 10^3 nt per J/cm^2). This is consistent with understanding that DNA is protected by the cellular structure resulting in lower lesion formation. However, determination of 64PP in DNA extracted from UVB irradiated CRL-2522 cells was preliminary due to the high

background from the control samples. To quantify 64PP reliably this problem must be dealt with.

I also made an attempt to apply this method for the study that involves the combined effects of two DNA-damaging agents (UV-light and BPDE).

6.2.4. Chapter 5: Synthesis and characterization of a fluorescent probe for CPD-lesions in DNA

I proposed a design of the fluorescent probe for CPD lesions in DNA. The probe includes a single CPD lesion and two fluorophores. Two fluorophores are used to increase the sensitivity of the fluorescently labeled standard (CPD*-90mer). The CPD*-90mer was synthesized using ligation reaction and partially characterized by CE-LIF immunoassay using interactions with anti-CPD monoclonal antibody (clone TDM-1) and competitive interactions with DNA extracted from UVB irradiated CRL-2522 cells.

6.3. Future research

With monoclonal antibodies available to bind CPD and other photoproducts, CE-LIF based immunoassay offers a useful approach to study the formation of photoproducts of interest. Using the basis of the calibration method, CE-LIF can also be applied to other photoproducts of interest. This may become a fairly powerful method compared to another method such as HPLC-MS/MS that requires lengthy digestion of DNA and as a result quantification of lesions may not be accurate.

My developed method may also be applied towards the combined studies of mutagenic and carcinogenic agents. We showed that it is applicable for both CPD- and BPDE detection. Therefore, the effect of UV light can be studied on the repair of the BPDE products. Repair studies can also be performed for UV-induced photoproducts in the presence of the other DNA damaging agents. CE-LIF immunoassay introduces a fast and easy way to measure two or more types of DNA adducts in the same sample. Such studies assist in understanding co-mutagenicity and co-carcinogenicity of multiple contaminants at environmentally relevant exposures. An example of such study is the effect of arsenic on the formation and repair of CPD lesions in DNA. (Appendix D).

The further characterization and application of the proposed fluorescently labeled CPD-probe with two fluorophores may be useful in projects related to DNA-protein studies at much lower detection limits.

6.4. Conclusions

We were able to develop, calibrate and demonstrate the applicability of the CE-LIF immunoassay method for detection and quantitative measurements of CPD and 64PP lesions in various isolated DNA samples and in cellular DNA. The detection limit was in the low femtomol range for CPDs. This method has many advantages, such as easy and quick solution preparation, inexpensive equipment, fast, sensitive and selective analysis. It measures the actual amount of lesions without changing or digesting the DNA.

The method also has its disadvantages. Development and synthesis of standards needed for calibration of the method may be challenging. This method does not allow the detection of different photoproducts simultaneously like HPLC-MS/MS analysis but.

The results of this project suggest further opportunities in related applications such as studying the effect of arsenic exposure on the formation and repair of UV-induced photoproducts.

6.5. References

1. R. Beukers, A.P.M. Eker and P.H.M. Lohman (2008), 50 years thymine dimer, DNA Repair, *7,* 530-543.

2. A.D. Woodhead, R.B. Setlow and M. Tanaka (1999), Environmental factors in nonmelanoma and melanoma skin cancer, J. Epidemiol. *9,* S102–S114.

3. J.L. Ravanat, T. Douki, and J. Cadet (2001), Direct and indirect effects of UV radiation on DNA and its components, J. Photochem. Photobiol. B: Biology, *63*, 88–102.

4. T. Douki, A. Reynaud-Angelin, J. Cadet and E. Sage (2003), Bipyrimidine photoproducts rather than oxidative lesions are the main type of DNA damage involved in the genotoxic effect of solar UVA radiation, Biochemistry *42*, 9221–9226.

5. D. Perdiz, P. Grof, M. Mezzina, O. Nikaido, E. Moustacchi and E. Sage (2000), Distribution and repair of bipyrimidine photoproducts in solar UV-irradiated mammalian cells. Possible role of Dewar photoproducts in solar mutagenesis, J. Biol. Chem., *275,* 26732–26742.

6. D.L. Mitchell (1988), The relative cytotoxicity of (6-4) photoproducts and cyclobutane dimers in mammalian cells, Photochem. Photobiol., *48*, 51–57.

7. Y.-H. You, D.-H. Lee, J.-H. Yoon, S. Nakajima, A. Yasui and G.P. Pfeifer (2001), Cyclobutane pyrimidine dimers are responsible for the vast majority of mutations induced by UVB irradiation in mammalian cells, J. Biol. Chem., *276*, 44688-44694.

8. D.L. Mitchell, J. Jen and J.E. Cleaver (1991), Relative induction of cyclobutane dimers and cytosine photohydrates in DNA irradiated

in vitro and *in vivo* with ultraviolet-C and ultraviolet-B light, Photochem. Photobiol., *54*, 741-746.

9. M. Yamada, M.U. Udono, M. Hori, R. Hirose, S. Sato, T. Mori and O. Nikaido (2006), Aged human skin removes UVB-induced pyrimidine dimers from the epidermis more slowly than younger adult skin in vivo, Arch. Dermatol. Res., *297*, 294-302.

10. M.S. Cooke, I.D. Podmore, N. Mistry, M.D. Evans, K.E. Herbert, H.R. Griffiths and J. Lunec (2003), Immunochemical detection of UV-induced DNA damage and repair, J. Immunol. Methods, *280*, 125-133.

11. H. Backvall, C. Wassberg, B. Berne and F. Ponten (2002), Similar UV responses are seen in a skin organ culture as in human skin *in vivo*, Experimental Dermatology, *11*, 349-356.

12. S. Courdavault, C. Baudouin, M. Charveron, B. Canguilhem, A. Favier, J. Cadet and T. Douki (2005), Repair of the three main types of bipyrimidine DNA photoproducts in human keratinocytes exposed to UVB and UVA radiations, DNA Repair, *4*, 836-844.

13. T. Douki, M. Court, S. Sauvaigo, F. Odin and J. Cadet (2000), Formation of the main UV-induced thymine dimeric lesions within isolated and cellular DNA as measured by high performance liquid chromatography-tandem mass spectrometry, J. Biol. Chem, *275*, 11678-11685.

14. S. Frelon, T. Douki, J.-L. Ravanat, J.-P. Pouget, C. Tornabene and J. Cadet (2000), High performance liquid chromatography-tandem mass spectrometry measurement of radiation-induced base damage to isolated and cellular DNA, Chem. Res. Toxicol., *13,* 1002-1010.

15. T. Douki, M. Court and J. Cadet (2000), Electrospray – mass spectrometry characterization and measurement of far-UV-induced

thymine photoproducts, J. Photochem. Photobiol. B: Biol. *54*, 145-154.

16. S. Sauvaigo, C. Serres, N. Signotini, N. Emmonet, M.-J. Richard and J. Cadet (1998), Use of the single cell gel electrophoresis assay for the immunofluorescent detection of a specific DNA damage, Anal. Biochem., *259*, 1-7.

17. M.P. Sastre, M. Vernet and S. Steinert (2001), Single-cell gel/comet assay applied to the analysis of UV readiation-induced DNA damage in *Rhodomonas sp.* (*Cryptophyta*), Photochem. Photobiol., *74*, 55-60.

18. J.P. Pouget, T. Douki, M.J. Richard and J. Cadet (2000), DNA damage induced in cells by γ and UVA radiation as measured by HPLC/GC-MS and HPLC-EC and comet assay, Chem. Res. Toxicol., *13*, 541-549.

19. V.J. Bykov, R. Kumar, A. Forsti and K. Hemminki (1995), Analysis of UV-induced DNA photoproducts by ^{32}P-postlabeling, Carcinogenesis, *16*, 113-118.

20. V.J. Bykov, K. Hemminki, (1995), UV-induced photoproducts in human skin explants analyzed by TLC and HPLC-radioactivity detection, 16, Carcinogenesis, 3015-3019.

21. S.E. Freeman, A.B. Blackett, D.C. Monteleone, R.B. Setlow, B.M. Sutherland and J.C. Sutherland (1986), Quantitation of radiation-, chemical-, or enzyme-induced single strand breaks in nonradioactive DNA by alkaline gel electrophoresis: Application to pyrimidine dimers, Anal. Biochem., *158*, 119-129.

22. I.D. Podmore, M.S. Cooke, K.E. Herbert and J. Lunec (1996), Quantitative determination of cyclobutane thymine dimers in DNA by stable isotope-dilution mass spectrometry, Photochem. Photobiol., *64*, 310-315.

23. K. Cahová-Kuchaříková, M. Fojta, T. Mozga, E. Paleček (2005), Use of DNA-repair enzymes in electrochemical detection of damage to DNA bases in vitro and in cells, Anal. Chem., *77*, 2920-2927.

24. X. Liu and M.J.Smerdon, (1995), A slot blot method for detection of ultraviolet photoproducts in DNA, Anal. Biochem., *229*, 323-328.

Appendix A

Optimization of experimental conditions
for non-competitive CE-LIF immunoassay

Starting conditions for non-competitive CE-LIF immunoassay were chosen based on the conditions reported for the determination of benzo[a]pyrene [1-7]. Because in reported results the complex peak was not completely resolved from the antibody peak and because the antibodies used in this work are different, we have experimentally optimized the experimental conditions to achieve optimum separation and detection.

A.1. Effect of the pH of the running buffer

Resolution in capillary electrophoresis (CE) can be adjusted by changing the electroosmotic flow or changing the degree of deprotonated silanol groups on the capillary walls. Change of the pH of the running buffer is the easiest and the simplest way to control resolution. Since we are separating antibodies (Ab*, positive charge) from the complex of antibodies with DNA (Ab*-DNA, combination of positive and negative charges), the pH of the running buffer should be in the range allowing deprotonation of silanol groups. Tris-glycine buffer was chosen as a running buffer due to its good buffering capacity and low mobility, which minimized current generation and thus Joule heating.

The pH of the running buffer varied from 7.0 to 9.0. The pH 7.0 – 8.0 were adjusted using acetic acid; pH 8.4 was the actual pH of the purchased Tris-glycine (TG) buffer; pH was adjusted to 9.0 using ammonium hydroxide.

At lower pH, resolution between Ab* and Ab*-DNA peaks was higher than at the higher pH (Figure A.1.1) due to the slower EOF and thus slower mobility of species (Figure A.1.2) and therefore resulting in a better separation between charged species (Ab*-DNA and Ab*). However, slower mobility at lower pH also means that proteins are more likely to adsorb on the capillary walls. Adsorption also results in the peak tailing, broadenning and lowering the signal intensity, which explains the maximum observed in Figure A.1.3. Since $PA_{relative}$ is the ratio of PA_{cmplx} (peak area due to Ab*-DNA complex) to PA_{total} (the peak area of all fluorescently labeled species), the pH of the running buffer should not affect the $PA_{relative}$ value, which was observed for pH < 9.0 (Figure A.1.4). At pH 9.0 the complex peak coeluted with the antibody peak resulting in data being different.
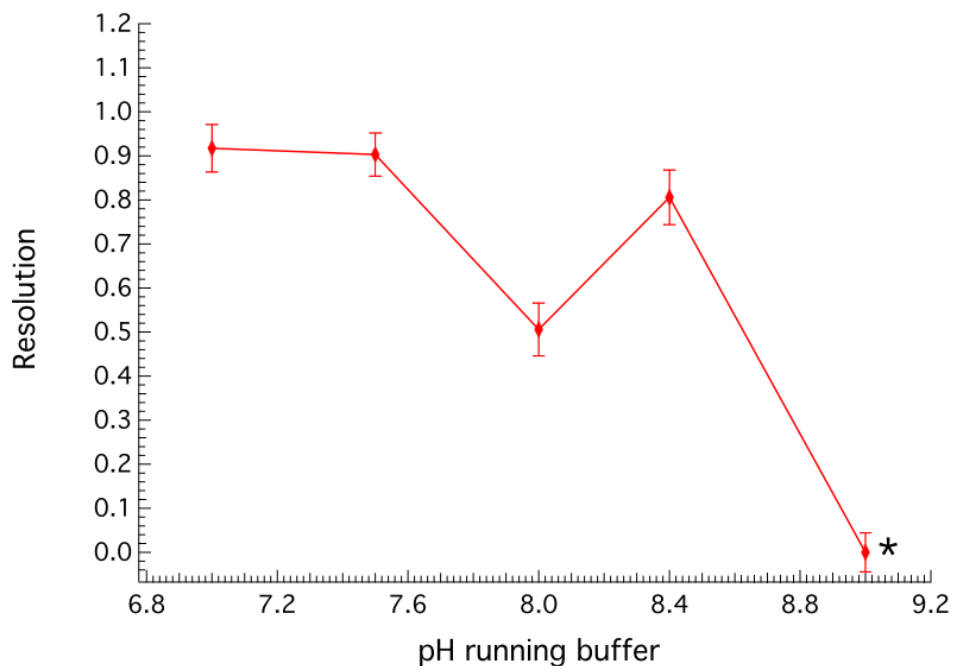
Figure A.1.1. Effect of pH of the running buffer on the resolution between antibody and complex peaks for electropherograms for CPD detection in UV-irradiated DNA

Each data point represents the mean value and the error bars represent ± standard deviation from a minimum of three independent experiments.

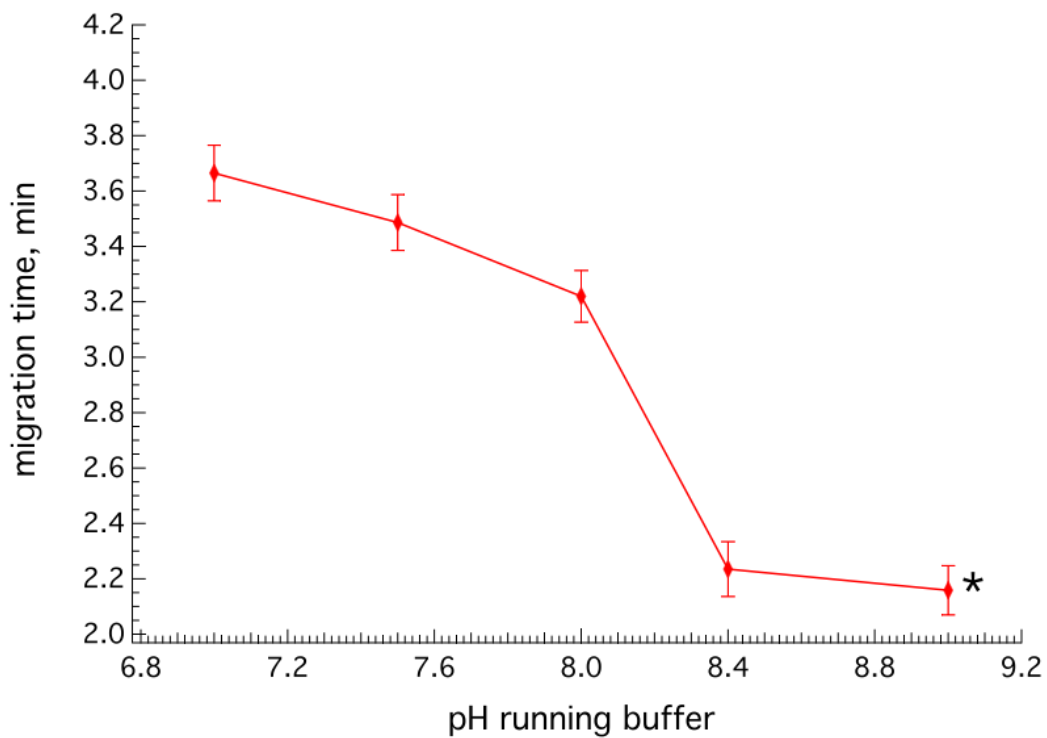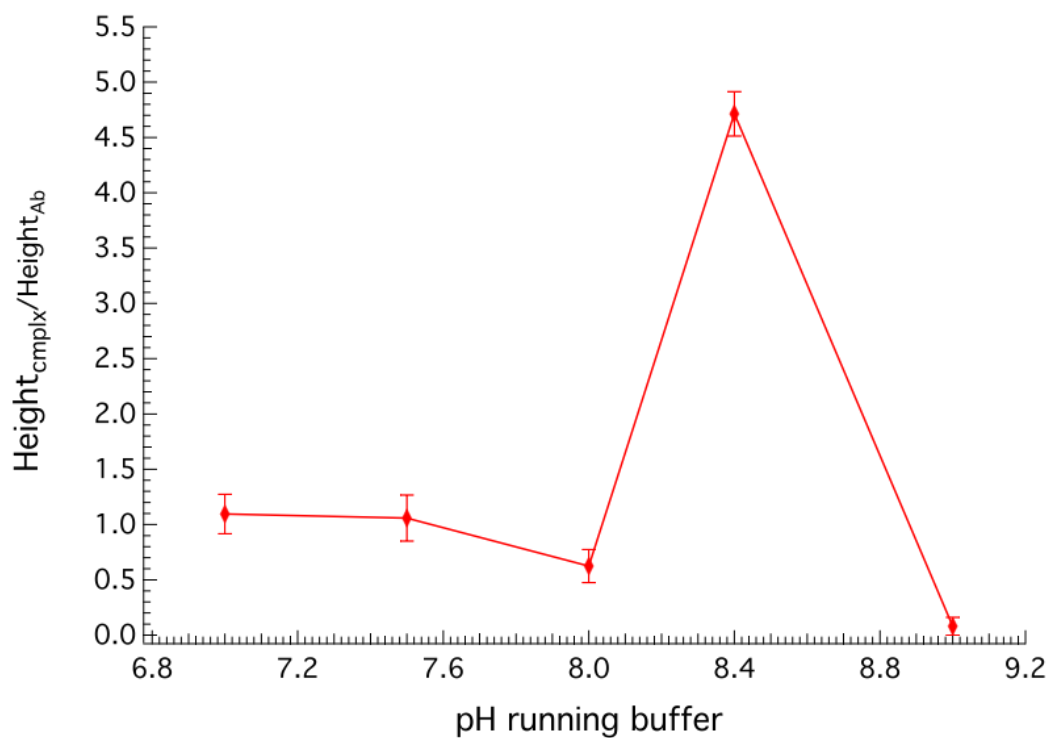(*) Antibody peak and ternary complex peak(s) coeluted together.

Figure A.1.2. Effect of pH of the running buffer on the migration time of the complex peak

Each data point represents the mean value and the error bars represent ± standard deviation from a minimum of three independent experiments.

(*) Antibody peak and ternary complex peak(s) coeluted together.

Figure A.1.3. Effect of pH of the running buffer on the signal produced during CE-LIF

Ratio of heights was used to monitor the signal suppression due to either adsorption of the solutes (pH < 8.4) or their co-elution (pH > 8.4).

Each data point represents the mean value and the error bars represent ± standard deviation from a minimum of three independent experiments.
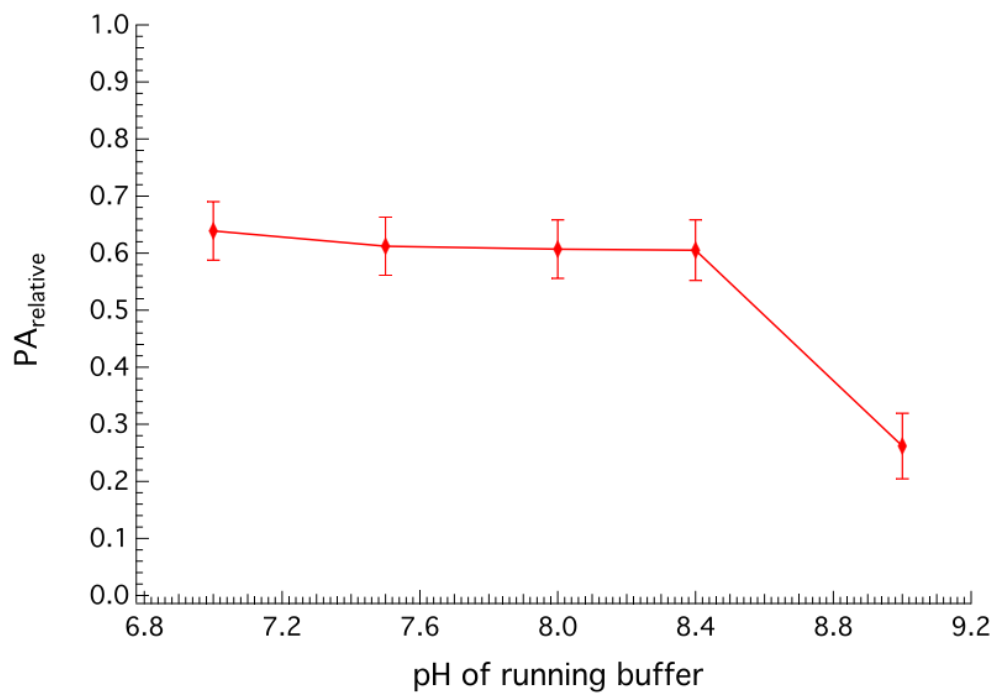
Figure A.1.4. Effect of pH of the running buffer on the response (PA$_{relative}$) for CPD lesions formed in UV-irradiated DNA

Each data point represents the mean value and the error bars represent ± standard deviation from a minimum of three independent experiments.

A.2. Effect of running buffer ionic strength

The ionic strength of running buffer (IS) is another factor that affects the EOF and thus resolution of species. At low IS, EOF increases resulting in shorter migration times. Faster EOF may also result in a poorer resolution between peaks. However, at higher IS, EOF slows down resulting in a better separation of differently charged species but it also may result in higher adsorption on the walls of the capillary.

Ionic strength for the Tris-glycine (TG) running buffer with pH 8.4, varied from 0.5× to 2×TG. Lowering IS resulted in coelution of both Ab* and Ab*-DNA peaks and not enough separation between them. Migration of complex peaks got longer with the increase of IS of running buffer (Figure A.2.1) confirming that mobility of species slowed down with EOF. Even though migration times increased, resolution for buffers with IS greater than 1× did not improve significantly (Figure A.2.2). Possible reason is an adsorption of proteins on the capillary walls, which results in peak tailing and thus not large improvement of resolution. Calculating PA$_{relative}$ for complex peak resulted in the highest value for 1×TG running buffer (Figure A.2.3), therefore we chose 1×TG as the running buffer.
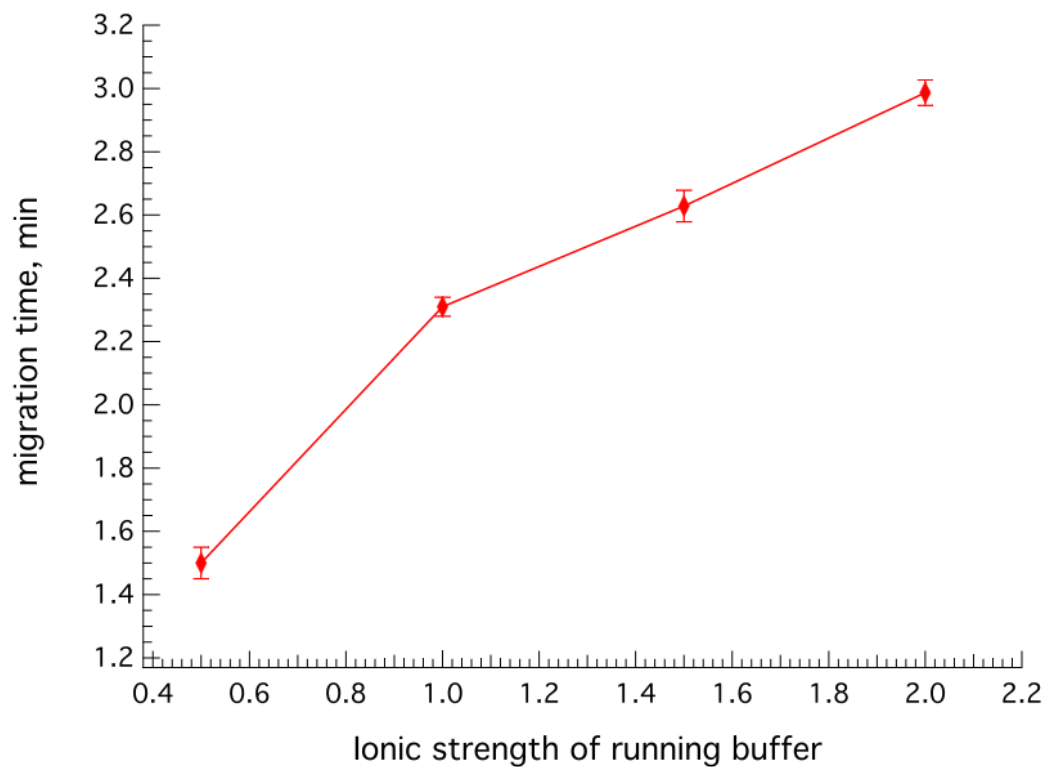
Figure A.2.1. Effect of the ionic strength of the running buffer on the migration time of the complex peak

Each data point represents the mean value and the error bars represent ± standard deviation from a minimum of three independent experiments.
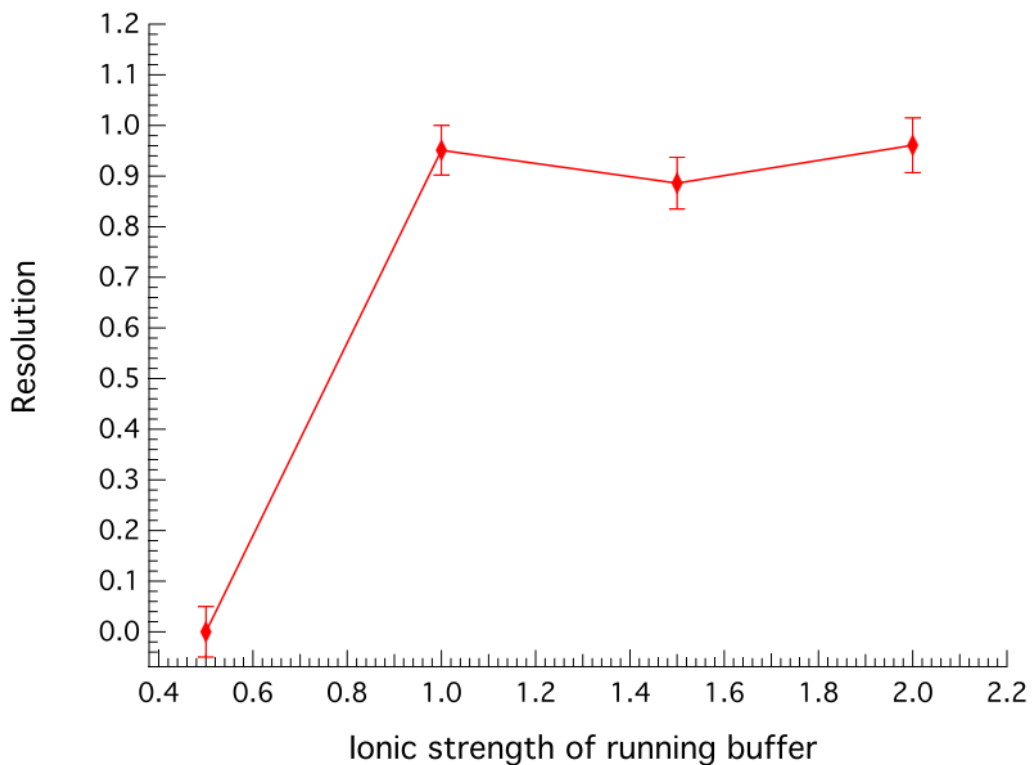
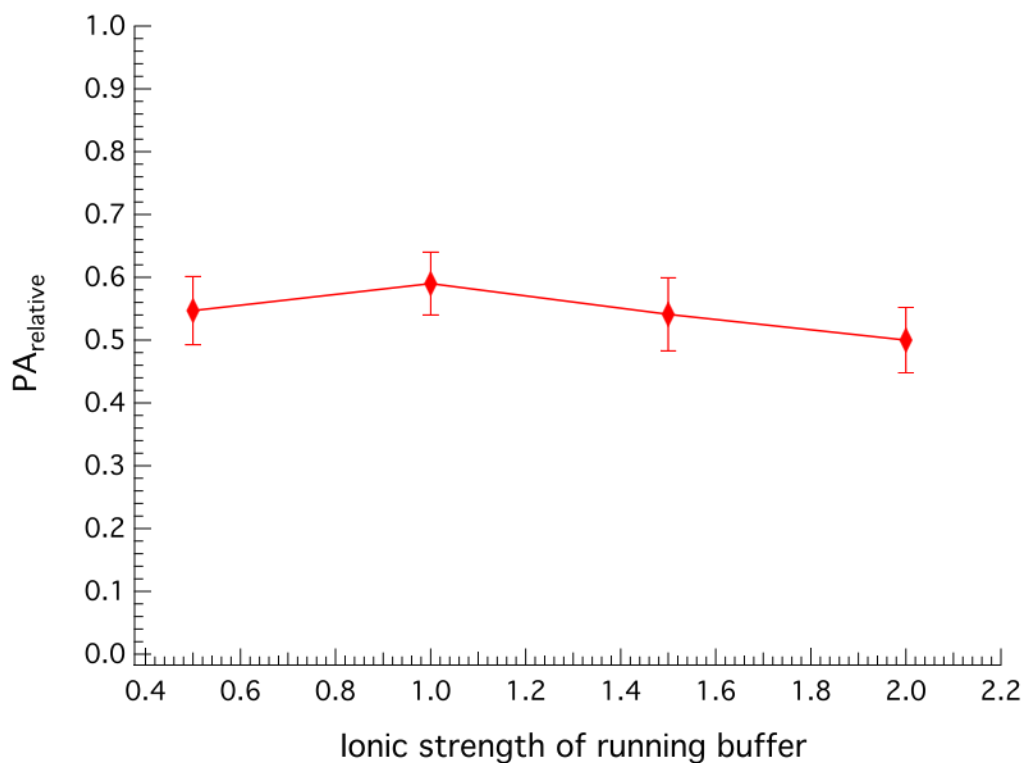**Figure A.2.2. Effect of the ionic strength of the running buffer on the resolution between antibody and complex peaks in electropherograms for CPD detection in UV-DNA**

Each data point represents the mean value and the error bars represent ± standard deviation from a minimum of three independent experiments.

Figure A.2.3. Effect of the ionic strength of the running buffer on the response (PA$_{relative}$) for CPD lesions formed in UV-irradiated DNA

Each data point represents the mean value and the error bars represent ± standard deviation from a minimum of three independent experiments.

A.3. Effect of the separation electric field

Electric field applied to the capillary also affects the EOF. The increase in the separation electric field will result in increased EOF and thus mobility of species, which may decrease the resolution. However lowering the electric field may not be beneficial. Lowering the separation electric field will lower the mobility of species thus leading to possible adsorption on the capillary walls.

In our experiments the separation electric field varied from 300 V/cm to 600 V/cm. As expected, migration times for peaks were shorter at the higher separation electric field (Figure A.3.1). Figure A.3.2 shows the effect of separation electric field on resolution. At 500 V/cm resolution reached a maximum (Figure A.3.2). This may be explained by the following possibilities: (i) predominant contribution of adsorption of positively charged proteins at electric fields lower than 500 V/cm resulting in the tailing, broadening and lowering the signal and therefore lower resolution; (ii) predominant contribution of too high EOF at 500 V/cm resulting increased mobility and thus insufficient time to separate species and therefore lower resolution. As a result, the chosen separation electric field was 500 V/cm. Separation electric field had no effect on the $PA_{relative}$ (Figure A.3.3)
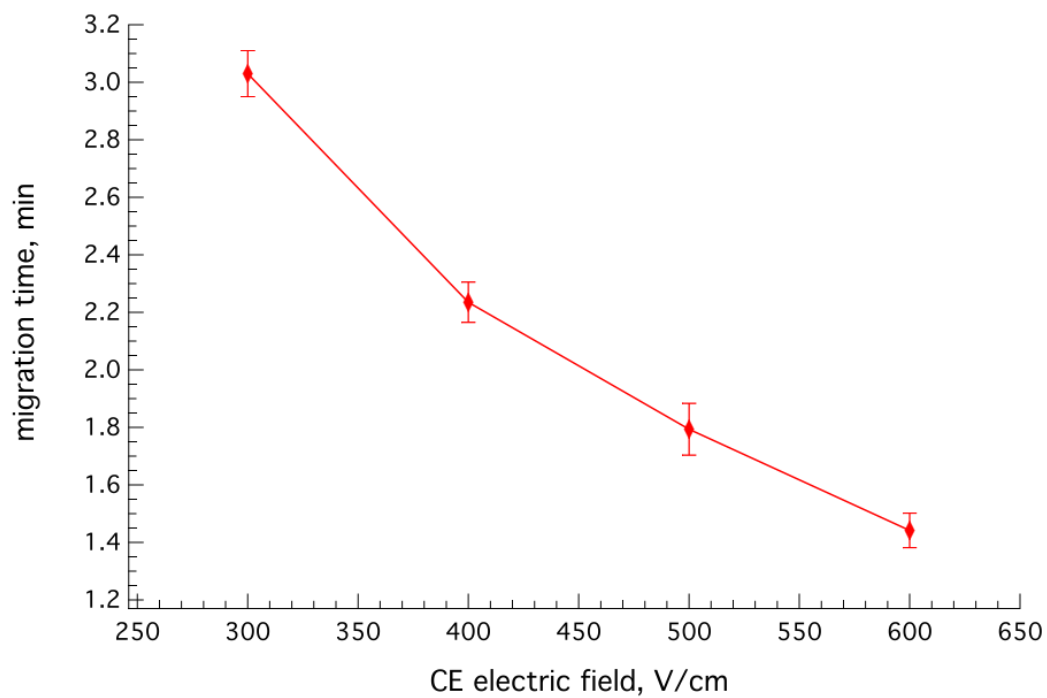
Figure A.3.1. Effect of the separation electric field (V/cm) on the migration time of the complex peak

Each data point represents the mean value and the error bars represent ± standard deviation from a minimum of three independent experiments.
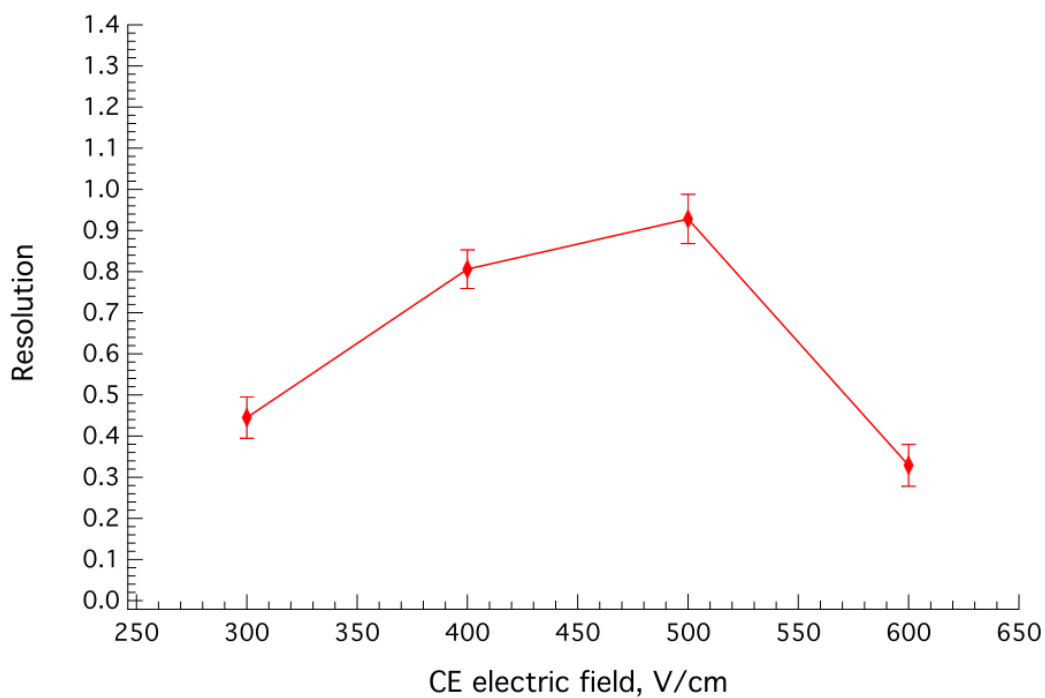
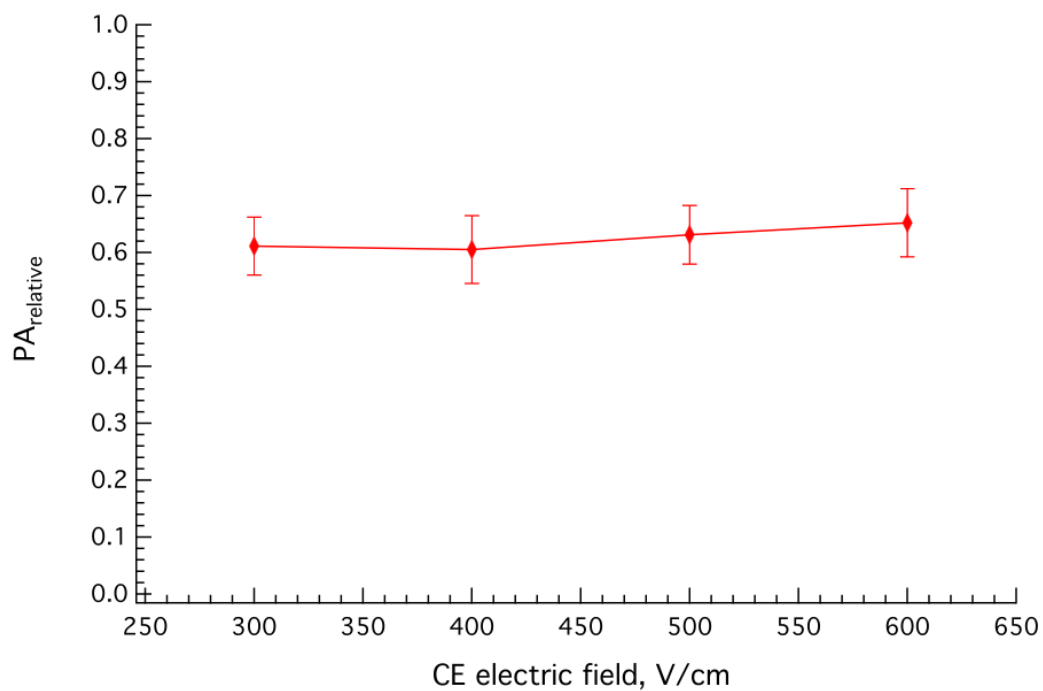**Figure A.3.2. Effect of separation electric field (V/cm) on the resolution between antibody and complex peaks in electropherograms for CPD detection in UV-DNA**

Each data point represents the mean value and the error bars represent ± standard deviation from a minimum of three independent experiments.

Figure A.3.3. Effect of the separation electric field (V/cm) on the response (PA_{cmplx}/PA_{total}) for CPD lesions formed in UV-irradiated DNA

Each data point represents the mean value and the error bars represent ± standard deviation from a minimum of three independent experiments.

A.4. Effect of the injection time and voltage

When optimizing the experimental conditions, we realized that conditions not only should focus on the resolution. For example, when choosing the pH of the running buffer, preferred conditions provided the highest signal. Better detection signal means higher sensitivity and, of course reproducibility of results, as well as it means lower detection limits.

In capillary electrophoresis, the amount of sample injected into the capillary depends on the injection time and injection voltage. Both parameters affect the size of the zone (zone length). Increasing injection time and voltage results in a larger zone. However, too long an injection will result in zone broadening. Length of the zone has to be smaller than the dispersion caused by diffusion of the molecule in order to keep the longitudinal profile to a minimum. Since proteins have low diffusivity, the zone length has to be fairly short.

The effect of the injection time and voltage was studied using the following conditions: injection times were varied at 3, 5 and 7 seconds; injection voltages were 10 kV (below the separation voltage), 15 kV (equivalent to the separation voltage) and 20 kV (above the separation voltage). Considering, that size of the zone is proportional to the signal detected, it should be also proportional to peak areas of detected fluorescent species thus leaving $PA_{relative}$ unchanged. At low injection voltage and short time, the size of the zone is small, however, it did not affect $PA_{relative}$

210

significantly as was expected (Figure A.4.1). At lower injection voltage and shorter injection times resolution of peaks was also the highest (Figure A.4.2). However, working with too low injection times and voltages may also mean working under the detection limits, which might be an issue while working with small amounts of DNA damage. Therefore, the injection time was chosen as 5 sec and the injection voltage was chosen to be the same as the separation voltage.
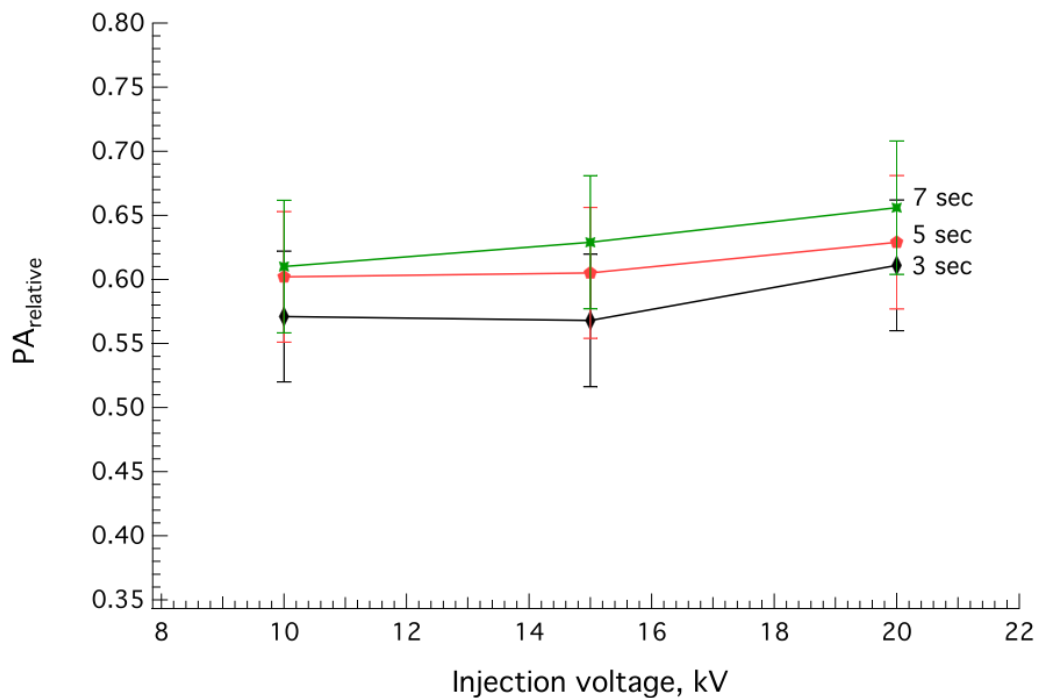
Figure A.4.1. Effect of the injection voltage (kV) and injection time (sec) on the response (PA_{cmplx}/PA_{total}) for CPD lesions formed in UV-irradiated DNA

Each data point represents the mean value and the error bars represent ± standard deviation from a minimum of three independent experiments.
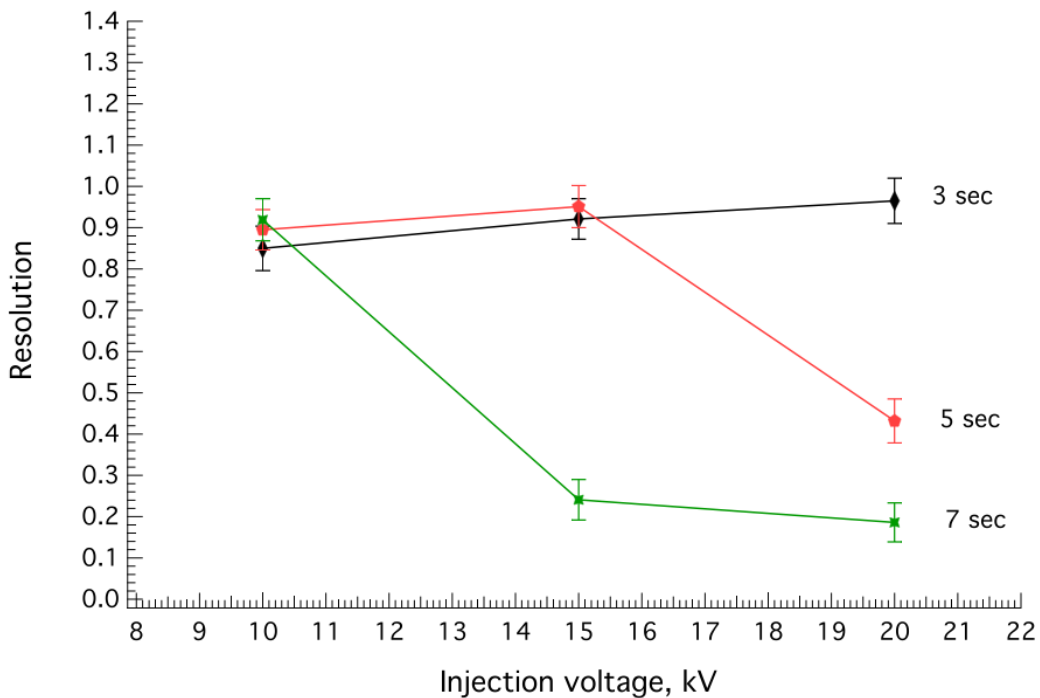
Figure A.4.2. Effect of injection voltage (kV) and injection time (sec) on the resolution between antibody and complex peaks in electropherograms for CPD detection in UV-DNA

Each data point represents the mean value and the error bars represent ± standard deviation from a minimum of three independent experiments.

A.5. Effect of the incubation buffer composition

Binding of an antibody to the damage in DNA is pH dependent [8, 9]. Therefore the pH of the incubation buffer may play a key role in damage recognition. The most common pH when antibody binds to DNA is neutral, pH 7.3 – 7.6 [8]. Mainly, pH of the buffer affects the structure of the antibody and thus recognition of the damage. Different compositions of the incubation buffers may also affect the stability of formed complexes. From our experiments, complexes formed between anti-CPD antibody and DNA samples were incubated in 1×TG incubation buffer at pH 7.4. These complexes were found to be stable for a fairly long period of time (results not shown). However, incubation buffer may also improve CE efficiency and resolution during non-competitive CE-LIF immunoassay. Wang *et al.* studied different buffer compositions on focusing of the eluting peaks, increase in sensitivity and resolution [7]. Wang *et al.* also showed that focusing best occurred when the difference in pH for incubation and running buffer is at least 1.0. Shen also studied effect of different pH and ionic strength of incubation buffer on the detection of BPDE adducts in DNA using CE-LIF immunoassay [9]. Both of these studies suggest use of neutral pH for complex formation. Therefore, the pH in our experiments was chosen as 7.5 and pH of the running buffer 8.4. However, different incubation buffer compositions were studied.

The following incubation buffers were chosen: $1 \times TG$ at pH 7.5 (our conditions); $2 \times TG$ at pH 7.5; $2 \times TG$ + 10 mM acetic acid (HAc) (conditions in [7]); $2 \times TG$ + 0.5 PBS (PBS is known to stabilize proteins). The listed order is also an order of increasing ionic strength of the incubation buffer. Increasing ionic strength of the incubation buffer decreases the migration time (Figure A.5.1). This effect is opposite to the one we saw for the ionic strength for the running buffer (Figure A.2.1). Since the running buffer was the same, EOF did not change but presence of more high mobility counter ions (from HAc or PBS) in the zone resulted in faster migration times for the analyte (Ab* and Ab*-DNA). Since $PA_{relative}$ was approximately the same for, $1 \times TG$ and $1 \times TG$ + HAc (Figure A.5.2), the resolution was the highest (Figure A.5.3) for $1 \times TG$. Therefore, the $1 \times TG$ incubation buffer was chosen in our experiment.
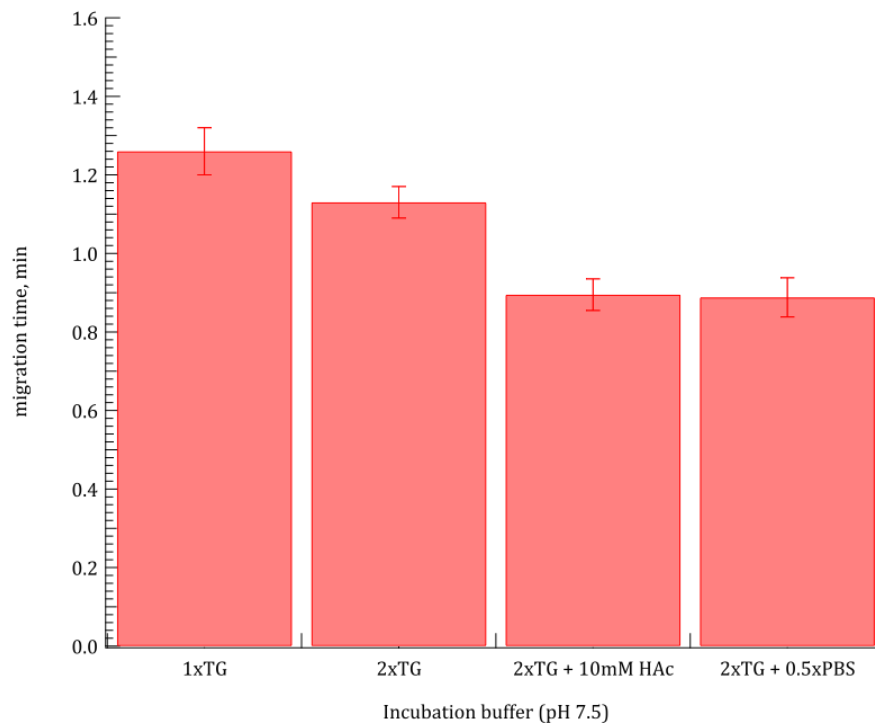
Figure A.5.1. Effect of the composition of the incubation buffer on the migration time of the complex peak

Each data point represents the mean value and the error bars represent ± standard deviation from a minimum of three independent experiments.
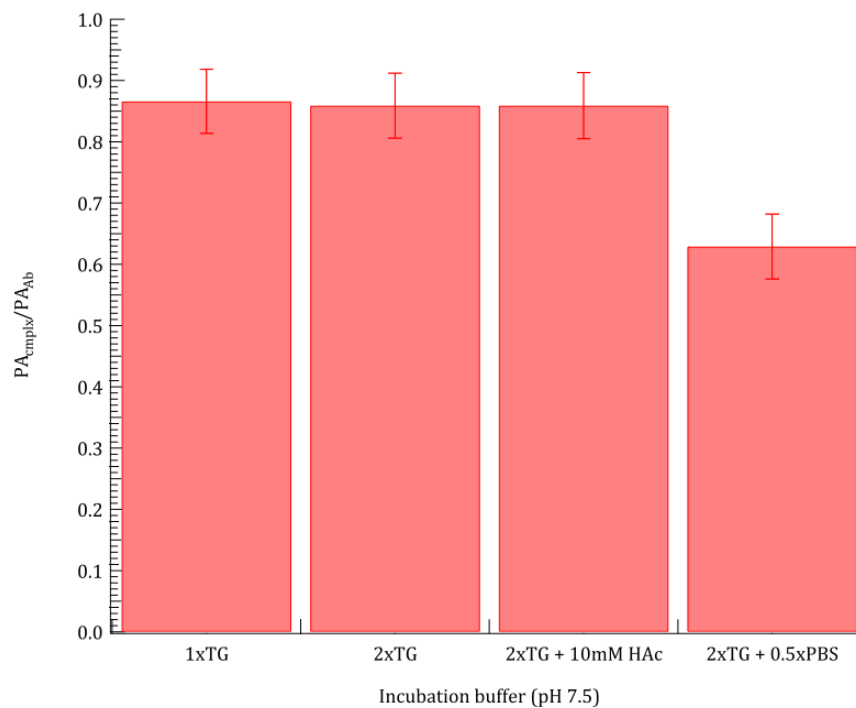
Figure A.5.2. Effect of the composition of the incubation buffer on the response (PA$_{cmplx}$/PA$_{total}$) for CPD lesions formed in UV-irradiated DNA

Each data point represents the mean value and the error bars represent ± standard deviation from a minimum of three independent experiments
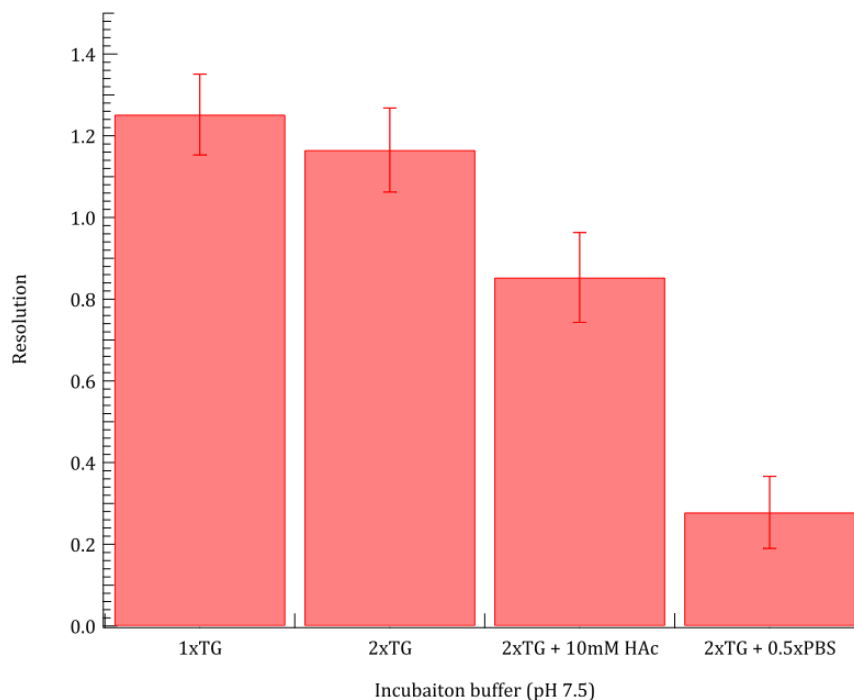
Figure A.5.3. Effect of the composition of the incubation buffer on the resolution between antibody and complex peaks in electropherograms for CPD detection in UV-DNA

Each data point represents the mean value and the error bars represent ± standard deviation from a minimum of three independent experiments

Summary of the condition under which CE-LIF analyses were performed:

- Injection: 5 sec at voltage equal to the separation voltage

- Separation: electric field of 500 V/cm and running buffer 1×TG, pH 8.4

- Incubation buffer: 1×TG, pH 7.5

A.6. References

1. T.J. Carnelley, S. Barker, H. Wang, W.G. Tan, M. Weinfeld and X.C. Le (2001), Synthesis, characterization and applications of fluorescent probe of DNA damage, Chem. Res. Toxicol., *14*, 1513-1522.

2. H. Wang, M. Lu, N. Mei, J. Lee, M. Weinfeld, X.C. Le (2003), Immunoassays using capillary electrophoresis laser induced fluorescence detection for DNA adducts, Anal. Chim. Acta, 500, 13-20.

3. W.G. Tan, T.J. Carnelley, P. Murphy, H. Wang, J. Lee, S. Barker, M. Weinfeld and X.C. Le (2001), Detection of DNA adducts of benzo[a]pyrene using immunoelectrophoresis with laser-induced fluorescence. Analysis of A549 cells, J. Chromatrogr. A, *924*, 377-386.

4. A. LeBlanc, S. Shen, K. Lew, M. Weinfeld and X.C. Le (2009), Detection of BPDE-DNA adducts in mononuclear white blood cells by capillary electrophoresis immunoassay and its application to studying the effect of glutathione depletion, Electrophoresis, *30*, 1558-1563.

5. S. Shen, J. Lee, X. Sun, H. Wang, M. Weinfeld and X.C. Le (2006), Elevation of cellular BPDE uptake by human cells: a possible factor contributing to co-carcinogenicity by arsenite, Environmental Health Perspectives, *114*, 1832-1837.

6. X.C. Le, V. Pavski, H. Wang (2005) Affinity recognition, capillary electrophoresis and laser induced fluorescence polarization for ultrasensitive bioanalysis, Canadian Journal of Chemistry, *83*, 185-194

7. H. Wang, M. Lu and X.C. Le (2005) DNA-Driven focusing for protein-DNA binding assays using capillary electrophoresis. Analytical Chemistry, *77*, 4985-4990

8. A. Travers, DNA-Protein Interactions, Springer, 1993.

9. S. Shen, Arsenic effects on the formation and repair of benzo[a]pyrene diol epoxide-DNA adducts, Ph.D. thesis, Edmonton, AB, 2006.

Appendix B

Results of HPLC separation, purification and MS characterization of the 16mer standards

B.1. Results of characterization of 16mer standards

16 nucleotide-long oligonucleotide (16mer) standards with a single UV lesion were synthesized by the Synthetic Organic Chemistry Lab (University of Texas Medical Branch, USA). Initially, 16mer was synthesized (SM-16mer) with one possible site for UV lesions (refer to Chapter 3). After SM-16mer UV irradiation, the mixture of 16mer standards was HPLC separated (Figure B.1). The chromatogram clearly shows 16mers with CPD (peak "a"), 64PP (peak "b") and other UV-lesions (peaks "c" and "d") and the 16mer with no damage (peak "SM"). Figure B.2 shows the same chromatogram as in Figure B.1 with the detection from absorption at 320 nm, the wavelength absorbed by 64PP lesions only [1-3].

After HPLC separation of the mixture of 16mer standards, the collected fractions with CPD-16mer (16mer with single CPD), 64PP-16mer (16mer with single 64PP) and SM-16mer (16mer with no damage) were HPLC/MS confirmed. Figure B.3 shows the results for CPD-16mer of HPLC (A) and MS (B) analyses; Figures B.4 shows the results for 64PP-16mer of HPLC (A) and MS (B) analyses; and Figures B.5 shows the results for SM-16mer of HPLC (A) and MS (B) analyses.
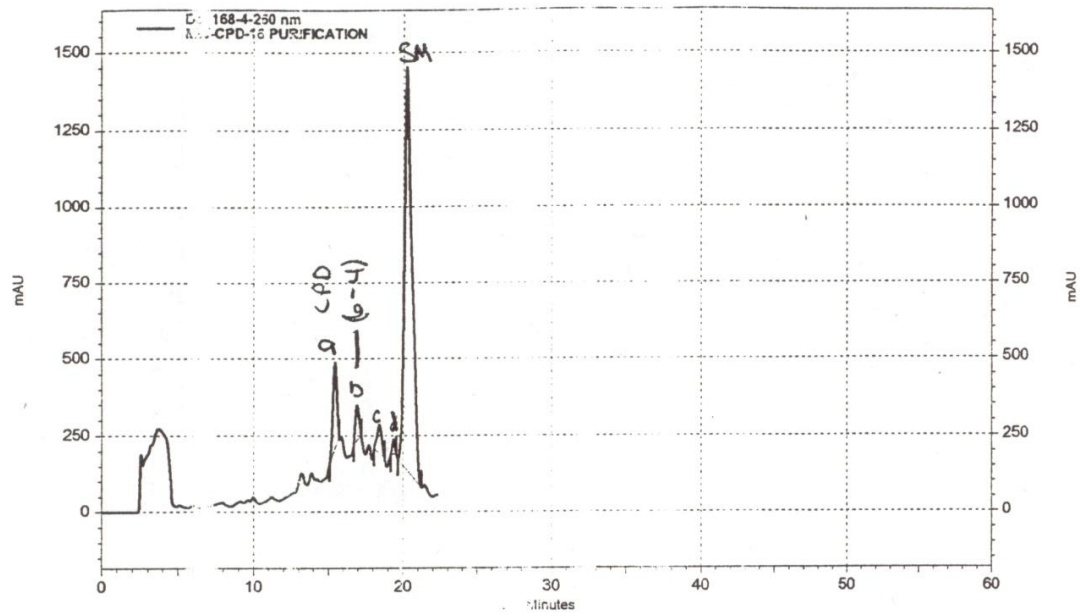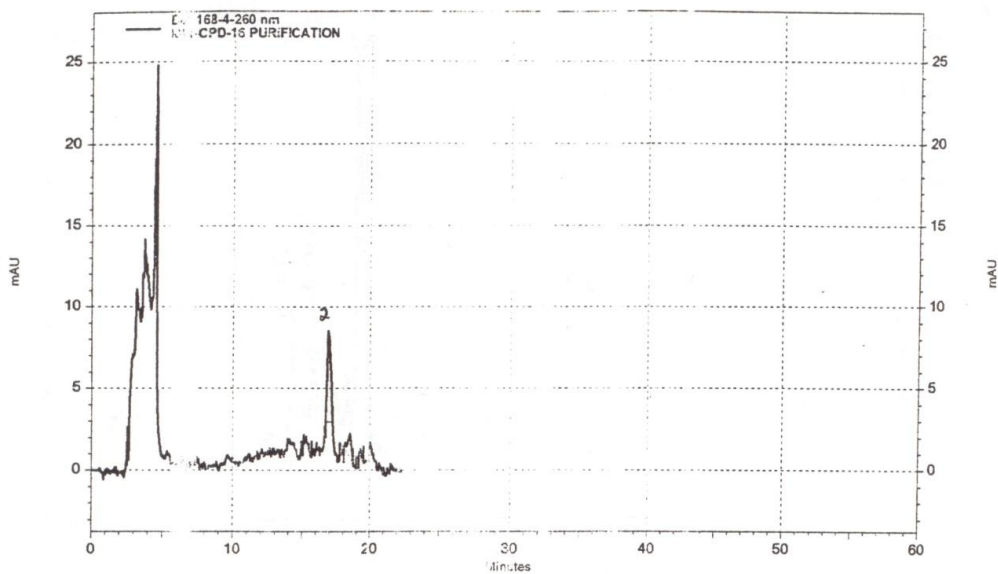
Figure B.1. HPLC separation of the UV irradiated SM-16mer using absorption at 260 nm

The scanned image of the provided HPLC chromatogram of the UV irradiated SM-16mer. Peaks were detected measuring the absorption at 260 nm.

Peak "a" or "CPD" – 16mer with CPD lesion

Peak "b" or "(6-4)" – 16mer with 64PP lesion

Peaks "c" and "d" – 16mer with another UV lesions (were not identified by the supplier)

Peak "SM" – 16mer with no UV lesions

Figure B.2. HPLC separation of the UV irradiated SM-16mer using absorption at 320 nm

The scanned image of the provided HPLC chromatogram of the UV irradiated SM-16mer. Peaks were detected measuring the absorption at 320 nm.
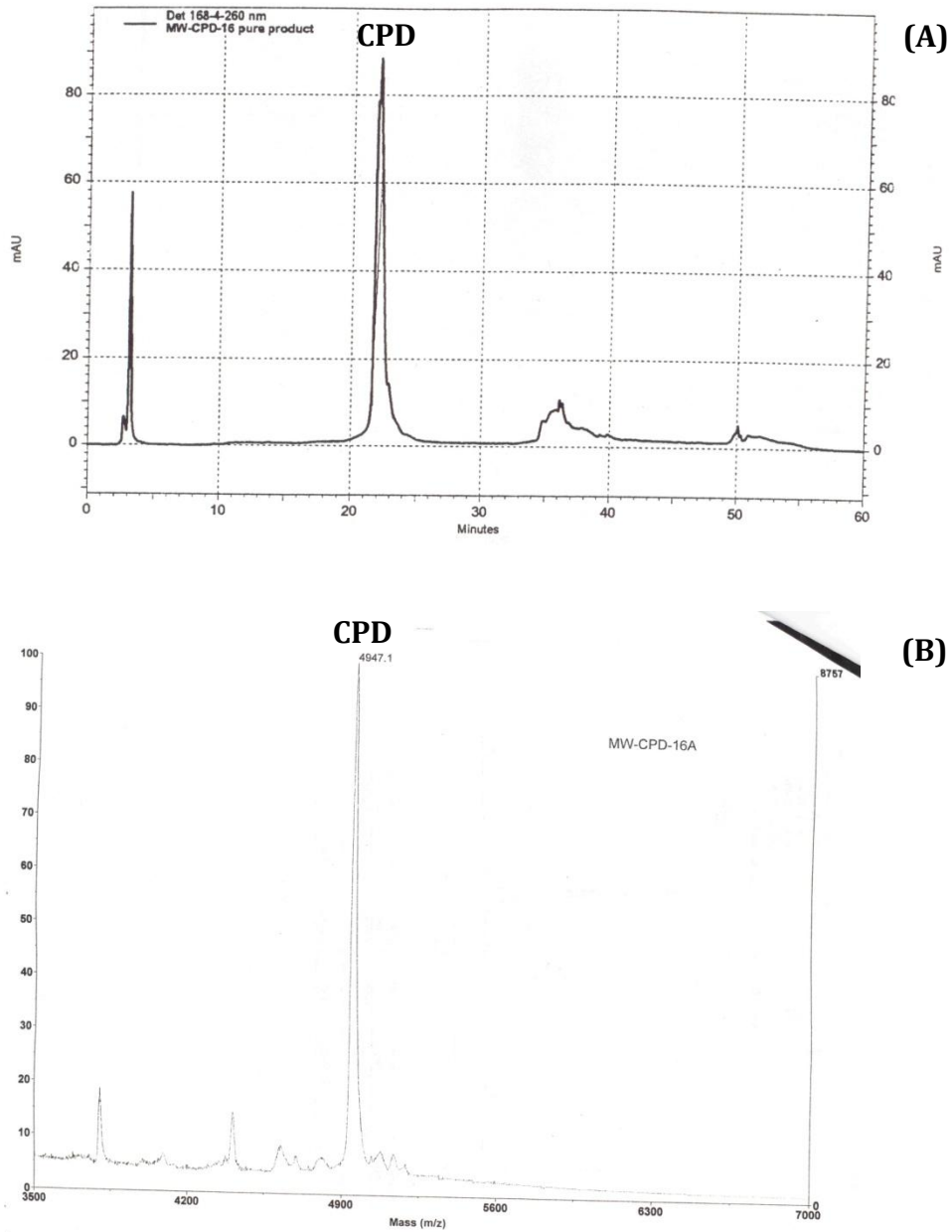
Peak "2" – 16mer with 64PP lesion

Figure B.3. HPLC (A) and MS (B) confirmation of CPD-16mer

The scanned images of the provided HPLC chromatogram (A) using the absorption at 260nm and MS spectrum (B).

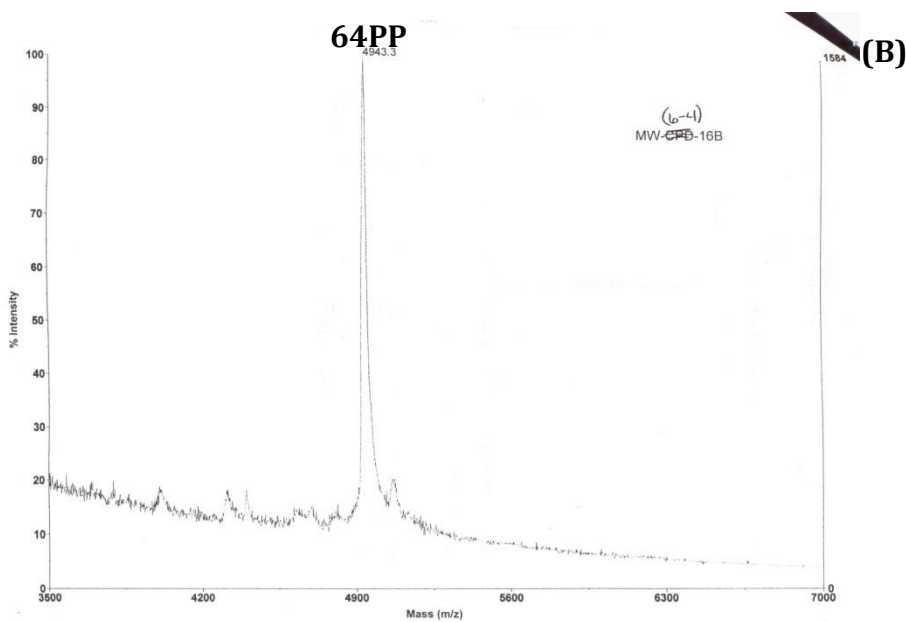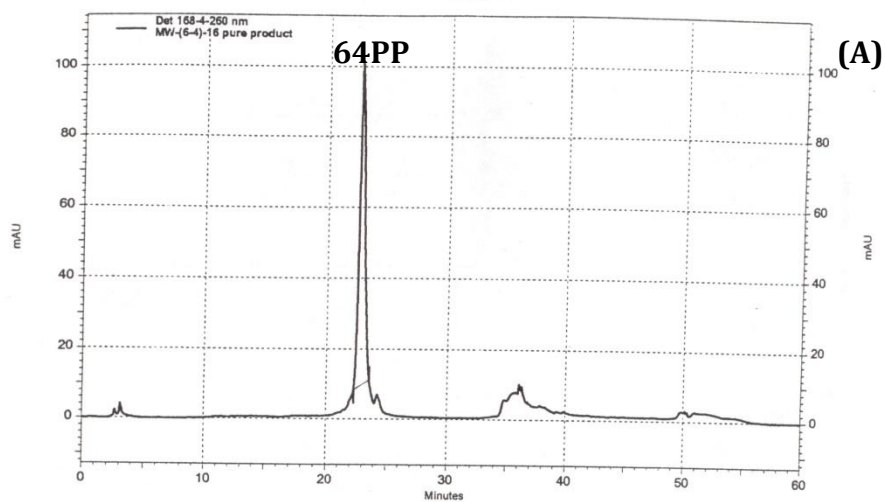Peak "CPD" – 16mer with CPD lesion

Figure B.4. HPLC (A) and MS (B) confirmation of 64PP-16mer

The scanned images of the provided HPLC chromatogram (A) using the absorption at 260nm and MS spectrum (B).
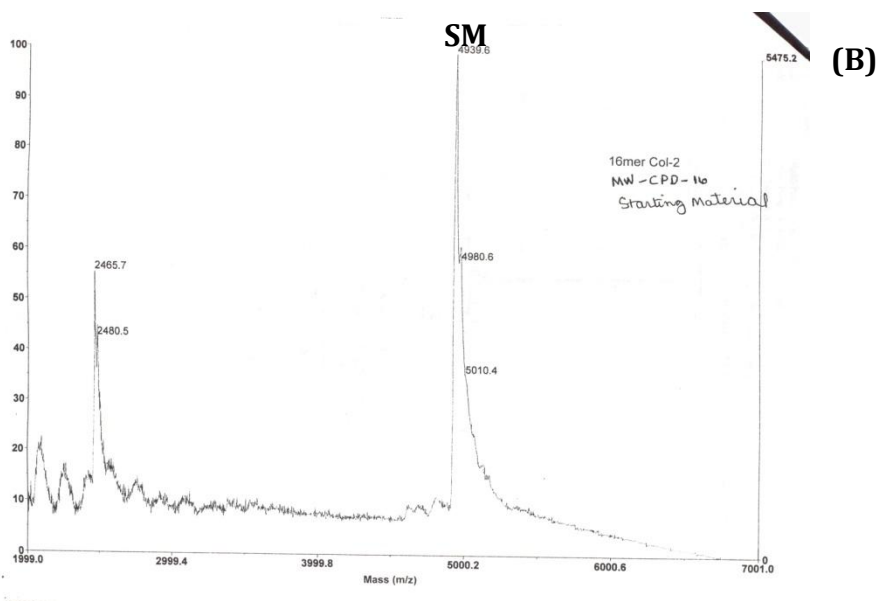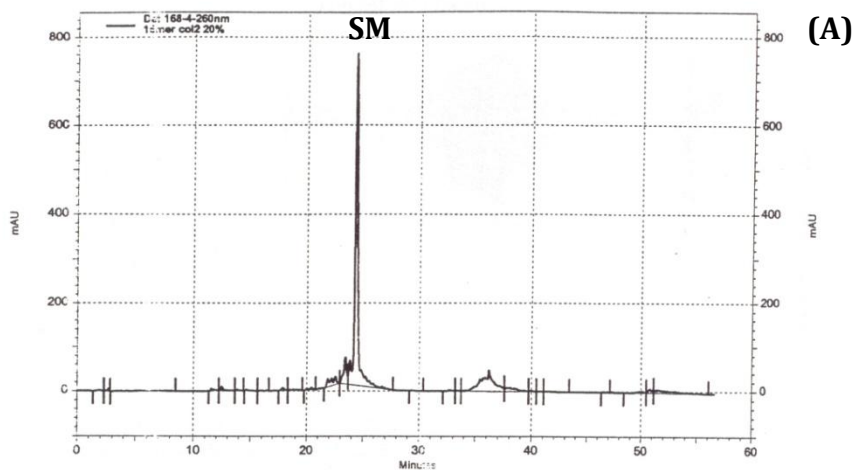
Peak "64PP" – 16mer with 64PP lesion

Figure B.5. HPLC (A) and MS (B) confirmation of SM-16mer

The scanned images of the provided HPLC chromatogram (A) using the absorption at 260nm and MS spectrum (B).

Peak "SM" – 16mer with no UV lesions

B.2. References

1. J.-S. Taylor and M.P. Cohrs (1987), DNA, light and Dewar pyrimidones: The structure and biological significance to TpT$_3$, J. Am. Chem. Soc. *109*, 2834-2835.

2. J.-S. Taylor, D.S. Garrett and M.P. Cohrs (1988), Solution-state structure of the Dewar photoproduct of thymidylyl-(3'→5')-thymidine, Biochemistry *27*, 7206-7215.

3. F. Gaecés and C.A. Dávila (1982), Alterations in DNA irradiated with ultraviolet radiation-I. The formation process of cyclobutylpyrimidine dimers : cross sections, action spectra and quantum yields, Photochem. Photobiol., *35*, 9-16.

Appendix C

Integration of peaks

Peaks were integrated using provided procedure files and plug-in for the IgorPro Software (version 6.0). Two approaches were used for integration of the antibody peak: Gaussian fit and vertical drop-down to baseline method. Comparison of results from both integration analyses showed no significant differences.

C.1. Comparison of integration analyses of antibody peak

An electropherogram corresponding to the CPD detection in 80nt DNA library irradiated with 1.6 J/cm^2 UVB light (Figure 2.3) was used to show the comparison of both methods.

Total peak area of all fluorescent species (PA_{total}) was calculated using base-to-base integration for both analyses (Figure C.1.1). Multiple peaks Gaussian fit procedure was used to integrate antibody peak (PA_{Ab}). The PA_{Ab} (Figure C.1.2) was used to calculate peak area for the ternary complex peak (PA_{cmplx}). The vertical drop-down to baseline method was also used (Figure C.1.3) to compare if results are much different. This comparison was needed when the CPD was measured in cellular DNA. Shape of the antibody peak was not perfectly Gaussian. Integrated peaks were used to calculate $PA_{relative}$, which is the ratio of PA_{cmplx} over PA_{total}.

1. Gaussian fit used to integrate antibody peak:

   $PA_{cmplx} = PA_{total} - PA_{Ab} = 0.5978 - 0.2131 = 0.3847$

   $PA_{relative} = PA_{cmplx}/PA_{total} = 0.3847/0.5978 = 0.6435$

2. Vertical drop-down to baseline method used to integrate antibody peak:

   $PA_{cmplx} = PA_{total} - PA_{Ab} = 0.5978 - 0.2301 = 0.3677$

   $PA_{relative} = PA_{cmplx}/PA_{total} = 0.3677/0.5978 = 0.6151$

Since standard deviation for $PA_{relative}$ among experiments was on average ± 0.05, both $PA_{relative}$ values are within experimental error. Thus both integration methods can be used in calculation of $PA_{relative}$.
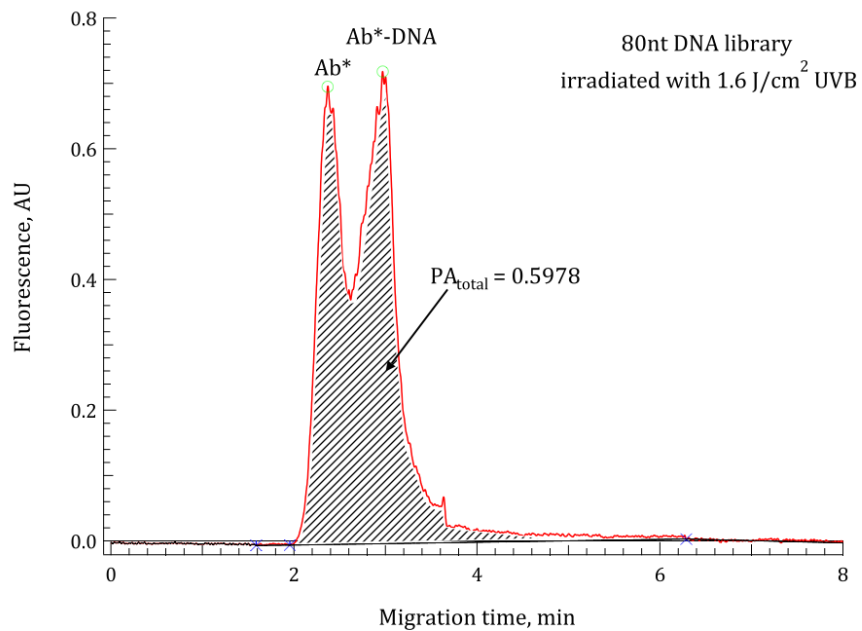
Figure C.1.1. Integration of all peaks using base-to-base integration method

Electropherogram from the CE-LIF analysis of CPD lesions in 80nt DNA library irradiated with 1.6 J/cm^2 UVB light,

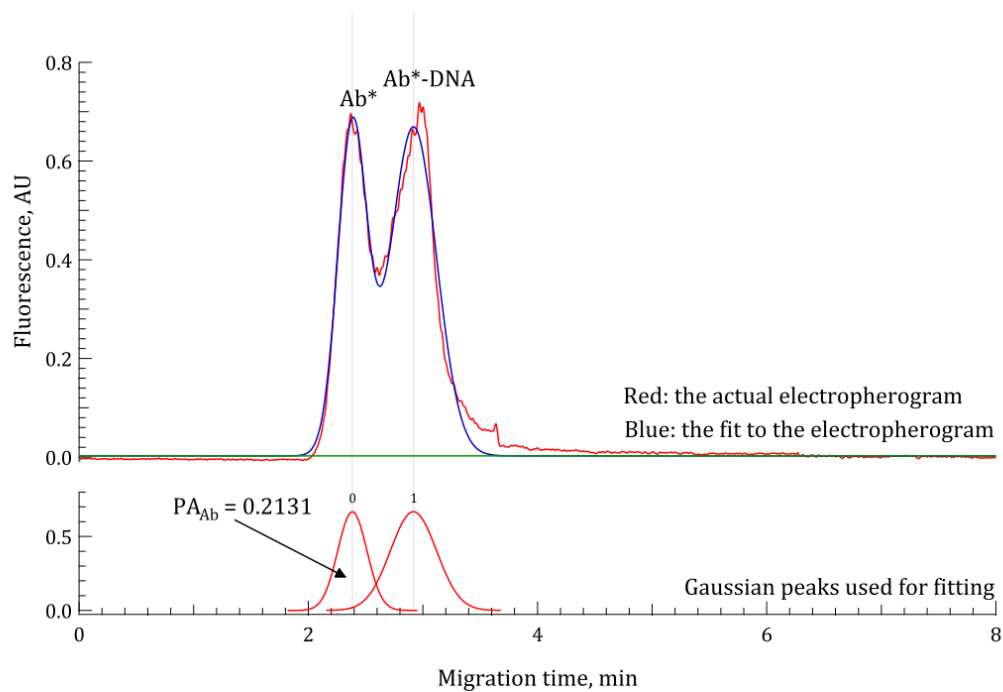Shaded area represents the area integrated by IgorPro Software.

Figure C.1.2. Integration of antibody peak using Gaussian fit

Electropherogram from the CE-LIF analysis of CPD lesions in 80nt DNA library irradiated with 1.6 J/cm^2 UVB light,

Shaded area represents the area integrated by IgorPro Software.

Figure C.1.2. Integration of antibody peak using the vertical drop down to baseline method

Electropherogram from the CE-LIF analysis of CPD lesions in 80nt DNA library irradiated with 1.6 J/cm² UVB light,

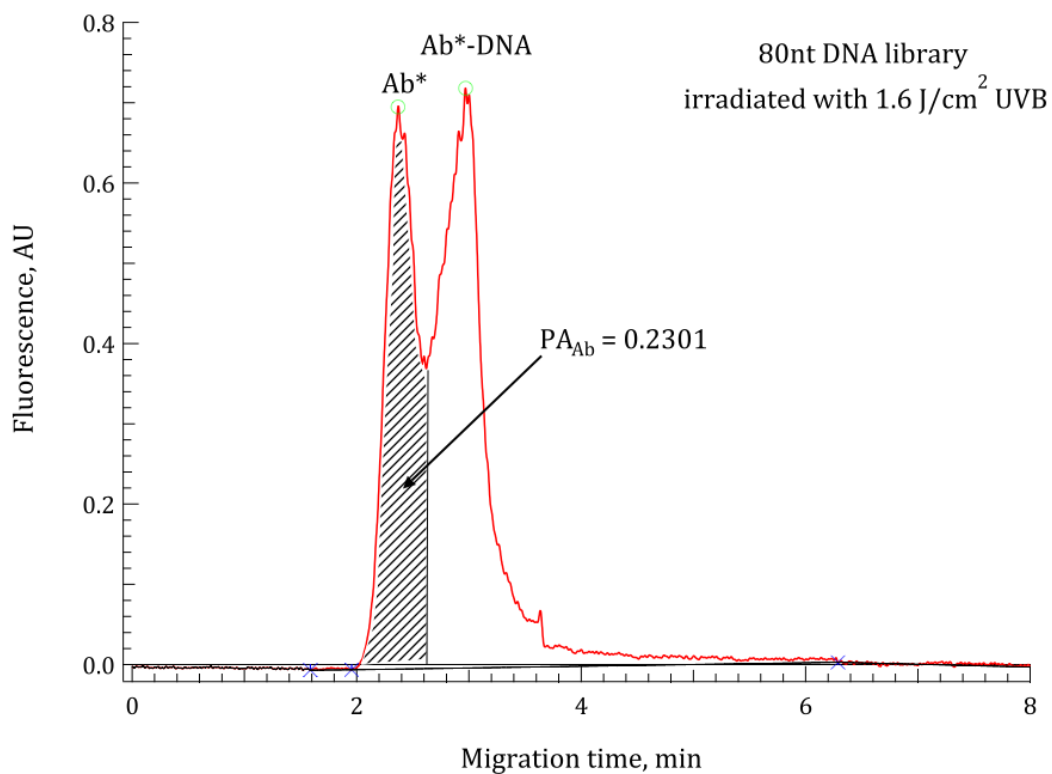Shaded area represents the area integrated by IgorPro Software.

C.2. Integration of peaks in CE-LIF immunoassay for human placenta DNA

Peaks obtained from the analyses of cellular DNA samples were more complex. Antibody peak did not have perfect Gaussian shape and control samples had a bit higher background. In these cases antibody peak was integrated using drop down to baseline method. In this part only calculations of $PA_{relative}$ for two electropherograms are shown as examples. First electropherogram is for a control HP-DNA sample and the second is for HP-DNA irradiated with 0.11 J/cm^2 UVB light. The electropherograms used are the same as the ones in Figure 2.9 for HP-DNA samples for CPD detection.

Figure C.2.1 shows integration of tall peaks for both electropherograms. Figure C.2.2 shows integration of the antibody peak for both electropherograms. Based on the integration results for PA_{total} and PA_{Ab} complex peak area (PA_{cmplx}) is calculated. From relative peak area ($PA_{relative}$) used in the dose response curves is calculated as the ratio of PA_{cmplx} over PA_{total}. Calculations for electropherograms shown in this Appendix are shown below.
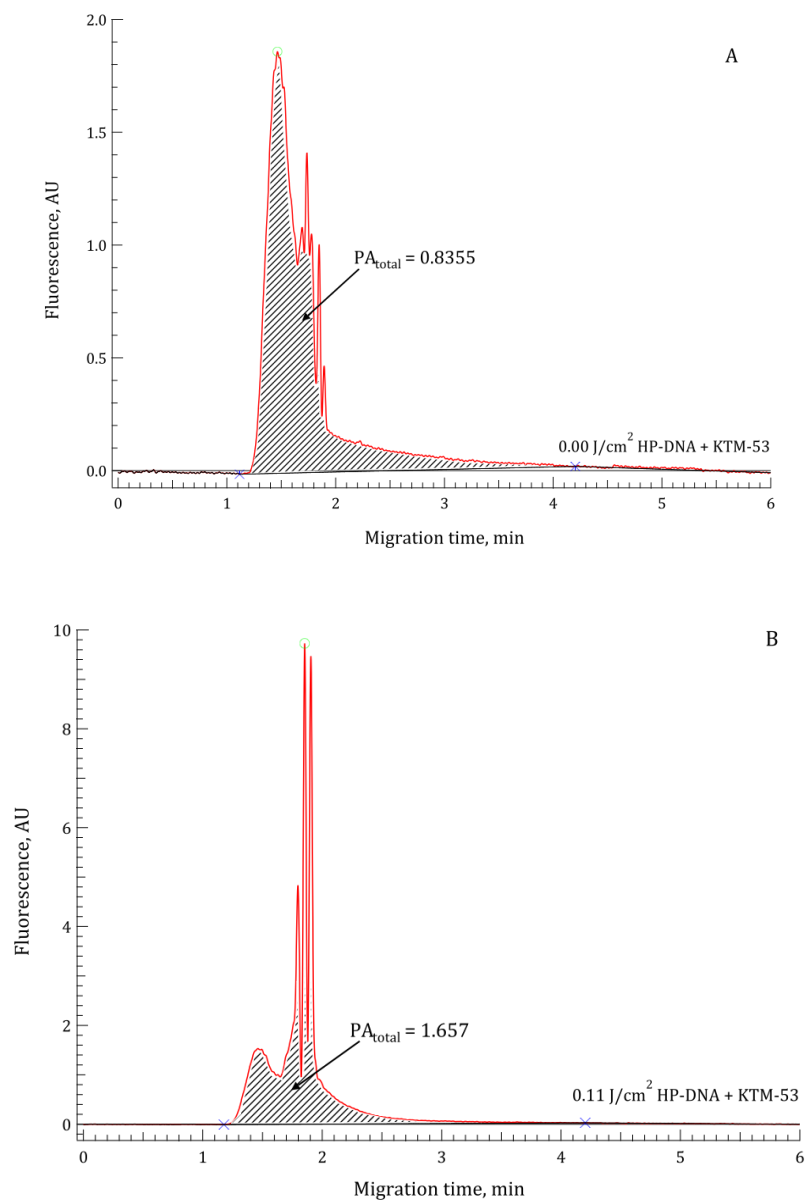
Figure C.2.1. Integration of all peaks using base-to-base method for the control HP-DNA (A) and HP-DNA irradiated with 0.11 J/cm² UVB (B)

Electropherograms from the CE-LIF analyses of CPD lesions in HP-DNA samples.

Shaded area represents the area integrated by IgorPro Software.
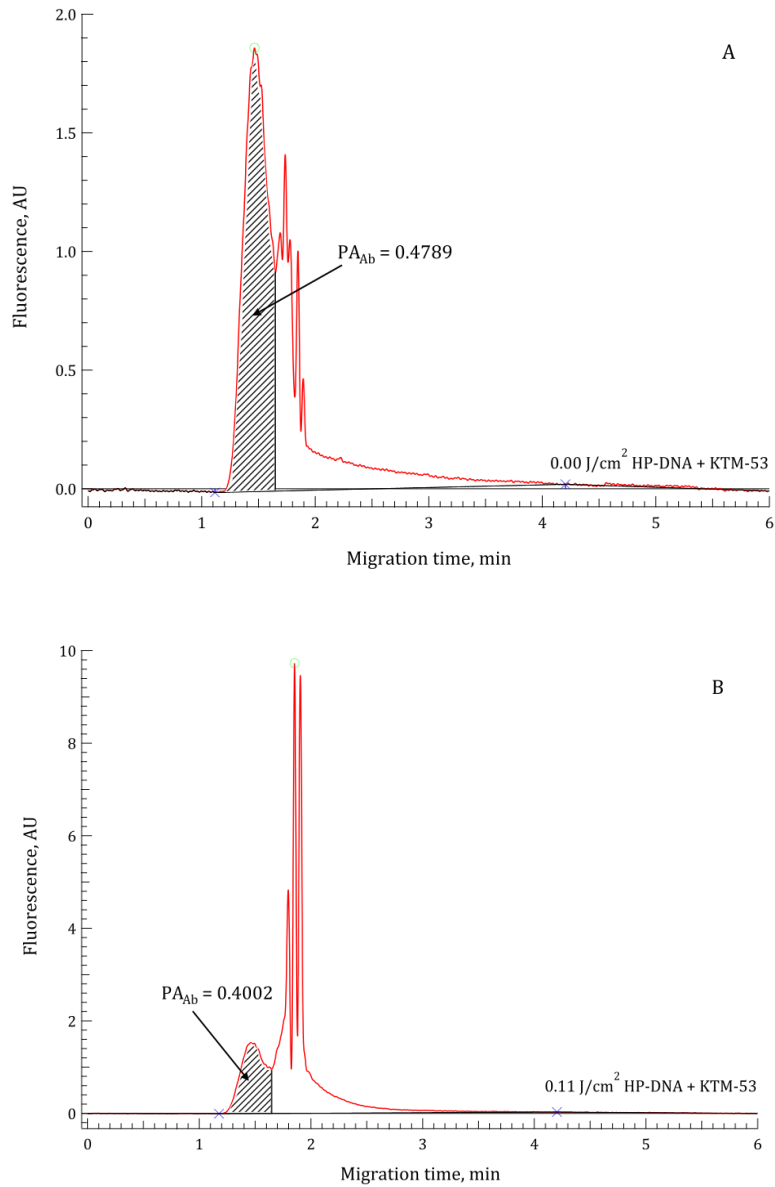
Figure C.2.2. Integration of the antibody peak using vertical drop down to baseline method for control HP-DNA (A) and HP-DNA irradiated with 0.11 J/cm² UVB (B)

Electropherograms from the CE-LIF analyses of CPD lesions in HP-DNA samples.

Shaded area represents the area integrated by IgorPro Software.

Calculations of PArelative for the control HP-DNA sample:

$$PA_{cmplx} = PA_{total} - PA_{Ab} = 0.8355 - 0.4789 = 0.3566$$

$$PA_{relative} = PA_{cmplx}/PA_{total} = 0.3566/0.8355 = 0.4268$$

Calculations of PArelative for the HP-DNA irradiated with 0.11 J/cm^2 UVB:

$$PA_{cmplx} = PA_{total} - PA_{Ab} = 1.657 - 0.4002 = 1.257$$

$$PA_{relative} = PA_{cmplx}/PA_{total} = 1.257/1.657 = 0.7585$$

All $PA_{relative}$ values for all experiments done in this work were calculated using this procedure.

.

Appendix D

Effect of arsenic species
on the formation and repair of CPD lesions in cells

Dr. X.C. Le and his group are studying the effect of arsenic on the formation and repair of DNA adducts as well as arsenic speciation in different matters [1-12]. One of the future directions of the research, using the developed CE-LIF immunoassay to detect CPD lesions in cells, could be studying the effect of arsenic species on the formation and repair of CPD lesions in cells.

D.1. Effect of arsenic on the formation of CPD lesions

1. Negative control for arsenic: fibroblasts CRL-2522 will be irradiated with environmentally relevant doses of UVB light (0.0 – 0.2 J/cm^2). After irradiation of cells are placed on ice to slow down repair mechanism until the DNA is extracted from cells. The CE-LIF assay will be used to measure CPD lesions.

2. Negative control for CPD lesions: fibroblasts CRL-2522 will be treated with various arsenic species (iAs$^{(III)}$, iAs$^{(IV)}$, MMA$^{(III)}$, MMA$^{(V)}$, DMA$^{(III)}$, DMA$^{(V)}$, etc.) in the growth medium at the indicated concentrations for, lets say, 24 hours. After treatment, DNA is extracted from cells and CPD lesions measured using the CE-LIF immunoassay.

3. Combined exposure of cells: fibroblasts CRL-2522 will be pre-treated with various arsenic species the same way as in part 2. The cells will then be irradiated with the same UVB doses as in part 1. After UVB irradiation cells are placed on ice to slow down repair mechanisms until DNA is extracted. CPD lesions are then measured using the CE-LIF.

D.2. Effect of arsenic on the repair of CPD lesions

Experiments in this part of project are similar to the ones described in the section D.1 with the exception, that cells after arsenic treatment and UVB exposure will be incubated for various times (example, 0 hrs, 3 hrs, 6 hrs, 12 hrs, 24 hrs, 48 hrs, 72 hrs) for cells to repair CPD lesions. At the end of each repair time period, DNA is extracted from cells and CPD measured using the CE-LIF assay.

All types of exposure and treatment will require at least 3 triplicates of cells.

D.3. References

1. S. Shen, J. Lee, X. Sun, H. Wang, M. Weinfeld and X.C. Le (2006), Elevation of cellular BPDE uptake by human cells: A possible factor contributing to co-carcinogenicity by arsenite, Environ. Health Perspectives, *114*, 1832-1837.

2. S. Shen, Arsenic effects on the formation and repair of benzo[a]pyrene diol epoxide-DNA adducts, Ph.D. thesis, Edmonton, AB, 2006.

3. S. Shen, J. Lee, M. Weinfeld and X.C. Le (2008), Attenuation of DNA damage-induced p53 expression by arsenic: A possible mechanism for arsenic co-carcinogenesis, Molecular Carcinogenesis, *47,* 508-518.

4. A. LeBlanc, S. Shen, K. Lew, M. Weinfeld and X.C. Le (2009), Detection of BPDE-DNA adducts in mononuclear white blood cells by capillary electrophoresis immunoassay and its application to studying the effect of glutathione depletion, Electrophoresis, *30*, 1558-1563.

5. C. Yuan, X. Lu, N. Orr, Z. Wang, Y. Xia, T. Wade, J. Mumford and X.C. Le (2008), Arsenic speciation analysis in human saliva, Clinical Chemistry, *54*, 163-171.

6. V. Charoensuk, W. Gati, M. Weinfeld and X.C. Le (2009), Differential cytotoxic effects of arsenic compounds in human acute promyelocytic leukemia cells, Toxicol. Applied Pharmacol., *239*, 64-70.

7. B. Chen, H. Narenmandula, M. Lu and X.C. Le (2009), Metabolism, toxicity, and biomonitoring of arsenic species, Progress in Chemistry, *21*, 474-482.

8. S. Shen, J. Lee, W.R. Cullen and X.C. Le (2009), Arsenite and its mono- and di-methylated trivalent metabolites enhance the formation of BPDE-DNA adducts in Xeroderma pigmentosum complementation group A cells, Chem. Res. Toxicol., *22*, 382-390.

9. H. Naranmandura, Y. Ogra, K. Iwata, J. Lee, K.T. Suzuki, M. Weinfeld and X.C. Le (2009), Evidence for toxicity differences between inorganic arsenite and thioarsenicals in human bladder cancer, Toxicol. Applied Pharmacol., *238*, 133-140.

10. C.F. McGuigan, C.L.A. Hamula, S. Huang, S. Gabos and X.C. Le (2010), A review on arsenic concentrations in Canadian drinking water. Environmental Reviews, *18*, 291-307.

11. L.W. Chen, X. Lu and X.C. Le (2010), Complementary chromatography separation combined with hydride generation - inductively coupled plasma mass spectrometry for arsenic speciation in human urine, Analytica Chimica Acta, *675*, 71-75.

12. K. Lew, J.A. Acker S. Gabosand X.C. Le (2010), Biomonitoring of arsenic in urine and saliva of children playing on playgrounds constructed from chromated copper arsenate-treated wood, Environmental Science and Technology, *44*, 3986-3991.